A STUDY OF THE QUADRUPOLE ION STORAGE SOURCE

BY

R.F. BONNER, B.Sc.

A thesis submitted for the degree of

Doctor of Philosophy

at the

University of Kent at Canterbury

Chemical Laboratory

August, 1974.

To my wife and

my parents.

Acknowledgements

Sincere thanks are due to my supervisor, Dr. J.F.J. Todd, for his encouragement, thoughts and helpful criticisms throughout this project.

In addition, it is a pleasure to acknowledge the assistance of my friends and colleagues; in particular Dr. G. Lawson who helped during both the work and the production of this thesis, and also to Messrs. D.A. Pugh, G.S. Jackson, P.R.J. Smith, R.J. Oliver and W.T. Povey for the construction of the original apparatus and for their continuing assistance with mechanical and electronic problems.

Finally, I am deeply grateful to Mrs. G. Lawson for typing the bulk of this thesis, and to Miss S. Hawkins and Miss S. Compston for their invaluable contributions to its production.

ABSTRACT

Although the three-dimensional quadrupole ion trap has received some attention as a mass spectrometer, few reports have been published describing the more general exploitation of its ion storage capabilities. This latter aspect is the subject of the present research.

Initially the general features of trapped ion techniques are surveyed in a review of the literature, after which the theory of the quadrupole ion storage trap (QUISTOR) is developed in general terms and a method for calculating the mean kinetic energy of stored ions derived.

The design of the QUISTOR is briefly described and the method of mounting this device as an ion source for a commercial quadrupole mass filter given in detail. Various modifications made to the remainder of other existing equipment are also described. Following this the performance is presented in two parts. Firstly, an account of the modes of operation and the details of a characterization of the electron optics and the storage capabilities is given, and secondly, the various types of ionic process that have been observed in the QUISTOR, including low-pressure Chemical Ionization employing air as a reagent gas, are detailed. It is shown that the QUISTOR is an extremely versatile device, being capable of operation in a manner akin to a normal ion source or as an ion storage source.

Finally, some suggestions for instrumental improvements and further research are included in a general discussion of the device.

Note on Units Employed Throughout This Work

The Units employed here are those more familiar to Mass Spectroscopists, rather than those defined under the Systeme Internationale (SI), and include the following:

Quantity	Unit
Pressure	Torr
Energy	Electron Volt (eV)
Length	Centimetre (cm)

The conversion factors to SI units are:

SI Unit	Non-SI Equivalent
Newton /square metre (Nm^{-2})	$^{1}/133.3$ Torr
Joule (J)	$^{1}/4.184$ Calorie
Metre (m)	10^{2} centimetre

In addition calculated ion velocities, Chapter 3, are expressed in metres per radian of the applied RF field; this is to maintain the generality of the expressions, and may be converted to metres sec^{-1} by multiplying by the radial frequency, Ω, of the applied RF.

Rate constants are given in the familiar units of cm^{3} $molecule^{-1}$ sec^{-1}; the conversion from pressure in Torr to molecules cm^{-3} is based on the law that one mole (i.e. 6.02×10^{23} molecules) at NTP ($0^{o}C$ and 760 Torr) occupies 22.4 litres.

TABLE OF CONTENTS

LIST OF FIGURES

CHAPTER 1

Introduction

1.1 Quadrupole Devices

The focussing properties of quadrupole and higher order electrostatic and magnetic fields are well-known, and they are widely used in particle accelerators, electron beam systems and mass spectrometers as charged particle lenses. The use of time-dependent quadrupole electric fields as mass spectrometers in their own right, however, was first proposed by Paul and Steinwedel[33], and was further developed by Paul and colleagues[118-121]. The quadrupole mass filter utilizes a two-dimensional quadrupole field, produced by connecting steady (DC) and alternating radio-frequency (RF) voltages, out of phase in the x- and y-directions, to pairs of a structure comprising four accurately parallel rods arranged at the corners of a square, as shown in Figure 1-1 (a). Such a field possesses two intersecting equipotential planes, which bisect the planes of the rods, as illustrated in Figure 1-1 (b), and has no field along the axis of the rods, the z-direction. Ions entering the array of rods along the z-axis undergo cyclic focussing and defocussing, again out of phase in the x- and y-directions, and as a result ions of only one particular m/e value remain bounded (are said to be stable) and can leave the device, all other ions being lost on the rods.

The correct field inside the device is ensured by careful choice of the rod geometry rather than voltage relationships; ideally the internal surfaces of the rods should be hyperbolic, although round rods are often used and chosen to approximate hyperbolae most closely. The particular m/e value which is stable depends on the magnitude of the voltages, the RF frequency and the size of the device, and may be selected by appropriate choice of these quantities; alternatively, the

Figure 1-1 Quadrupole Mass Filter Geometries

(a) Array of Circular Rods

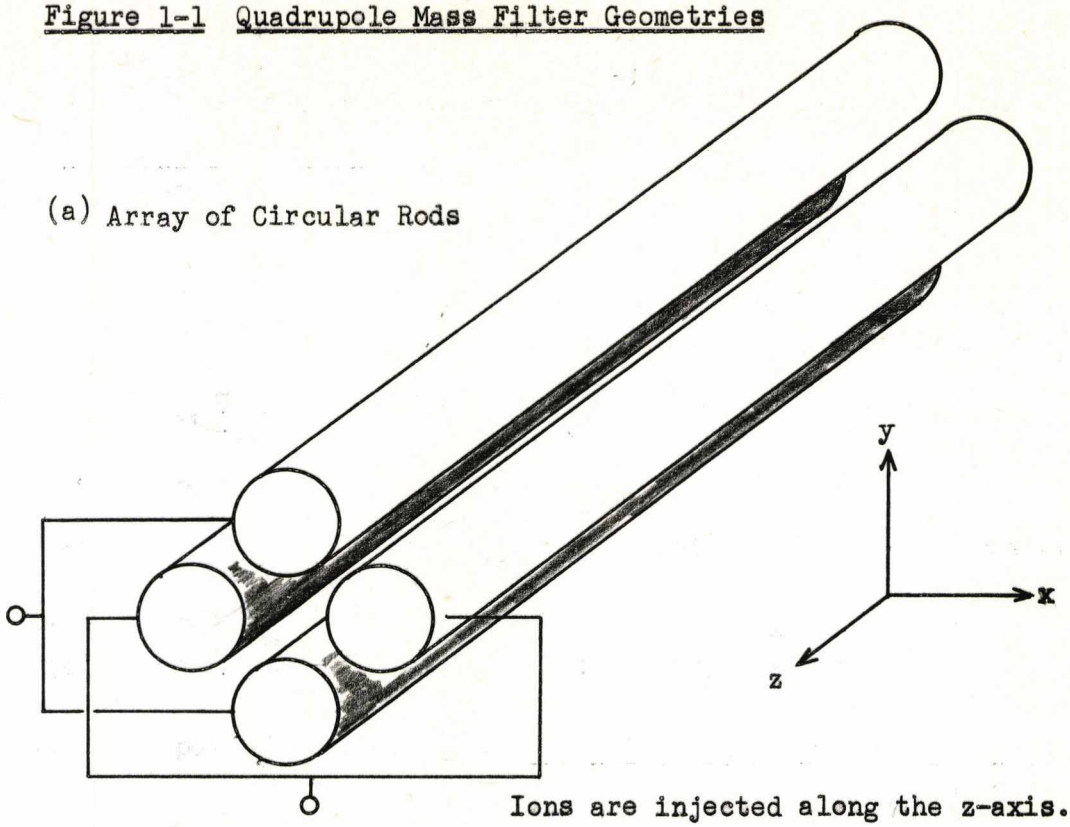

Ions are injected along the z-axis.

(b) Cross Section of Hyperbolic Rods, Showing Zero Equipotential Planes (Dashed)

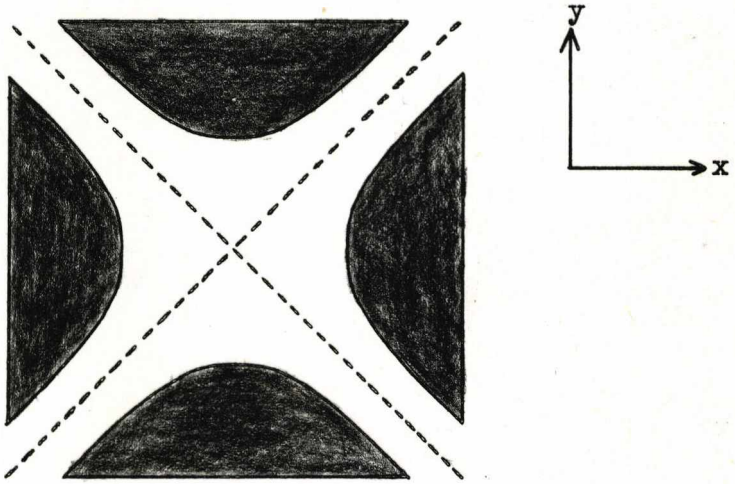

device may be scanned over a given range by varying the voltage amplitudes. A second mode of operation exists, in which a range of m/e values can pass through; this is achieved with zero DC potential applied to the rods, and is known as the 'total pressure' or 'ion gauge' mode, since a signal proportional to the source pressure is obtained.

A related instrument, the monopole mass spectrometer, first described by von Zahn[97], is essentially one quarter of a mass filter, as it consists of one rod and an earthed 'V-block' electrode which replaces the zero equipotential planes of the mass filter. The applied voltages and operation of this device are similar to those for the mass filter, described above.

These devices have been widely used in many fields where compactness and ease of operation are required, for example space-flight, other portable applications, partial and total pressure measurement and residual gas analysis. Commonly, mass filters are a mere 12.5 cm. in length and, being totally voltage operated, lend themselves readily to remote and automatic control; furthermore, their relative insensitivity to the ion kinetic energy and the lack of high accelerating voltages has made them popular as ion and molecular beam detectors. The applications of quadrupole devices have been recently reviewed by several authors,[103,122,123] and will not be repeated here, although a more detailed account of the theory and operation of these devices is given in Chapter 3.

In contrast to the mass filter and monopole, the three-dimensional quadrupole, or ion trap, has received little attention. As its name implies, the field is three-dimensional and is again generated by RF and DC voltages applied to a set of three electrodes having hyperbolic faces. Unlike the mass filter, the electrodes are not all identical, (this is demonstrated and illustrated in Chapters 2 and 3), and the device has cylindrical symmetry. In many ways the lack of interest in

this device is surprising, as it would appear to have several advantages over the mass filter. It can be made smaller, typical instruments have the dimensions of a cylinder 5 cm. in diameter and 5 cm. in height, and with greater ease, Dawson, Hedman and Whetten[36] having reported acceptable performance from a device roughly shaped from wire mesh. In the mass filter the resolution depends on the number of RF cycles an ion experiences, and hence increases with mass since heavy ions have lower velocities for a fixed ion energy; this results in a mass spectrum which is invariably different to that obtained from a magnetic instrument, owing to discrimination against high mass ions. In the three-dimensional device, however, stable ions are stored for a fixed time to allow unstable ions to be lost and, since this time does not depend on mass, the spectrum should not show discrimination against higher masses. Furthermore, the resolution should be dependent on the storage time and easily adjustable. In addition to these more mass spectrometric advantages, the storage capabilities are of great interest, and the reported uses of these devices in this mode are reviewed in Chapter 2.

1.2 Historical Introduction to This Work

This work is a continuation of that performed and described by Dr. G. Lawson[37], also of this Laboratory, the original research proposal being to employ a three-dimensional quadrupole ion trap as an ion source for a mass spectrometer, in order to enable the source residence time to be increased and long-lived metastable ions to be studied. The mass analyzer was a quadrupole mass filter, chosen because of the previously mentioned advantages - insensitivity to ion kinetic energy and lack of high accelerating voltages - the actual model being an ELECTRONIC ASSOCIATES INC. (PROCESS ANALYZERS INC. - E.A.I.) QUAD 250 A. Two Quadrupole Ion Stores (QUISTORs) were constructed, one accurately machined from stainless steel and the other roughly shaped

from wire mesh. The former was not used, because of the experimental difficulties described in Chapter 4, but it was shown that ion-molecule reactions could be observed in the mesh device. While similar chemical phenomena resulting from ionic collisions had been observed in quadrupole traps by other workers, for example Dawson and Whetten[103] and Rettinghaus[39], they had been regarded as being undesirable owing to the likelihood of a reduction in storage capabilities occurring through ion-molecule scattering (see Chapter 5). The employment of such a device solely for the observation of ion collision processes is, therefore, unique to this Laboratory; the technique resembles both Space Charge Trapping and Ion Cyclotron Resonance (ICR), and is compared to these in the following chapter.

1.3 Aims of This Work, and the Organization of the Thesis

Essentially, the aims of this work were two-fold :

(i) To re-examine the stainless steel QUISTOR, and to study its behaviour, particularly to enable a comparison with the mesh device to be made, and to theoretically and experimentally characterise the ion kinetic energy;

(ii) To determine the type of ionic processes that could be observed in such a device, for instance Chemical Ionization. The possibility of this latter phenomenon was suggested by Dr. Lawson[37] following the observation of ion-molecule reactions in methane, the most usual reagent gas in Chemical Ionization studies.

In order to achieve (i) above, it was necessary to devise a method of mounting the QUISTOR on, or near, the analyzer so that the previously encountered experimental difficulties (see Chapter 4) were overcome. This is described in Chapter 4, along with the various modifications made to the apparatus, which was otherwise as previously described[37].

The theory of ionic motion in quadrupole fields is developed and discussed in Chapter 3, and leads to a method for calculating the mean kinetic energy of stored ions.

Before the description of the types of ionic collision phenomena that have been observed in the QUISTOR, including Chemical Ionization and Spectrum Simplification (Chapter 6), the behaviour and storage characteristics are examined in detail, and the results are presented in Chapter 5.

In order to place the main contents of this thesis in perspective, the description of the work performed during this project is preceded by a literature review of the various ion storage methods, and uses, that have been reported. The review is intended to demonstrate the growing employment of ion traps, particularly in ion collision studies, and to indicate the place of the QUISTOR among these other devices. Included are references to reports which became available before June 1974.

Much of the work concerning ion-molecule reactions was performed in conjunction with Dr. G. Lawson, Dr. R.E. March (during his short stay at Kent as a Visiting Research Fellow) and, more recently, Mr. R. E. Mather, B.Sc., who is continuing these and other studies with special reference to Chemical Ionization.

A list of the papers that have been published and presented as a result of this work, is given in the Appendix.

CHAPTER 2

Review of Ion-Storage Methods

2.1 Scope of the Review

The purpose of this review is to examine the role of ion-storage methods as experimental tools in modern gas phase chemistry, and to show the place of the three-dimensional, radio-frequency quadrupole electric trap in this field. 'Ion-storage' meaning the confinement of an ion in a particular volume by suitable electric and/or magnetic fields. Specifically, Electron Beam, Quadrupole and Pulsed Ion Cyclotron Resonance (ICR) Traps will be considered in detail, and a brief description of Drift Tubes and Ion Cyclotron Resonance Mass Spectrometry will be given. These latter two techniques do not come into the category of ion-storage methods, as defined above, since the ions are not contained, but pass slowly, and with a well defined velocity, through a particular region. This does, however, often result in an increase in the time between ion creation and detection, as in ion traps. The major application of all these methods is in the field of ion-particle reactions, which has become in recent years a large part of gas-phase chemistry. Consequently, a description of the traps is prefaced by an examination of ion-particle reactions, and the more important methods employed for their study (excluding ion trapping techniques). Finally, the various ion traps are discussed and compared.

2.11 Ion-Particle Reactions

The rapid development in the study of ion-particle reactions, has occurred in two distinct areas:

i) The reactions of ions with photons and electrons, leading to the production of multiply charged ions.

ii) The reactions of ions and neutral molecules involving charge- and heavy particle-transfer, leading directly to the technique of 'Chemical Ionization'.

Data on these reactions can also provide information on the energy levels in atoms and molecules, and enables comparisons with theoretical reaction rates and collision data.

The reactions of ions with photons and electrons is clearly important in the production of multiply charged ions, since it is unlikely that such ions will be produced by a one-step process:

$$M + e^- \longrightarrow M^{n+} + (n + 1)e^-$$

unless the ionizing particle is highly energetic. More probable is a multi-step process :

$$M + e^- \longrightarrow M^+ + 2e^-$$

$$M^+ + e^- \longrightarrow M^{2+} + 2e^- \quad \text{etc.}$$

Interest in ion-neutral reactions has been promoted by realization of the large number of naturally occurring reactions of this type, for example in the upper atmosphere, flames and plasmas. In the upper atmosphere, a wide range of reactions occur by ions resulting from photo-ionization and account for many phenomena, such as the aurora borealis and radio wave propagation. The development of space flight and air- and rocket-borne mass spectrometers has provided an experimental method of examining the ionic and neutral composition of the upper atmosphere. Similarly, many of the combustion products in flames and the reaction products in plasmas can be explained by the reactions of ions produced by thermal ionization.

The concept of ion-neutral reactions has been used, since the earliest days of mass spectrometry, to explain the presence of ions, which could not be formed simply by ionization and subsequent dissociation; in particular ions with m/e 3 and 19. The persistent formation of these ions was attributed to the reactions :

$$H_2^+ + H_2 \longrightarrow H_3^+ + H$$

and $$H_2O^+ + H_2O \longrightarrow H_3O^+ + OH$$

The design of conventional mass spectrometer ion sources permits the observation of only the faster ion-molecule reactions, and the products can often present undesirable complications in the resulting mass spectra. The reason for this is that only a small number of collisions between ions and molecules can occur under the operating conditions of a normal source with a correspondingly low probability of reaction, unless the reaction rate is high. Thus, studies of ion-particle reactions necessitate special sources in which the collision number can be increased, and then varied. A simple, conventional ion source is shown in Fig. 2-1.

Figure 2-1 Schematic Representation of a Conventional Ion Source

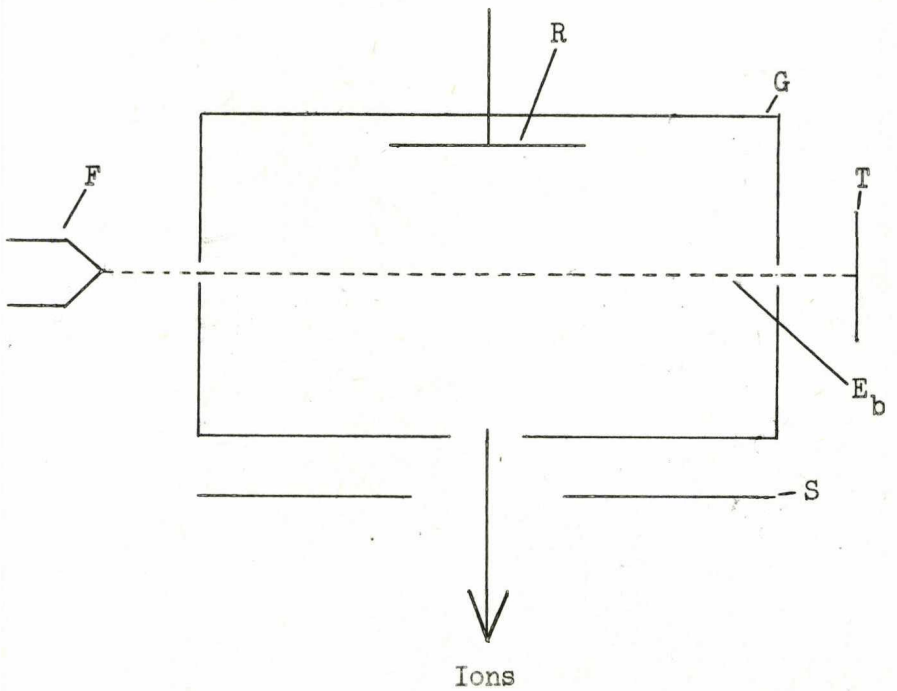

Electrons, produced by a heated filament F, pass through an essentially field free region or Faraday cage. G, and are collected on a trap, T. The electron beam, E_B, is often collimated by the application of a magnetic field parallel to the beam. Ions, produced by collisions between the beam and the neutral molecules in G, move under the influence of a small positive potential applied to the repeller, R, towards the exit slit, S, where they are accelerated and enter the analyzer. During the time an ion spends in the source, usually about 10^{-6} seconds, it is in an environment containing molecules and electrons with which it may undergo collisions. As an approximate calculation, the number of collisions per second, Z, may be written :

$$Z = kN$$

where k is the rate constant for collisions between ions and molecules, and is known to be of the order of 10^{-9} cm^3 $molecule^{-1}$ sec^{-1}; and N is number density of gas molecules, which is approximately 10^{11} at 10^{-5} torr and room temperature. Consequently under these conditions an ion will undergo 100 collisions per second, but since the residence time is usually short, the actual probability of collision is vanishingly small. Field[1], has estimated that in a chemical ionization source, operated at 1 torr and with a residence time of ca 10^{-5} seconds, the number of collisions an ion undergoes is approximately 200, and this sort of figure must be approached if ion-molecule reactions are to be observed. From the above calculation, it is apparent that the collision number may be increased in one of two ways :

i) the number density (i.e. pressure) of neutrals can be increased, or

ii) the source residence time can be increased.

In theory an increase in the source operating pressure is simple,

and ion-neutral reactions may be observed at short residence times with a conventional source. Practically, several difficulties arise; in particular high-speed differential pumping must be incorporated, to maintain the analyzer at high vacuum, and there is danger of high-voltage breakdown in the source and filament burn-out. Nevertheless, standard mass spectrometers, operated at both high and low pressure, have been widely used in ion reaction investigations (see reference 2 for many examples and further references). The occurrence of ion-neutral reactions in high pressure sources led to the development of the technique known as 'Chemical Ionization', first reported by Munson and Field[3]. Conventional electron impact ionization frequently causes considerable fragmentation of sample molecules, and low abundance of molecular ions. From the point of view of sample analysis, large molecular ion currents are desirable, in order to determine the molecular weight, M, and these can be achieved by employing Chemical Ionization. The sample under examination is mixed with a large excess of reagent gas, so that the total pressure in the ion source is 1-2 torr. Methane is commonly used as a reagent gas, although other substances, including the rare gases, have been used. The mixture is subjected to electron impact during which the reagent molecules are ionized and undergo ion-molecule reactions forming charge or proton donating agents, which in the case of methane are CH_5^+ and $C_2H_5^+$. These then donate protons to, or abstract electrons from, the sample, forming ions at M or (M + 1). This technique has been widely adopted as a means of ionization preferable to electron impact in analytical applications, and has been reviewed elsewhere[1].

On the other hand, increasing the residence time of the ions in the source, permits the use of much lower pressures, but necessitates the construction of special sources. An exception to this is the Space Charge Trap, which utilises a conventional ion source.

In addition to mass spectrometers, the other major techniques used in ion reaction studies are Ion Beams and Afterglows. These will be briefly examined, to permit comparison with ion trapping techniques, more detailed reviews may be found elsewhere[2,4,5]. They have mainly been used to study the effects on ion-molecule reactions of varying the ion kinetic energy, which are often large, altering both the reaction rate and pathway.

2.111 Beam Methods

In this technique a beam of ions, often mass and energy selected by a source mass spectrometer, is injected into a collision region containing a neutral species. Frequently the reaction chamber is subjected to a uniform potential gradient to ensure a constant ion energy. Emergent ions, which may be either products or un-reacted reagents are then detected; if the detector is another mass spectrometer, the technique is known as Tandem Mass Spectrometry. This basic, simplified principle has been widely adopted and various workers have described equipment for crossing or merging the beam of ions with a second beam, of ions, neutrals, electrons or photons. Thus many reactions have been studied, and information on scattering obtained. This latter process is often examined by employing a detector which is rotatable about the collision region, and provides data on the angular distribution of products.

Since the collimation of the ion beam deteriorates rapidly as the ion-energy is reduced below one electron-volt, this technique has been used for ion energy studies greater than this value, and up to several thousand electron-volts.

2.112 Afterglow Methods

In this technique, an arc is struck in a region containing a neutral species, which is partially ionized. Ion-neutral reaction products are normally detected by a mass spectrometer. The neutral

species may be passed through the discharge region (flowing afterglow) or it may be static. The latter technique has mainly been used for the study of the reactions between ions and neutrals of their own kind, e.g.:

$$Ar^+ + Ar \longrightarrow Ar + Ar^+$$

although the presence of trace amounts of other neutrals permits examination of more complex systems, e.g.:

$$Ar^+ + H_2 \longrightarrow ArH^+ + H$$

In a flowing afterglow, the reaction time depends on the flow-rate of the neutral species, and consequently provides an extremely versatile technique for the study of ion-molecule reactions. Helium is commonly employed as the flowing gas, other materials being injected downstream of the discharge.

The energy of ions produced by a discharge is essentially thermal, and consequently these techniques have been used in studies of the reactions of low kinetic energy ions.

From the above outline of these experimental methods, it is apparent that they cannot be used in the region of ion energies between thermal ($\underline{ca}$0.01 ev) and several electron volts. In this region, the most widely used techniques are Drift Tubes, ICR and Ion Storage. The types of ion traps will now be reviewed in detail; where the devices have been used in applications, other than as ion traps (for example as massive charged particle traps or mass spectrometers) these are included for the sake of completeness.

2.2 Types of Ion Trap

The three types of ion trap considered in this review are Electron Beam Traps, Radio-frequency Quadrupole Electric Field Traps and Pulsed Ion Cyclotron Resonance Traps. The latter, although considered in detail, is included with ICR and Drift Tubes in Section 2.23, 'Other Traps'.

2.21 Electron Beam Traps

Two types of Electron Beam Trap have been reported in the literature, known as the Space Charge Trap and the Hollow Electron Beam Trap. In both ions are stored in the space charge of the electron beam that produced them, but they differ in the shape and method of formation of the ionizing beam. These traps have been used in the field known as 'Sequential Mass Spectrometry', where ions are created, stored and then undergo further ionization, by collisions with electrons, and ion-molecule reactions.

2.211 Space Charge Traps

The principle of trapping ions in the space charge of an electron beam was used by Field, Spagenberg and Helm[6] to explain the observed phenomena of 'gas focussing', in which the dispersion of an electron beam was found to decrease as the residual pressure was increased. They showed that the trapping of ions by the beam, results in partial space charge neutralization, thus eliminating defocussing effects. The ions are trapped in a radial potential well which has the electron beam as its centre, and most negative part. Linder and Hernqvist[7] designed an electron beam source which incorporated this principle, and allowed the passage of electron beam currents some thirty times greater than those obtainable in conventional sources. They also included results on the rate of ion build-up as a function of pressure, and on beam noise in the presence of trapped ions. Plumlee[8] described a mass spectrometer ion source which incorporated space charge neutralization, and he reported that this allowed the use of higher ionizing beam currents, and increased the effective volume of the source from which a stable ion current could be drawn. He reported the observation of ion currents one or two orders of magnitude greater than those from a conventional ion source, and also greater fragmentation which he ascribed

to the probability of an ion experiencing several collisions with electrons and neutrals.

In 1966 Baker and Hasted[9] described an apparatus for studying the production of multiply charged ions by successive collisions of ions with electrons. Ions are created by an electron beam, are then trapped in the radial space charge of the beam, and undergo further collisions with electrons. In this technique, known as Sequential Mass Spectrometry, multiply charged ions are produced with electron beam energies less than the relevant ionization potential. The apparatus used was an un-modified A.E.I. MS 10 mass spectrometer, and further work has been described[10,11]. Typically trapping times are of the order of 10mS with this device. Redhead[12,13,14] has also reported results obtained by Sequential Mass Spectrometry. His apparatus differs from that of Baker and Hasted in having an additional grid, which permits better trapping. Figure 2-2 compares Redhead's source with a conventional source.

Figure 2-2 Comparison of Redhead and Conventional Ion Source

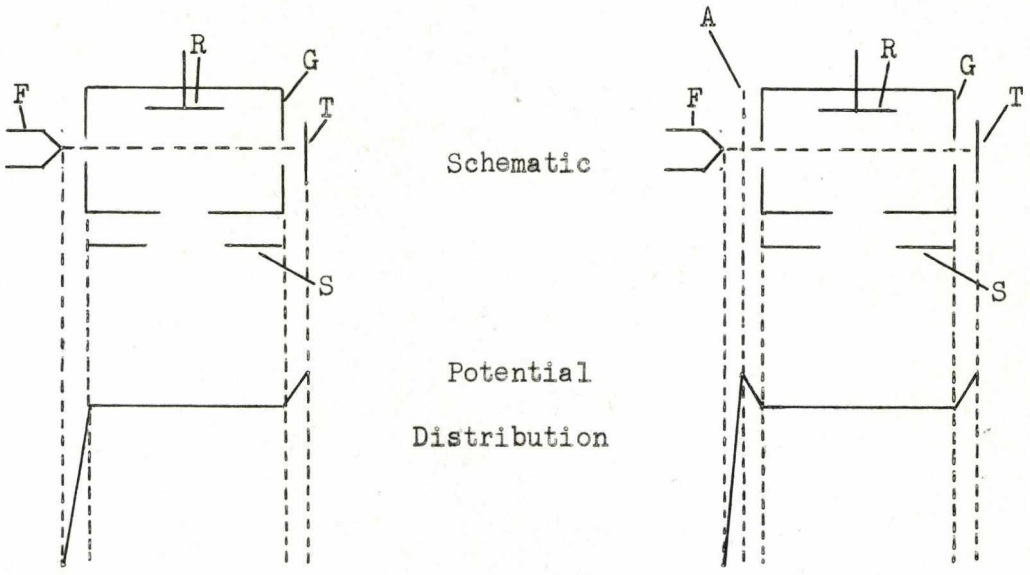

2-2(a) 2-2(b)

The additional grid, A in Figure 2-2b, was maintained positive with respect to the cage, G, causing a potential depression in the direction of the beam; the trapping time obtained, at similar pressures to those used by Baker and Hasted, was of the order of one second. Results on electron collisions with various ions, studied by this method, have also been reported by Daly and Powell[15,16,17] and Cuthbert, Farren, Prahallada Rao and Preece[18,19,20].

The adaptation of this technique to the study of unimolecular ion decomposition or bimolecular ion-molecule reactions was proposed by Bourne and Danby[21]. A conventional A.E.I. MS 2 was used, and the pulse train shown in fig. 2-3 applied to the ion source. The filament was operated at -5v and periodically pulsed to -30v, with a repetition rate of 2Hz. Ions created by the 30eV electrons are trapped in the space charge of the 5eV beam.

Figure 2-3 Pulse Train Employed by Bourne and Danby for Space Charge Trapping

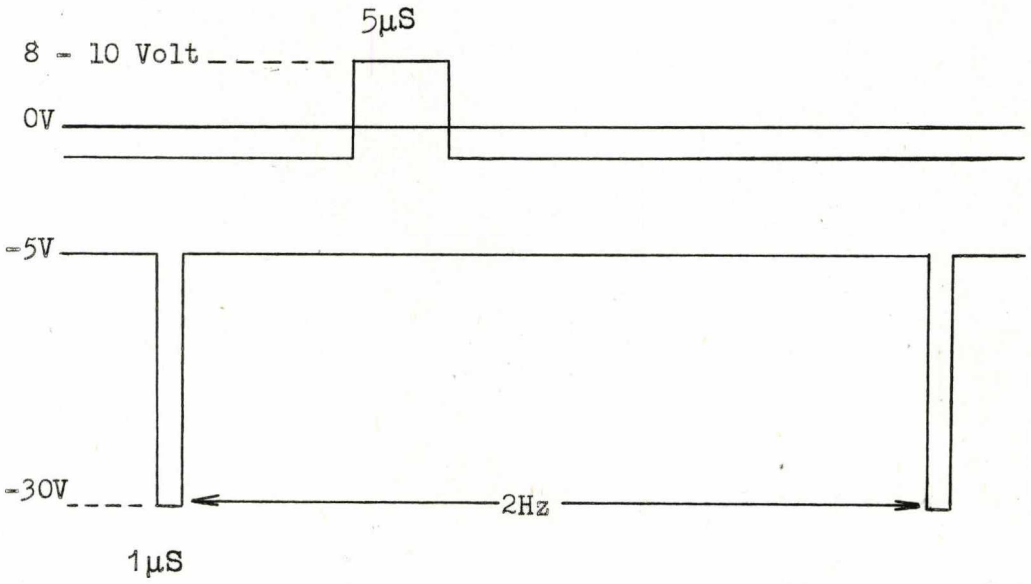

After a variable reaction time, the ions were ejected by a 8 or 10 volt pulse applied to the repeller, which was otherwise maintained slightly negative to prevent ion loss by disturbance of the space charge. Although Bourne and Danby succeeded in storing argon ions for several hundred microseconds, they did not study any systems in which ion-molecule reactions were likely. Studies of this kind were later reported by Herod and Harrison[22], who employed a 6 inch 90° sector magnetic instrument having a conventional ion source (e.g. Figure 2-2a) to which a similar pulse train to that shown in Figure 2-3 was applied. They examined the ion-molecule reactions occurring in methane, ethylene, acetylene and propylene using storage times of up to 2.5 mS, and estimated the ion kinetic energy to be in the range 0.3 to 0.5 eV With this technique the ion kinetic energy can be varied by altering the repeller potential[23]. In addition to these reports, Harrison *et al* have described the reactions occurring in several systems, in a series of papers entitled 'The Bimolecular Reactions of Trapped Positive Ions'[24].

2.212 Hollow Electron Beam Trap

The Hollow Electron Beam Trap was first proposed by Hasted, for use in Sequential Mass Spectrometry[11]. The essential features of this instrument are shown in Figure 2-4.

Ions are confined by the space charge of a hollow beam, produced by a toroidal cathode, C_T, of the type developed by Hartnagel[25] in his studies on microwave radio valves and the production of noise in such valves by ions. The indirectly heated cathode is operated under space charge limited conditions, and is maintained at a voltage V_T, with respect to the earthed collision chamber. The beam enters and leaves the collision chamber *via* grids - shown dotted - and is collected on the anode, A. Hartnagel and Herkmann[26] have recently shown that the beam becomes more cylindrical as the trap fills with ions and the

Figure 2-4. Hollow Electron Beam Trap

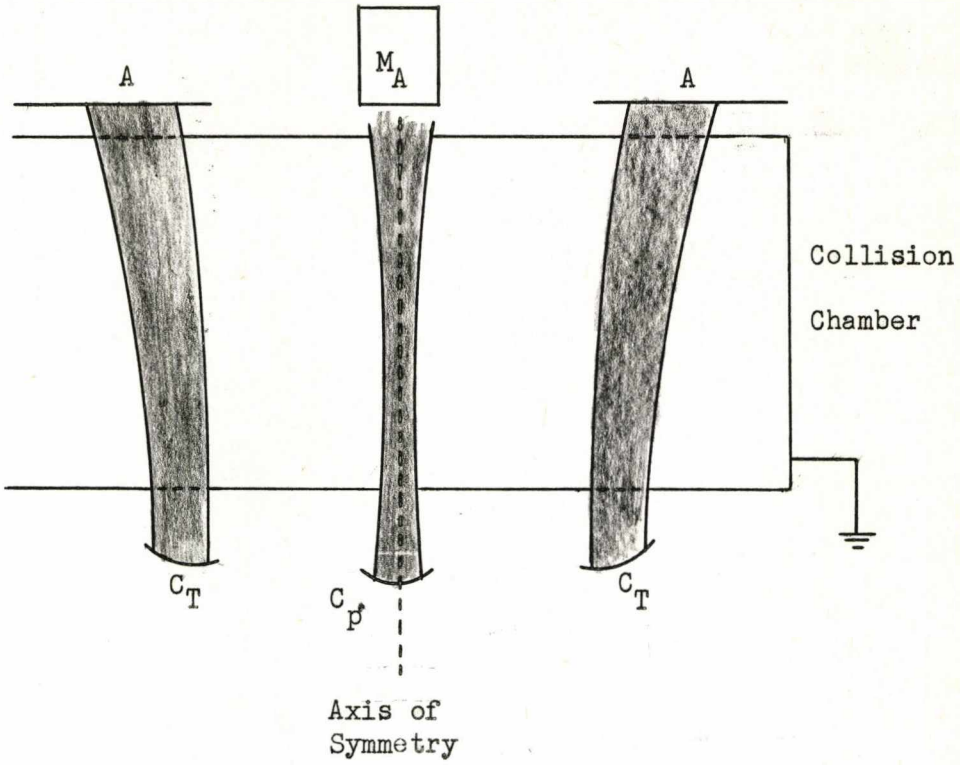

space charge is neutralized. Analysis indicates that the space charge, and consequently the ion density, is greatest on the axis of the hollow beam. A second 'pencil' electron beam may be introduced along the axis, thereby causing further ionization of the trapped ions which then drift out of the collision region and enter the mass analyzer, M_A. Hartnagel Hartnagel[25,26,27] has reported on the electron optical aspects and design considerations of hollow electron beams, and Hasted and Awad[28] have reported results on Sequential Mass Spectrometry using these devices. Typical storage times are of the order of one second at a pressure of 10^{-7} Torr[29].

2.213 Charged Particle Electron Beam Traps

For completeness it must be noted that several workers, notably Schulz[30], have described a space charge trap employed in the study of molecular energy levels. Basically, the apparatus is as shown in Figure 2-5. Two grids, A and B maintain a small potential depression

Figure 2-5. Slow Electron Trap Described by Schulz

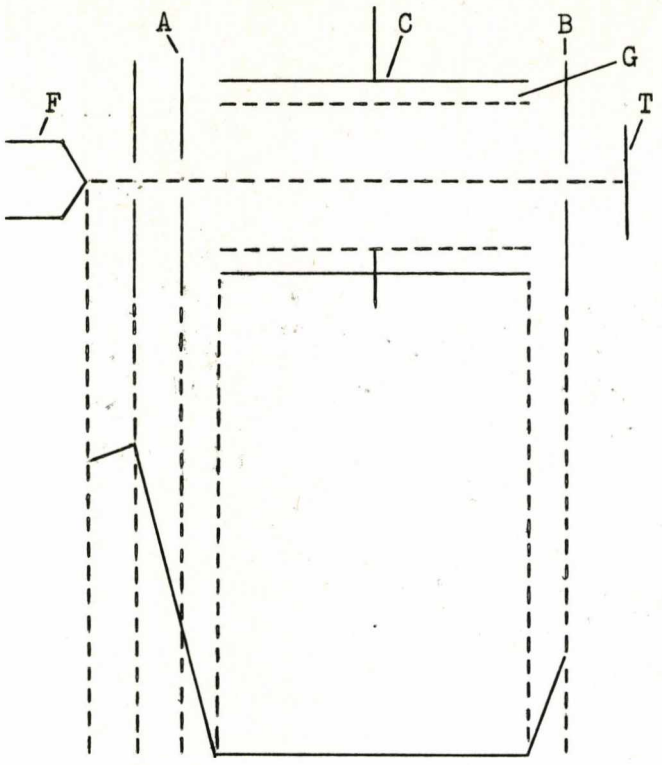

with respect to the cylindrical mesh cage, G. Fast electrons from the filament, F, pass through the cage and are collected by the trap, T. As the incident electron beam energy approaches an energy level of the neutral species in G, slow electrons are produced which, being unable to escape parallel to the beam, drift through the cage, and are collected at the cylindrical collector, C. Thus the energy of the molecular levels is indicated by the appearance of slow electrons.

2.22 Radio-frequency, Electric Field Traps

Although the most widely reported trap in this group is the three-dimensional quadrupole, several authors have described traps employing radio-frequency electric fields, which are not strictly quadrupolar. Essentially, the operation of these devices depends on the ion, or other charged particle, always experiencing a force directed towards the centre of the trap, so that it is contained within a definite volume. In true quadrupole traps the forces, produced by a radio-frequency field, act in three dimensions, whereas many of the other traps use radio-frequency

confinement in two directions, and a static electric or magnetic field, to overcome gravity, in the third direction. The advantage of the quadrupole trap is that it may be operated so that either ions of particular m/e values, or a range of values can be stored. The use of non-quadrupolar radio-frequency traps has been largely concerned with charged particle, rather than ion, storage. Consequently, this section will be mainly concerned with quadrupole traps, and has been divided into three parts :

1) The Three electrode Quadrupole Trap.

2) The Race-back Quadrupole Trap.

3) The Six-electrode Quadrupole Trap.

Again, the Six-electrode Quadrupole Trap has only been reported as a charged particle trap, and will only be briefly examined. Studies on, and experiments with Three-electrode Quadrupole Traps form the rest of this thesis, and further details on the theory and operation of such traps may be found elsewhere. (See Chapters 3, 4, 5 and 6).

2.221 Quadrupole Traps

A general quadrupole field can be expressed by :

$$\Phi = \Phi_o \frac{(\alpha_x x^2 + \alpha_y y^2 + \alpha_z z^2)}{r_o^2} \qquad (2\text{-}1)$$

where Φ_o is of the form $(U - V \cos \Omega t)$, U being a steady DC voltage, and V the amplitude of an alternating RF voltage of radial frequency, Ω . r_o is a constant having the dimensions of length, and the α_x, α_y, α_z are constrained to certain values by Laplace's equation :

$$\nabla^2 \Phi = 0$$

which gives :

$$\alpha_x + \alpha_y + \alpha_z = 0 \qquad (2\text{-}2)$$

For the case of the quadrupole mass filter, which utilises a two-dimensional field, a_z is zero and a_x and a_y are of equal magnitude but opposite sign. In the three-dimensional case, a family of solutions exist, the simplest being :

$$a_x = a_y \; ; \; a_z = -2a_x \qquad (2\text{-}3)$$

and

$$a_y = 2a_x \; ; \; a_z = -3a_x \qquad (2\text{-}4)$$

which correspond to the three-electrode and six-electrode quadrupole traps, respectively. It can be shown, see Chapter 3, that for certain values of U, V, Ω and r_o ions of specific m/e values will be stored, all others being lost on the electrodes, this is known as the 'mass spectrometric' mode of operation. Alternatively, if U is made equal to zero, a range of m/e values can be stored; this is the 'ion gauge' or 'total pressure mode'.

2.221(i) Three-electrode Quadrupole Traps

Substitution of equation (2-3) in (2-1) yields the equation for a three-electrode quadrupole field :

$$\Phi = \Phi_o\left(\frac{x^2 + y^2 - 2z^2}{r_o^2}\right)$$

which can be conveniently expressed in circularly cylindrical co-ordinates, with x and y equivalent :

$$\Phi = \Phi_o\left(\frac{r^2 - 2z^2}{r_o^2}\right)$$

This field is produced by a suitable choice of electrode geometry, rather than voltages, which then need only have opposite signs. The electrode geometry is shown in cross-section in Figure 2-6.

The electrode faces are complementary hyperbolae with the relationship :

$$r_o^2 = 2z_o^2$$

where r_o and z_o are the distances to the points of closest approach of

the electrodes to the origin, as shown in the figure. The electrodes in the z-direction are commonly known as the 'end-caps', while that in the r-direction is called the 'ring'. This device, first described by Paul and colleagues[31,32], is a development of the quadrupole mass filter reported by Paul and Steinwedel[33].

In early devices of this type, the presence of ions was detected by resonant absorbtion from a constant power RF generator, in a manner similar to that used in NMR studies. An alternative method of detection was described by Dawson and Whetten[34,35] in which ions are ejected from the device by application of a suitable voltage pulse to one of the end caps, and are collected on a Faraday Cup or Electron Multiplier. To ease the application of voltage pulses to the end-caps, Dawson and Whetten also showed that the alternating RF voltage need only be applied to the ring electrode, and that the DC voltage, U, could be applied to the end-caps. Dawson, Hedman and Whetten[36] have also shown

Figure 2-6. Cross-section of Three-electrode Quadrupole Trap

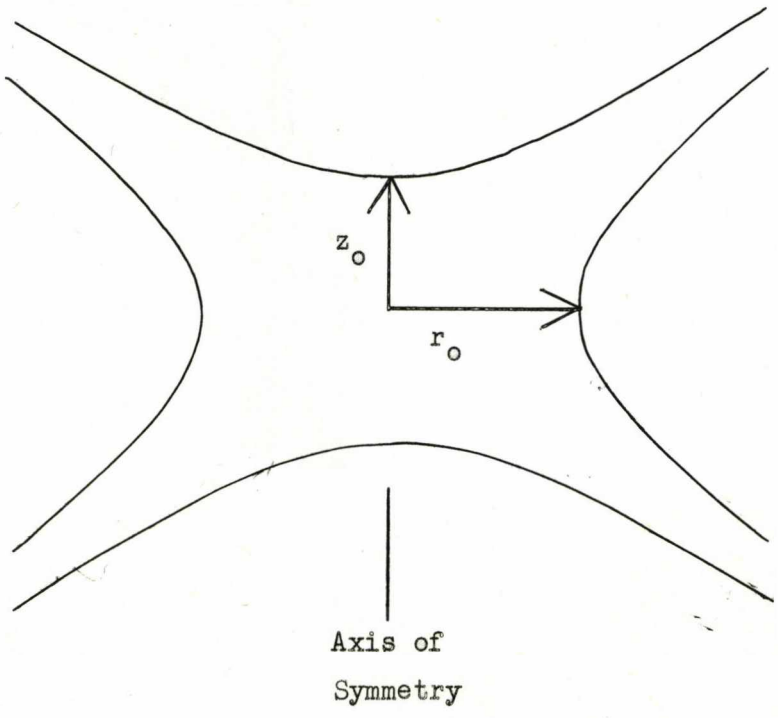

that accurately shaped hyperbolic electrodes, although possibly being advantageous, are not vital. They have described the operation of a device constructed from stainless steel mesh. A similar device made from copper mesh has been constructed by Lawson[37,38]. Rettinghaus[39] has reported on the use of such a device as a partial pressure gauge, employing electrodes fabricated from spherical sections to approximate hyperbolae. Using this he was able to detect a minimum partial pressure of 10^{-10} torr, corresponding to approximately four ions contained in the trap. The disadvantage of employing non-ideal electrodes is that, as shown by Dawson and Whetten[40], abnormal resonances can occur, resulting in peak splitting and other undesirable effects, although these are more obvious in the mass spectrometric, rather than ion gauge, mode.

Three-dimensional quadrupoles have received considerably less attention than the mass filter, and most workers have described their usage as mass spectrometers, with comparatively few exploiting their storage capabilities. Among the mass spectrometric users of these devices are Dawson and Whetten[34,35], Harden and Wagner[41,42], Sheretov *et al*[43,44,45] and Mastoris[46]. Since the mass resolution in quadrupole devices is dependent on the number of cycles of the RF voltage that an ion experiences[47,48], the three-dimensional quadrupole should show greater resolution than the mass filter, increasing with storage time. This is not apparent from the literature, however.

The applications relying more on the storage property of these traps can be broadly divided into two classes - physical and chemical. Reports on the physics of stored ions have been given by Dehmelt[49,50], whose colleagues have also demonstrated radiative cooling in quadrupole traps[51]. Dehmelt[52] has also studied the magnetic resonance and RF spectra of spin-polarized ions, produced by spin-exchange collisions. For example, helium ions were stored and bombarded with polarized

caesium atoms, causing production of trapped, polarized helium atoms by the reactions :

$$Cs\uparrow + He^{+}\uparrow \longrightarrow Cs\uparrow + He^{+}\uparrow$$

$$Cs\uparrow + He^{+}\downarrow \longrightarrow Cs\downarrow + He^{+}\uparrow$$

The hyperfine structure of the helium ions was then determined. Dehmelt[49], has also proposed a method of calculating the kinetic energies of ions in quadrupole traps. Briefly, this method considers an ion as moving a known distance at a known frequency, under conditions of simple harmonic motion, thus allowing calculation of the velocity and energy (see Chapter 3 for a detailed account).

The chemical applications of quadrupole ion traps have been demonstrated by Todd and colleagues[37,38,53,54]. In their system, ions are created inside a quadrupole ion store (QUISTOR), allowed to react for a variable time and then injected into a conventional mass filter for analysis. This allows examination of reactions as a function of storage time, rather than pressure as is more usual. A variety of chemical phenomena have been observed, including low-pressure ion-molecule reactions and chemical ionization, charge transfer reactions and spectrum simplification (see Chapter 6). Observation of this latter phenomenon, which is akin to chemical ionization, has also been indicated by Harden and Wagner[41].

The three-electrode quadrupole trap, and variants, has also been used to store other charged particles. Wuerker, Shelton and Langmuir[55] have confined charged particles of iron and aluminium, and also electrons, in a true three-electrode trap. Whetten[56], has recently reported similar experiments using a three-electrode trap constructed from stainless steel mesh, operated at atmospheric pressure with an applied voltage of 1500V at 60Hz. Both these groups have used photographic methods to observe the motions of the large charged particles. Karras and Lindman[57]

have determined the cyclotron resonance frequency of trapped electrons, and the simulation of micrometeorites by the acceleration of stored micron sized diamond particles has been described by Vedder[58].

Several workers have described devices in which the ring and end-cap electrodes are approximated by a cylinder and two flat plates, respectively, in particular Langmuir, Langmuir, Shelton and Wuerker[59] and Byrne and Farago[60], who also employed a magnetic field in the z-direction. This apparatus was used to store electrons, which were then spin-polarized by spin-exchange collisions with an atomic beam. Devices of this kind have recently been subjected to a numerical analysis by Benilan and Audon[61]. Instruments of several geometries have been reported by Staubel[62], and Berg and Gaulker[63,64] for suspending large (up to 200 μgm.) particles and droplets. In all these cases, a RF voltage is applied to a cylindrical or annular 'ring' electrode, and a DC voltage is applied between two 'end-caps' in order to overcome gravitational forces. The use of direct optical or photographic methods of observation is usual.

2.221(ii) Race-track Quadrupole Trap

Dehmelt and colleagues[52] observed that the linewidths obtained in their hyperfine splitting studies were dependent on the ion temperature, which could be reduced by radiative cooling. Using a Penning Trap they discovered that the degree of cooling was limited by the storage time[65], and in an attempt to increase this they employed quadrupole traps. These were operated in ultra-high vacua to reduce ion loss by scattering; radiative cooling in such traps was demonstrated by Church[66], who obtained storage times of up to six minutes at 5×10^{-11} Torr. A previous attempt to demonstrate radiative cooling in a 'storage ring trap' had proved unsuccesful, but further details of this trap have been given by Church[66]. This device was constructed by bending the rods of a linear mass filter so that they became continuous. The difficulty

of obtaining accurate curvatures was later overcome by using machined circular electrodes. The device was normally operated with one pair of rods earthed; ions were created inside by electron bombardment and detected by resonant adsorption. At pressures below 10^{-9} Torr storage times measureable in minutes were observed.

2.221(iii) Six-electrode Quadrupole Traps

The field used in this instrument is obtained by substitution of equation (2-4), section 2.221, into (2-1) :

$$\Phi = \Phi_o \left(\frac{x^2 + 2y^2 - 3z^2}{r_o^2} \right) \qquad (2\text{-}6)$$

It is produced by a structure having cubic geometry, as shown in Figure 2-7.

Figure 2-7 Reported Six-electrode Quadrupole Trap Geometries

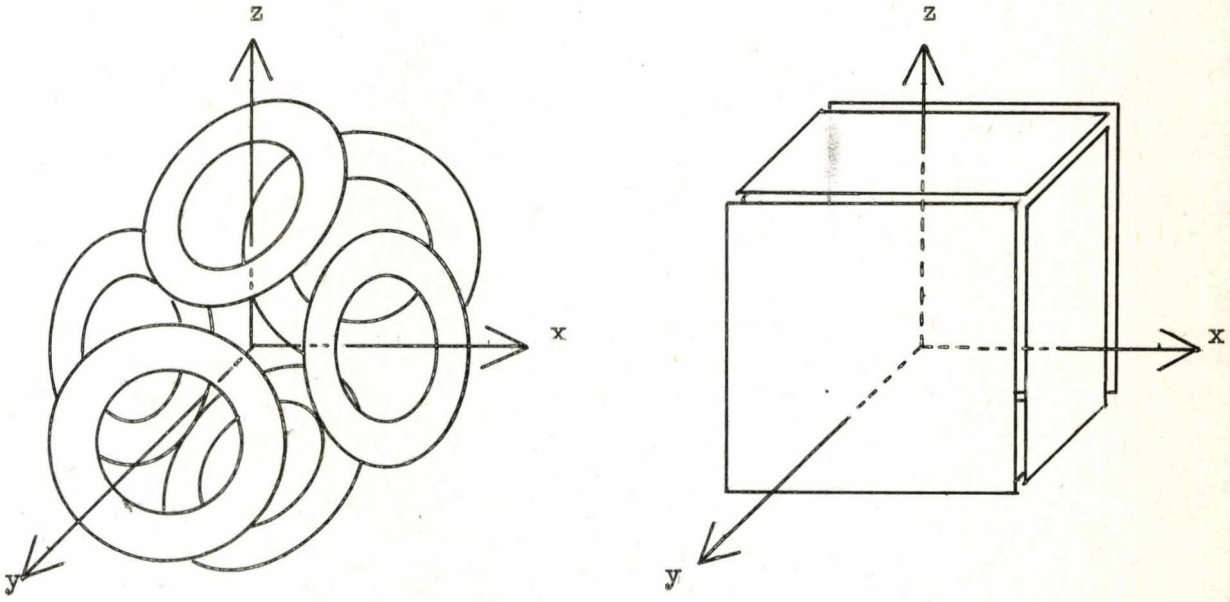

2-7 (a) 2-7 (b)

Ideally, the electrodes should be hyperbolic, but such a device has not been reported. In this case, the choice of geometry is not sufficient to produce the required field, and the DC components of Φ_0 applied to each pair of opposite electrodes must differ; a three-phase RF generator is also required.

The various accounts of this device in the literature have mainly been concerned with massive charged particle storage[59,67,68], although there have been some reports on more physical applications. In the work described by Waniek and Jarmuz[69], and Haught and Polk[70], six-electrode structures were used to store charged particles, which were then subjected to laser beams. In the former case, the workers were examining the acceleration of such particles by vapour emission, and they used optical methods of detection (Figure 2-8).

Figure 2-8. Optical Detection of Massive Charged Particles

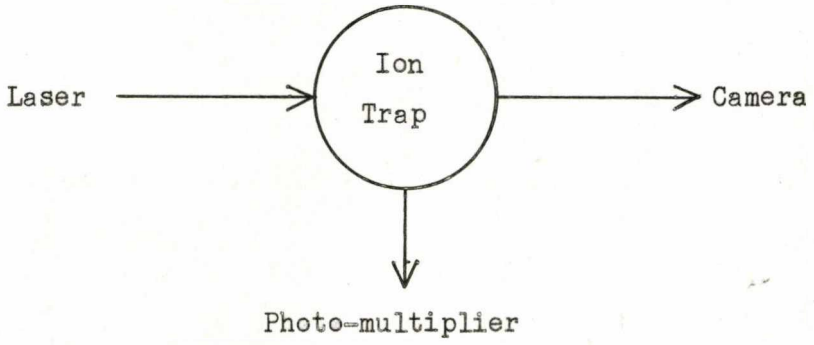

Permanent records were obtained from a camera containing high speed (10000 ASA) film, located in the path of the laser beam, while scattered radiation was observed by a photomultiplier placed at 90° to the beam. A similar system was used by Haught and Polk for investigating the confinement properties of magnetic fields, using hot, fully ionized plasmas produced by subjecting suspended particles to the pulses of a 20 MW laser. In both of these laser studies the amplitude of the RF voltage was chosen so that the suspended particle remained at all times in the focus spot of the laser; they also used

annular electrodes, Figure 2-7(a), as did Zaritskii[68]. The other reported six-electrode devices have employed square, planar electrodes as shown in Figure 2-7(b).

2.23 Other Types of Ion Trap

This section deals particularly with the recent development of Trapped Ion Cyclotron resonance, but first Drift Tubes and Ion Cyclotron Resonance (ICR) are considered. The reason for this is not only to introduce trapped ICR, but to provide a comparison with true ion traps, as defined in Section 2.1 References to detailed texts on these topics are included.

2.231 Drift Tubes

The essential feature of a drift tube is an enclosed region containing a set of field electrodes, as shown in Figure 2-9.

Figure 2-9. Drift Tube Electrode Arrangement

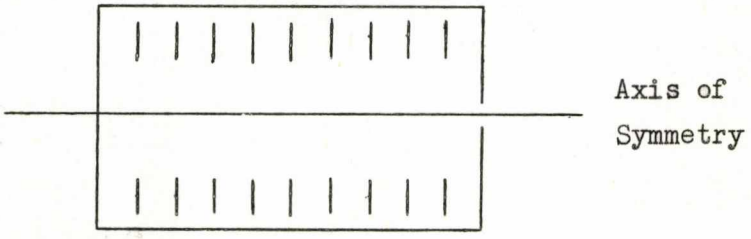

The field electrodes are accurately aligned grids or annuli to which suitable DC voltages are applied, forming a uniform potential gradient in the direction of the axis of the tube. The enclosed region permits neutral molecules to be contained inside the field. Ions may be either created inside the tube, or may enter along the axis and are detected on leaving. During their passage through the tube, ions gain energy from the field and lose it by collisions with neutrals; since the ionic and molecular masses are generally comparable, equilibrium is quickly reached, and the ions settle down to a steady drift, with a velocity v_d. Clearly the mean ion energy is some function of the electric field, E, and the pressure of neutrals, p;

more particularly, it can be shown to depend on the parameter E/p. Originally, drift tubes were used to determine ionic mobilities by observing the variation of drift velocity with field strength; more recently they have been widely used in the study of ion-neutral reactions. This work has been led by McDaniel[3,4,71] and colleagues, who have examined reaction rate variations with both ion energy (field strength) and pressure. Studies using drift tubes are unavoidably linked to certain physical properties, such as mobility and diffusion coefficients. Although ions possess a steady drift velocity, space charge causes a tendency to both radial and axial diffusion. McDaniel[71] has shown that careful analysis of the peak shape, resulting from the passage of a pulse of ions, can lead to information on these quantities.

The complexity of the apparatus, in addition to the drift tube itself, depends on the particular application. For mobility studies a simple ion-source and detector are required, although gating systems are often included to permit accurate velocity determination. The study of ion-neutral reactions necessitates the use of a product ion analyzer, conveniently a mass spectrometer. A typical instrument, after McDaniel[71], is shown in Figure 2-10. The apparatus is differentially pumped to maintain the analyzer under high vacuum while permitting the use of a higher pressure in the drift tube. Ions are created by an axial ion source, and on emerging, the central 'core' is removed for mass analysis by a skimmer. Quadrupole mass filters are frequently used as the analyzer since they are relatively insensitive to changes in ion energy, and do not require large accelerating voltages. McDaniel[71] has also discussed the advantages of employing a moveable ion source; with this modification 'end-effects', occuring in both the source and analyzer, can be eliminated, and the calculation of diffusion coefficients is eased.

Figure 2-10. Drift Tube, Gas After McDaniel[71].

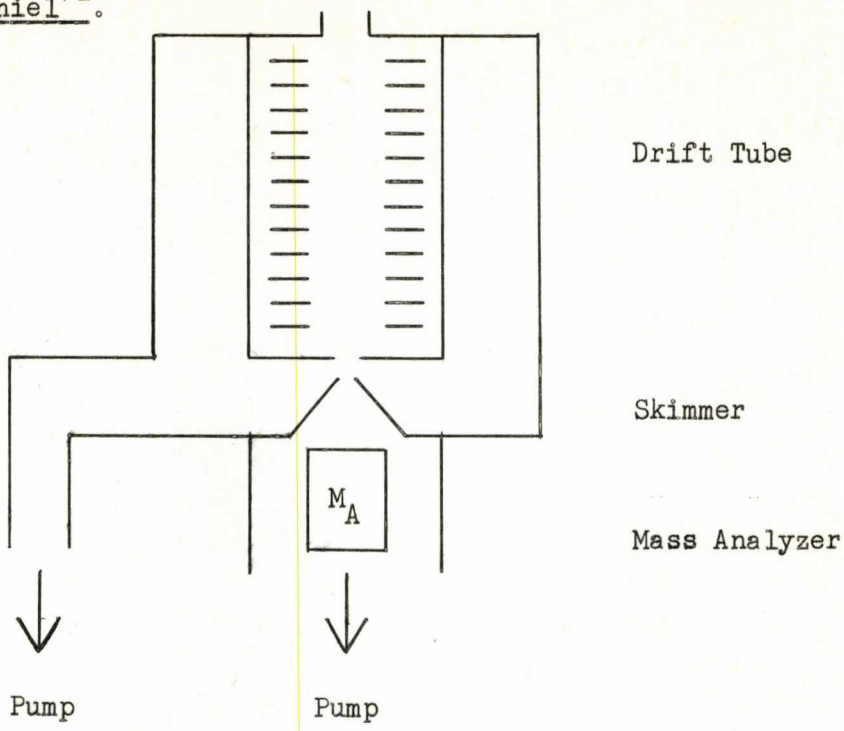

2.232 Ion Cyclotron Resonance Mass Spectrometry (ICR)

From the point of ion storage, the recent development of trapped ICR is undoubtedly the most interesting, but before discussing this technique in detail, conventional ICR will be briefly examined. Although ICR bears a passing resemblance to a Drift Tube in that the ions pass slowly through, the major difference is the method of ion detection, ICR being a complete mass spectrometer. The various advantages of ICR and the many variations on the basic technique have been reviewed in detail by several authors[72,73,74], and their work will not be repeated here.

ICR is a direct development of the 'Omegatron', described by Sommer, Hipple and Thomas[75,76,77], which is shown in Figure 2-11. This device, which was constructed for the precise determination of atomic constants, was capable of resolving the $H_2^+ - D^+$ doublet, indicating a mass resolution of approximately 35,000. It consists of a set of 'picture-frame' electrodes, P, assembled between two plates E, and connected to a RF generator, R. The homogenity of the RF field produced is maximized

by the guard rings, G, which are slightly positive to trap the ions within the cell. The device is placed in a magnetic field, B, which is shown running from left to right in Figure 2-11(a), and also assists collimation of the electron beam produced by conventional electron optics.

Ions are created inside the device and describe circular trajectories, in a plane perpendicular to the magnetic field, at the cyclotron frequency, ω_c, given by :

$$\omega_c = \frac{eB}{m}$$

If the cyclotron frequency of a particular ion is equal to the radial frequency of the RF generator, that ion will absorb power from the field and describe a spiral path, as shown in Figure 2-11(b), eventually being

Figure 2-11. Schematic Representation of Omegatron Mass Spectrometer

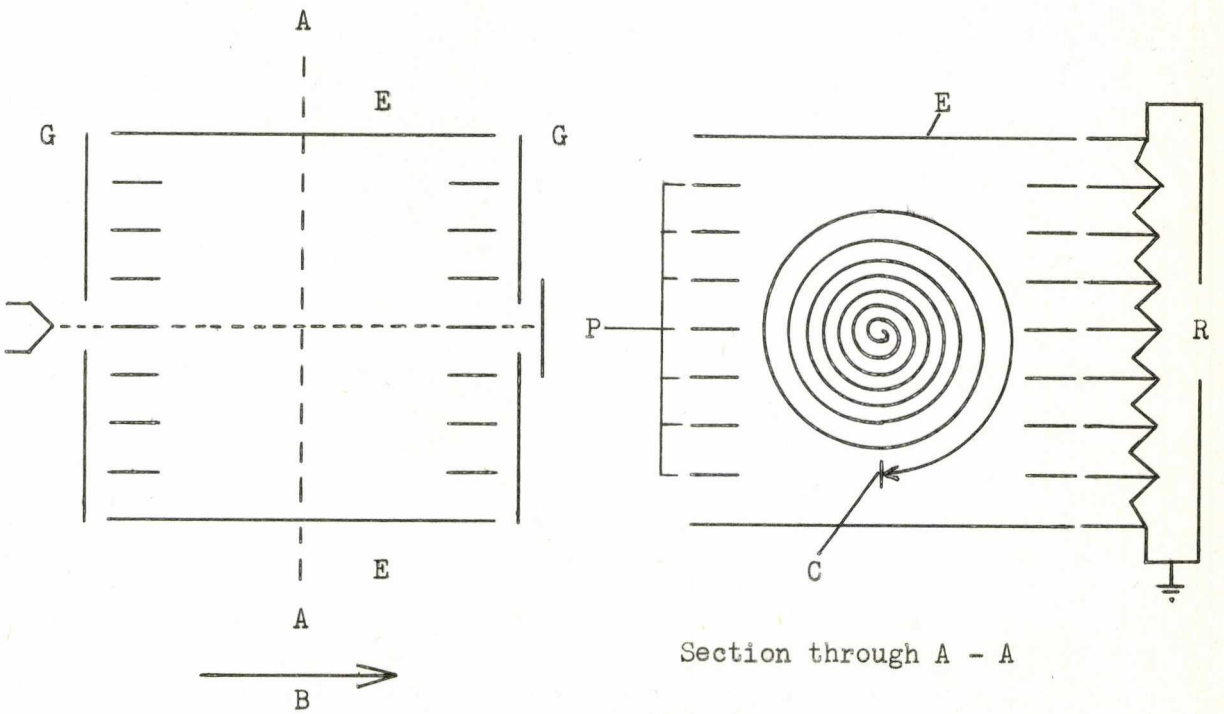

2-11(a) 2-11(b)

detected by the collector, C. A given mass range may be scanned by sweeping either the magnetic field or the RF frequency. The motion of ions in these fields has been examined in greater detail by Blauth[78].

Commercially, the omegatron has been mainly used as a small partial pressure gauge, having a mass range of approximately 0 - 50 amu. The main disadvantage of this instrument is that the trajectories of resonant ions are affected by space-charge repulsion, especially caused by non-resonant ions. This was overcome in a device designed by Llewelyn (Varian Associates) and Baldeschwieler (Stanford University), and marketed by Varian Associates under the trade name 'Syrotron'. A typical instrument, more commonly known as an ICR cell, is shown in Figure 2-12. It has separate source and analyzer regions, thereby lessening the effects of space charge.

Figure 2-12. Diagram of ICR Cell

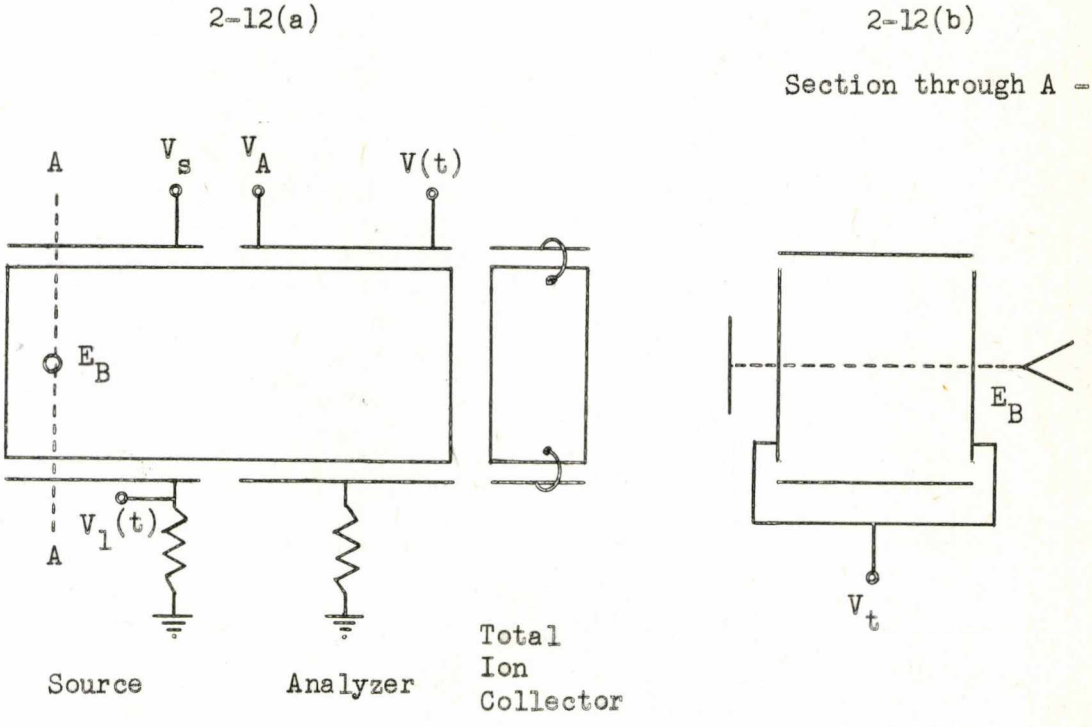

A small, positive voltage, V_T, is applied as shown in Figure 2-12(b), to prevent ion loss by collision with the walls. The electron beam and magnetic field run into the plane of the page in Figure 2-12(a).

Migration of the ions from source to analyzer is controlled by the source drift voltage, V_S; drift through the analyzer region is governed by the analyzer drift voltage, V_A. The four plates comprising the total ion collector are connected together, and to a small negative voltage; ions entering this region quickly strike one of these plates producing a signal, which can be amplified in the usual way. There are two possible methods of detection :

(i) The power loss in a constant power observing oscillator, V(t), caused by resonant ions, can be detected.

(ii) The observing oscillator can be used to completely remove a specific ionic species from the analyzer, and the corresponding drop in total ion current recorded.

The efficiency of ion detection is not affected by the ion kinetic energy, since this only alters the radius of the trajectory and not the cyclotron frequency. The instrument is scanned by varying either the magnetic field or observing oscillator frequency, as in the omegatron. Usually, a phase sensitive detector is employed, and referenced to modulation of either the electron energy, the electron beam or the magnetic field. Since power adsorption by an ion causes it to accelerate, specific ions may be accelerated to a desired energy by application of a field at their cyclotron frequency, by an irradiating oscillator, $V_1(t)$.

In general, ion-molecule reactions may be complex, one ion being the precursor of several others, for example :

$$A^+ + B \xrightarrow{k_1} C^+ + D$$

$$A^+ + B \xrightarrow{k_1} E^+ + F$$

$$X^+ + Y \xrightarrow{k_3} C^+ + G$$

where k_1, k_2 and k_3 are the relevant rate constants. Conventionally, k_1 would be determined by measuring the increase of C^+, or the decrease of A^+, as a function of the collision number. This is obviously confusing here, however, since A^+ also produces E^+, and C^+ is produced from X^+. In order to obtain data in cases like this, and to ascertain which product ions result from a particular reagent ion, several workers have proposed modifications to the basic technique of ICR, notably Ion Cyclotron Double Resonance (ICDR) and Source Ejection.

2.232(i) Ion Cyclotron Double Resonance

Ion Cyclotron Double Resonance was introduced to investigate reaction pathways by Anders, Beauchamp, Dunbar and Baldeschwieler[79], who reasoned as follows. If a product ion, C^+, is in fact produced from a reagent ion, A^+, then there will be some 'chemical coupling', via charge or heavy particle transfer, between A^+ and C^+. A^+ will normally be in thermal equilibrium with the background molecules, assuming the energy gained between collisions is equal to that lost in collisions, and this will vary with the translational energy of A^+, and hence the power it absorbs. Consequently, the shape of the C^+ peak, which is dependent on the number of collisions per second, should alter as the translational energy of A^+ is varied. Also, since the rate of formation of C^+ is probably dependent on the translational energy of A^+, the yield of C^+ should change as this is varied. To examine these ideas, they devised ICDR, in which another oscillator $V_2(t)$ is connected to the source region, and tuned to the cyclotron frequency of A^+, ω_A. The observing oscillator, V(t), is tuned to the cyclotron frequency of C^+, ω_c. Any changes in the peak shape or intensity of C^+ are observed as A^+ ions are excited. Originally, $V_2(t)$ was switched on and off, the output from V(t) being referenced to this 'chopping' frequency, allowing direct comparison of the effects of 'normal' and 'excited' A^+ ions.

This technique has received considerable attention, notably from Clow and Futrell[80], although several authors have pointed to the fact that care must be taken in interpretting ICDR data, since the results are often ambiguous (see reference 81 for example).

2.232(ii) Source Ejection

A method for the removal of specific ionic species from the source region, to ease the study of systems such as (7), has been proposed by Beauchamp and Armstrong.[82] The use of a small positive trapping voltage, V_T, connected to the source side plates, causes the ions to execute simple harmonic motion with a radial frequency, ω_T, given by :

$$\omega_T = \left(\frac{4eV_T}{md^2}\right)^{\frac{1}{2}}$$

where d is the separation of the side plates. If a RF generater is connected to the trapping plates, then specific ions will absorb power from this, quickly strike the side plates and be lost. This is achieved as shown in Figure 2-13.

Figure 2-13. Connection of an RF Generator to Source Trapping Plates, for Source Ejection

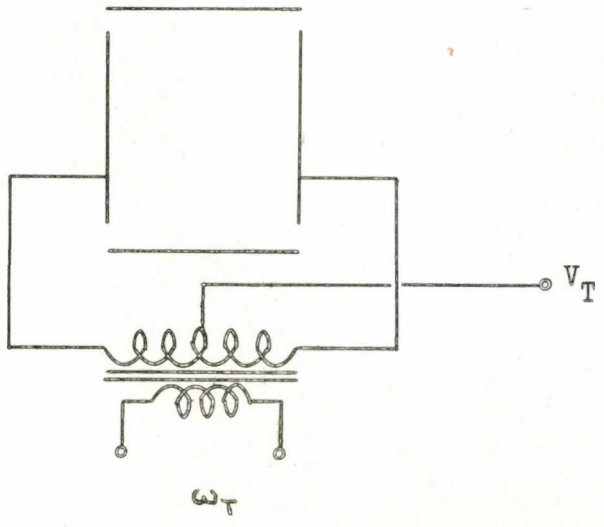

The side plates are connected to the secondary of a transformer, having a centre-tap connected to a supply, V_T, the primary of which is excited at a frequency ω_T. Again this RF is usually chopped, allowing the effect of ion ejection to be directly compared to normal operation.

Care must be taken to ensure complete ion ejection of the desired ions. This has been highlighted in recent studies on ammonia, using this method, by Marx and Mauclaire[83], and Huntress[84]. The reactions in ammonia :

$$NH_3^+ + NH_3 \xrightarrow{k_8} NH_4^+ + NH_2 \qquad (2\text{-}8)$$

$$NH_2^+ + NH_3 \xrightarrow{k_9} NH_4^+ + NH \qquad (2\text{-}9)$$

$$NH_2^+ + NH_3 \xrightarrow{k_{10}} NH_3^+ + NH_2 \qquad (2\text{-}10)$$

are confused because of the proton transfer reactions producing NH_4^+ (2-8) and (2-9), and the additional production of NH_3^+ (2-10). Complete ion ejection of NH_2^+ allows examination of k_8, while ejection of NH_3^+ allows the determination of k_9 and k_{10}.

2.233 Trapped Ion Cyclotron Resonance

This technique, also known as Pulsed Ion Cyclotron Double Resonance, was described by McIver[85,86]. The original apparatus was similar to a conventional ICR cell, but was totally enclosed as shown in figure 2-14. The important feature of this device is that it allows an increase in ion storage time from 1 - 5 mS (conventional ICR) to 100 mS, while retaining the capability of ICDR for reaction pathway determination. The unit is placed in a magnetic field, which passes into the page in Figure 2-14(a), as does the electron beam, E_B. Unlike ICR, ions are not removed from the source region, but remain trapped by the small voltages shown. The operation is totally pulsed; ions are created by a burst (100 μS) of electrons, and since the electron beam is off most of the time, space charge effects are negligible. The reaction products are

observed, after a variable time, by an RF pulse applied to the lower plate. After analysis the trap is emptied by application of a small, positive quench pulse to the upper plate which forces all the ions to collide with the lower plate. As with ICDR, the reagent ions may be either thermal or kinetically excited by application of an RF pulse to the upper plate. A more detailed account of this apparatus has been given by McIver and Dunbar[87]; this report also describes a method for observing and exciting the same ion. This is usually difficult, since the observing and irradiating oscillators are tuned to the same frequency, and the stronger irradiating oscillator interferes with the weaker observing oscillator. Since in this technique they are both pulsed, McIver and Dunbar applied an out-of-phase irradiating pulse to the observing plate, the amplitude of which could be adjusted to negate the effect of the irradiating pulse on the observing oscillator.

Figure 2-14. Pulsed ICR Cell, after McIver[85]

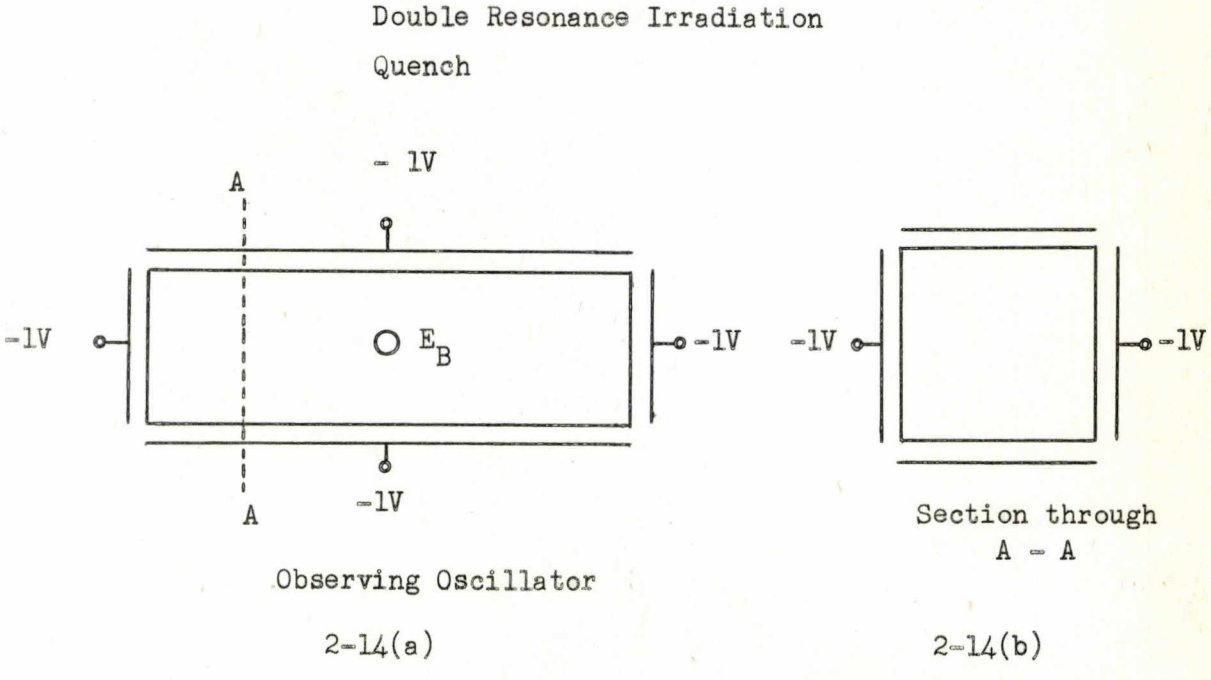

More recently, McIver[88] has described a solid-state observing oscillator, and has shown spectrum simplification in methanol (see Section 2.221(i) and Chapter 6). In a series of reports, McIver and colleagues[89] have also described studies on the gas-phase acidities and basicities of various compounds.

A simple modification to a standard ICR cell, allowing trapping in the 100 mS region, has been described by McMahon and Beauchamp[90]. The essential feature of this device is that the source is effectively closed by an additional plate, as shown in Figure 2-15.

Figure 2-15. Modification to a Standard ICR Cell to Allow Ion Trapping

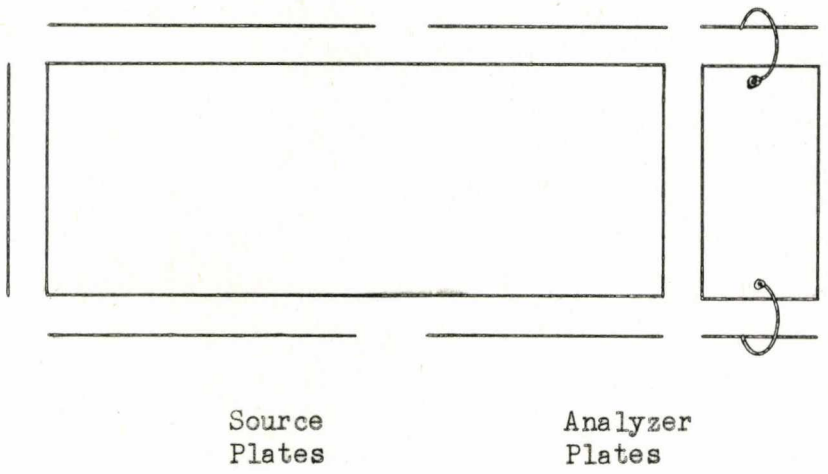

The voltages required to operate this device are shown schematically in Figure 2-16; from which it may be seen that the additional plate is connected to the lower source plate. In order to trap ions, created by a pulse of electrons typically 5 mS long, the source plates are earthed and the analyzer plates connected to a negative supply (Figure 2-16(a)). After a desired storage time, the conditions are altered to those of a

Figure 2-16. Modes of Operation of Modified ICR Cell

2-16(a) Ion Trapping Mode.

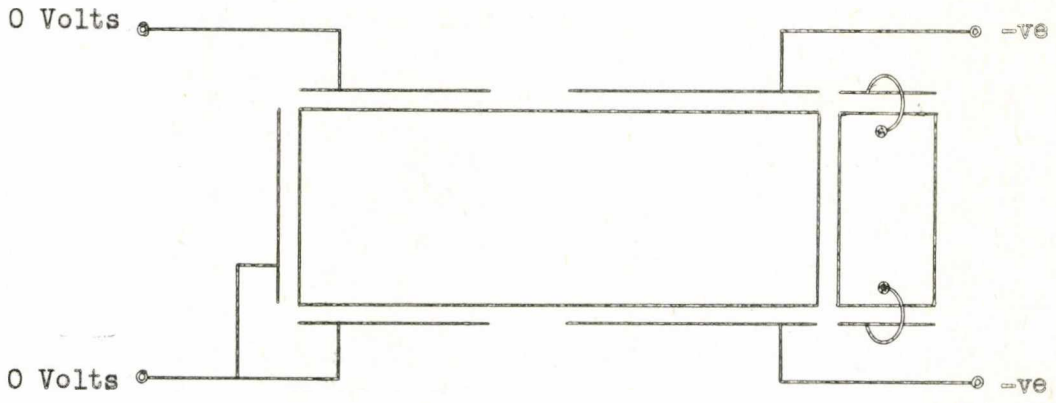

2-16(b) Ion Detection Mode.

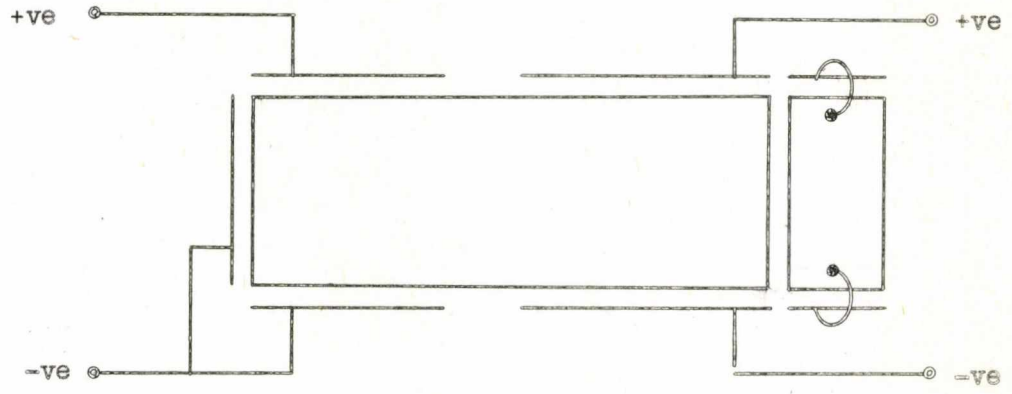

Key : -ve = Negative Voltage

+ve = Positive Voltage.

conventional ICR cell (Figure 2-16(b)) causing the ions to drift into the analyzer region for detection. The major advantage that this device has over McIver's design is that all the capabilities of a standard ICR cell are retained, particularly ICDR and Source Ejection. The use of such an instrument with source ejection has been described by Huntress and Pinnizzotto[91,92] to determine pathways and rate constants in the CH_4, H_2O, H_2S and NH_3 systems.

2.3 Discussion and Comparison of Ion Traps

The examination of ion-molecule reactions with reaction time is fast becoming a popular alternative to the more usual technique of varying the pressure. Although this method usually requires the construction of a special ion trap, it has the advantage that the pressure may be kept low, obviating the need for complex vacuum systems. Of the available ion trapping techniques, Pulsed ICR[85-92] seems most attractive, the reaction time may be very long - up to 100 m S - and the ICR capabilities for reaction pathway determination are fully retained. Results obtained in this manner, however, require careful consideration; ICDR is often ambiguous[81] and source ejection can only remove one ion selectively, resulting in a mass spectrum caused by the absence of that ion. The Three-dimensional Quadrupole Ion Trap would appear to present a viable alternative to the problem of pathway determination. Possibly such a trap could be operated as an ion source for a conventional mass filter, as in the method of Todd et al[53,54], but mass selectively, thereby operating as a Tandem Mass Spectrometer. Storage of one ionic species could be followed by relaxation of the operating conditions to allow trapping of the reaction products with subsequent ejection and analysis.

Comparison of the traps will be considered under three headings :

(i) Construction and Operating Requirements

(ii) Storage Capability

(iii) Applications.

The basic properties of each of the traps is summarised in Table 2-1.

2.31 Construction and Operating Requirements

Undoubtedly the simplest is the Space Charge Trap which requires a conventional mass analyzer and ion source, to which a pulse train is applied. The electron beam is usually collimated by a small magnetic field. Construction of an ICR cell is simple, but several electric, in addition to a magnetic, fields must be supplied. The minimum requirement is an observing RF field and two DC drift fields, while employment of ICDR or source ejection requires additional RF fields. Pulsed ICR necessitates pulsing the electron beam and the irradiating and observing RF supplies. The RF voltages required in ICR are, however, no greater than one volt; in comparison the Quadrupole Traps utilize extremely large voltages, frequently up to 1000 volts. Ideally the latter has hyperbolic electrodes, although these can be approximated using roughly shaped wire mesh[36,37]. Hollow Electron Beam Traps need to be carefully constructed, particularly the toroidal cathode. Details have been given by Hasted and Awad[28] and Hartnagel[25,26].

In addition, all these traps require vacuum systems capable of achieving background pressures of less than 10^{-5} torr.

2.32 Storage Capabilities

From Table 2-1 it is apparent that the longest reported storage time was obtained with a Three-dimensional Quadrupole Trap, with little loss of ions during storage. The figure of 5 sec. for Pulsed ICR was reported by Huntress and Pinnizzotto[91] and was accompanied by an approximately 50% ion loss. The use of such long storage times is, however, unusual; typically ion traps are operated with storage times in the region 1 10 mS. The available storage times are generally

Table 2-1.

	Construction	Fields Required	Max. Storage Time (Secs) at	Pressure (Torr)	Typical Storage Time	Uses	Refs.
Space Charge	Simple	M[b]	1	$\sim 10^{-7}$	10^{-3} - 10^{-2}	SMS IM	9-24
Hollow Electron Beam	Complex	-	1	$\sim 10^{-7}$	10^{-3} - 10^{-2}	SMS	25,28
Three-dimensional Quadrupole	Complex[a]	RF,DC[c]	10^{3}	3×10^{-10}	10^{-3} - 10^{-2}	IM MS P	31-46,49-56
Pulsed ICDR	Simple	RF,[d]DC,M	5	10^{-6}	10^{-3} - 10^{-1}	IM	85-92

Key : M = magnetic

RF = radio-frequency electric

DC = steady electric

SMS = sequential mass spectrometry

IM = Ion-molecule reactions

P = physical

MS = mass spectrometric

Notes : (a) simplified by use of mesh.

(b) magnetic field used for beam collimation only.

(c) DC required for mass spectrometric operation.

(d) Two RF fields needed, both pulsed.

limited by scattering of ions by neutral molecules and other ions. The effect of the former is reduced by operating at low pressure, while the latter is a slow process, since pulsed operation creates few ions. Some space-charge repulsion is desirable in the case of the Hollow Electron Beam Trap, since ions are removed by this means. Whetten[56], using a Three-dimensional Quadrupole Trap at atmospheric pressure, has observed that under these conditions the storage may be enhanced, presumably as a result of damping of the ion motion caused by collisions with a large number of molecules.

In Pulsed ICDR trapped ions may be excited to a known kinetic energy (up to 10 ev) with reasonable accuracy. This is not possible in the other traps, and only average values can be calculated.

2.33 Applications of Ion Trapping Techniques

Generally the major application of ion traps has been to the study of ion-particle reactions, although the Three-dimensional Quadrupole Trap has also been employed as a mass spectrometer and a massive charged particle trap.

Hollow Electron Beam Traps have only been employed in Sequential Mass Spectrometry, while the Space Charge Trap has also been used in the investigation of ion-molecule reactions, although it has received little attention, considering its simplicity, all reports coming from Harrison et al.[22,23,24] Similarly the use of a Three-dimensional Quadrupole Trap as a reaction chamber has only been reported by Todd and colleagues.[38,53,54] Although the most recently reported development in the field of ion-storage, Pulsed ICR promises to be widely adopted and is already employed by McIver[85-89], Beauchamp[90] and Huntress and Pinnizzotto.[91,92]

CHAPTER 3

Theory of Quadrupole Devices, and a Numerical Examination of the QUISTOR

3.1 Introduction

The theory of ionic motion in quadrupole fields is developed and shown to reduce to a form of Mathieu's equation, solutions of which are obtained in an outline discussion. In view of the proposed QUISTOR investigation of ionic collision processes, which are often strongly dependent on the ion kinetic energy, some estimation of the latter quantity is of interest. The expressions of Dehmelt[49] are discussed, and examined for validity at moderate values of q. An alternative method of calculating the mean ion energy is proposed, and details of its use given. The method is based on a general solution to Mathieu's equation, and is further described in Chapters 5 and 6.

3.2 Ion Motion in Quadrupole Fields

A quadrupole field may, in general, be expressed by the relationship :

$$\Phi = \frac{\Phi_o}{r_o^2} \left(a_x x^2 + a_y y^2 + a_z z^2\right) \qquad (3\text{-}1)$$

where r_o is a constant having the dimensions of length, and is dependent on the geometry of the device, and a_x, a_y, a_z are defined by fulfillment of Laplace's equation :

$$\nabla^2 \Phi = 0$$

where ∇ is the Laplacian Operator, $\partial/\partial x + \partial/\partial y + \partial/\partial z$.

Consequently, a_x, a_y and a_z are constrained by :

$$a_x + a_y + a_z = 0 \qquad (3\text{-}2)$$

The choice of these constants is dependent on the geometry required, and this is described in Section 3.5. Since there are no cross products in equation (3-1) each direction is independent of the

others, and a one-dimensional model is adequate, although all dimensions must be considered in a practical device.

Φ_o is composed of a steady (DC) voltage and an alternating radio-frequency (RF) voltage, and has the form :

$$\Phi_o = U - V \cos \Omega t$$

where U is the magnitude of the DC voltage, and V is the amplitude of the RF voltage, which has a radial frequency, Ω . For the x-direction, the field gradient, E_x, is given by :

$$E_x = \frac{-d\Phi}{dx} = \frac{-\Phi_o}{r_o^2} 2a_x x$$

$$= -\frac{(U - V \cos \Omega t)}{r_o^2} \cdot 2a_x x$$

Consequently, an ion in this field will experience a force, F_x, given by :

$$F_x = eE_x = -\frac{(U - V \cos \Omega t)}{r_o^2} 2a_x xe \qquad (3\text{-}3)$$

where e is the charge on the ion. F_x must also be equal to the product of the mass of the ion, m, and its acceleration, d^2x/dt^2, so :

$$F_x = eE_x = m \frac{d^2x}{dt^2} \qquad (3\text{-}4)$$

Therefore, equating (3-3) and (3-4) :

$$\frac{d^2x}{dt^2} + \frac{e}{m} (U - V \cos \Omega t) 2a_x x = 0 \qquad (3\text{-}5)$$

Similar equations are obtained for the y- and z- directions, and application of the transformations :

$$\Omega t = 2\gamma \; ; \quad a_u = \frac{8eUa_u}{m\Omega^2 r_o^2} \; , \; q_u = \frac{4eV}{m\Omega^2 r_o^2} \; a_u \qquad (3\text{-}6)$$

yields :

$$\frac{d^2u}{d\gamma^2} + (a_u - 2q_u \cos 2\gamma)u = 0 \qquad (3\text{-}7)$$

where u = x,y or z. Equation (3-7) is the canonical form of Mathieu's equation, which is well known.

3.3 Properties of Mathieu's Equation

Many of the works on Mathieu's equation (see references 93 and 94 for example, and further references) are concerned with the conditions necessary to obtain periodic solutions. In quadrupole devices, however, the most important property of the solution is its stability. If a solution of equation (3-7) has the form $u(\gamma)$, then the stability depends on its behaviour as γ tends to infinity; $u(\gamma)$ is said to be unstable if it also tends to infinity, and stable if it remainds bounded at all times. Whether a particular solution is stable or not, depends only on the values of a_u and q_u, in equation (3-7). The mathematical definition of stability is, however, inadequate for a practical instrument, since the amplitude of ion motion cannot exceed the dimensions of the device. Consequently, investigation of the maximum amplitude of ion oscillation is of interest.

A simplified account of Mathieu's equation theory follows. It is not intended to be a rigorous mathematical treatment, but rather an outline of the method of solution. The general solution to Mathieu's equation is derived, and used to obtain expressions for the maximum amplitude of oscillation and the mean ion energy in a three-dimensional quadrupole device.

3.31 Solutions of Mathieu's Equation

Although equation (3-7) has periodic coefficients, the solutions are not periodic unless a_u has certain values, known as characteristic values or exponents. From the theory of differential equations, the solution, $u(\gamma)$, of equation (3-7) may be expressed as a sum of two

independent solutions, $u_1(\gamma)$ and $u_2(\gamma)$, thus :

$$u(\gamma) = Au_1(\gamma) + Bu_2(\gamma) \tag{3-8}$$

where A and B are constants of integration related to the initial position, u(o) and velocity, $\dot{u}(o)$. Throughout this account, primes indicate differentiation with respect to γ . The independence of $u_1(\gamma)$ and $u_2(\gamma)$ is indicated by their Wronskian determinant, W, given by :

$$W = \begin{vmatrix} u_1(\gamma) & \dot{u}_1(\gamma) \\ u_2(\gamma) & \dot{u}_2(\gamma) \end{vmatrix} \tag{3-9}$$

which is non-zero if the solutions are independent. It can be shown that W is independent of the initial phase of γ , γ_o. Since the coefficients of equation (3-7) are periodic, Floquet's theorem may be applied, that is : Although solutions of the form

$$u\ (\gamma+\pi) = u(\gamma)$$

may not exist, solutions of the form

$$u\ (\gamma+\pi) = \sigma\, u(\gamma)$$

can exist (σ is a constant). A corollary of this is that equation (3-7) will always have a solution of the form :

$$u(\gamma) = e^{\mu\pi}\, \psi(\gamma)$$

where μ is a constant, and $\psi(\gamma)$ has a period π . The corollary may be established as follows :

If σ and $\psi(\gamma)$ are defined by :

$$\sigma = e^{\mu\pi} \; ; \; \psi(\gamma) = e^{-\mu\gamma}\, u(\gamma)$$

then : $\psi(\gamma + \pi) = e^{-\mu(\gamma + \pi)} \cdot u(\gamma + \pi)$

$= e^{-\mu\gamma} \cdot e^{-\mu\pi} \cdot \sigma \cdot u(\gamma)$

$= e^{-\mu\gamma} u(\gamma)$ (Since $e^{-\mu\pi} = \sigma^{-1}$)

$= \psi(\gamma)$

Floquet's theorem, and the corollary, are true for all linear, homogenous differential equations with coefficients of period π .

As $u(\gamma)$ will generally be neither odd nor even, it is convenient to make $u_1(\gamma)$ and $u_2(\gamma)$ even and odd respectively. Hence :

$$u_1(\gamma) = u_1(-\gamma)$$

and $$u_2(\gamma) = -u_2(-\gamma)$$

Thus equation (3-8) becomes :

$$u(\gamma) = Ae^{\mu\gamma} \psi(\gamma) + Be^{-\mu\gamma} \psi(\gamma) \qquad (3\text{-}10)$$

By Fourier's theorem any periodic function may be expressed as an infinite sum of exponentials :

$$f(t) = \frac{1}{T} \sum_{\kappa=-\infty}^{\infty} B_\kappa \exp(2\pi f_\kappa i)$$

where T is the period, and f_κ is equal to κ/T. Since $\psi(\gamma)$ has a period π, it may be written :

$$\psi(\gamma) = \sum_{n=-\infty}^{\infty} C_{2n} \exp(2n\gamma i)$$

and so :

$$\psi(-\gamma) = \sum_{n=-\infty}^{\infty} C_{2n} \exp(-2n\gamma i)$$

Substituting these results in equation (3-10) gives :

$$u(\gamma) = Ae^{\mu\gamma} \sum_{n=-\infty}^{\infty} C_{2n}\exp(2n\gamma i)+Be^{-\mu\gamma} \sum_{n=-\infty}^{\infty} C_{2n}\exp(-2n\gamma i) \qquad (3\text{-}11)$$

The constant, μ , may be either real, imaginary or complex, and hence may be expressed :

$$\mu = \alpha + i\beta$$

where α and β are real.

Equation (3-11) becomes, therefore :

$$u(\gamma) = Ae^{\alpha\gamma}.e^{i\beta\gamma} \sum_{n=-\infty}^{\infty} C_{2n}\exp(2ni\gamma)+Be^{-\alpha\gamma}.e^{-i\beta\gamma} \sum_{n=-\infty}^{\infty} C_{2n}\exp(-2ni\gamma)$$

which reduces to :

$$u(\gamma) = Ae^{\alpha\gamma} \sum_{n=-\infty}^{\infty} C_{2n}\exp(2n+\beta)i\gamma+Be^{-\alpha\gamma} \sum_{n=-\infty}^{\infty} C_{2n}\exp-(2n+\beta)i\gamma \qquad (3\text{-}12)$$

It can be seen by inspection of this equation that if α is real, either $e^{\alpha\gamma}$ or $e^{-\alpha\gamma}$ will tend to infinity as γ tends to infinity, and hence solutions are unstable if α is non-zero. Since only stable solutions are of interest in quadrupole devices, μ can be re-written :

$$\mu = i\beta$$

and equation (3-12) becomes :

$$u(\gamma) = A \sum_{n=-\infty}^{\infty} C_{2n}\exp(2n+\beta)i\gamma + B \sum_{n=-\infty}^{\infty} C_{2n}\exp-(2n+\beta)i\gamma$$

Applying the relationship :

$$\exp(i\theta) = \cos\theta + i\sin\theta$$

gives :

$$u(\gamma) = A \sum_{n=-\infty}^{\infty} C_{2n}[\cos(2n+\beta)\gamma + i\sin(2n+\beta)\gamma]$$

$$+ B \sum_{n=-\infty}^{\infty} C_{2n}[\cos-(2n+\beta)\gamma + i\sin-(2n+\beta)\gamma]$$

and therefore :

$$u(\gamma) = (A+B) \sum_{n=-\infty}^{\infty} C_{2n} \cos(2n+\beta)\gamma + (A-B) \sum_{n=-\infty}^{\infty} C_{2n} \sin(2n+\beta)\gamma$$

In the rest of this work, therefore, the complete general solution to Mathieu's equation has been taken as :

$$u(\gamma) = A \sum_{n=-\infty}^{\infty} C_{2n} \cos(2n+\beta)\gamma + B \sum_{n=-\infty}^{\infty} C_{2n} \sin(2n+\beta)\gamma \qquad (3\text{-}13)$$

where A and B differ from those used previously.

The parameters α , β - and hence μ - depend only on a and q in equation (3-7) and it is convenient to divide a - q space into regions of stability and instability, thus indicating the values of a and q necessary to produce stable, or unstable solutions. Such a division is shown in Figure 3-1, and is termed a stability diagram.

The boundaries, marked in the nomenclature of Mclachlan[93], correspond to solutions having periods π or 2π , and are given by the characteristic values of a; the overall diagram is symmetrical about the a-axis, although the boundaries are not.

The general solution, equation (3-13) is, essentially, an expression for the frequency spectrum of the solution $u(\gamma)$; that is each term in the solution corresponds to an oscillation with an amplitude given by the relevant C_{2n} coefficient, and a radial frequency, ω_n , which may be obtained by transforming to real time, thus :

$$\omega_n t = (2n+\beta)\gamma$$

but $$\gamma = \frac{\Omega t}{2} \qquad (3\text{-}6)$$

therefore $$\omega_n t = (2n+\beta)\frac{\Omega t}{2}$$

and $$\omega_n = \left(n + \frac{\beta}{2}\right)\Omega \qquad n = (-\infty, \ldots\ldots, 0, \ldots +\infty)$$

so $$\omega_n = \left(\frac{\beta}{2} \pm n\right)\Omega \qquad n = 0, 1, \ldots\ldots\infty$$

Figure 3-1. Stability Diagram for One Dimension

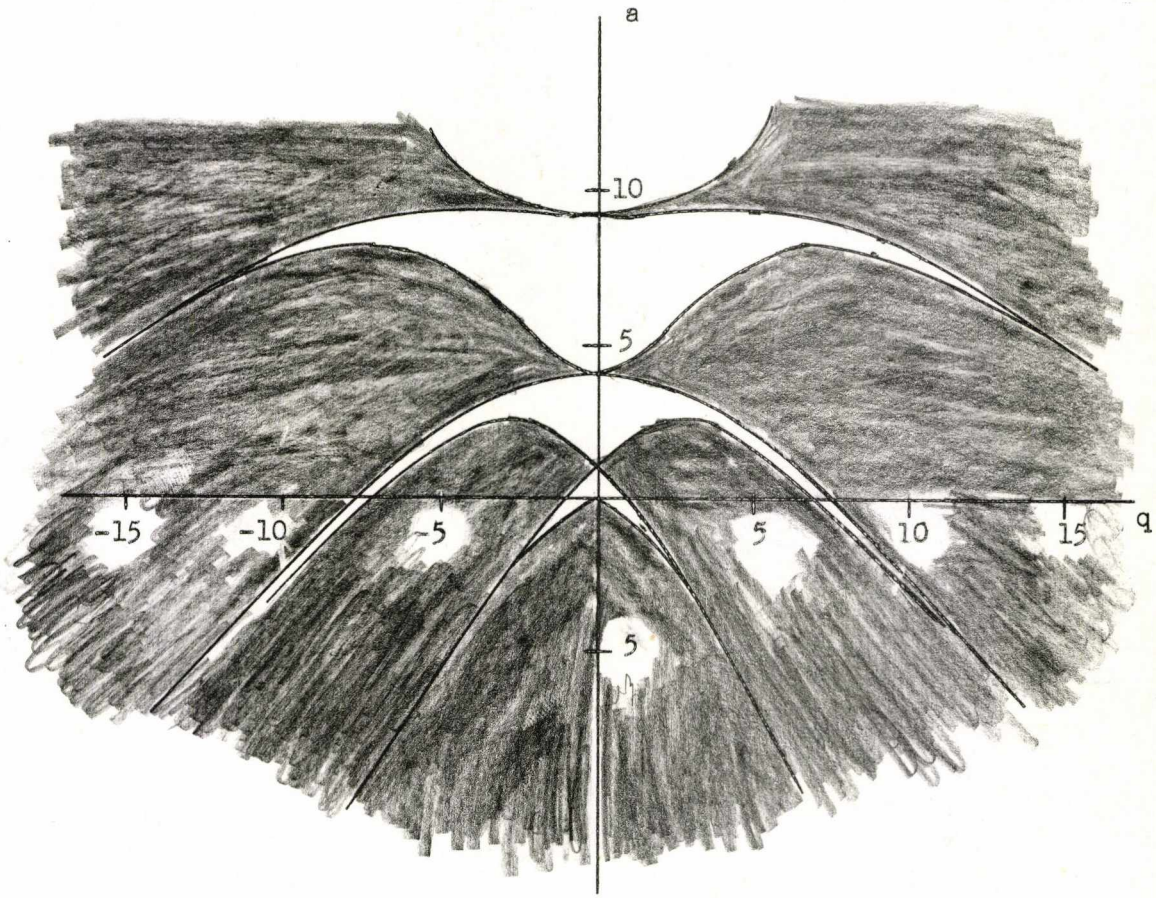

N.B. Areas of Stability are Unshaded.

Figure 3-3 - Combination of Two One-dimensional Stability Diagrams

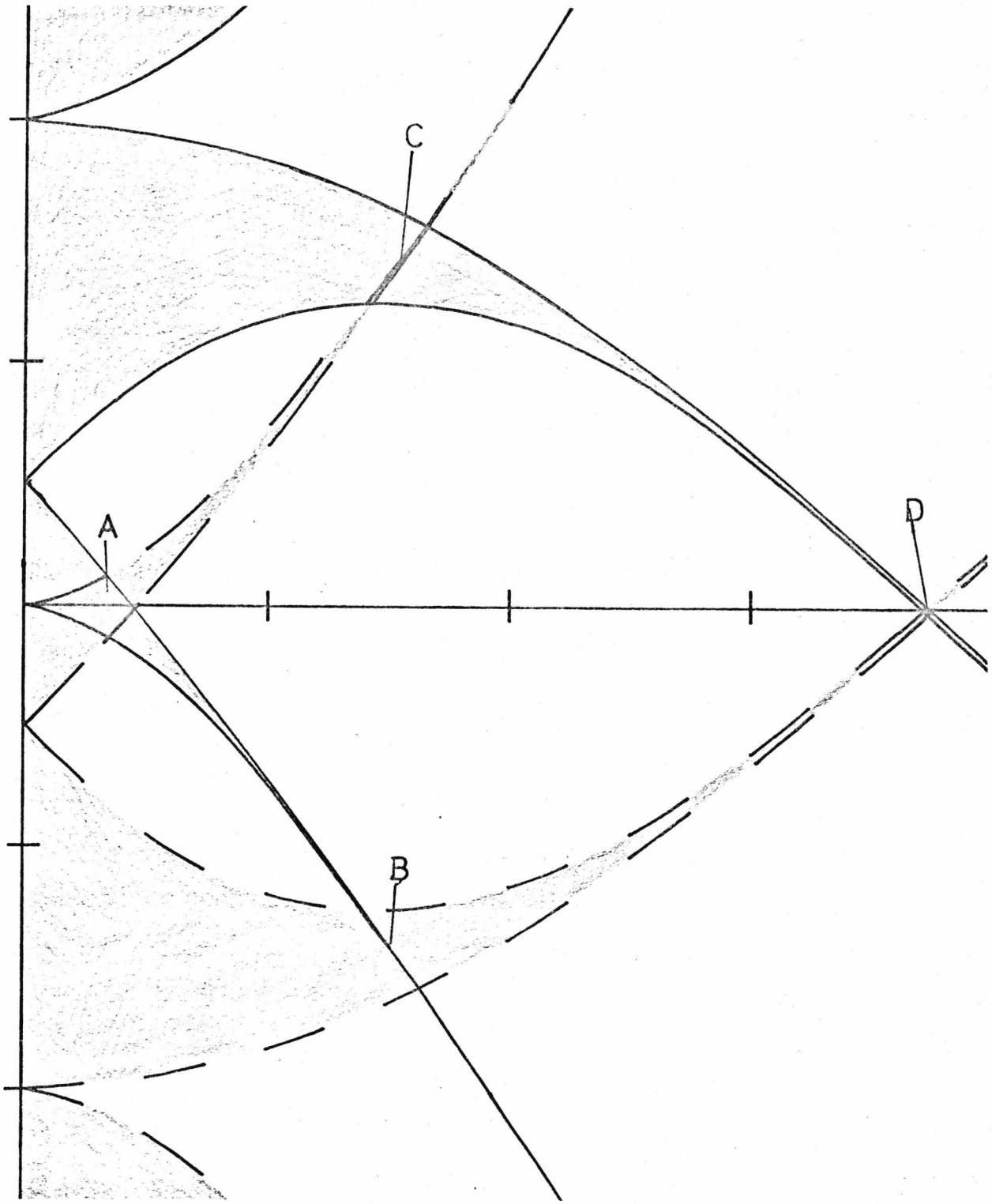

Consequently, it is apparent that β governs the frequency of ionic oscillation, and that the overall solution comprises a fundamental frequency, n = 0, and an infinite number of sidebands occuring in pairs.

The fundamental frequency, ω_o, is given by :

$$\omega_o = \frac{\beta\Omega}{2} \qquad (3\text{-}14)$$

Since equal values of β give rise to equal frequencies of vibration, points in a - q space having equal β- values are joined giving iso-β lines. This is shown in Figure 3-3, which is a magnified diagram of the region nearest the origin.

Although the frequencies of oscillation are constant along an iso-β the amplitude, C_{2n}, of each component will vary. The notation used in Figure 3-2 is again that of Mclachlan[93]; the β- values lie

Figure 3-2. Enlargement of Stability Diagram Showing iso-β Lines

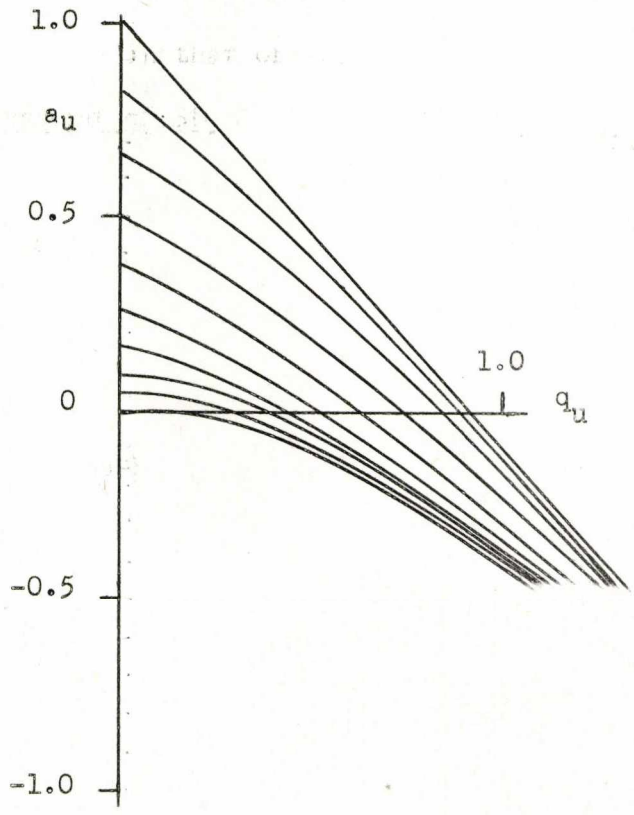

between 0 and 1 for each stability region, and are added to a constant, zero for the region shown, which is generally ignored. Some authors, for example Tamir[95], do not ignore the constant, and their β - values can be greater than unity.

3.32 Evaluation of A and B

The use of equation (3-12) necessitates calculation of A and B. If the initial phase of γ is γ_o, then the value of $u(\gamma)$ initially, $u(\gamma_o)$, is given by :

$$u(\gamma_o) = Au_1(\gamma_o) + Bu_2(\gamma_o) \tag{3-15}$$

Differentiating yields :

$$\dot{u}(\gamma_o) = A\dot{u}_1(\gamma_o) + B\dot{u}_2(\gamma_o) \tag{3-16}$$

Rearranging and equating, gives values for A and B :

$$A = \frac{u_o \cdot \dot{u}_2(\gamma_o) - \dot{u}_o \cdot u_2(\gamma_o)}{u_1(\gamma_o) \cdot \dot{u}_2(\gamma_o) - \dot{u}_1(\gamma_o)\, u_2(\gamma_o)} \tag{3-17}$$

$$B = \frac{u_o \cdot \dot{u}_1(\gamma_o) - \dot{u}_o \cdot u_1(\gamma_o)}{u_1(\gamma_o) \cdot \dot{u}_2(\gamma_o) - \dot{u}_1(\gamma_o) \cdot u_2(\gamma_o)} \tag{3-18}$$

where u_o is the initial position, $u(\gamma_o)$, and $\dot{u}_o$ the initial velocity, $\dot{u}(\gamma_o)$. In addition, the denominators of (3-17) and (3-18) are equal to the Wronskian Determinant, **W** .

3.33 Calculation of the C_{2n} coefficients and β

Although equation (3-13) is similar to a Fourier series, and has often been so described, it is improper since the C_{2n} coefficients are from recursion formulae[1], rather than integration. These formulae lead to the continued fractions :

$$\frac{C_{2n}}{C_{2n-2}} = \frac{-q}{(2n+\beta)^2}\left(1 - \frac{a}{(2n+\beta)^2} - \frac{q}{(2n+\beta)^2(2n+2+\beta)^2}\right(\quad \text{etc.} \qquad (3\text{-}19)$$

and

$$\frac{C_{2n}}{C_{2n+2}} = \frac{-q}{(2n-2+\beta)^2}\left(1 - \frac{a}{(2n-2+\beta)^2} - \frac{q}{(2n-2+\beta)^2(2n-4+\beta)^2}\right(\qquad (3\text{-}20)$$

etc.

Although these are infinite series, for computational purposes terms involving denominators greater than those shown may be ignored (see Section 3.9), since the denominators become very large. Normalization is achieved by assigning C_o the value of unity. Replacing n, in equation (3-20) by n - 1, yields another relationship between C_2 and C_{2n-2}. Elimination of C_{2n} and C_{2n-2} between this expression and equation (3-19) leads to a continued fraction relating β, a and q :

$$\frac{\beta^2 - a}{q} = \cfrac{q}{(2+\beta)^2 - a - \cfrac{q^2}{(4+\beta)^2 - a - \cfrac{q^2}{(6+\beta)^2 - a - \cfrac{q^2}{\ddots}}}} + \cfrac{q}{(\beta-2)^2 - a - \cfrac{q^2}{(\beta-4)^2 - a - \cfrac{q^2}{(\beta-6)^2 - a - \cfrac{q^2}{\ddots}}}} \qquad (3\text{-}21)$$

This may be used to determine any of the parameters a, q or β, for fixed values of the other two, as described in section 3.9 .

3.4 Investigation of the Maximum Amplitude of Oscillation

As mentioned in Section 3.3, operation of a practical quadrupole device also places a constraint on the maximum values, u_m, that the solution can have. An extremum of $u(\gamma)$ will occur when :

$$u'(\gamma) = 0$$

that is when :

$$A \sum_{n=-\infty}^{\infty} C_{2n}(2n+\beta)\sin(2n+\beta)\gamma = B \sum_{n=-\infty}^{\infty} C_{2n}(2n+\beta)\cos(2n+\beta)\gamma$$

which will occur when :

$$\sum_{n=-\infty}^{\infty} \tan(2n+\beta)\gamma = \frac{B \sum_{n=-\infty}^{\infty} C_{2n}(2n+\beta)}{A \sum_{n=-\infty}^{\infty} C_{2n}(2n+\beta)} = \frac{B}{A}$$

The corresponding values of $\sum_{n=-\infty}^{\infty} \sin(2n+\beta)\gamma$ and $\sum_{n=-\infty}^{\infty} \cos(2n+\beta)\gamma$ will be given by :

$$\sum_{n=-\infty}^{\infty} C_{2n} \sin(2n+\beta)\gamma = B/\sqrt{(A^2+B^2)}$$

and: $$\sum_{n=-\infty}^{\infty} C_{2n} \cos(2n+\beta)\gamma = A/\sqrt{(A^2+B^2)}$$

Substitution of these values into equation (3-13) gives an expression for u_m :

$$u_m = A \sum_{n=-\infty}^{\infty} C_{2n} \cdot \frac{A}{\sqrt{(A^2+B^2)}} + B \sum_{n=-\infty}^{\infty} C_{2n} \cdot \frac{B}{\sqrt{(A^2+B^2)}}$$

Which reduces to :

$$u_m = (A^2 + B^2)^{\frac{1}{2}} \sum_{n=-\infty}^{\infty} \left| C_{2n} \right| \qquad (3\text{-}22)$$

Physically, this means that the displacement will be a maximum when all the components of the motion reach their maxima in phase. Squaring (3-21) and substituting for A and B (equations (3-16) and (3-17)) gives :

$$\frac{w^2 u_m^2}{\left| \Sigma C_{2n} \right|} = u_o^2 [\dot{u}_1^2(\gamma_o) + \dot{u}_2^2(\gamma_o)] + \dot{u}_o^2 [u_1^2(\gamma_o) + u_2^2(\gamma_o)] - 2u_o \dot{u}_o [u_1(\gamma_o) . \dot{u}_1(\gamma_o) + u_2(\gamma_o) . \dot{u}_2(\gamma_o)] \qquad (3\text{-}23)$$

This is an equation of second degree, having the general formula :

$$ax^2 + 2hxy + by^2 + 2gx + 2fy + c = o$$

and it can be shown, for example[162], that the form of this equation is only dependent on the quantity $h^2 - ab$, thus :

(i) $h^2 - ab = 0$, the equation represents a parabola which may also include the case of two coincident straight lines;

(ii) $h^2 - ab < 0$, the equation represents an ellipse or circle;

(iii) $h^2 - ab > 0$, the equation represents a hyperbola, including the case of two intersecting straight lines.

Investigation of this quantity for equation (3-23) yields :

$$h^2 - ab = -W^2$$

which is always negative. The significance of this result is that, for fixed u_m, ellipses are obtained in $u_o - \dot{u}_o$ space which indicate the maximum values of u_o and $\dot{u}_o$ simultaneously possible, so that u_m is achieved exactly. If the initial conditions lie inside such an ellipse, the ion will be stable, otherwise it will be unstable.

Since, however, the maximum amplitude will be attained once in each period of oscillation, which may be large, ions may emerge from a device of finite length even though u_m is greater than the dimensions of the device.

This analysis is based largely on that of Paul, Osberghaus and Fischer[31].

3.5 Application of the Theory of Mathieu's Equation to Quadrupole Devices

Although the preceding discussion relates to one-dimension, all dimensions must be examined in practical devices. This is because the constraint applied to α_x, α_y and α_z :

$$\alpha_x + \alpha_y + \alpha_z = 0 \tag{3-2}$$

places similar constraints on a and q :

$$\begin{aligned} a_x + a_y + a_z &= 0 \\ q_x + q_y + q_z &= 0 \end{aligned} \tag{3-24}$$

Consequently an ion may be stable in one direction, and yet unstable in another.

3.51 The Quadrupole Mass Filter

For this device, there is no quadrupole field in the z-direction, consequently $\alpha_z = 0$ and :

$$\begin{aligned} \alpha_x &= -\alpha_y \\ a_x &= -a_y \\ q_x &= -q_y \end{aligned} \tag{3-25}$$

An overall stability diagram is obtained by superimposing x- and y- stability diagrams; because of the simple relationship between

a_x, a_y and q_x, q_y, the y stability diagram is the x diagram reflected in the q- and a- axes. Since the stability diagram for one direction (Figure 3-1) is already symmetrical about the a axis, only inversion in the q-axis is necessary. The combined diagram is shown in Figure 3-3, with the axes marked in terms of a_x and q_x. Operation must be in an overlapping region, for example those marked A, B, C, D, for stability in both directions. In practice only region A is of use, since operation in the others requires high voltages and leads to very large amplitudes of oscillation. Since this region is symmetrical about the q-axis, only the upper half ($a > 0$) need be shown (Figure 3-4), and selection of stable values of a_x and q_x automatically give stable values for the corresponding y parameters. The associated β values, β_x and β_y, will differ, however, as will the C_2n coefficients.

3.511 Operation of the Mass Filter

Substitution of equations (3-25) in equation (3-1) gives the quadrupole field required by the mass filter :

$$\Phi = \Phi_o\left(\frac{x^2-y^2}{r_o^2}\right) \qquad (3\text{-}26)$$

Ideally, this is generated by an array of four rods having hyperbolic cross-sections, as shown in figure 3-5.

Commonly, however, four round rods are used, their radius, r, being chosen to approximate hyperbolae as closely as possible; this occurs when :

$$r = 1.1487\ r_o$$

where r_o is the radius of the inscribed circle, as defined in Figure 3-5. This value has often been mis-quoted as $r = 1.16\ r_o$ but the correct value has been re-established by Denison[96]. Pairs of rods in the x- and y- direction are coupled, and connected to voltages of $(U - V\cos\Omega t)$ and $-(U - V\cos\Omega t)$ respectively. These voltages are generated by

Figure 3-4 Enlargement of Region A (Figure 3-3)

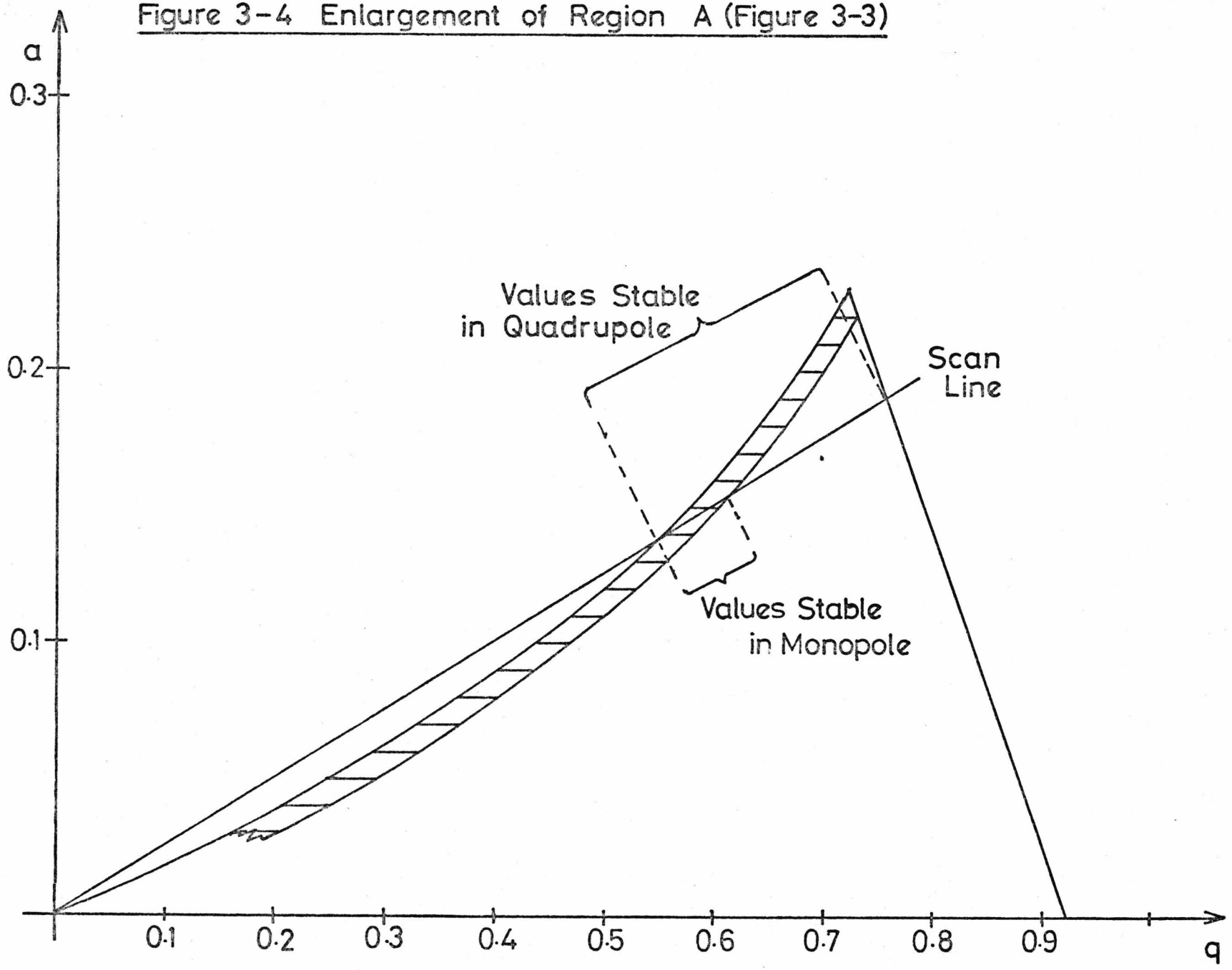

Figure 3-5. Cross Section of Mass Filter with Hyperbolic Rods

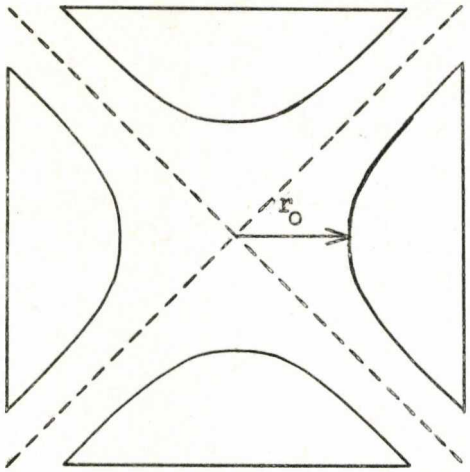

N.B. Zero Equipotential Surfaces shown dashed.

combining two DC levels of opposite polarity with two RF signals exactly 180° out of phase.

Such a device can be used to produce a mass spectrum by scanning the applied voltages so that masses are sequentially stable, pass through the array of rods and are detected. This is achieved by varying U and V such that a/q is a constant and can be represented by a scan line, as shown in Figure 3-4. Ions having a, q values on this line and inside the stability diagram are stable and detected, whereas all others are lost. The mass resolution obtainable is dependent on the range of a- and q- values simultaneously stable, i.e. the length of scan line intersecting the stability diagram, and can be increased by increasing the value of a/q. Consequently, the maximum resolution corresponds to operation at the tip of the stability diagram. Quadrupole mass filters

are renowned for their discrimination against high masses; this is because the resolution is dependent on the number of RF cycles an ion experiences, which is proportional to the flight time. For a fixed ion energy, heavy mass ions will be travelling slower, and are more likely to be rejected. This mode of operation is termed 'mass spectrometric'.

If the chosen scan line is co-incident with the q-axis, i.e. $a = 0$, a range of masses, having $0 < q \ll 0.92$, is simultaneously stable; the resolution is low but the sensitivity (a measure of the minimum number of neutrals detectable) much higher. This is known as the 'ion gauge' or 'total pressure' mode, and is widely used in pressure measuring quadrupoles.

3.52 The Monopole Mass Spectrometer

The development of the monopole was due to von Zahn[97]; it is essentially a quadrupole mass filter with one rod, and the zero equi-potential surfaces (Figure 3-5) replaced by an earthed 'V-block' electrode. This places greater restriction on the ion motion, and although the stability diagram is similar to the mass filter, only a-, and q- values at the left hand edge (shown shaded in Figure 3-4) are usable. This region cannot be drawn definitively as it depends on the geometry of individual devices.

3.521 Operation of the Monopole

The method of operation of the monopole is identical to the mass filter, except that only one voltage ($U-V\cos\Omega t$), is required. Both the mass spectrometric and total pressure modes are available.

3.53 The Quadrupole Ion Trap

The three-dimensional quadrupole, or ion trap, is conveniently described in circularly cylindrical co-ordinates, with x and y equivalent, giving :

$$a_z = -2a_r \qquad \text{and} \qquad q_z = -2q_r \qquad (3\text{-}27)$$

As with the mass filter, the field required is generated by specifying the shape of the electrodes, rather than alter the magnitudes of the voltages. In this case, the field, given by substitution of equations (3-27) in equation (3-1), is :

$$\Phi = \Phi_o\left(\frac{z^2 - 2r^2}{r_o^2}\right)$$

which is generated by the electrode structure shown in Figure 3-6. The two electrodes in the z-direction are known as 'end-caps', while that in the r-direction as the 'ring'. The cross-section of the device has the form of complementary hyperbolae having the relationship :

$$r_o^2 = 2z_o^2$$

Since a_z, q_z and a_r, q_r differ by -2, the overall stability diagram is no longer symmetrical about the q-axis, and has the form shown in Figure 3-7.

It can be seen from this diagram that in the total pressure mode, i.e. $a_z = a_r = 0$, that the range of β values is different in the

Figure 3-6. Cross Section of Ion Trap Electrodes

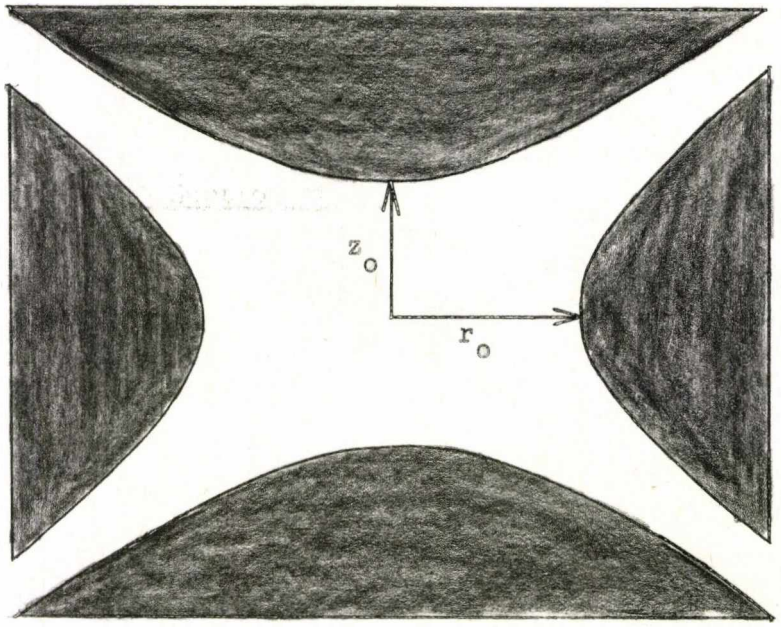

Figure 3-7. Ion Trap Stability Diagram, Showing Iso-β lines.

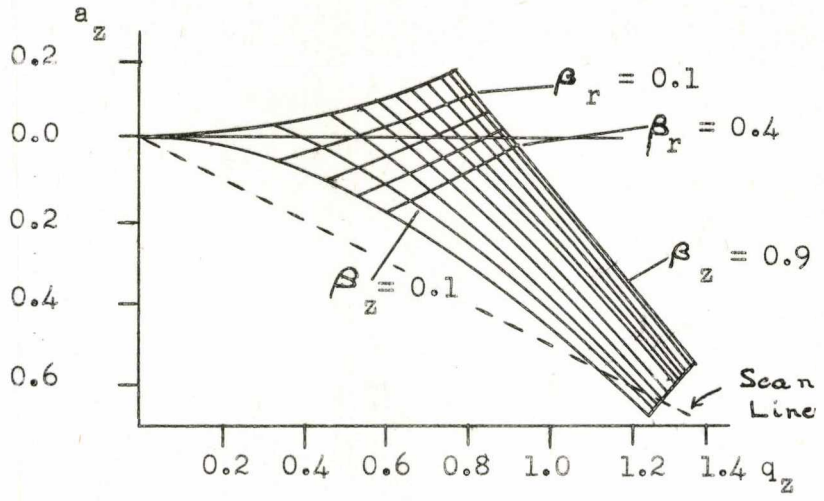

two directions, that is $0 < \beta_z < 1.0$ while $0 < \beta_r < \sim 0.35$, indicating different frequencies of oscillation.

3.531 Operation of the Ion Trap

Although a method of operating the ion trap, comparable to the mass filter, would entail application of voltages $(U-V\cos\Omega t)$ and $-(U-V\cos\Omega t)$ to the end-caps and ring respectively, Dawson and Whetten[34] have shown that it may be operated with the end-caps earthed, and $(U-V\cos\Omega t)$ applied to the ring only. Under these conditions, the centre of the device does not remain at zero voltage, but oscillates in phase with the RF and with about half its amplitude. To an ion at the centre of the device, therefore, the end-caps appear to be oscillating out of phase with the RF. Thus the required field is produced in the z-direction, although RF is only applied in the r-direction. Consequently, the value of q (see Section 3.6) is altered, but correct operating is not affected. The main advantage of this method is that it facilitates application of voltage pulses to the end-caps in order to eject ions. This provides a method for ion detection and was proposed by Dawson and Whetten[34] as an alternative to the measurement of the power absorbed by ions, at specific frequencies,

from an auxillary RF generator, used by Paul et al[31].

Mass spectrometric usage of this device necessitates pulsed operation since an ion sample must be stored, to allow unstable ions to be lost on the electrodes, before detecting the stable ions. Scan lines may be drawn on the stability diagram, as shown in Figure 3-7. The device may also be operated in a total pressure mode, that is with U equal to zero causing a range of masses to be stable, which in the mass filter is given by $0 < q < \sim 0.92$.

3.6 Note on Definition of q

Since operation of the ion trap with uni-polar RF, as described above, alters the definition of q from that given in equation (3-6), a convention has been adopted throughout this work such that the same equation is used for all devices, but V is altered. The relationship used is :

$$q = \frac{2eV}{m r_o^2 \Omega^2} \qquad (3\text{-}28)$$

where V is defined as being the maximum potential difference between opposite pairs of electrodes. Consequently, in the case of the mass filter V is equal to twice the zero-to-peak amplitude of the applied RF. For the ion trap, with unipolar RF, V is equal to the amplitude of the RF.

Considerable confusion has arisen owing to the different definitions of q and V used by different authors; the convention described above is therefore proposed as a reasonable alternative.

3.7 Treatment of Ion Energy in the Ion Trap

Any treatment of the ion kinetic energy in a quadrupole ion trap must, necessarily, be an estimation since there are a large number of ions ($\sim 10^8$) which have been created at various RF phases and initial positions. At any given instant there will be an energy spread

dependent on the creation conditions, but an instant later the spread will be the same. Consequently, a reasonable method of estimating the mean kinetic energy is to obtain an expression for the velocity variation of a particular ion, and average it over some period. Since the two directions are independent, only one need be examined so long as the other is considered when evaluating the energy.

In the treatment reported by Dehmelt[49], a simple sinusoidal waveform is used to approximate the position of an ion, considered to execute simple harmonic motion in a 'pseudo-potential' well of depth $\bar{D}$ volts. The maximum velocity will occur in an ion that just touches the electrodes, i.e. has an amplitude z_o in the z-direction. Consequently Dehmelt has :

$$u(t) = z_o \cos \bar{\omega}_z t \qquad (3\text{-}29)$$

where $\bar{\omega}_z$ is the secular frequency of ion motion. Dehmelt further defines $\bar{\omega}_z$ by :

$$= \frac{q\Omega}{2\sqrt{2}} \qquad (3\text{-}30)$$

which when compared to the fundamental of ion motion :

$$= \frac{\beta\Omega}{\sqrt{2}} \qquad (3\text{-}14)$$

delete $\sqrt{}$

shows that Dehmelt has :

$$\beta = \frac{q}{\sqrt{2}} \qquad (3\text{-}31)$$

At the very low q and β values with which Dehmelt is concerned, equations (3-29) and (3-31) are reasonable approximations, however, they deteriorate as β increases. Consequently the aim of this discussion is to examine the validity of these equations and to derive an

alternative method of ion energy calculation.

A simplification may be introduced by considering the initial velocity of an ion to be zero; this is reasonable, since the original thermal velocity of a molecule will be small and it will receive little additional energy in a collision with an electron compared to the subsequent ion velocity. If

$$\dot{u}\,(\gamma_o) = 0$$

then B in equation (3-13) becomes zero, and the equation of motion reduces to :

$$u(\gamma) = A \sum_{n=-\infty}^{\infty} C_{2n} \cos(2n+\beta)\gamma \qquad (3\text{-}32)$$

If only the fundamental mode of vibration is important, i.e. $C_{2n} = 0$ for $n \neq 0$, then :

$$u\,(\gamma) = A \cos \beta\gamma$$

or

$$u\,(t) = A \cos \frac{\beta \Omega\, t}{2} \qquad (3\text{-}33)$$

These equations (3-29), (3-32) and (3-33) will be referred to as Dehmelt's Solution, the Smoothed General Solution (SGS) and the Complete General Solution (CGS) respectively. A comparison of the merits of Dehmelt's Solution and the Smoothed General Solution is shown in Figure (3-8), which is a computer plotted trajectory for $\beta = 0.1$, obtained as described later in Section 3.9; z_o has been taken as unity, and the coefficient A in (3-32) selected to produce a maximum displacement of unity. It can be seen that both Dehmelt's and the Complete Solutions reach z_o, but the Smoothed Solution does not; nevertheless, the maximum error in Dehmelt's is twice that in the Smoothed Solution. Both are, however, fairly good approximations to the Complete Solution.

Figure 3-8. Computer Plotted Ion Trajectory for $\beta = 0.1$

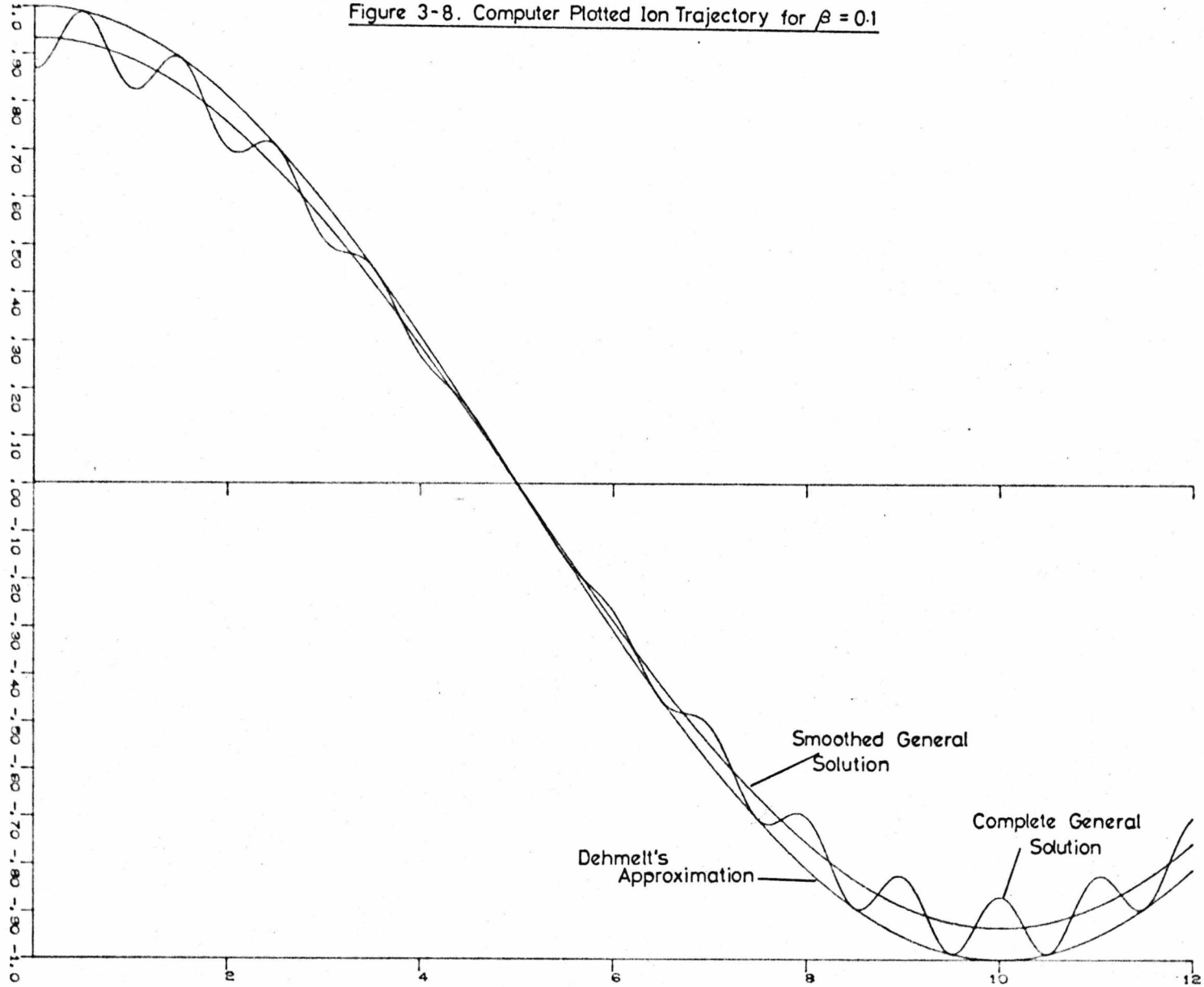

DISPLACEMENT

G-GO. UNITS OF PI

Differentiating equations (3-29), (3-32) and (3-33) gives

from (3-29) :

$$\dot{u}(t) = -z_o \bar{\omega}_z \sin \bar{\omega}_z t = \frac{-z_o q\Omega}{2\sqrt{2}} \sin \bar{\omega}_z t \qquad (3\text{-}34)$$

from (3-32) :

$$\dot{u}(\gamma) = A \sum_{n=-\infty}^{\infty} (2n+\beta)\sin(2n+\beta)\gamma \qquad (3\text{-}35)$$

$$\therefore \quad \dot{u}(t) = -A \sum_{n=-\infty}^{\infty} (2n+\beta)\sin(2n+\beta)\frac{\Omega t}{2}$$

from (3-33) :

$$u(t) = A \cos \frac{\beta\Omega t}{2} \qquad (3\text{-}36)$$

$$\dot{u}(t) = -A\frac{\beta\Omega}{2} \sin \frac{\beta\Omega t}{2}$$

It can be seen from Figure 3-9 that the approximate velocities are very different to the Complete Solution velocity. These curves are again computer drawn, using equations (3-34) to (3-36) and the same conditions as Figure 3-8. The maximum velocities predicted by Dehmelt's and the Smoothed Solutions will occur when :

$$\sin \bar{\omega}_z t = \sin \frac{\beta\Omega t}{2} = 1$$

and will be given by :

$$v_{max_{Dehmelt}} = \frac{z_o q\Omega}{2\sqrt{2}} \qquad (3\text{-}37)$$

$$v_{max_{SGS}} = \frac{A\beta\Omega}{2} \qquad (3\text{-}38)$$

Since, however, the velocity of the General Solution is clearly some low frequency drift with a superimposed high frequency ripple, the mean velocities may well be in reasonable agreement.

Figure 3-9. Computer Plotted Ion Velocities vs. Time($\gamma - \gamma_0$) for $\beta = 0.1$

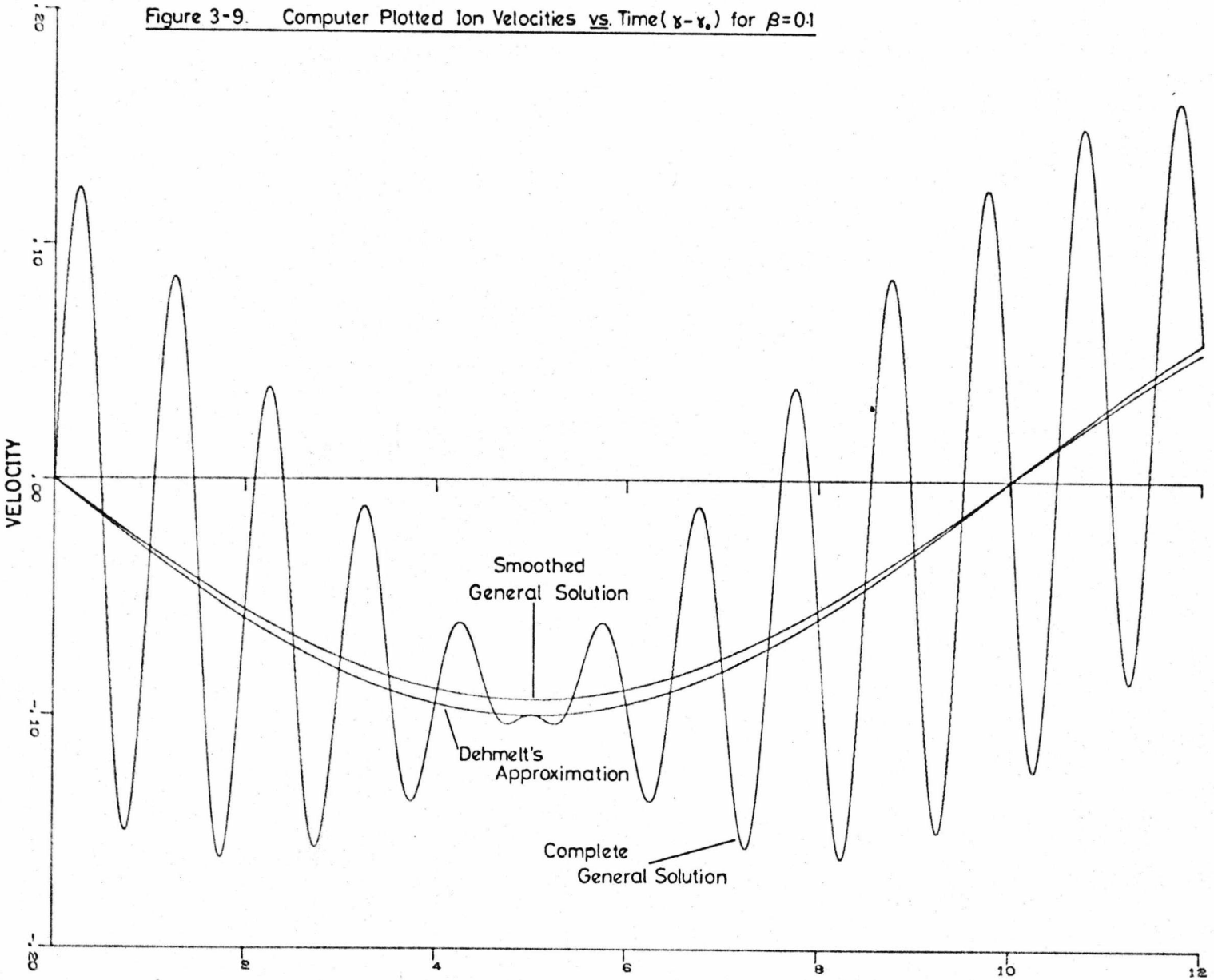

The mean velocity is found from :

$$\langle \dot{y}(t) \rangle = \frac{\int_0^{T_1} \dot{y}(t)\, dt}{\int_0^{T_1} dt}$$

where $\langle \dot{y}(t) \rangle$ is the mean velocity over the period T_1. In this case averaging over a half-period is sufficient, and therefore :

$$T_1 = \frac{\pi}{\bar{\omega}_z} \quad \text{or} \quad \frac{\pi}{\omega_o}$$

Also, as :

$$\int \dot{y}(t)dt = y(t)$$

the mean velocity is given by :

$$\langle \dot{y}(t) \rangle = \frac{[y(t)]_0^{T_1}}{\int_0^{T_1} dt} \qquad (3\text{-}39)$$

Applying equation (3-39) to (3-29) gives :

$$\langle \dot{y}(t) \rangle_D = \frac{[z_o \cos \bar{\omega}_z t]_0^{\pi/\bar{\omega}_z}}{\pi/\bar{\omega}_z}$$

$$= \frac{z_o \bar{\omega}_z}{\pi} [\cos \pi - \cos o)$$

$$= \frac{-2z_o \bar{\omega}_z}{\pi}$$

Neglecting the minus sign and substituting for $\bar{\omega}_z$ from equation (3-30) :

$$\langle \dot{y}(t) \rangle_D = \frac{q\Omega z_o}{\sqrt{2}\pi} \qquad (3\text{-}39)$$

Similarly for the Smoothed General Solution :

$$\langle \dot{y}(t) \rangle_{SGS} = \frac{A[\cos \frac{\beta\Omega}{2} t]_0^{2\pi/\beta\Omega}}{2\pi/\beta\Omega}$$

$$= \frac{A\beta\Omega}{\pi} \qquad (3\text{-}40)$$

For the General Solution, the situation is more complex :

$$\langle \dot{y}(t) \rangle_{CGS} = \frac{A\,[\Sigma C_{2n} \cos \omega_n t]_0^{\pi/\omega_0}}{\int_0^{\pi/\omega_0} dt}$$

where $\omega_n t = (2n + \beta)\gamma$

therefore : $\langle \dot{y}(t) \rangle_{CGS} = \frac{A\,\omega_0}{\pi}[\Sigma C_{2n} \cos \frac{\omega_n}{\omega_0} \pi - \Sigma C_{2n}]$

$$= \frac{A\,\omega_0}{\pi}[\Sigma C_{2n}(\cos \frac{\omega_n}{\omega_0} \pi - 1)] \qquad (3\text{-}41)$$

Consider the term : $\cos \frac{\omega_n}{\omega_0} \pi$

Since : $\omega_n t = (2n+\beta)\gamma$

$$\omega_n = (2n+\beta)\frac{\Omega}{2}$$

and $\omega_0 = \frac{\beta\Omega}{2}$

Therefore $\frac{\omega_n}{\omega_0} = \frac{(2n+\beta)}{\beta}$

and $\cos \frac{\omega_n}{\omega_0} \pi = \cos \frac{(2n+1)\pi}{\beta}$

$$= \cos \frac{(2n\pi+\pi)}{\beta}$$

Using the identity :

$$\cos (x + y) = \cos x \cdot \cos y - \sin x \cdot \sin y$$

gives :

$$\cos\left(\frac{2n\pi + \pi}{\beta}\right) = \cos\frac{2n\pi}{\beta} \cdot \cos\pi - \sin\frac{2n\pi}{\beta} \cdot \sin\pi$$

$$= -\cos\frac{2n\pi}{\beta}$$

Therefore, equation (3-41) becomes :

$$\langle \dot{y}(t) \rangle_{CGS} = \frac{A\beta\Omega}{2\pi}\left[\sum C_{2n}\left(\cos\frac{2n\pi}{\beta} + 1\right)\right] \qquad (3\text{-}42)$$

An important check which may be verified by inspection, is that this last equation gives equation (3-40) on substituting $n = 0$.

Thus three equations for the mean velocity have been obtained :

Dehmelt	$q\ \Omega\ z_o\ /\sqrt{2}\pi$
Smoothed General Solution	$A\ \beta\ \Omega\ /\ \pi$
Complete General Solution	$\frac{A\beta\Omega}{2\pi}\left[\sum C_{2n}\left(\cos\frac{2n\pi}{\beta} + 1\right)\right]$

(3-43)

The behaviour of the last equation is likely to be unpredictable as β increases since the cosine term may reduce to a cancelling term (e.g. $\beta = 1.0$, $\cos 2n\pi/\beta = \cos 2n\pi = 1$ for all n). This indicates that the averaging period should also vary as β increases, and the low frequency drift becomes less dominant. Nevertheless, these equations have been shown to give good agreement for $0 < B \lesssim \sim 0.4$ indicating that either of the approximations is reasonable at moderate values of β. Results of these calculations are given in Section 3.93, and are shown to be in good agreement with the experimental data in Chapters 5 and 6.

3.8 The Application of Numerical Analysis Techniques to Quadrupole Devices

The numerical analysis of quadrupole devices has been performed by

several workers using one of two methods :

(i) Numerical integration of Mathieu's equation (3-7) using a standard numerical integration technique. A study of this kind was first reported by Lever[98] for the monopole, but it has also been used for the mass filter (for example, by Dawson and Whetten[34,40]). Numerical integrating methods are step procedures, that is from the starting point x_o, with known values of $y(o)$ and $\dot{y}(o)$, a value for y at $x_o + h$ is calculated, and used in turn to calculate y at $x_o + 2h$. The term h is a small interval. Errors, proportional to powers of h, are therefore cumulative over the range of integration. A further disadvantage of this method is that Mathieu's equation is only applicable to ideal quadrupoles with hyperbolic electrodes, whereas round rods are more common in mass filters.

(ii) Examination of the field by solving Laplace's equation. This method has been applied by Denison[96] and Chisolm and Stark[99] to examination of real quadrupoles, with an array of round rods in an earthed cylindrical housing. Essentially the method is as follows. A cross-section through the device is taken and covered with a square mesh (since the quadrupole is symmetrical, this need only be performed on one quadrant, although the sign changes in two of the others). An array of simultaneous equations is then set up,

relating the potential of each node in the mesh to that of its neighbours. The array of equations is repeatedly calculated, ensuring that voltages on the electrodes are not changed, until an error requirement is satisfied. Each node voltage is then known, and can be used to evaluate field gradients and hence particle trajectories. Conceivably, Laplace's equation could be replaced by Poisson's equation :

$$\nabla^2 \Phi = -\rho/\epsilon_0 \qquad (3\text{-}44)$$

where ρ is the space charge density (coulomb m^{-3}) and ϵ_0 is the dielectric constant of the medium (F m^{-1}), thereby allowing inclusion of space charge terms, but this has not been reported in the literature.

In addition to the above methods, the use of the solution of Mathieu's equation has been reported by Powell[100], and several workers (for example Kando[101] and Yinon and Klein[102]) have described the use of analogue computing techniques.

All these authors have concerned themselves with investigation of quadrupole devices as mass analysers, particularly at high resolution obtained near the tip of the stability diagram. In the present application, however, the QUISTOR is to be operated in the total pressure mode, and consequently this mode is of interest. In particular

two things were demanded of the numerical analysis :

(i) An explanation of the total pressure peak obtained in both the mass filter and the ion trap. If the RF voltage is scanned, with zero DC applied, it is found that the peak height obtained varies with RF amplitude, i.e. q, such that a maximum always occurs at a q value in the range $\langle\sim 0.15 < q < \sim 0.2$; this is shown in Figure 3-10. This effect appears to be a result of several phenomena, and is discussed in Section 3.92.

Figure 3-10. Total Pressure Peak Shape

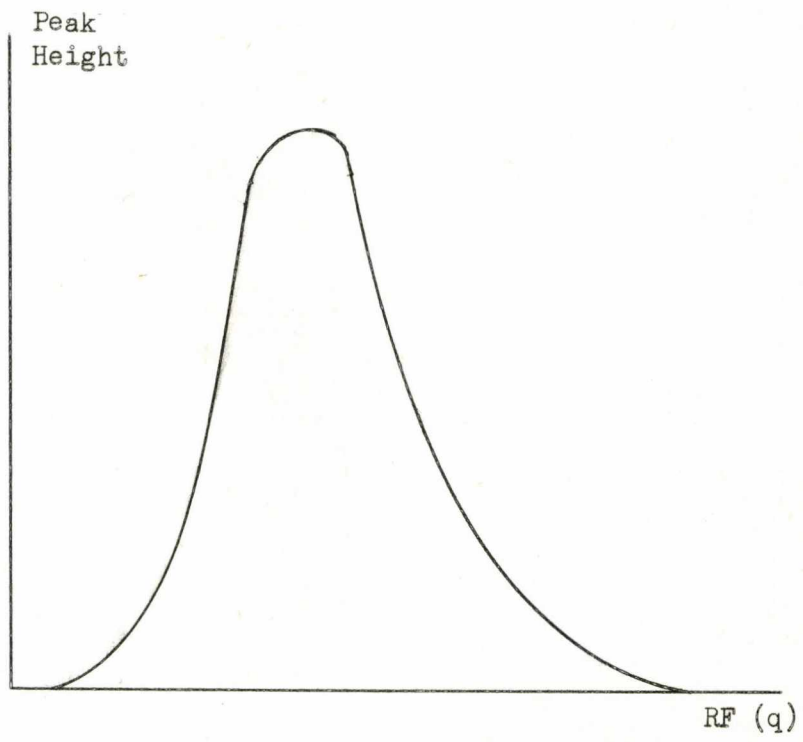

(ii) Estimation of the mean ion kinetic energy, and comparison with the work of Dehmelt. This is clearly important in the proposed QUISTOR investigations, since ion collision phenomena are often strongly dependent on ion energy. Results are given in Section 3.93 and are shown to be in good agreement with experimental data in Chapters 5 and 6.

3.9 Description of Numerical Examination of the QUISTOR

The method adopted was based on the Complete General Solution, and subsequent formulae developed in Sections 3.3, 3.4 and 3.6 This was chosen for three reasons:

(i) it is more accurate than a step-wise procedure;

(ii) estimation of the position at any time is possible without computing the preceding steps;

(iii) equations can easily be developed for the maximum amplitude of oscillation and ion energy, whereas with conventional integration procedures these quantities can only be found by examination.

This method is, however, slower than a numerical integration technique, if a complete trajectory is to be produced, owing to the number of calculations required per step. In a Runge-Kutta type procedure, six or eight calculations are performed whereas this method requires approximately twenty calculations. Although most of the computations were performed for a QUISTOR operating in total pressure

mode and assuming zero initial ion velocity, the programs used were capable of greater flexibility, and were checked by comparison with the results of Lever[98].

3.91 Description of the Programs Employed

This section briefly describes the programs devised to permit analysis of the General Solution, equation (3-13). These were written as a library of sub-routines which could be used as desired to permit calculations on specific formulae. Programs were required for the following functions :

(i) Calculation of β from a and q - also a from β, q and q from a, β using equation (3-21).

(ii) Generation of the C_{2n} coefficients, with $C_o = 1$, from equations (3-19) and (3-20).

(iii) Calculation of A and B from the initial conditions employing equations (3-17) and (3-18); this also entails calculation of W from equation (3-9).

The programs were written in ALGOL for use on an INTERNATIONAL COMPUTERS LTD. (ICL) 4130.

The methods were as follows :

(i) The relevant equation was :

$$\frac{\beta^2-a}{q} = \frac{q}{(2+\beta)^2 - a - \dfrac{q^2}{(4+\beta)^2 - a - \dfrac{q^2}{(6+\beta)^2 - a - q^2 \text{ etc.}}}}$$

(3-21)

$$+ \frac{q}{(\beta-2)^2 - a - \dfrac{q^2}{(\beta-4)^2 - a - \dfrac{q^2}{(6-\beta)^2 - a - q^2 \text{ etc.}}}}$$

In practice, terms up to $(12+\beta)$ and $(12-\beta)$ were used, it having been shown that the difference introduced by using higher terms was in the sixth decimal place. The procedure adopted was to treat each series separately, compute the highest terms, then the next highest and so on, finally adding the two series. Calculation of a and β from the above formula was straightforward since these can be written on the left hand side, an approximation (to either β or a) guessed and a better approximation calculated. This was repeated until successive approximations differed by less than 1×10^{-6}. As q cannot be written on the left hand side of (3-21), the formula was re-written for β on the left, and q calculated, based on the flowchart shown in Figure 3-11, to produce a β -value disagreeing with that required by less than 10^{-6}.

Essentially q is stepped by an index (initially 0.1) until the calculated β is greater than the required β. q is then reduced by the index, which is itself divided by ten. This is repeated with the new index (0.01) until β calculated is again

Figure 3-11. Flowchart Representation of Program to Calculate q

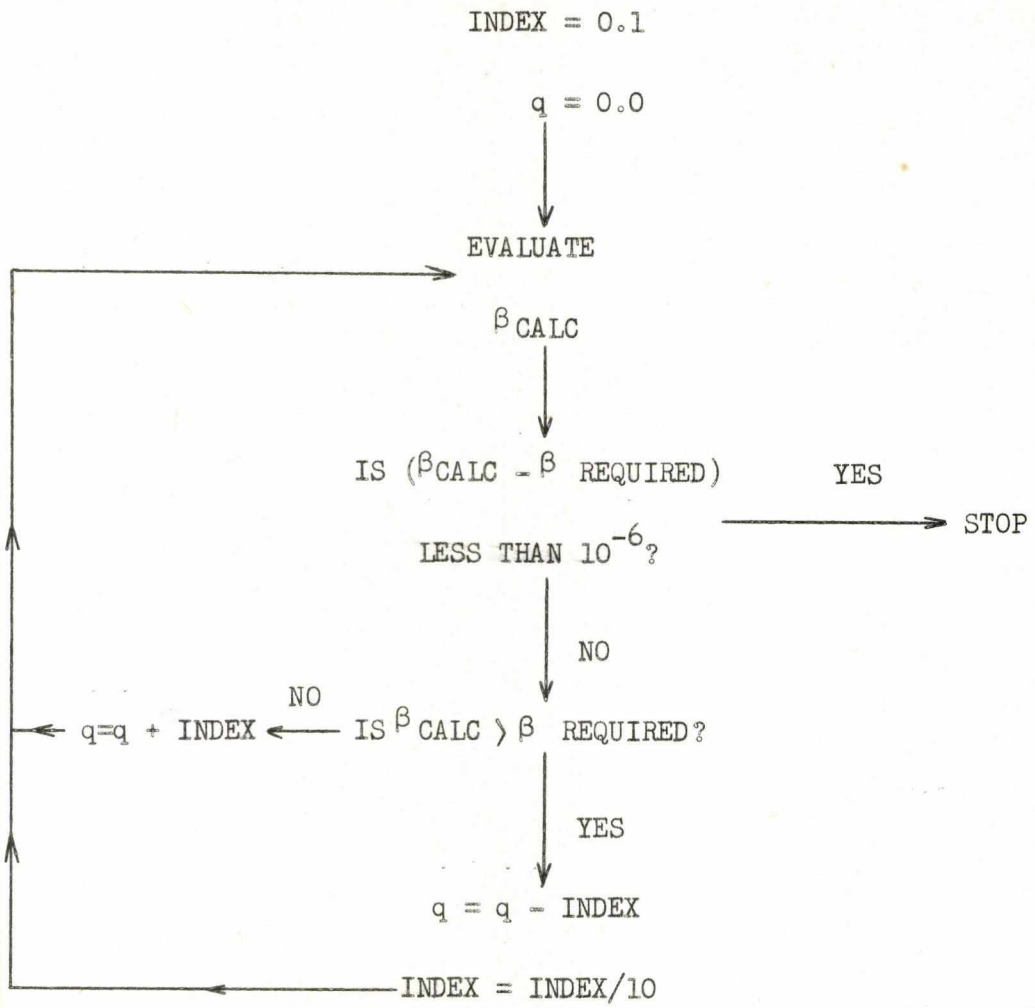

greater than the required value. The cycle is repeated until β calculated differs by less than 10^{-6} from the required β.

(ii) Equations (3-19) and (3-20) are used directly, considering only the terms shown with an error of the order of 10^{-6}. The procedure was to compute the highest terms and work towards the beginning of each series. C_o is taken as unity in both cases. Clearly program (i) must be employed first to calculate a, β and q.

(iii) Calculation of A and B, equations (3-17) and (3-18) required knowledge of the quantities $u_1(\gamma_o)$, $\dot{u}_1(\gamma_o)$, $u_2(\gamma_o)$ and $\dot{u}_2(\gamma_o)$ and also W, which depends on the other four. Comparison of equations (3-13) and (3-8) gives :

$$u_1(\gamma_o) = \Sigma\, C_{2n} \cos (2n+\beta)\gamma_o$$

$$u_2(\gamma_o) = \Sigma\, C_{2n} \sin (2n+\beta)\gamma_o$$

$$\dot{u}_1(\gamma_o) = -\Sigma\, C_{2n}(2n+\beta)\sin(2n+\beta)\gamma_o$$

$$\dot{u}_2(\gamma_o) = \Sigma\, C_{2n}(2n+\beta)\cos(2n+\beta)\gamma_o$$

Consequently, having evaluated a, q, β and the C_{2n} coefficients, the above quantities may also be readily calculated for definite initial conditions. As a check on the correct functioning of these programs, a stability diagram was obtained for $0 \ll \beta \ll 1$ and was the same as that given by McLachlan[93], the results were also compared with the work of Tamir[5]. A graph of β against q for a = 0, Figure 3-12, from the exact equation, and from Dehmelt's approximation (equation 3-31), shows that the latter is reasonable for $0 < q < 0.14$. Generally, Dehmelt has q - values within this region. The actual curve is also in agreement with that produced by Berkling, and reported by Dawson and Whetten[103]. Table 3-1 shows the important results for β = 0.1, 0.2 ..... 0.8. The conditions chosen were $\dot{u}(o) = 0$, and a = 0. The rows, from top to bottom, are : β ; the q - value necessary to produce this; the initial position, u_o, needed to produce a maximum

Figure 3-12. Variation of β With q, for a = 0.

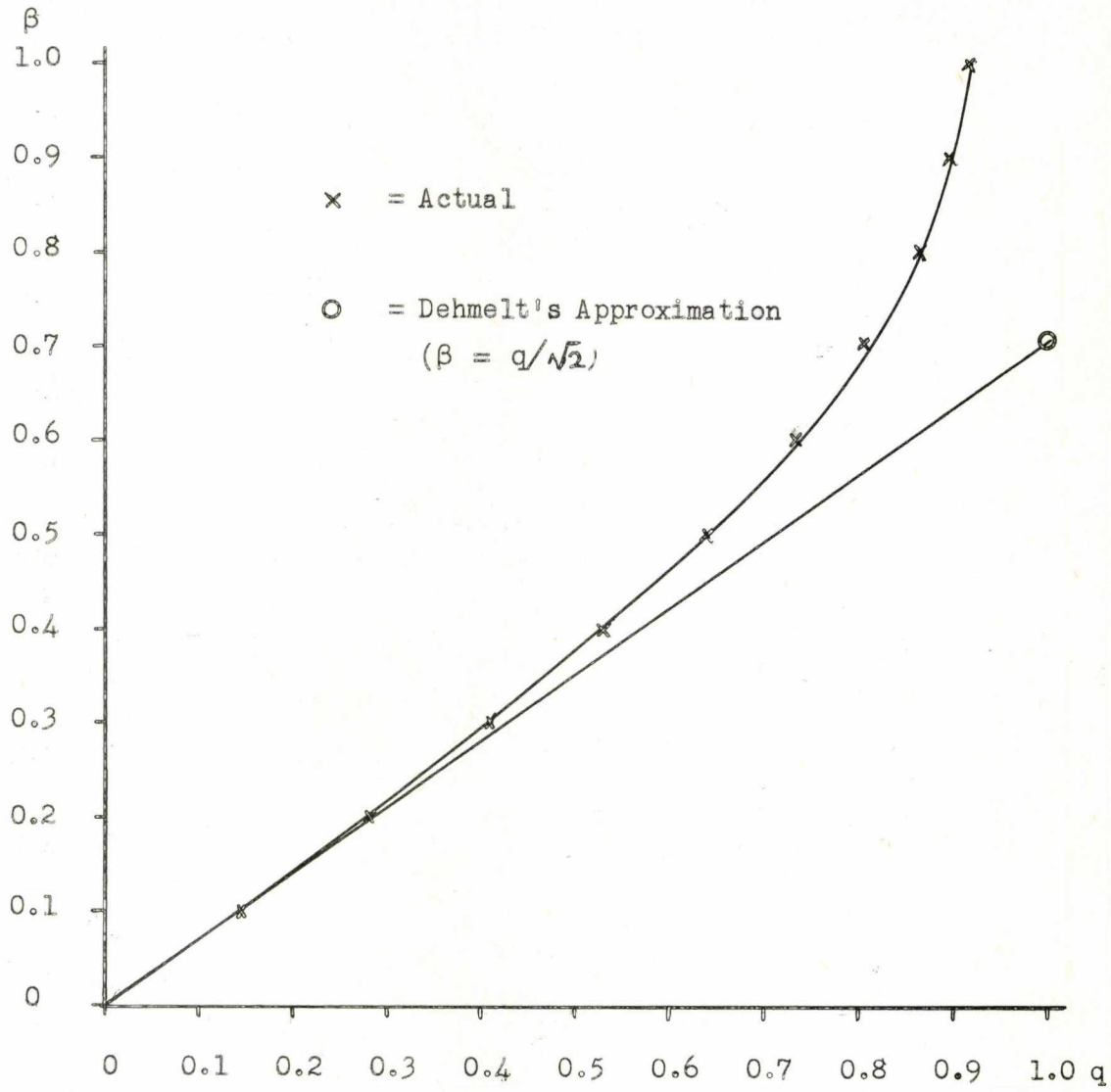

Table 3-1

β	0.1	0.2	0.3	0.4	0.5	0.6	0.7	0.8
$q_a=0$	0.1408692	0.2784354	0.4094425	0.5320734	0.63931500	0.7324250	0.807624	0.86288340
U_o for $U_m = 1$	0.86750856	0.74930391	0.64125942	0.53939771	0.4446986	0.35248858	0.26265781	0.17436138
A	0.93316702	0.87241062	0.81575586	0.76114343	0.70935773	0.65778334	0.60651581	0.55525264
C-8	0.0	0.0	0.00000037	0.00000135	0.00000362	0.00000816	0.00001605	0.00002835
C-6	-0.00000146	-0.00001374	-0.00005365	-0.00014652	-0.00031855	-0.00061031	-0.00105921	-0.00170276
C-4	0.00036155	0.00166007	0.00425690	0.00863066	0.01506907	0.02429001	0.0368245	0.05333069
C-2	-0.03903604	-0.08607951	-0.14227869	-0.20993960	-0.28842182	-0.38276335	-0.49548216	-0.63118230
C_o	1.0	1.0	1.0	1.0	1.0	1.0	1.0	1.0
C_2	-0.03195168	-0.05758027	-0.07753226	-0.09251914	-0.10262195	-0.10875495	-0.11123600	-0.11051747
C_4	0.00026777	0.00090897	0.00171727	0.00254228	0.00324144	0.00376660	0.00406953	0.00414194
C_6	-0.00000101	-0.00000658	-0.00001772	-0.00003302	-0.00004906	-0.00006334	-0.00007323	-0.00007731
C_8			0.00000011	0.00000025	0.00000043	0.00000063	0.00000078	0.00000086
ΣC_{2n}	0.92963912	0.85888903	0.78609232	0.70853626	0.62690316	0.53587338	0.43306012	0.31402170
$\Sigma \lvert C_{2n} \rvert$	1.0716195	1.1462492	1.2258570	1.3138128	1.4097260	1.5202574	1.6487616	1.8009820

displacement, u_m of one; the corresponding value of A; the C_{2n} coefficients C - 8 to C8; the sum of the C_{2n} coefficients; the absolute sum of the C_{2n} coefficients.

A typical ion trajectory plot is shown in Figure 3-8; the conditions were $u'_o = 0$, a = 0 with q chosen to give $\beta = 0.1$, and u_o chosen to produce $u_m = 1.0$.

3.92 Explanation of the Total Pressure Peak Shape

The shape of the total pressure peak height plotted against RF, Figure 3-10, is believed to be mainly dependent on two conflicting factors :

(i) Adopting Dehmelt's model, see Section 3.7, of ions oscillating in a potential well, as the RF is increased then the number of ions stored will also increase, since $\bar{D}$ is related to V, and hence to q. In fact, examination of Dehmelt's equations gives :

$$\bar{D} = \frac{m z_o^2 q^2 \Omega^2}{10e}$$

where q $\propto$ V.

Physically, the significance of this result is that as V is increased the force on each ion is increased, such that more ions are retained.

(ii) The conflicting factor is the number of ions which will have maximum amplitudes less than the geometry of the device. For a particular β_z value, there is a value of u(o) which yields a trajectory

of maximum amplitude z_o, and similarly for the r - direction. Consequently there is a volume in space, inside the device, in which ions must be created to remain stable, this is shown schematically in cross-section in Figure 3-13.

The cross-section of this volume is elliptical, and on rotating it yields an oblate spheroid of volume :

$$\text{Volume} = \frac{4}{3}\pi a^2 b$$

where a and b are the half-lengths of the major and minor axes, respectively.

The volume of the spheroid is plotted against β in Figure 3-14, and is seen to decrease as β increases.

Obviously, both the above treatments are gross simplifications, and combination is complex, since many unknown factors will affect it, for example, the space-distribution of the electron beam, the ion density and any field imperfections. However, these results do predict that an optimum value for q will exist, such that storage is maximized. Further, they suggest that observation of rate constants will not be afftected by the RF amplitude, other than from kinetic energy considerations, although the actual peak height may alter. This is shown to be the case in Chapter 5.

3.93 Calculation of Maximum and Mean Ion Energies

Maximum ion velocities were calculated from equations (3-37) and (3-38), allowing calculation of the maximum kinetic energy of an

Figure 3-13. Volume in which Ions must be Created to Remain Stable

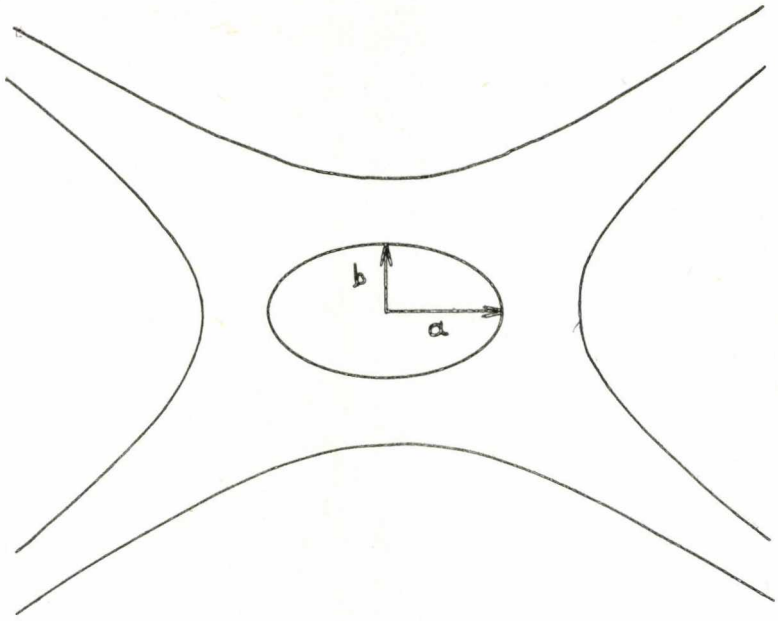

ion of known mass. Plots of these equations against β are shown in Figure 3-15, for a maximum permissible displacement of 7.07×10^{-3} m (i.e. z_o for the QUISTOR). Velocity is in the units of metres radian^{-1} of the RF field; this retains the generality, since these figures may be converted to metres second^{-1} for any device by multiplying by the radial frequency of the applied RF. These units are also used for the mean velocities.

Figure 3-16 shows plots of mean velocity, from equations (3-43). The erratic behaviour of the results from the Complete General Solution is a consequence of the invariant averaging period employed. Clearly, in a more rigorous treatment, this effect should also be considered.

Figure 3-14. Volume of QUISTOR in Which Ions Can Be Created and Remain Stable vs. q.

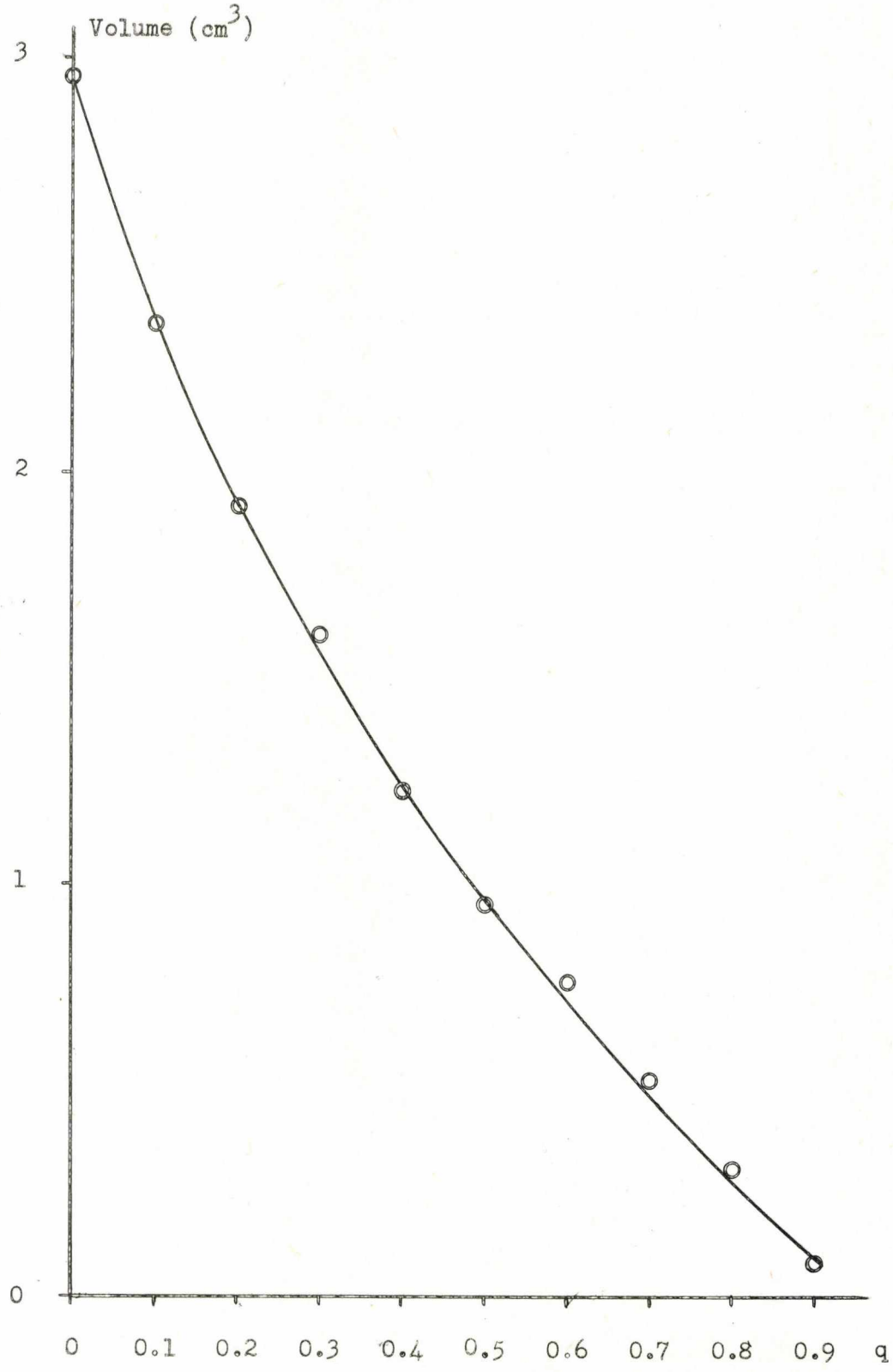

Figure 3-15. V_{max} vs. β ; Calculated for a Maximum Displacement of 0.707×10^{-2} metre

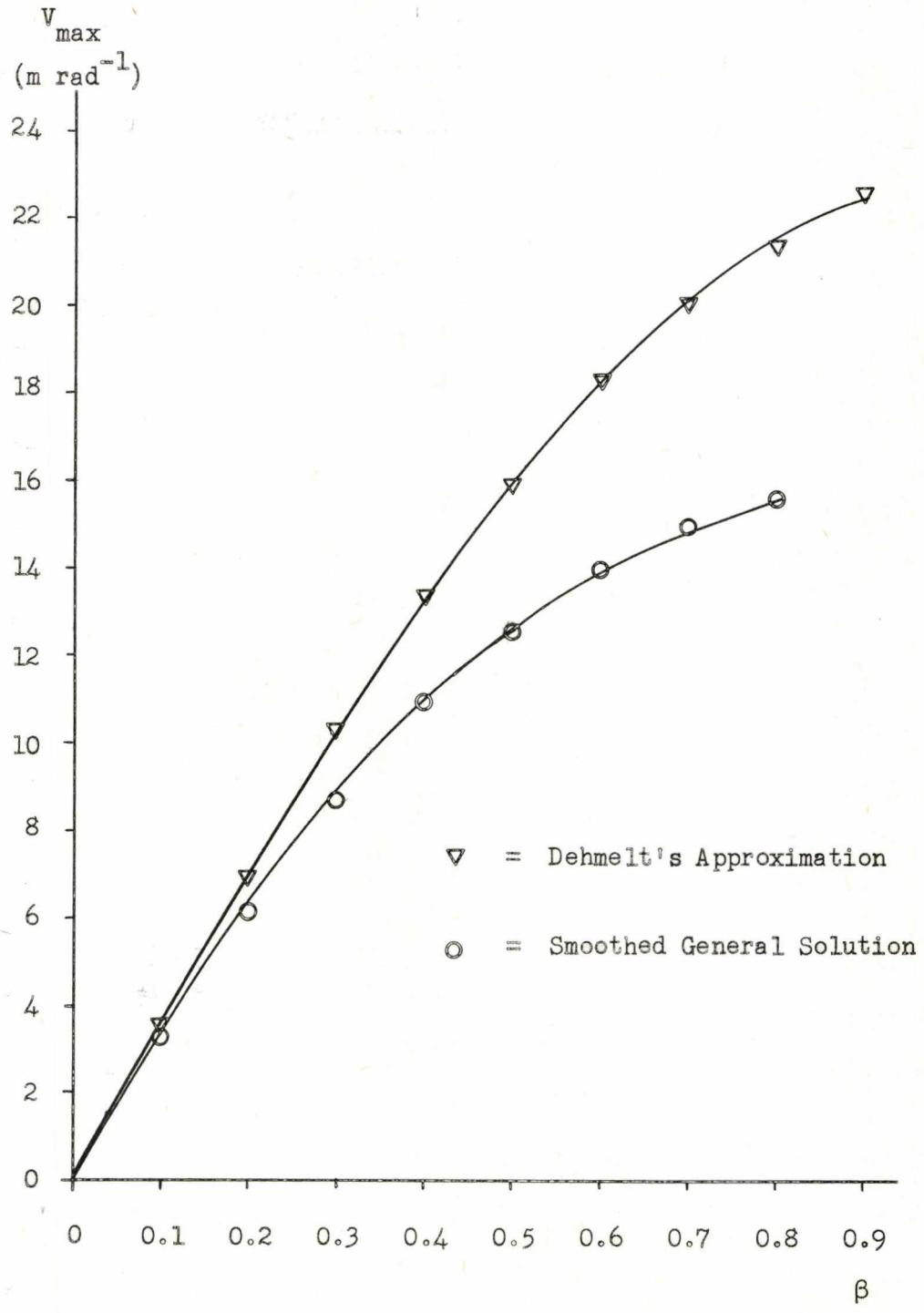

Figure 3-16. Mean Velocity vs. β for $z_o = 7.07 \times 10^{-3}$ metre.

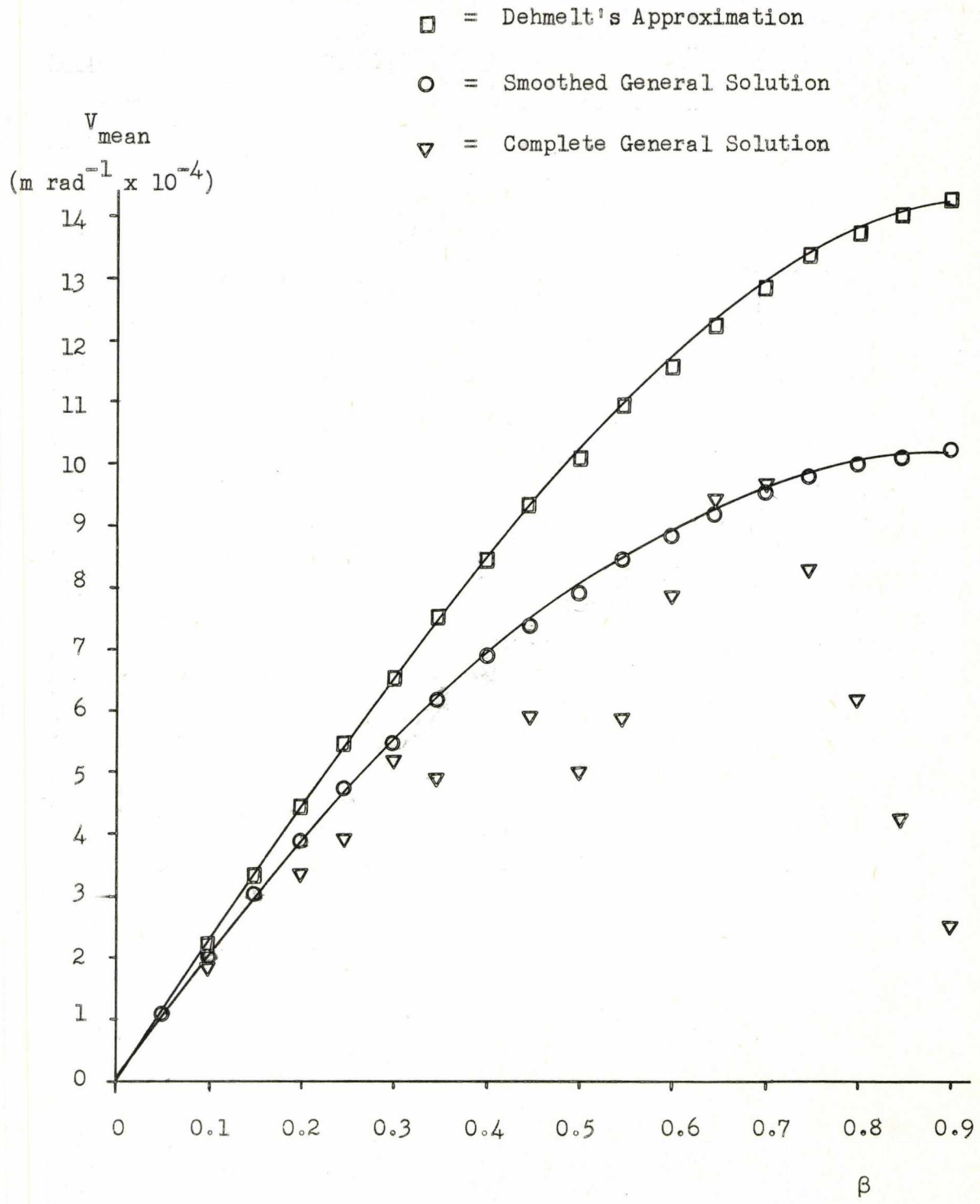

The results, however, are in excellent agreement in the region $0 < \beta < \sim 0.3$, which was the usual operating range of the QUISTOR.

As mentioned in Section 3.7, both directions must be considered for a practical device. The amplitude permissible in the r - direction is a factor of $\sqrt{2}$ greater than that in the z - direction, but the frequency is approximately one half, consequently :

$$\langle \dot{V} \rangle = (\langle V_r \rangle^2 + \langle V_z \rangle^2)^{\frac{1}{2}}$$

where $\dot{V}$ is velocity, and the subscripts denote direction.

where $V_z \propto z_o \omega_z$

$$V_r \propto r_o \omega_r = \sqrt{2} z_o \frac{\omega_z}{2}$$

$$\therefore \langle V \rangle^2 \propto \left(z_o^2 \omega_z^2 + \frac{z_o^2 \omega_z^2}{2}\right)$$

$$\therefore \langle V \rangle^2 \propto 1.5\, z_o^2 \omega_z^2$$

and $\langle V \rangle \propto 1.225 \langle V_z \rangle$

The results obtained from the preceding curves must, therefore, be multiplied by a factor of 1.225 to allow for ion motion in both directions.

In order to obtain either the mean or maximum energy of a particular ion, the relevant q - value must be determined from equation (3-28). The corresponding value of β is then obtained, either by calculation as described in Section 3.91 or from the graph shown in Figure 3-12. This then allows evaluation of the required velocity, again either by

calculation or from Figures 3-15 or 3-16, which may be expressed in the conventional units of metre second^{-1} by multiplying by the radial frequency of the applied RF. To obtain the energy in eV, the following equation is used

$$Ee = \tfrac{1}{2}mv^2$$

where E is the ion energy in electron volts. Finally, the motion in the r - direction is taken into account, and E multiplied by 1.5.

CHAPTER 4

The Experimental System

4.1 Introduction

The mounting of the QUISTOR on the analyzer - an ELECTRONIC ASSOCIATES INC. (PROCESS ANALYZERS INC.) EAI QUAD 250 A - is described in detail. The chapter is divided into three sections :

(i) Mechanical Construction - the mounting of the QUISTOR and electron gun are discussed.

(ii) Electronic Requirements - the various units required are described.

(iii) Ancillary Equipment - a description of the recording equipment, the analyzer and the vacuum system is given.

The first two sections consist of an account of the equipment that had previously been constructed, followed by a description of the modifications made during the course of this work. The ancillary equipment is discussed more generally, since the alterations made were of a minor nature.

Although the stainless steel QUISTOR had already been constructed, it had been abandoned because of experimental difficulties and a simpler mesh device employed. Accounts of the constructional details of both QUISTORs and the operation of the mesh device may be found elsewhere[37,38].

4.2 Mechanical Apparatus

4.21 Construction of the Original QUISTOR and Electron Gun

In the design of any quadrupole device, the main consideration is the desired mass range, which is dependent on :

(i) the size of the device (i.e. r_o), and

(ii) the RF power (frequency and voltage) to be applied,

and can be determined from the expression :

$$q = \frac{2eV}{m\Omega^2 r_o^2} \qquad \text{(Symbols as defined in Chapter 3)}$$

where, for total pressure operation, $0 < q < 0.9$.

A policy of duplicating commercial equipment was adopted, and the RF generator built was a copy of the ELECTRONIC ASSOCIATES INC. (E.A.I.) QUAD 250 A unit. As a result, condition (ii) above was specified as having a maximum voltage of 1200 Volts, at several fixed frequencies up to 3.3 MHz, using either laboratory-constructed coils or the E.A.I. originals. A value for r_o of 1 centimetre was chosen, allowing a mass range of 1-100 a.m.u. at 3.3 MHz, but small errors were introduced, however, by taking $r_o = 0.400$ inches, since all available lathes were graduated in inches. (0.400 inches = 1.016 cm).

The dimensions of the three electrodes are shown in Figure 4-1; each electrode was machined from 2 inch diamter stainless steel (18/8) rod, to an accuracy of 0.001 inches, the relevant co-ordinates being generated by a computer from the equations :

$$\frac{r^2}{r_o^2} - \frac{z^2}{z_o^2} = 1 \qquad \text{(End Caps)}$$

and

$$\frac{r^2}{r_o^2} - \frac{z^2}{z_o^2} = -1 \qquad \text{(Ring)}$$

with

$$r_o^2 = 2z_o^2$$

After machining, the electrode faces were highly polished to minimize surface irregularities. The flat areas surrounding each electrode were incorporated to allow accurate assembly by the insertion of suitable ceramic spacers.

The choice of material for the ceramics was governed by the necessity of their withstanding 1200 V at radio frequencies, and being

Figure 4-1 Stainless Steel QUISTOR Electrode Dimensions

METASTABLE ION EXPERIMENTS.
THREE DIMENSIONAL QUADRUPOLE ION STORAGE CELL. (QUISTOR).
UNIVERSITY OF KENT.

1 0·200" Radius curve uniform round centre electrode.
2 0·190" Radius centred on axis thro' 4.
3 Ion exit region 0·028" thick, containing 0 0·031" diam' holes.
4 Electron entrance and exit holes 0·064" diameter 0·064" long.

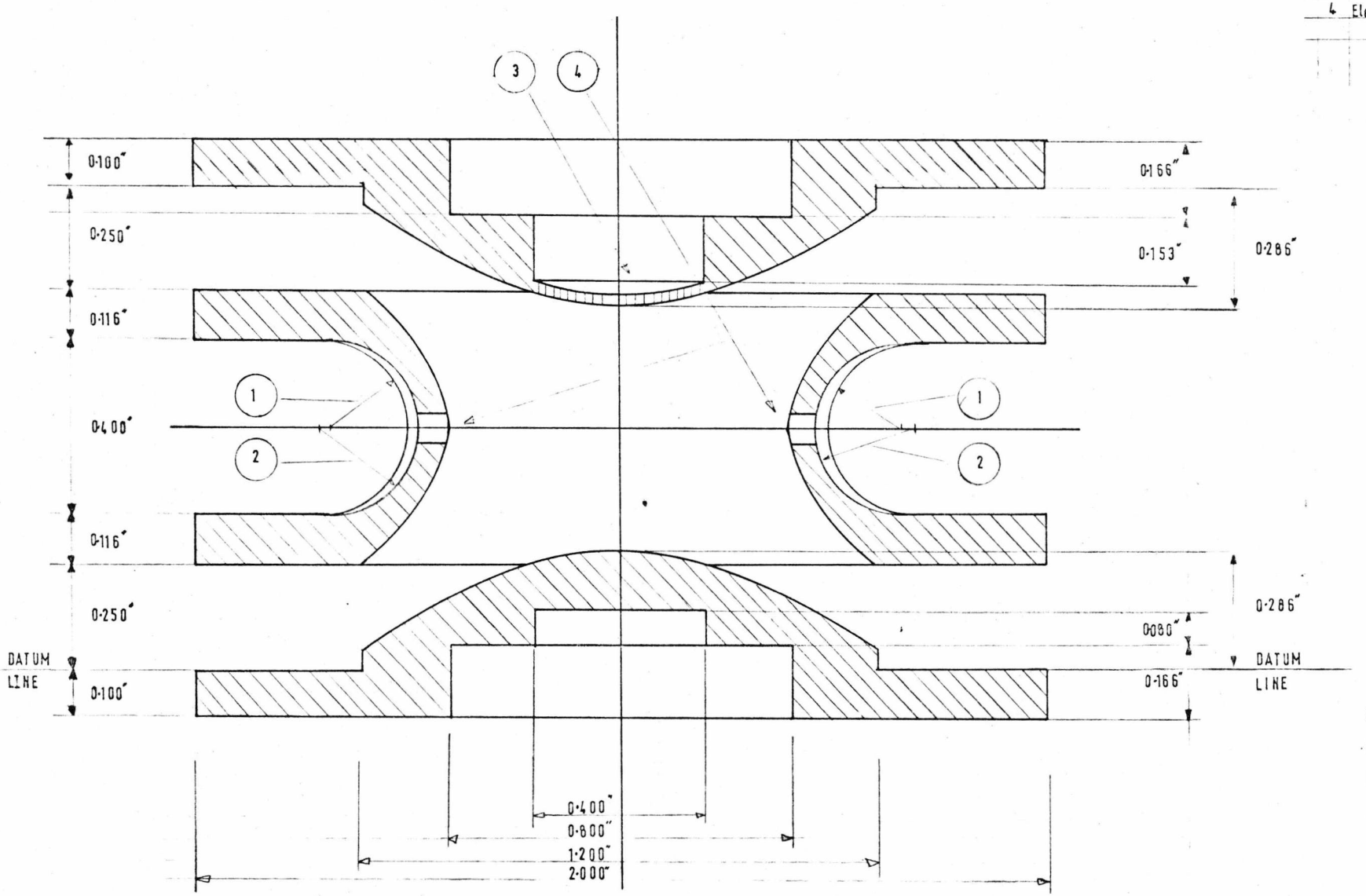

DIMENSIONS.	INCHES
SCALE.	4:1
DRAWN.	G. LAWSON.
APPD.	J.F.J. TODD.
DATE	2/11/69 9/1/69
DRAWING NO.	300/6

Figure 4-2 INSULATING CERAMIC DETAILS

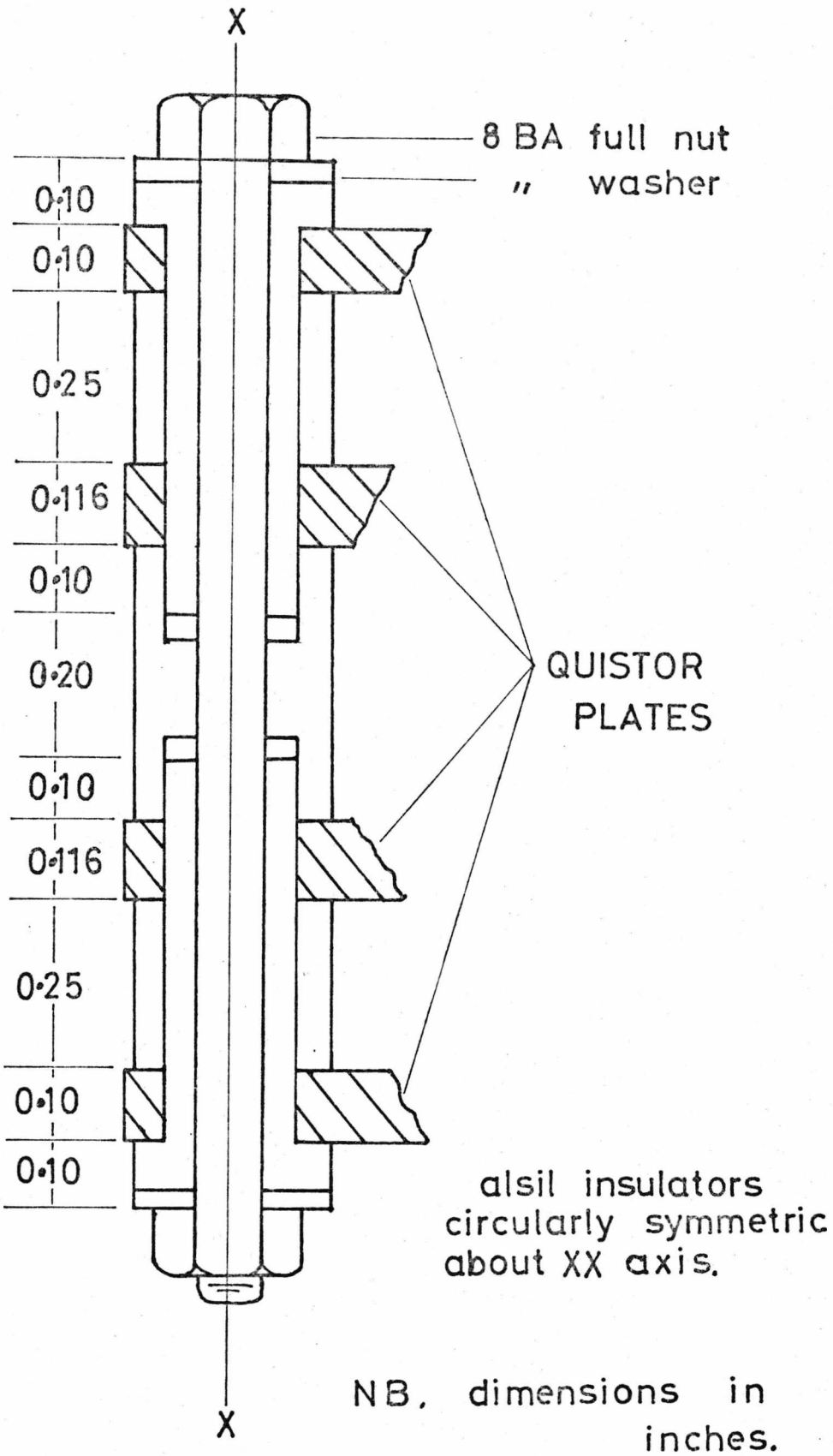

Figure 4-3 ASSEMBLED QUISTOR

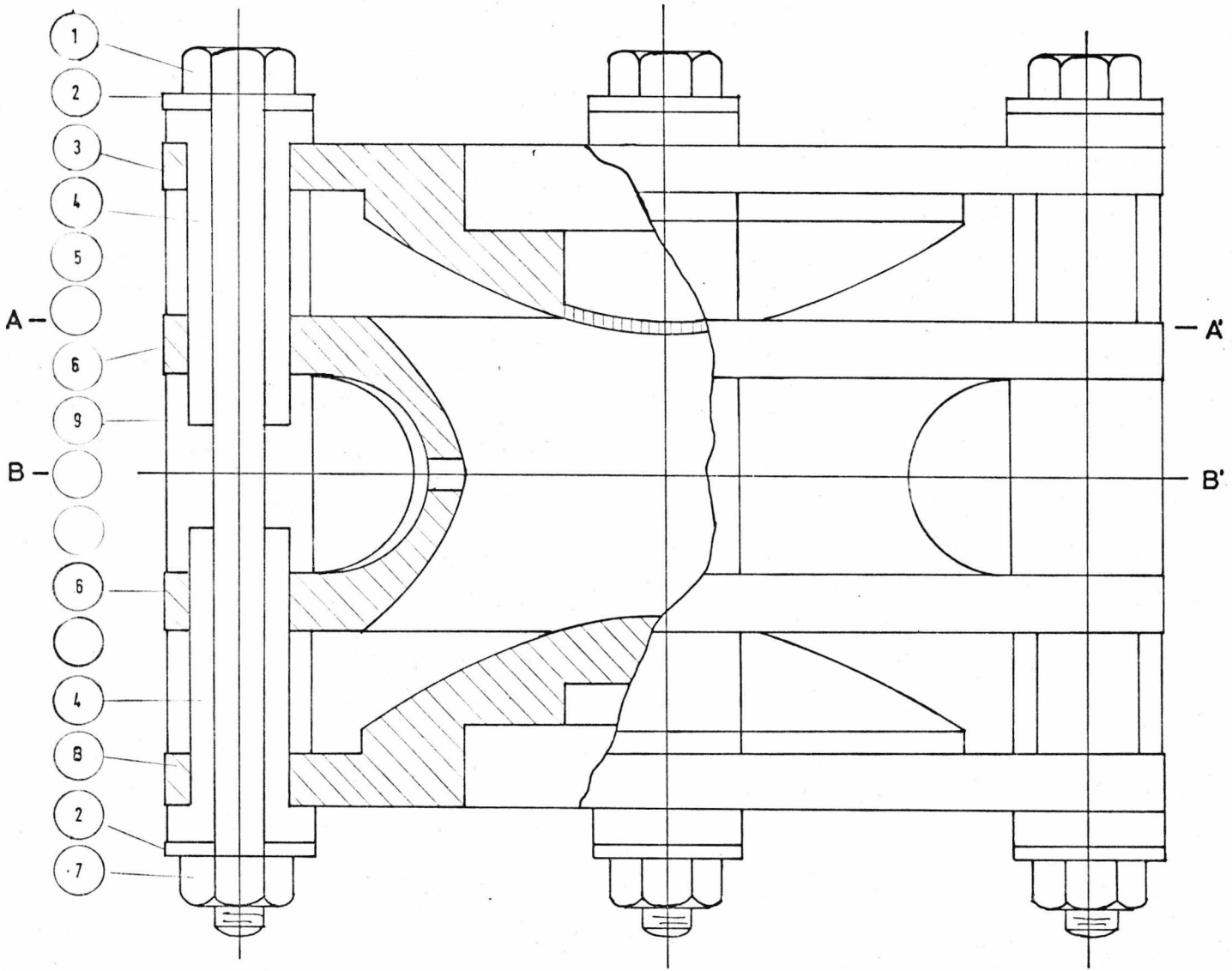

capable of machining to 0.001 inch accuracy; the chosen material was pyropholite (Trade Name : ALSIL). To maintain physical strength, and maximize the RF breakdown path length, the spacers were designed as shown in Figure 4-2.

The QUISTOR was designed to be supported by stainless steel rods, having 8 B.A. threads on each end, as shown in Figure 4-3. Figures 4-4 and 4-5 show sections through A - A' and B - B' (Figure 4-3) respectively. The upper electrode (Figure 4-4) was perforated, to allow ion extraction, this was accomplished by machining the central region as thin as possible, consistent with retaining mechanical strength - 0.015 inches - and drilling thirty 0.031 inch holes through the steel. The ring electrode was recessed, as shown in Figure 4-5, to allow close positioning of an electron gun.

In the original electron gun, electrons were produced by a heated ASSOCIATED ELECTRICAL INDUSTRIES (A.E.I.) Tungsten/Rhenium filament, supplied for use on an MS 10 mass spectrometer, the electron energy being defined by the steady potential difference between the filament and the ring electrode. Between the filament and the ring were positioned an electron beam gating plate, and two focussing plates.

The QUISTOR and electron gun were designed to be mounted on a 2 inch square stainless steel plate, fastened to a bellows assembly. Several experimental difficulties (see Section 4.22) necessitated extensive alterations, and a wire mesh QUISTOR and simpler electron gun were constructed, and mounted on the bellows. The assembly was inserted into the vacuum tank, and the bellows adjusted to position the QUISTOR next to the entrance aperture of the analyzer. A schematic diagram of the simplified electron gun is shown in Figure 4-6.

The electron gate was constructed from stainless steel sheet (20 gauge), in the shape of a five-sided box, to minimize RF pick up

Figure 4-4 (Upper). Section through A-A' (Figure 4-3).

Figure 4-5 (Lower). Section through B-B' (Figure 4-3).

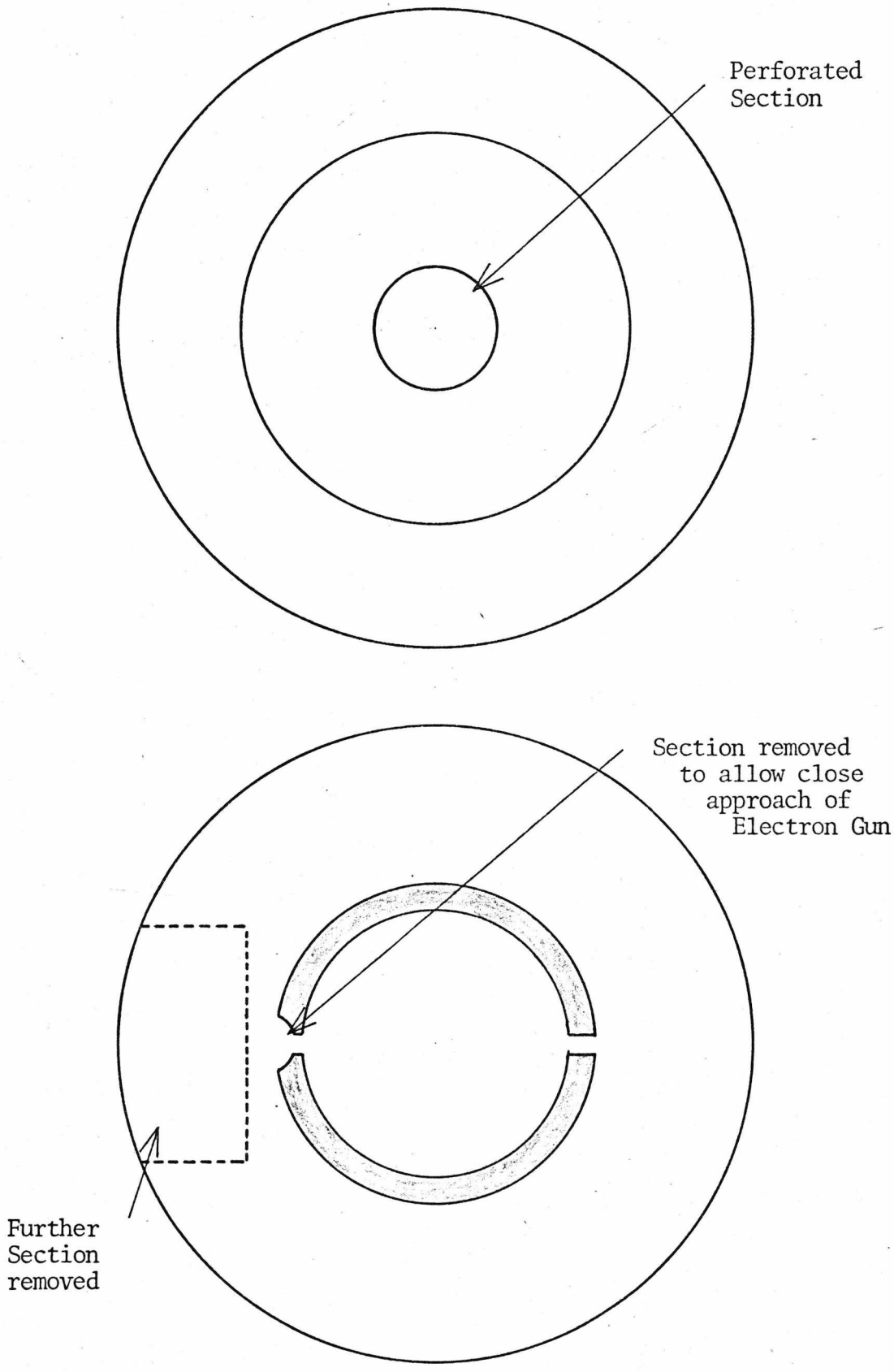

by the filament. The filament itself was supported by stainless steel barrel connectors in turn supported by shaped ceramics, Figure 4-6b, mounted on a stainless steel back plate. Connection to the filament was also made via the barrel connectors. The focussing and gating electrodes were mounted on 10 B.A. stainless steel bolts, and insulated with suitable ceramic spacers.

4.22 Modification and Mounting of the QUISTOR and Electron Gun

Attempts to use the experimental (stainless steel) system, previously described, were hampered by two major difficulties:

(i) It proved impossible to maintain alignment of the electron beam through the apertures in the ring electrode. This arose from vibrations of the rotary pumps causing the electron gun mounting bolts to loosen.

(ii) The resistance of the feedthroughs incorporated in the bellows assembly was found to be too large to allow the passage of adequate filament currents.

To overcome these difficulties, it was decided in this work to dispense with the bellows assembly, and to mount the QUISTOR directly on the QUAD 250 A, utilising source mounting components supplied by E.A.I. This allowed connections to the QUISTOR to be made via the low resistance feedthroughs on the QUAD 250 A support flange, but did present two minor disadvantages :

(i) The distance between the QUAD 250 A and the QUISTOR could not be varied easily, as was possible with the bellows assembly, and would entail dismantling and re-building the apparatus.

(ii) The apparatus must be mounted vertically in the vacuum tank to avoid possible distortion of the QUAD 250 A rods, owing to the additional weight of the QUISTOR.

Figure 4-6(a) Schematic of Original Electron Gun Design

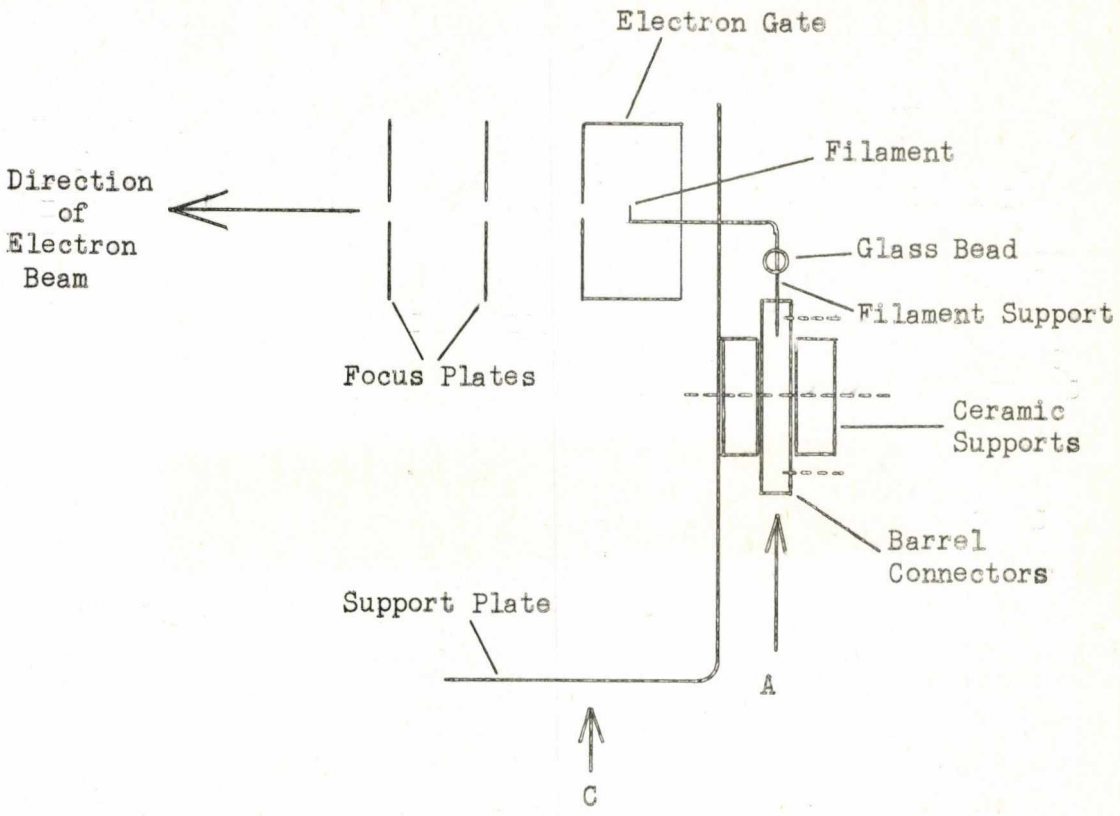

Figure 4-6(b) Support Ceramics and Barrel Connectors, Viewed from A.

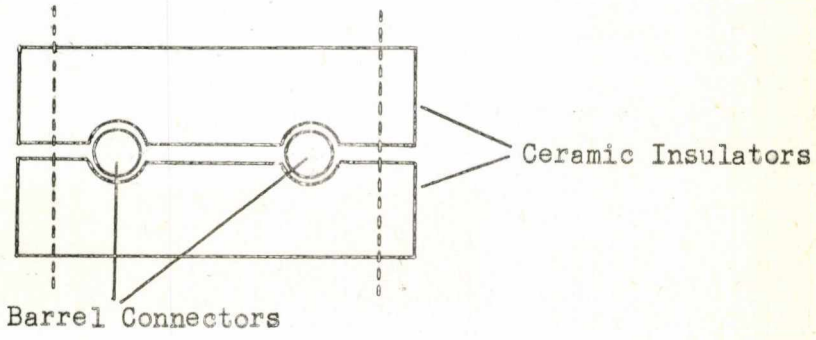

N.B. Dashed lines represent a 10 B.A. stainless steel nut and bolt. Electron Gate and focus plate supporting insulators omitted for clarity.

Figure 4 7

QUISTOR MOUNTING

SCHEMATIC

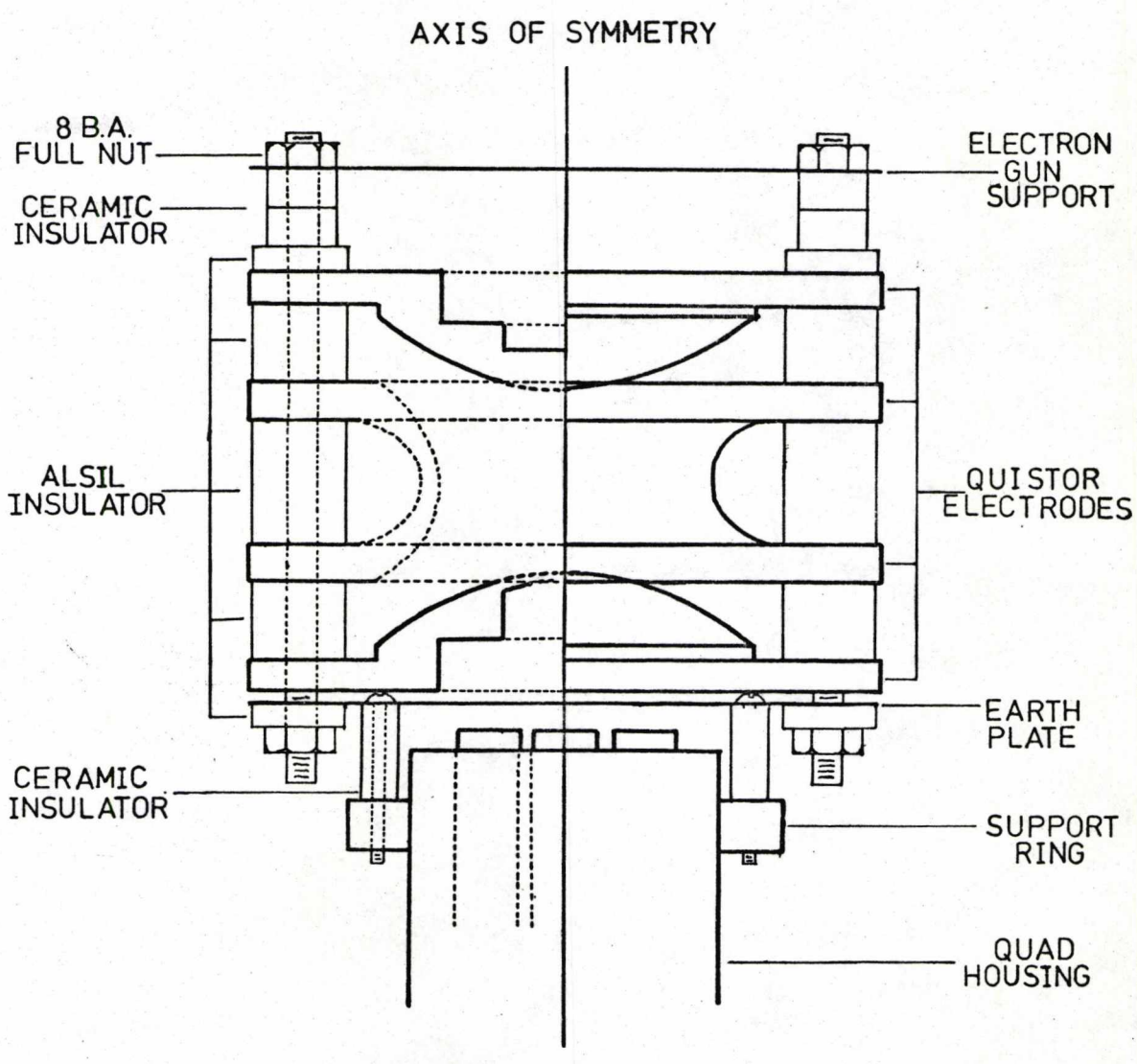

Scale: Twice Real Size.

N.B. Two Sets Of Bolts and Spacers Omitted For Clarity.

The method of mounting is now described in detail, and is illustrated schematically in Figure 4-7 and by a photograph of the assembled apparatus, Figure 4-8.

As can be seen from Figure 4-9, components of the conventional E.A.I. source are mounted on a stainless steel plate, which is bolted to a stainless steel ring, and separated from it by 8.5 mm alumina insulators. The support ring is attached to the cylindrical rod housing by four self-tapping screws. A similar method was adopted for mounting the QUISTOR; a 2 inch diameter plate was drilled in an identical manner to the normal ion source plate, but with a central $\frac{3}{4}$ inch aperture and the QUISTOR assembled with the ion-exit end-cap flush with the support plate (labelled 'earth plate' in Figure 4-7). This was then mounted on the support ring as shown (Figures 4-7 and 4-8). The stainless steel assembly rods were removed and replaced with 8 B.A. mild steel studding;

Figure 4-9. Schematic Diagram of E.A.I. Ion Source

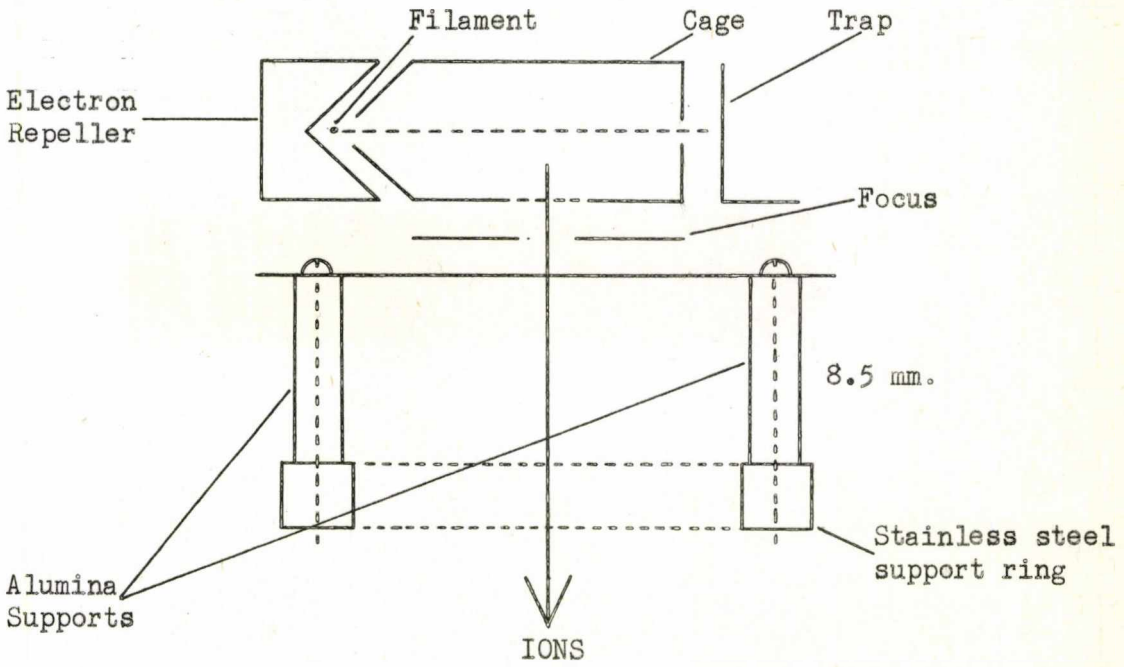

Figure 4-8. Photograph of Assembled QUISTOR Mounted on the Analyzer

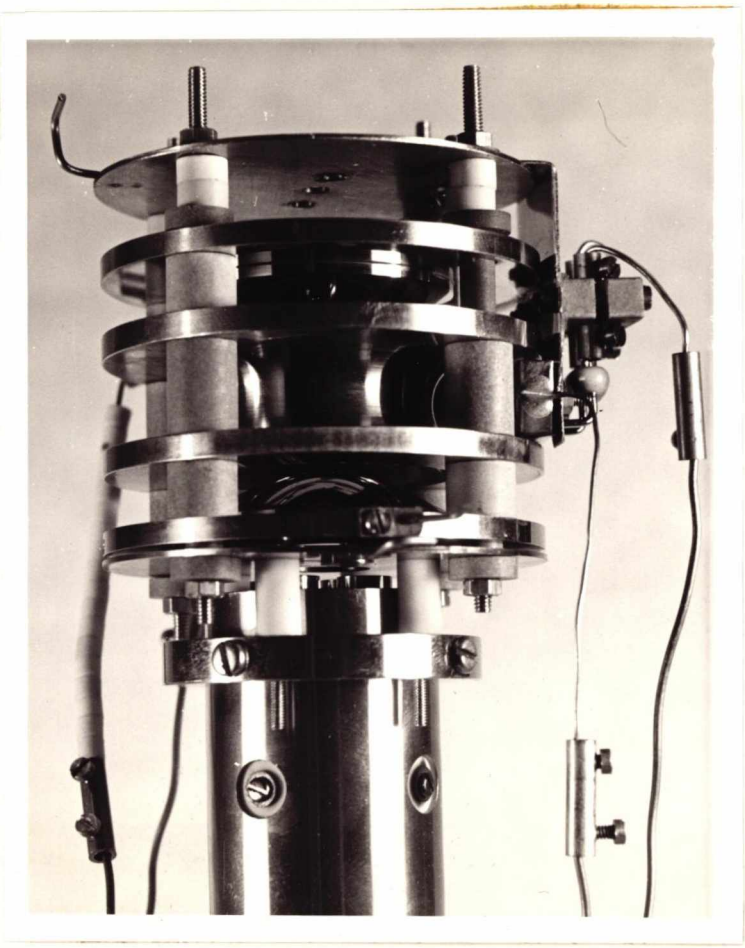

this allowed greater flexibility in mounting, particularly permitting the inclusion of two 3 mm ceramic insulators and the electron gun support plate. This method of mounting connected the ion-exit end-cap and the electron gun support plates to earth, and these, therefore, did not need further connection. The electrical connections to the other two QUISTOR electrodes were made *via* lengths of stainless steel wire spot-welded to small pieces of stainless steel plate, which were fastened to the electrodes by means of 10 B.A. bolts locating in 10 B.A. tapped holes. An example of these may be clearly seen in Figure 4-8.

Figure 4-8 also shows the electron gun and filament. The gun was similar to that described in Section 4.21 (see Figure 4-6), with the exception that the focussing plates were removed, allowing closer approach of the electron gate to the ring electrode, and no electron trap was used. The gun was supported by attaching the back plate (Figure 4-6) to the support plate (Figure 4-7) with a 6 B.A. stainless steel nut, bolt and washer. Two mutually perpendicular slots, as shown in Figure 4-10, were filed in the back and support plates to permit adjustment of the electron gun with respect to the ring electrode. Alignment of the electron gun proved fairly straightforward, and was effected by viewing the filament through both the holes in the ring electrode, and moving the gun assembly until the filament bisected these holes. Connection to the electron gate was made *via* a length of stainless steel wire silver-soldered in place.

Although this system worked quite well, several small drawbacks were encountered, and consequently avoided in a later mounting design.

(i) As mentioned earlier, the ion-exit end-cap electrode was permanently earthed; this did not permit examination of the effect of attractive, rather than repulsive, ion removal.

(ii) It was found that, while the electron gate was efficiently

shielding the filament from stray RF pick-up, it was itself suffering from this effect with consequent deterimental results.

(iii) The mounting and positioning of the electron gun were critical, since it was conceivable that the back plate might come into contact with the ring or upper end-cap (Figure 4-8) with subsequent shorting of the RF and/or pulse voltage to earth. This possibility was thought even more likely because of the vibration caused by the rotary pumps, and in this design small pieces of mica sheet were inserted between the upper end-cap and the back plate, between the ring and back plate, and between the ring and the electron gate, as preventative measures.

In order to overcome (i) above, and allow separate connection to the ion-exit end-cap, the mounting system shown in Figure 4-11 was adopted.

Figure 4-10 Electron Gun Support

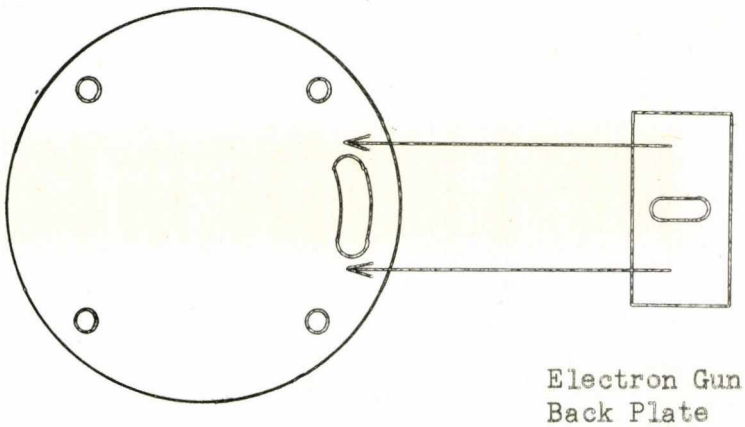

Figure 4-11 Diagram of Modified Mounting

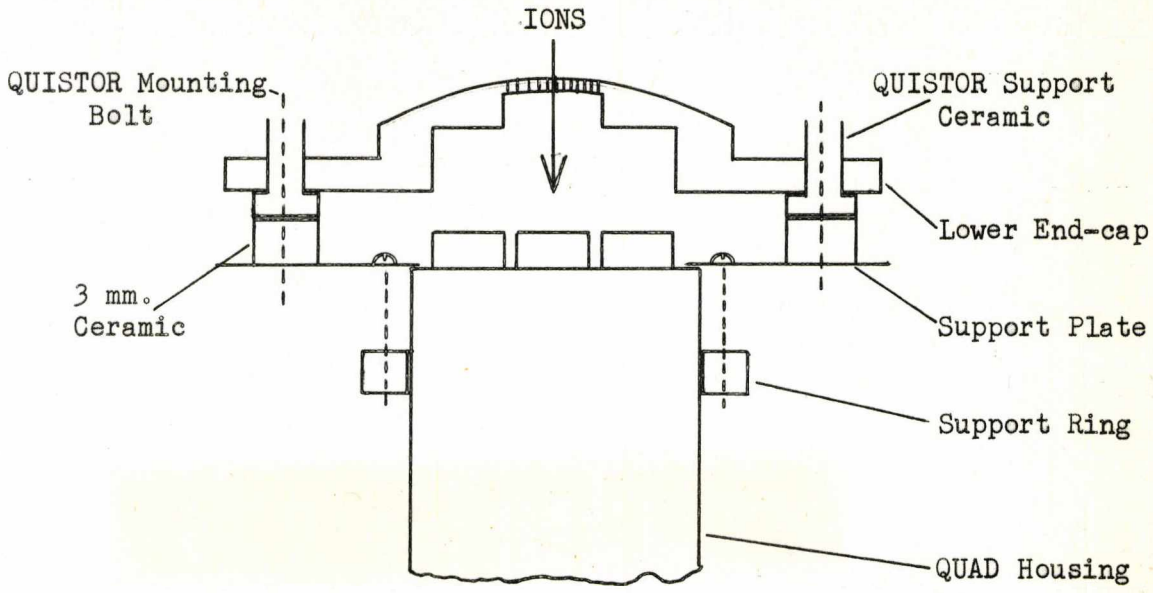

The same QUISTOR support plate as described earlier was used, but the diameter of the central hole was increased to 1 inch, to enable it to rest on the rod housing. The ion-exit end-cap was spaced 3 mm away from this plate with suitable ceramics.

To enable fast interchange of the QUISTOR and conventional ion sources, a separate brass support ring, of similar dimensions to the stainless steel version previously employed, was constructed for the QUISTOR.

At this stage, the necessity of employing sheets of mica as insulators was removed by having a section of the ring electrode milled away; this is shown dotted in Figure 4-5 and is clearly visible in Figure 4-12. The section was 1 inch long, and was centered on a line joining the mounting holes adjacent to the electron entrance in the ring electrode. Metal was removed until the thickness of flat area (before the start of the hyperbolic face) was approximately 0.1 inches.

Figure 4-12. Photograph of Modified Mounting, shown Schematically in Figure 4-11.

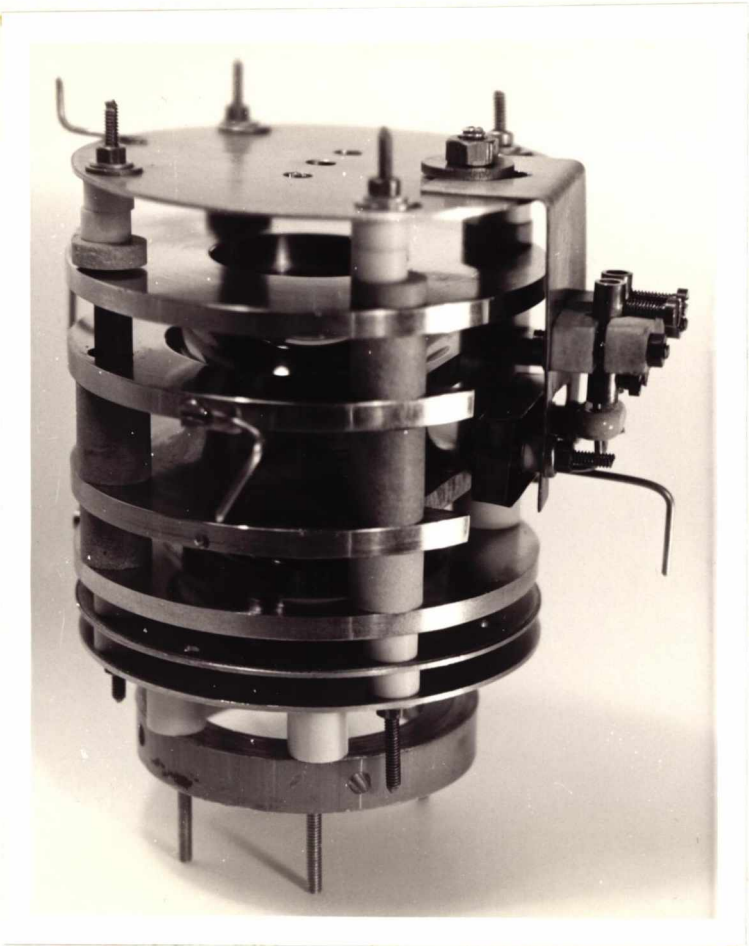

Figure 4-12 also shows the mounting of the electron gun, which was re-designed to prevent RF pick-up by the electron gate, (iii) above. This was achieved by the inclusion of a small stainless steel rectangle as the electron gate, and the use of the previous box-shaped gate as an earthed shield, Figure 4-13 depicts this schematically.

Using this arrangement, minimal RF breakthrough to the electron gate was encountered, connection to the gate being made via a length of stainless steel wire attached by spot-welding.

At a later date, the 3 mm spacers, shown in Figure 4-11, were each replaced by two 2 mm ceramic spacers and an additional 2 inch diameter plate with an 0.5 inch central hole, as may be seen in Figure 4-12. This modification was incorporated to examine the effects of some focussing of the ion beam but, unfortunately, the available voltage supplies (0 $\pm$ 100 V DC) did not improve the focussing noticeably; in fact since the QUAD-QUISTOR distance had been increased, the signal output deteriorated, and the design shown in Figure 4-11 was reverted to.

Figure 4-13 Modified Electron Gate

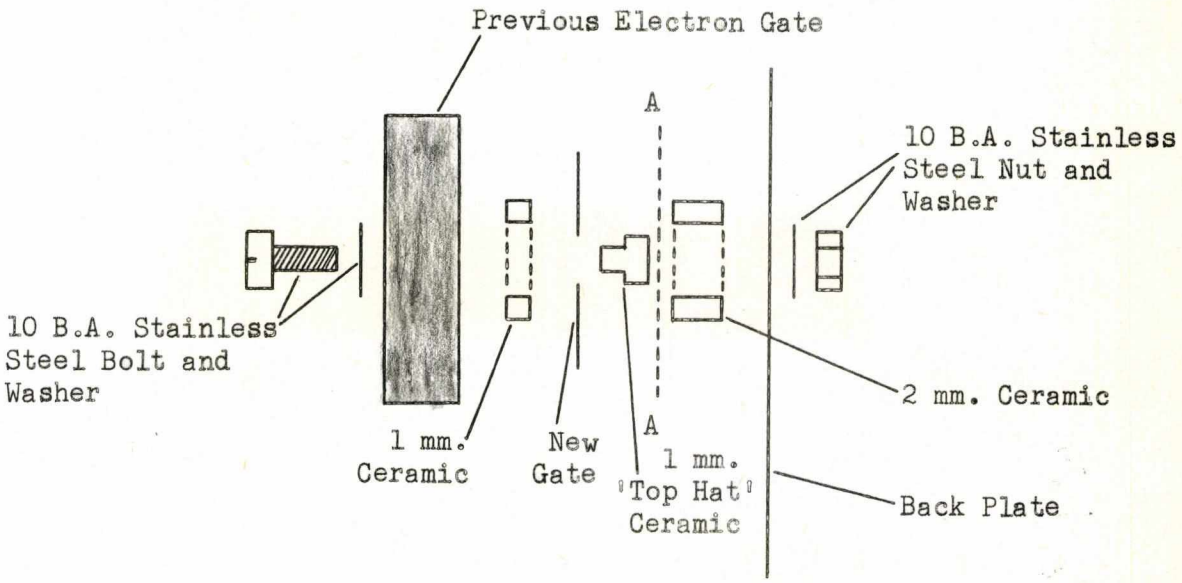

N.B. A - A represent the filament position

The A.E.I. filaments, used in the earlier part of this work, became unobtainable and replacement filaments were constructed using old supports, which were carefully cleaned with a small file, to remove old connections, before spot-welding a new length of filament wire in place. Three types of filament were constructed in this way :

(i) 0.007 inch rhenium wire;

(ii) 0.005 inch tungsten wire;

(iii) 0.001 x 0.030 inch tungsten ribbon.

All of these required a nickel 'sandwich' to be welded to the molybdenum supports, before the actual filament wire could be welded. The spot-welder used was a HUGHES AIRCRAFT COMPANY VTA-60 High Precision Welding Head. The tungsten ribbon filaments proved to be the most satisfactory, because of their high durability and the relatively large electron currents produced.

4.3 Electronic Requirements

4.31 Original Electronic Apparatus

As mentioned in Section 4.21, a policy of duplicating commercial electronic equipment had been adopted, and the two basic units required for operation of the QUISTOR were constructed in this manner. The RF generator was a laboratory-built copy of the E.A.I. QUAD 25C A, somewhat modified for available British components, and simplified by removal of the scanning circuitry, since the intended operation was at fixed RF amplitudes. An AC filament supply was constructed, based on the design of a unit supplied by A.E.I. for use with the MS 10 mass spectrometer.

The QUISTOR RF generator consisted of an EHT power supply and a high voltage oscillator. The former delivered 1200 Volts at 1500 mA, with a maximum ripple of 20 mV, while the oscillator supplied two outputs, mutually 180° out of phase, although only one of these was

employed. The amplitude of the output was controlled by a 0 → -100 Volt level, supplied to the unit in the opposite sense, that is the lower the DC bias, the higher the RF output. The RF frequency was varied by switching between plug-in coils; a 1 MHz coil was constructed giving, in conjunction with E.A.I. units, outputs at 1.0, 1.8 and 3.3 MHz. On connection of these supplies to the QUISTOR each frequency underwent a ca. 20% decrease, owing to the large additional capacitive loading introduced. The oscillator was equipped with two variable capacitors in the output circuitry, permitting slight adjustment of the RF frequency and waveform.

A schematic diagram of the A.E.I. MS 10 'Electron Beam Control Unit', showing the various voltage outputs, is given in Figure 4-14.

The filament supply provided ca. 5 Amps with a 2 Volt, 100 Hz, potential drop across the filament; the DC level of the filament could be set between -5 and -105 Volts by means of a ten-turn helipot

Figure 4-14 A.E.I. Electron Beam Control Unit

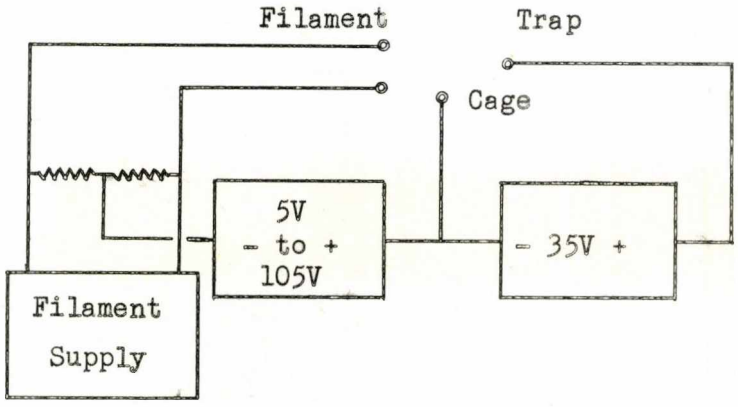

'Electron Energy' control. Operating with an MS 10, 35 Volts would be applied to the electron trap, causing a fraction of the electron current to be collected and 'fed back' to stabilize the filament supply. The cage, in this circuit, acts as a reference point for the filament and trap voltages; and a connection was made between this and the ring electrode via a low pass filter. This allowed the ring to be operated at a fixed DC level, without disturbing the electron optics or permitting RF to reach the filament supply unit. The circuit of the filter is shown in Figure 4-15. With 1000 Volts applied to the ring electrode, the voltage output from this unit to the cage was less than 1 Volt.

The units described above were capable of operating the QUISTOR under storage conditions, but with no control over the storage time. To 'gate' the electrons a negative voltage was applied to the electron gate, and periodically nullified by application of a positive pulse applied via a filter. Consequently, two pulse generators were required; the units used were Hewlett-Packard (HP) 214A's, having the following specification :

Figure 4-15 RF Interface

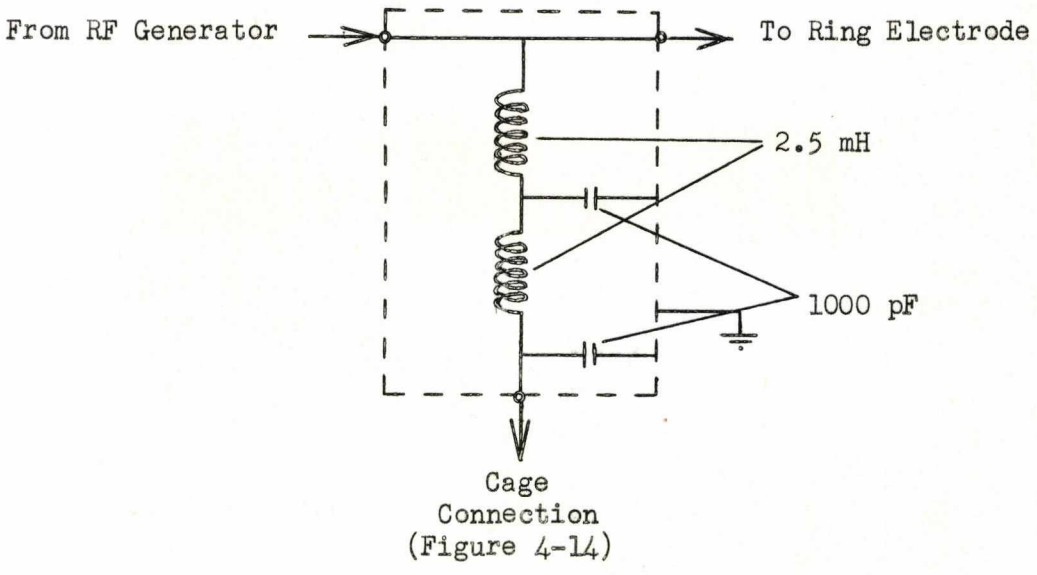

Output Pulse : Continuously variable between 8 mV and 100 Volts, with either polarity, in 9 ranges. Typically, the rise and fall times are better than 15 nSec.

Repetition Rate : 10 Hz to 1 MHz continuously variable in 5 ranges (internal triggering) or DC to 1 MHz (external triggering).

Three internal modes of operation permit :

(i) Setting of the output pulse to occur from 0 to 10 mS before the trigger output.

(ii) Setting of the output pulse to occur from 0 to 10 mS after the trigger output.

(iii) Double pulsing with variable delay between pulses.

In addition, when triggering one generator from another, the triggered generator may have its output delayed by 0 to 75 or 80% of the pulse repetition period.

To prevent pulses from reaching the electron gate bias supply, a further low-pass filter was incorporated. This was resistive-capacitive and, while working adequately, caused some loss of height and distortion of the shape of the pulse reaching the QUISTOR.

4.32 Modification to the Original Electronic Equipment

During the course of this work it became apparent that a DC filament supply would be advantageous, since the AC unit imposed a 100 Hz modulation on the ion current pulses. The E.A.I. 'Ionizer Control' unit was employed for this purpose, and also delivered 5 Amps at 2 Volts. This supply differed in that it was emission, rather than trap, current stabilized, the emission current being measured between filament and cage (see Figure 4-9). In operation here, the trap was disconnected and the cage connected to earth; it was found that the 'Emission' meter still registered a current, corresponding to the

electron current striking the earthed plate. Consequently the filament was stabilized with this unit, and the emission could be controlled; this is in contrast to the AC supply which, since a trap was not used with the stainless steel QUISTOR, drove the filament to the limit of the available power. Correct operation of the electron gate could be verified by ensuring that the emission current dropped to zero as the bias on the gate was increased.

The original low-pass filter in the gating circuitry was replaced by that shown in Figure 4-16; this introduced no measurable distortion to either the amplitude or shape of the pulses.

4.4 Ancillary Equipment

4.41 Recording Equipment

The original SERVOSCRIBE MODEL 1 X-T pen recorder was replaced by a BRYANS SOUTHERN INSTRUMENTS LTD. MODEL 26000 A3 X-Y recorder. This had the advantage that the scans at different storage times could be displaced in the Y-direction only, allowing direct comparison between spectra. The X-drive was provided by the analyzer control unit, and the Y-drive taken directly from the electron multiplier output. Typically,

Figure 4-16 Ion Creation Pulse/DC Interface

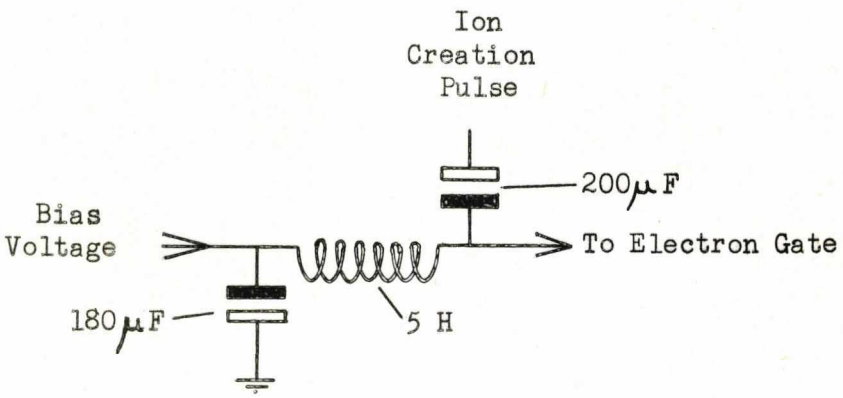

scan speeds were in the region of 1 amu/second causing 100 ion pulses per amu at the recorder (for a source repetition frequency of 100 Hz). This pulsed signal was averaged by the pen recorder over the pulse period, with a corresponding reduction in intensity. This is discussed further in Chapter 5.

For examining ion pulse shapes, measuring storage times and checking system behaviour, a TEXTRONIX INC. Model 585A oscilloscope was employed; this instrument was equipped with a Type 82 dual-trace plug-in unit having a frequency response of DC to 85 MHz.

Two operation amplifiers were available, although their use was avoided since the gain is dependent on signal frequency. They were obtained from ANCOM LTD. and were a type 15 A-1 and 15A-71 having current gains of x 10 and x 2000 respectively.

4.42 The Quadrupole Mass Filter

The QUAD 250 A, supplied by E.A.I., had the following brief specification :

Mass Ranges :	LOW	1 - 100 amu
	MEDIUM	10 - 250 amu
	HIGH	50 - 500 amu
	HIGH	50 - 800 amu

Resolution : Better than twice the mass number on the Low and Medium mass ranges (e.g. >200 at m/e 100). Better than unity on the High mass ranges (e.g. >300 at m/e 300).

Scan Speeds :
(i) Continuously variable from 50 mSec. to 30 min. for each mass range.
(ii) Continuously variable from 500 mSec. to 6 min per amu.

Figure 4-17

VACUUM SYSTEM SCHEMATIC

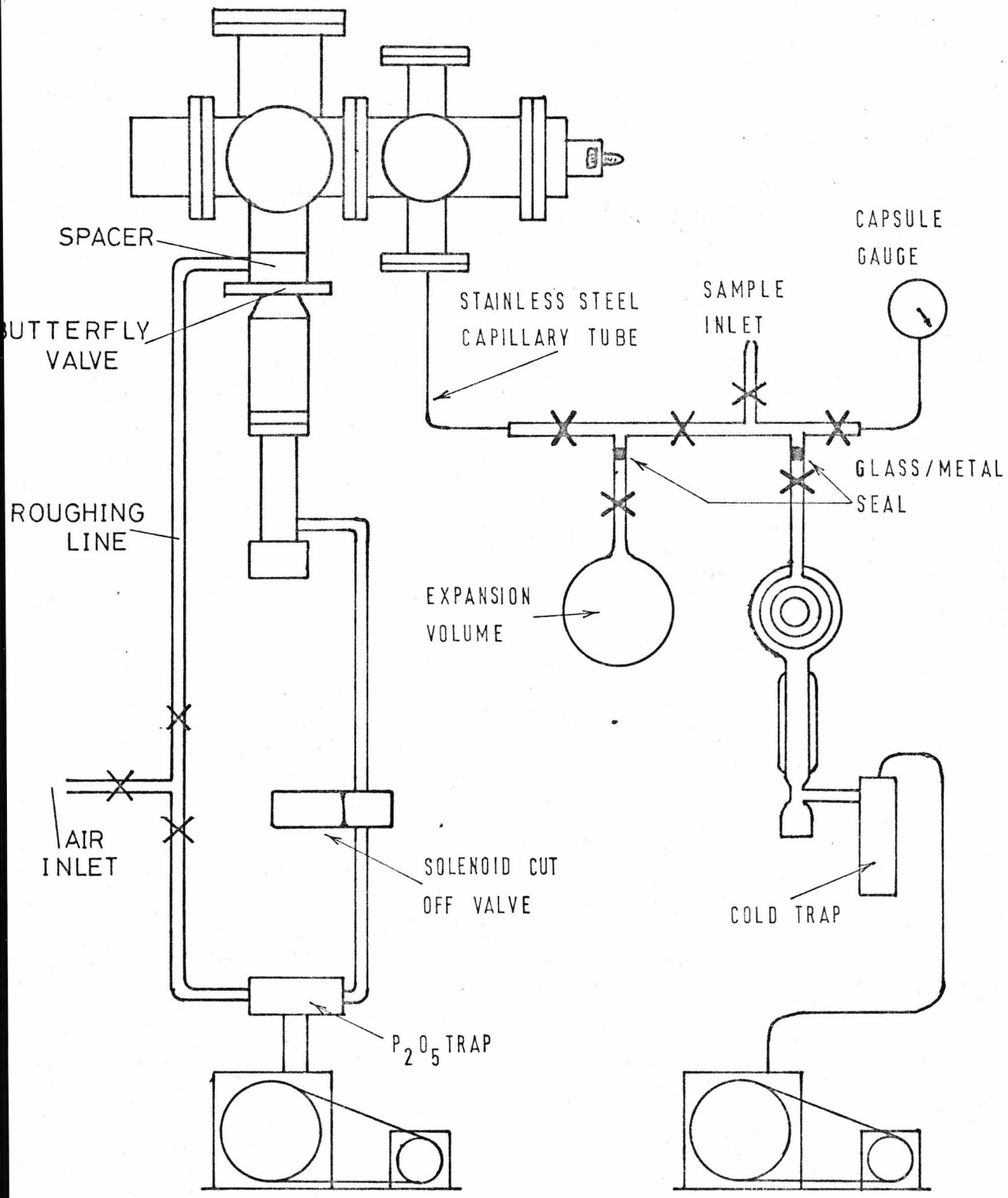

This instrument also has the facility for single peak and total pressure monitoring.

4.43 The Vacuum System

A schematic diagram of the vacuum system and inlet system is shown in Figure 4-17. The only modification made to this section of the apparatus was the inclusion of a Quarter Swing Butterfly valve (Model QSB2) and a 2 inch spacer, to allow the roughing line to be included. These were provided to enable fast removal of the QUISTOR system, for inspection and maintenance, followed by quick re-evacuation. The additional vacuum components were supplied by EDWARDS HIGH VACUUM LTD.

The system was pumped by an EDWARDS E02 2 inch oil diffusion pump, capable of a pumping speed of 150 litre second^{-1}, backed by an EDWARDS ED35 double stage rotary pump. Pressure measurement was by a VACUUM GENERATORS VIG10 ion gauge and IGP2 controller.

The inlet system was evacuated by a laboratory-constructed mercury diffusion pump, backed by an EDWARDS ES50 single stage rotary pump, pressures being measured with an EDWARDS GC3 0-100 Torr Capsule gauge. Samples could either be expanded into the 2 litre volume or not, as desired. Unfortunately, the inlet system was un-heated, and consequently only samples with high volatility could be admitted.

CHAPTER 5

Characteristics of the QUISTOR, When Employed as an Ion Source

5.1 Introduction

This chapter contains a description of experiments which were performed in order to optimise the operation of the QUISTOR; in particular the effect of varying the amplitude of the applied RF was examined, since it was observed that the signal strengths obtained were dependent on this quantity. It is shown that this had no effect on measured rate constants, other than caused by variations of the primary ion kinetic energy. All calculated ion energies, quoted throughout this and the following chapters, were evaluated by considering contributions from the ion motion in both the r- and z- directions, that is energies for the z-direction were calculated from the equations and graphs presented in Chapter 3, and multiplied by a factor of 1.5. It is also shown experimentally that ion kinetic energies calculated in this manner were within the correct range.

The inlet system capsule gauge was calibrated employing the well-known rate constant for the disappearance of the CH_4^+ species in methane :

$$CH_4^+ + CH_4 \longrightarrow \begin{cases} CH_5^+ + CH_3 \\ CH_3^+ + H_2 \end{cases}$$

In addition, data on ion build-up and decay processes in the QUISTOR were collected and are compared with similar quantities reported by other workers.

5.2 The Electron Gun

Since the major proposed investigation of the QUISTOR was a study of its use in the ion storage mode, the particular characteristic of interest of the electron gun was its behaviour in the presence of an RF voltage. As the maximum amplitude of the RF was 1000 Volts, it seemed

probable that the electron energy would oscillate widely with the RF, and that it would be 'cut-off' when the oscillating voltage resulted in the ring electrode being more negative than the filament. The electron beam intensity was examined by mounting a small trap in its path, and its energy spread investigated by two methods :

(i) attempting ionization efficiency plots for argon and other rare gases.

(ii) by measuring the trap current as a function of a negative voltage applied to the electron gate.

The AC filament supply had previously been characterized in detail,[37] and consequently this work was concerned with the E.A.I. unit.(See Section 4.32). Although in the storage mode the electron beam was pulsed, these measurements were performed with continuous ionization in order to facilitate electron current observation; this did not invalidate the results, since the beam characteristics would not be altered by pulsing. In all cases the emission current, that is the current between the filament and the earthed shielding box, was indicated as being 3mA.

Two electron beam traps were constructed; the first comprised a 4 x 1 cm. strip of stainless steel sheet, bent into a right angle and spot-welded to a 2 inch diameter stainless steel plate. This plate was mounted in place of the upper end-cap (Figure 4-7) so that the trap was in the centre of the ring electrode, and intersected the electron beam. This is shown schematically in Figure 5-1.

As it was intended to operate the QUISTOR without an electron collector, electron currents were measured between the trap and earth with a MODEL 8 AVOMETER, without the inclusion of a positive collector voltage. It was hoped that the large time constant of the AVOMETER, compared to the RF period, would result in the effect of the RF voltage being averaged to zero permitting direct observation of the electron currents.

Figure 5-1. Mounting of First Electron Trap

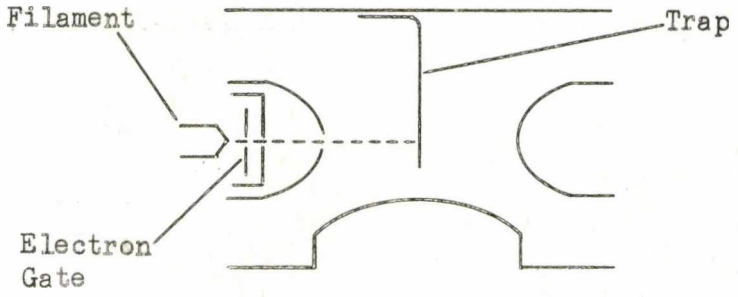

In practice, this was not found to be the case: the various metal-metal junctions caused partial rectification of the RF, resulting in a large DC current at the AVOMETER which completely swamped the fairly small trap currents. Consequently, the use of this trap was abandoned, although some measurements, made without RF applied to the device, indicated currents in the range 20-30 μA.

The second trap was constructed from a 1 cm. square of 18 gauge copper sheet, securely soldered to 16 gauge copper support wires. It was mounted outside the ring electrode, intersecting the electron beam after its passage through both apertures. A reduction in measured trap currents was expected, but this arrangement did have the advantage that the upper end-cap was retained, permitting simultaneous ion and electron current measurements. Trap currents recorded in this manner were in the range 15-25 μA, indicating fair electron focussing, which was supported by the observation that the electron burns on the ring electrode were centred on the entrance and exit apertures.

5.21 Measurements on the Electron Beam in the Absence of an Applied RF Voltage

The electron energy was displayed on the E.A.I. unit as the voltage between the filament and ring electrode, normally earthed, and this measurement tended to be inaccurate owing to the junction potentials and resistances of the leads and connections. Consequently, this voltage was measured across the connections to the vacuum tank, using a SOLARTRON LM 1450 Digital Voltmeter, and plotted against the nominal electron energy. A schematic diagram of the experimental system employed is shown in Figure 5-2.

The three QUISTOR electrodes, and the electron gate, were connected to earth, trap currents again being measured with the AVOMETER. The results, shown in Figure 5-3, indicate that maximum electron currents were obtained at high electron energies, as a result of focussing effects. Consequently, maximum ion currents would be obtained with the electron energy as high as possible, consistent with the ability to switch off the electron beam when operating in the ion storage mode. Information on the energy spread inherent in the electron beam, and the voltage required to turn it off, was obtained by connecting a DC voltage generator (0→-100Volts) to the electron gate, and recording the trap current as a function of this voltage. The results obtained, for electron energies of 50, 60 and 70 eV, are reproduced in Figure 5-4, the horizontal axis of which is the quantity (Electron Energy - Electron Gate Voltage). Ideally the trap current should vanish when this quantity becomes zero, but it is apparent from Figure 5-4, that this was not the case, and that a large proportion of the electrons have energies greater than the filament voltage. Consequently, a large negative voltage was necessary to switch off the electron beam. The electron beam energy spread was also investigated by performing ionization

Figure 5-2. Mounting of Second Electron Trap

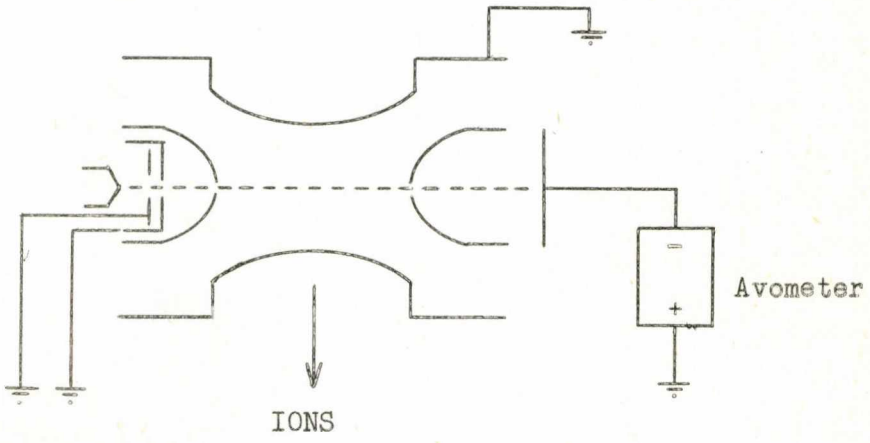

potential plots, using the experimental arrangement shown in Figure 5-2, but with a positive DC generator connected to the upper end-cap to ensure continuous ion removal. A possibility existed of the electrons undergoing acceleration towards the positive end-cap after entering the device with a resultant increase in electron energy. The results obtained, shown in Figure 5-5, indicated that while this effect was occurring to a small extent, the curve at 10 Volts ion extraction being shifted by approximately 10 Volts while that at 40 Volts was only shifted by approximately 12 Volts, most of the energy spread was in the beam itself.

5.22 Measurements on the Electron Beam with an RF Voltage Applied to the Ring Electrode

Although the second electron trap also suffered from RF pick-up, direct observation of the trap current was possible up to certain RF

Figure 5-3(a). Indicated vs. Actual Electron Energy

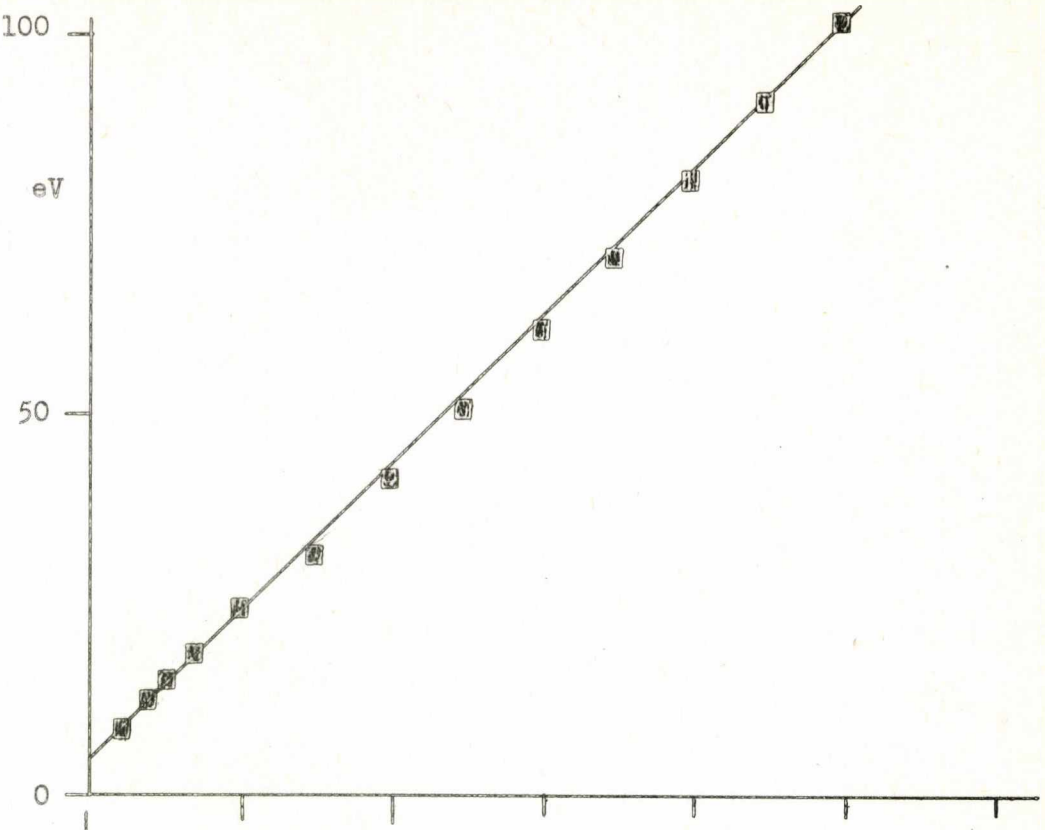

Figure 5-3(b). Trap Current vs. Electron Energy

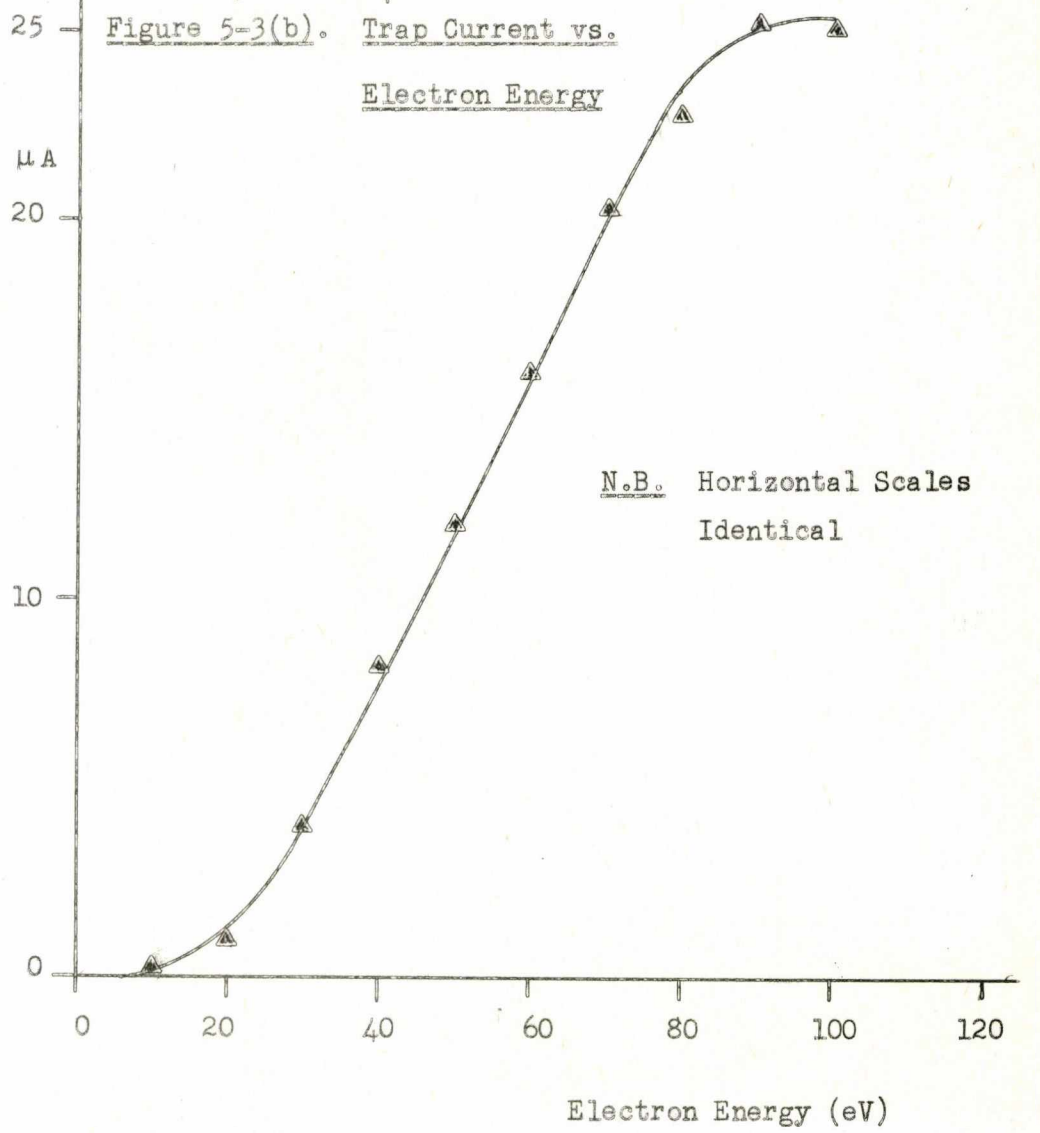

N.B. Horizontal Scales Identical

Figure 5-4. Trap Current vs. Electron Gate Voltage

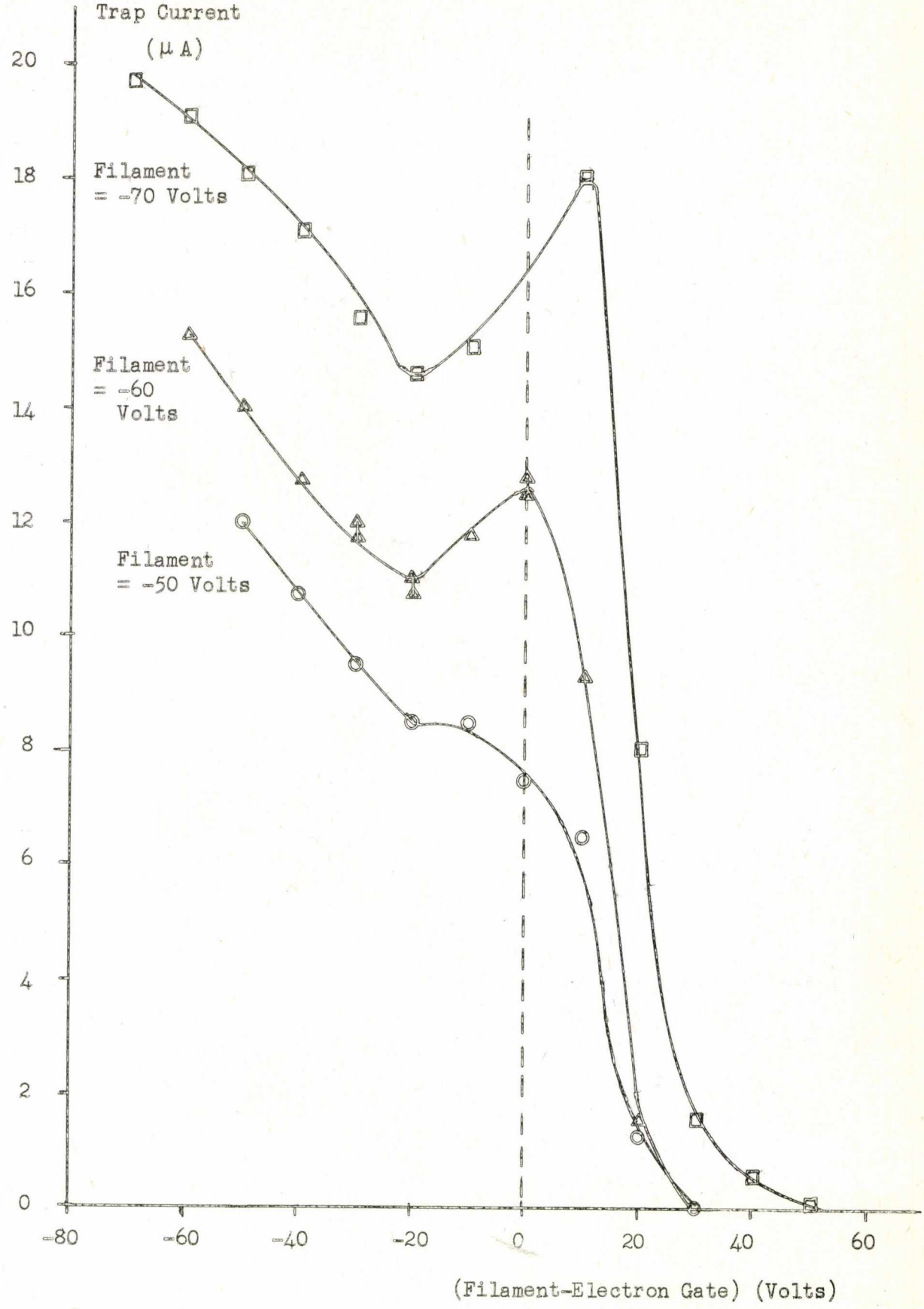

Figure 5-5. Ionization Potential Plots for Argon

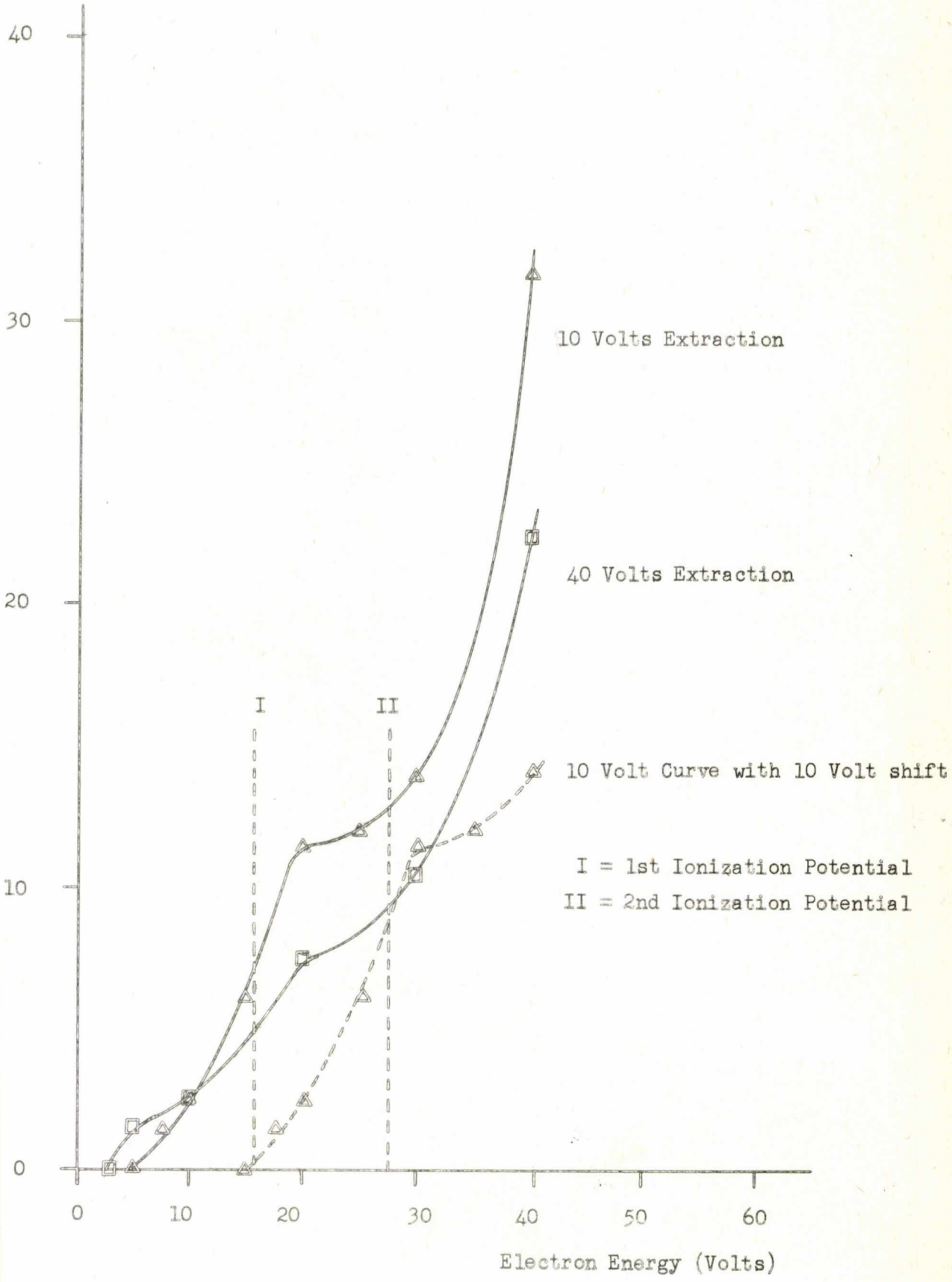

voltages. Above these the DC level introduced proved excessive, although the behaviour of the electron beam could be estimated by comparison of the trap currents obtained with the filament on and off. Plots obtained for the trap current against RF voltage are shown in Figure 5-6; the trap current (with the filament switched on) was observed to decrease and then to increase, but comparison of the two curves shows that the increase was purely due to RF pick-up. The initial decrease, to approximately one half of the trap current at zero RF voltage, was thought to result from the beam being switched off during the portion of a cycle when the RF was negative. Apart from this reduction at low RF, however, the electron current was constant over the range of RF voltages available; the results shown were obtained at an RF frequency of 2.75 MHz, but identical behaviour was observed at 0.8 MHz. Direct observation of the electron switching, by connecting the oscilloscope to the trap, proved impossible owing to the magnitude of the RF pick-up.

An ionization potential plot for argon, shown in Figure 5-7, was obtained using the same experimental arrangement as previously described, but with 500 Volts of RF applied to the ring electrode and zero extraction voltage (the ions leaving the device because of space-charge repulsion). This showed that the RF introduced an additional energy spread into the electron beam but, somewhat surprisingly, that the magnitude was considerably less than the amplitude of the RF. The maximum electron energy spread was estimated from Figure 5-7 as being ca.25eV, greater than the indicated energy; further experiments with helium showed an energy spread of up to 20eV, at an RF amplitude of 200 Volts.

Figure 5-6. Trap Current vs. RF Amplitude

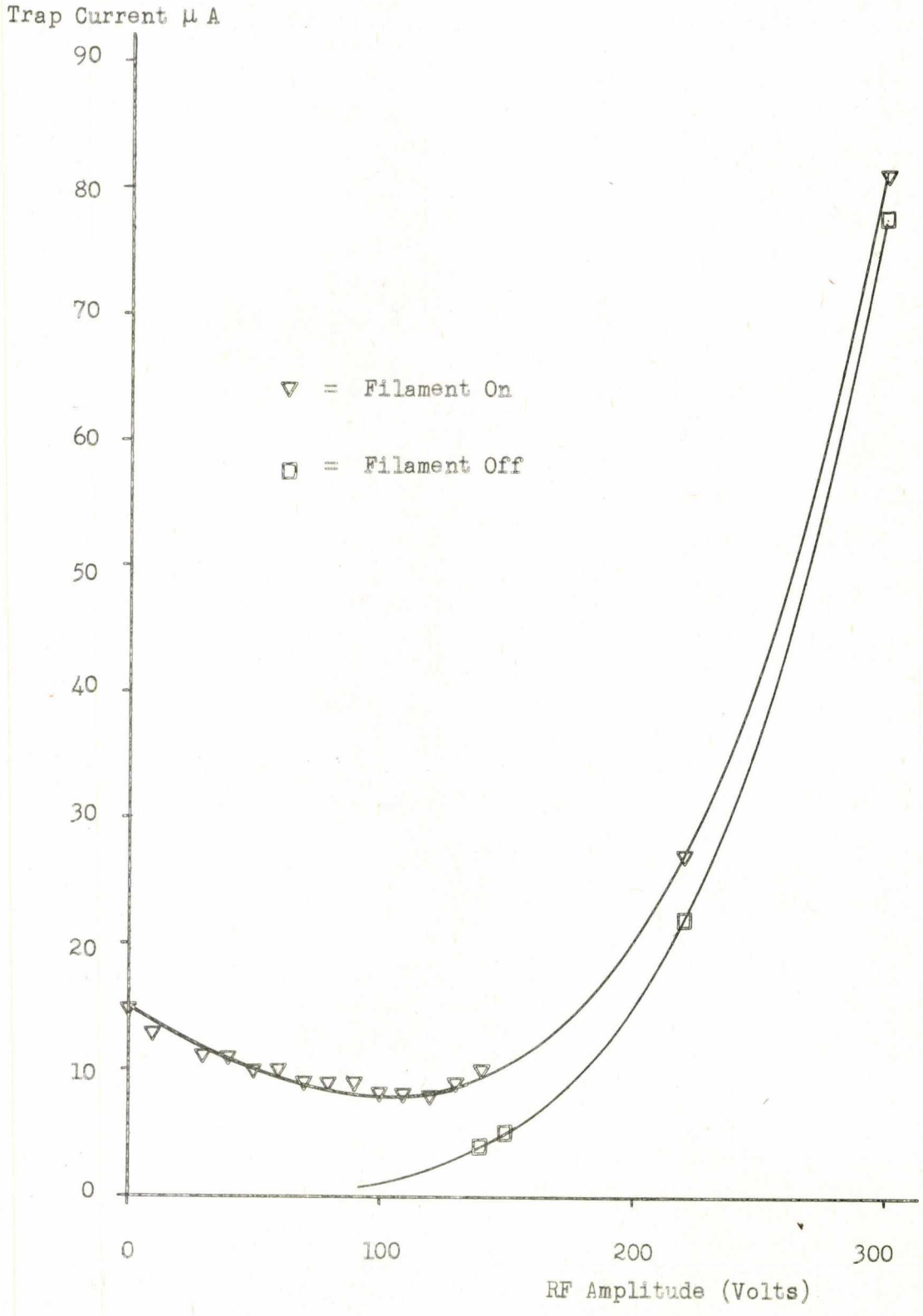

Figure 5-7. Ionization Potential Plot for Argon, Ion Storage Mode

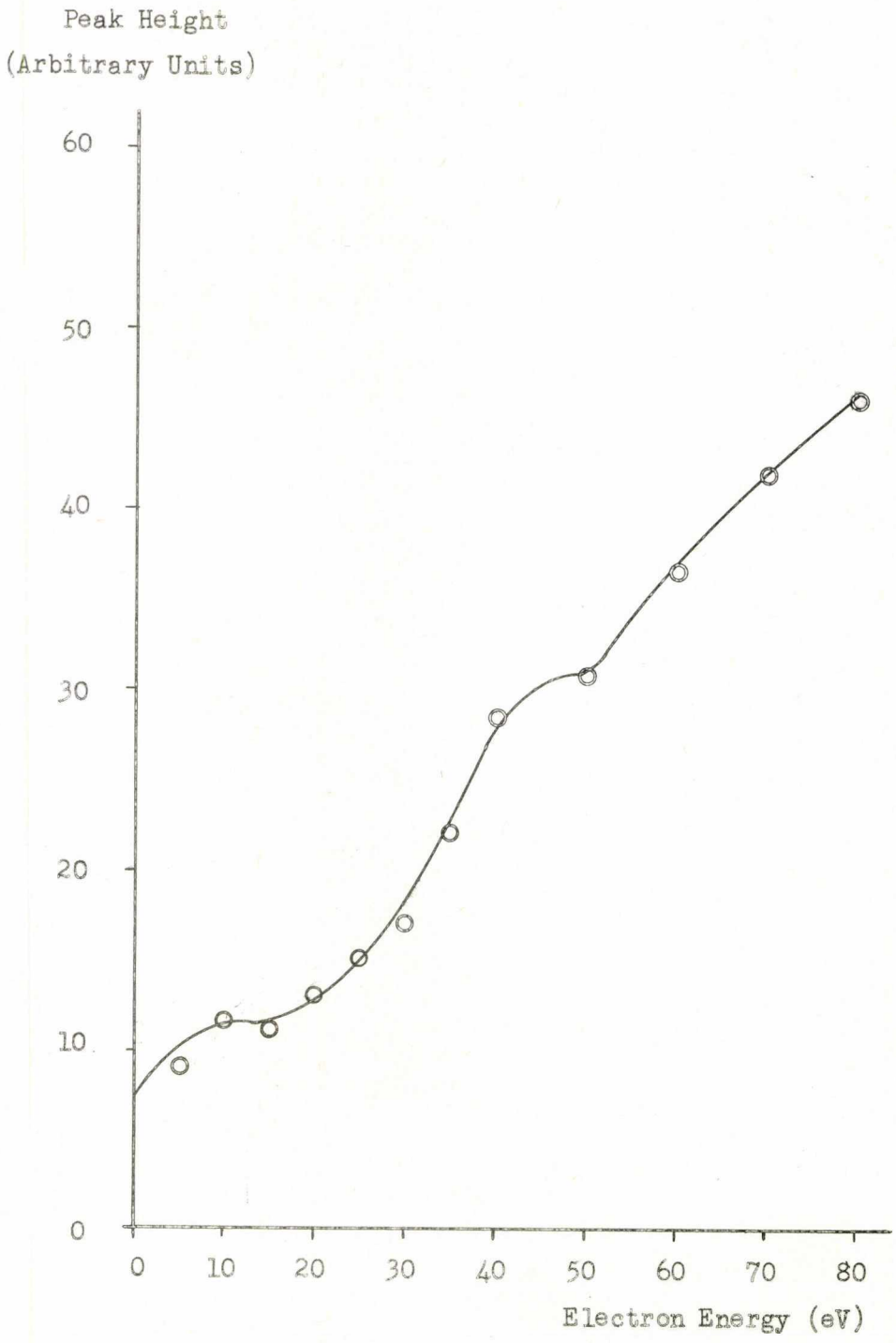

5.23 Conclusion

The application of an RF voltage to the ring electrode was shown to affect both the intensity and energy of the electron beam. In the case of the former, a reduction by approximately 50% was experienced, although the current obtained was roughly constant over the range of voltages available. The effect on the beam energy was to introduce an additional spread, although this was not as large as expected. The results also suggested that a filament voltage of -50 Volts and an electron gate voltage of -110 Volts would ensure complete beam extinction, but permit a reasonable current through the device when the beam was then switched on.

5.3 The QUISTOR as an Ion Source

The QUISTOR could, basically, be operated in one of two modes. In the first ('static' operation) the electron beam was operated continuously, and continuous ion removal ensured by application of a positive potential to the upper end-cap (see Figure 5-8). Alternatively, with RF applied to the ring electrode, the ions could be allowed to 'self-eject' under the influence of space-charge repulsion. In this mode, the QUISTOR was comparable to a conventional ion source, and yielded similar mass spectra. The second mode of operation ('ion storage' mode) entailed pulsing the electron beam and ion ejection, allowing direct control of the storage time. Since this mode was of greater interest, it was examined in greater detail, the static mode is, however, briefly described.

5.31 The QUISTOR as a Static Ion Source - Without RF

The connection of the QUISTOR for operation as a static source is shown in Figure 5-8. The lower (ion-exit) end-cap and the electron gate were earthed, and the upper end-cap and ring electrode connected to the trap output of the filament supply, in order to obtain a variable DC ion

Figure 5-8. Connection of the QUISTOR as a Static Source.

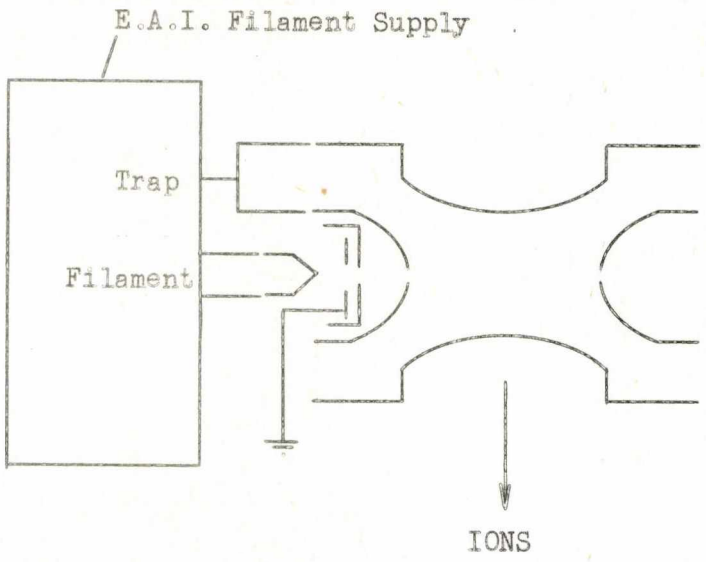

extraction voltage. Figure 5-9 shows a typical spectrum of benzene obtained in this mode, with an indicated pressure of 8×10^{-5} Torr and at a nominal electron energy of 70 eV. The ion extraction voltage was 40 Volts, resulting in a large energy spread in the electron beam. Table 5-1 compares the fragmentation pattern of this spectrum with data listed in the American Petroleum Institute (API) Tables of Mass Spectral Data, from which it may be seen that the major difference was the greater relative abundance of low mass ions in the QUISTOR spectrum. This was a function of the quadrupole analyzer rather than the QUISTOR; since the resolution of a particular ion is dependent on the number of RF cycles it experiences, low mass ions are less resolved than high mass ions, for a fixed ion energy, as their velocity is greater. Consequently, for identical samples, the relative intensity of high mass ions is always lower in quadrupoles than in magnetic sector instruments.

Figure 5-9

Benzene Spectrum - QUISTOR as a Static Source.

Sensitivity 160 mv/cm.

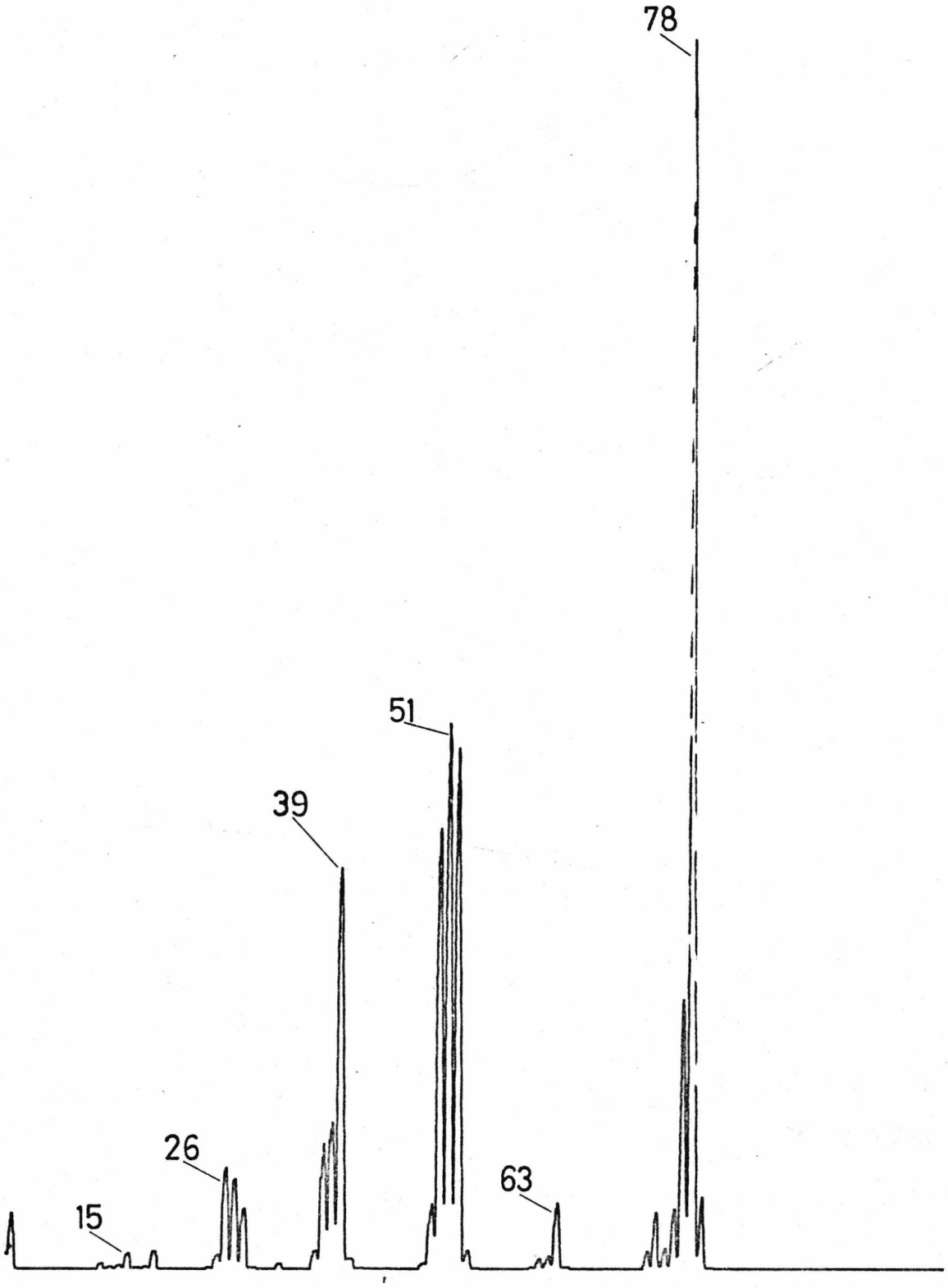

Table 5-1 Benzene Spectrum. Comparison of the QUISTOR as an Ion Source (Static) with a Conventional Mass Spectrometer

m/e	Standard[a]	QUISTOR No RF	QUISTOR 450V RF	QUISTOR 575V RF
79	6.44	5.90	5.83	5.99
78	100.00	100.00	100.00	100.00
77	14.4	21.70	20.0	23.34
76	5.99	4.87	2.5	4.73
75	1.61	1.54	--	1.26
74	4.59	4.62	1.67	3.47
73	1.47	1.28	--	0.95
63	2.78	5.13	5.83	4.10
62	0.63	1.03	--	0.63
61	0.54	0.77	--	0.31
52	19.4	42.31	44.17	25.55
51	18.6	44.36	45	24.29
50	15.7	35.64	37.5	18.61
49	2.51	5.13	5	2.52
39	14.2	32.56	62.5	8.52
38	5.75	11.80	26.67	3.15
37	4.1	10	20.83	2.21
28	0.59	4.87	7.5	--
27	3.04	7.18	12.5	--
26	3.4	7.95	15.83	0.63
15	0.78	1.28	1.67	--

a) Data obtained from the American Petroleum Institute (API) Tables of Mass Spectral Data, Spectrum Serial No. 175, originally obtained from a Consolidated Electrodynamics Corporation (CEC) 21-102 Magnetic Sector Mass Spectrometer.

In more recent quadrupole mass filters, this disadvantage is often overcome by increasing the ion energy with mass, thereby maintaining the flight time through the quadrupole constant for all ions.

The sensitivity was less with the QUISTOR than with the E.A.I. source, and this was a result of the respective designs. The E.A.I. source is designed specifically to encourage ions to enter the mass analyzer, whereas this was not the case for the QUISTOR.

5.32 The QUISTOR as a Static Source - with RF Applied

For operation in this mode, the QUISTOR was connected as in Figure 5-8, with the exception that the ring electrode was coupled to the RF generator. The spectra obtained, Figure 5-10, were similar to that obtained without the RF, with the following differences :

(i) The observed ion currents were reduced by ca. 50%, owing to the cyclic switching of the electron beam, already mentioned.

(ii) The QUISTOR could be made to mass discriminate, causing the spectrum to alter, by varying the RF voltage.

This latter effect is analagous to the total pressure behaviour of a normal quadrupole mass filter, in which the ion current varies with RF voltage in a manner similar to that represented in Figure 5-11, for a single ion species.

The maximum of this curve is always observed at an RF voltage corresponding to a q-value of ca. 0.2. The effect is additive, if different ionic species are present, resulting in the curve shown in Figure 5-12 for a binary mixture of two equally intense ions. The reasons for this behaviour is described in Section 3.92. As a result the spectrum could be significantly altered by varying the RF voltage.

The mass spectra shown in Figure 5-10, were obtained for benzene under the same conditions as Figure 5-9, but with two different RF voltages. Spectrum (b) was obtained with 575 Volts applied, this being

Figure 5-10

Benzene Spectrum - QUISTOR as a Static Source with RF applied.

Sensitivity = 80 mv/cm.

a) 450 Volts

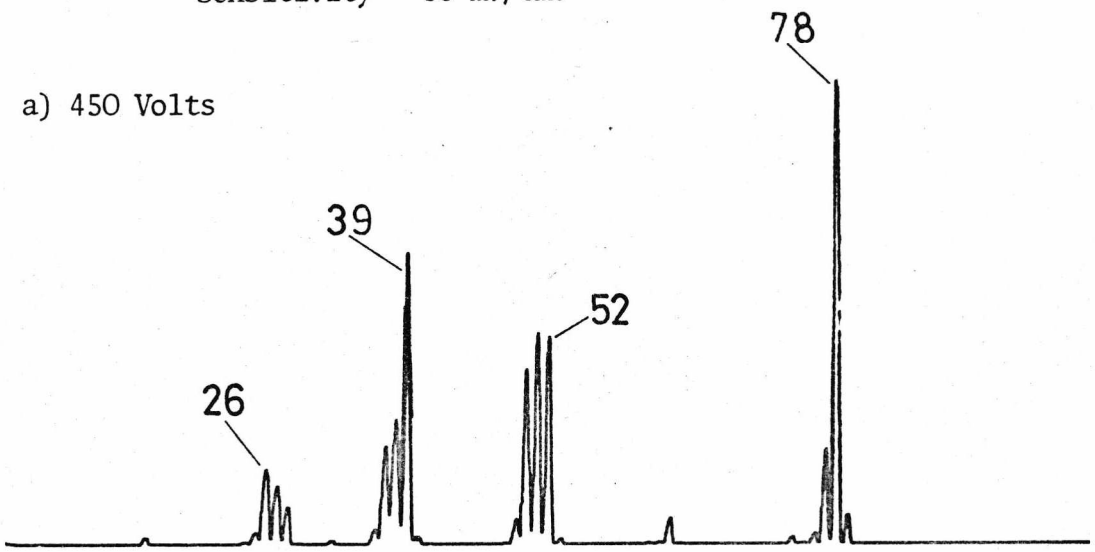

b) 575 Volts

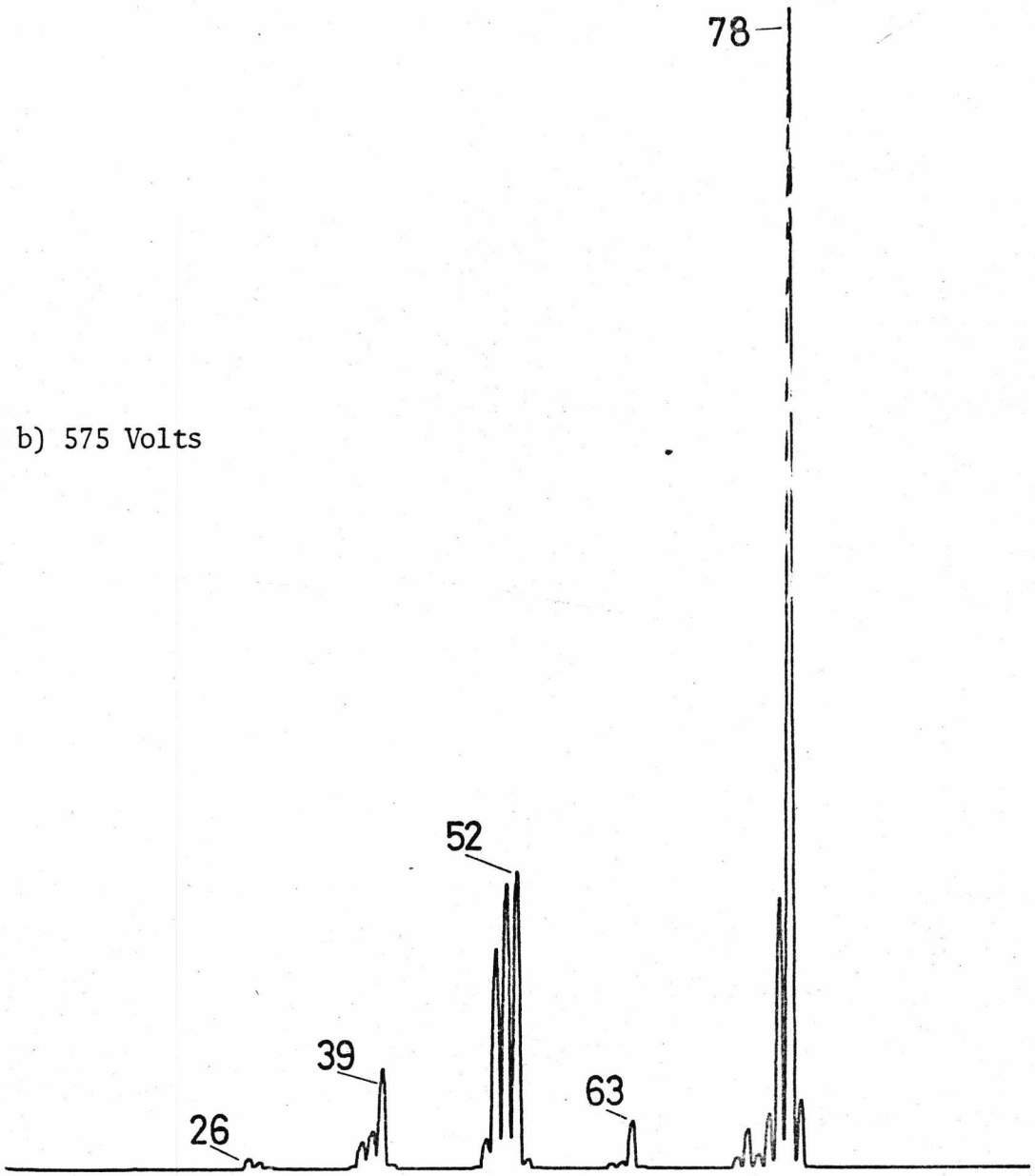

Figure 5-11. Behaviour of Total Pressure Peak

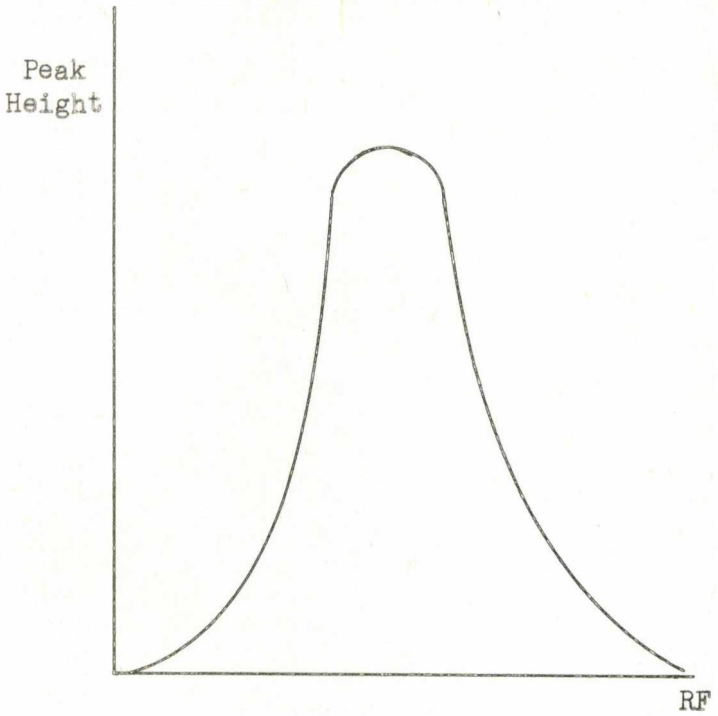

Figure 5-12. Additive Behaviour of Total Pressure Peak

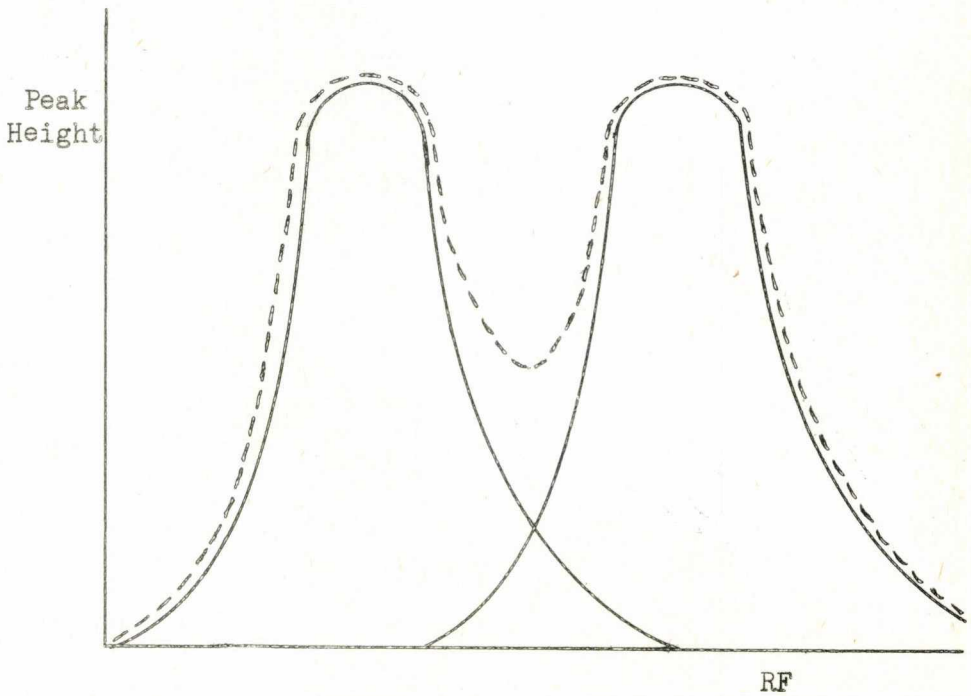

the optimum value for m/e 78; the QUISTOR was effectively nullifying the mass discrimination of the analyzer by itself discriminating against lower mass ions. The resulting fragment pattern was, therefore, very similar to that obtained in a magnetic instrument (Table 5-1). In spectrum (a), 450 Volts were applied - the optimum value for m/e 39 - and heavy discrimination against the high mass ions was apparent.

Ion storage was found to be possible in this mode, particularly if an insufficient ion extraction voltage was applied. As a result, Sequential Mass Spectrometry (see Chapter 2) was observed, ions being stored in the presence of an electron beam and undergoing several ionizing collisions to produce multiply charged ions. For example, in the spectrum of argon the ratio of m/e 40 (Ar^+) to m/e 20 (Ar^{++}) decreased as the ion extraction voltage was reduced.

5.33 The QUISTOR as an Ion Storage Source

The experimental system and procedure are described in Sections 5.331 and 5.332, including a discussion of the method of evaluating ion-molecule reaction rate constants, and possible sources of error. The behaviour of the QUISTOR as an ion storage source is detailed in Section 5.333, its storage capabilities being discussed in terms of ion-molecule and ion-ion scattering rate constants, after the method of Dawson, Hedman and Whetten,[36] and compared to similar quantities obtained by these authors, Harden and Wagner,[42] and Lawson.[37]

5.331 Experimental System

A schematic diagram of the apparatus is shown in the upper part of Figure 5-13, the lower part of which illustrates the pulse train applied to the QUISTOR. It had previously been shown[37] that biassing the electron gate such that the electron beam was extinguished and then nullifying this bias with a short pulse, to obtain a burst of electrons was more satisfactory that switching the beam off when <u>not</u> required,

Figure 5-13. Schematic Representation of Experimental Apparatus and Pulse Train Applied in Ion Storage Mode.

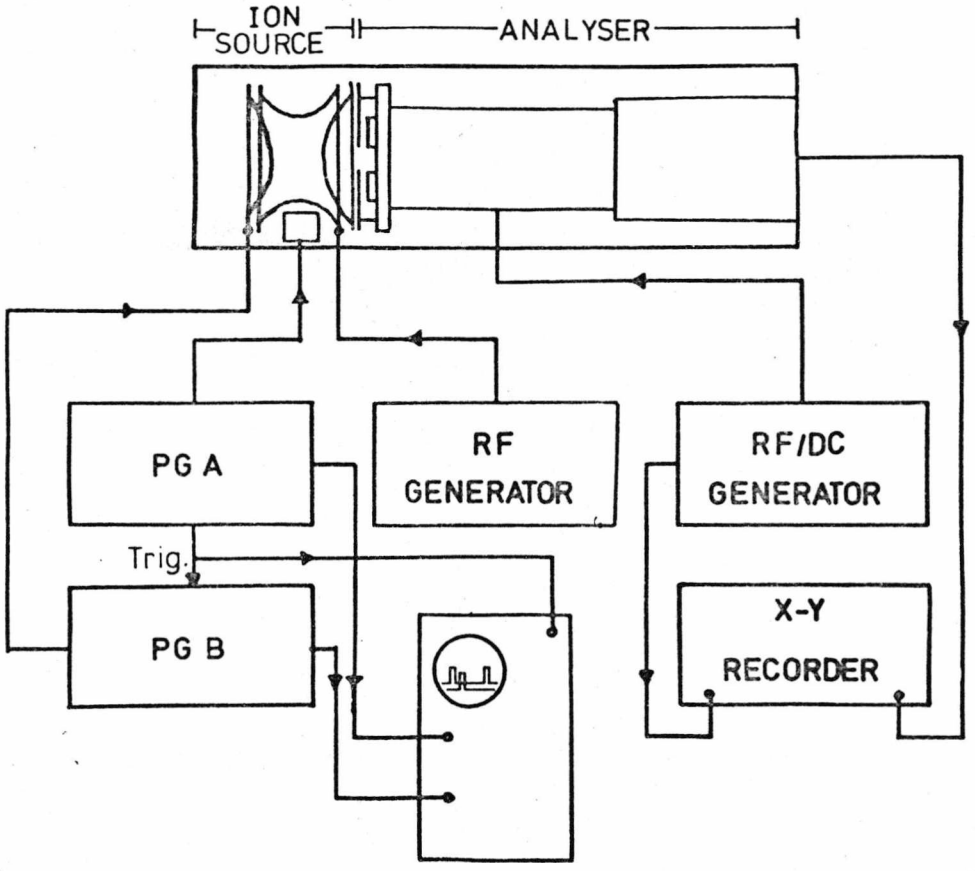

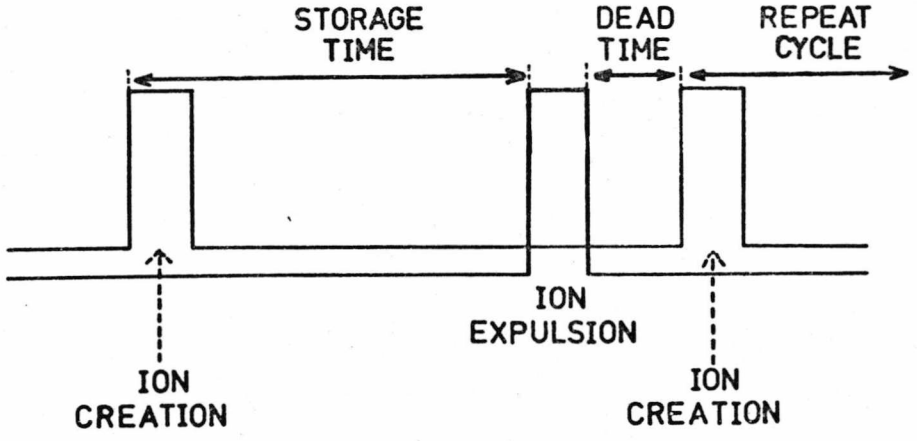

using long pulses. Consequently, this method of operation was adopted; the electron gate was biassed negative with respect to the filament, and a burst of electrons admitted to the device by the application of a positive pulse from pulse generator A, PG A in Figure 5-13. This generator also provided an external trigger pulse to the ion expulsion generator, PG B, and the oscilloscope. The delay time, measured using the oscilloscope, could be set to a maximum value of ca. 70-80% of the pulse repetition period, this limitation being imposed by the available output power of the Pulse Generators. Typically, repetition rates of 100 Hz or 200 Hz were employed, permitting maximum storage times of 3.5 and 8 mS respectively. Generally, ion creation and expulsion pulse widths were in the range 10-20 μS. Ion extraction could be either repulsive, with positive pulses applied to the left-hand end-cap (Figure 5-13), or attractive with negative pulses applied to the right-hand end-cap; these alternatives are discussed in Section 5.333.

Operating in this mode caused a further reduction in sensitivity, for two reasons :

(i) The electron beam was only switched on for short periods, resulting in relatively few ions; for example, with 20 μS pulses at 200 Hz the beam was switched on for 4 mS in every second, or a factor of 4×10^{-3} of the total time.

(ii) The pen recorder was unable to respond to individual pulses, and averaged each pulse over the whole duty cycle; again, with 20 μS pulses at 200 Hz, this results in further reduction by a factor of 250. Clearly, some form of pulse height analysis would have been beneficial, but this was not available.

Experimentally, it was found that storage was best at the highest frequency available, i.e. 2.75 MHz. At 0.8 MHz, observation of the output signal on the oscilloscope showed that the ion pulses were

coincident with the expulsion pulse. At 1.5 MHz either extreme, or partial ion ejection at both pulses, could be obtained, depending on the RF amplitude. These phenomena may be explained by Dehmelt's pseudo-potential well model, that ions are trapped in such a well of depth $\bar{D}$ Volts, proportional to the amplitude of the applied RF, and the square of its radial frequency (see Section 3.7); under given conditions the number of ions, N_t, that can be trapped is proportional to $\bar{D}$. It has already been shown, Section 5.2, that the electron current is constant with frequency, and hence the number of ions created, N_c, is also constant. At 0.8 MHz, N_t is very much lower than N_c, whatever the applied voltage, and the excess are immediately ejected, whereas at 2.75 MHz, N_t is always greater than N_c, and ions are stored until an extraction pulse is applied. At 1.5 MHz, N_t and N_c are comparable and their relative magnitudes critically dependent on the RF amplitude. Similar behaviour has been reported by Dawson and Whetten[104] in three traps having Zo's of 0.4, 0.8 and 2.0 cm and at RF frequencies of 1.8 MHz, 1.0 MHz, 0.5 MHz and 60-200 kHz. They found that although ions could be stored at 20 kHz, the number stored and the mean storage time decreased with frequency.

Harden and Wagner[42] have reported that a quadrupole ion trap, employed as a mass spectrometer, often required a length of time to 'condition' before mass selective operation was possible. This was not observed in the QUISTOR, although cleanliness was found to be extremely important. When the electrodes were dirty ions always emerged on the creation pulse, even at 2.75 MHz. This may well explain the behaviour observed by Harden and Wagner, the 'conditioning time' required being a function of the time required to remove condensable material from the trap, this removal being expedited by having the filament on.

In this work, the QUISTOR electrodes were treated with great care, and were cleaned in a 1 : 1 : 8 solution of formic acid, hydrogen peroxide (100 volume) and distilled water; the faces were then polished with 'DURAGLIT' before washing with water and acetone.

5.332 Experimental Procedure

Rate constants were obtained from peak height *versus* time plots, based on equations derived in the following manner.

Consider the reaction :

$$A^+ + B \longrightarrow C^+ + D \qquad (5\text{-}1)$$

Then the rate of loss of A^+ is given by :

$$\frac{-d[A_t^+]}{dt} = k\,[A_t^+]\,[B]$$

where k is the rate constant, the square brackets indicate concentration and the subscripts, time.

Throughout an experiment $[B]$ is constant and may be equated to the pressure, or partial pressure, p. Thus, rearranging gives :

$$\frac{-d\,[A_t^+]}{[A_t^+]} = k\,p\,dt$$

Which on integrating becomes :

$$-\ln [A_t^+] = k\,p\,t + c$$

where c is a constant, and may be evaluated by substitution of the initial condition that $[A_t^+] = [A_o^+]$ when $t = 0$, hence :

$$\ln \frac{[A_o^+]}{[A_t^+]} = k\,p\,t \qquad (5\text{-}2)$$

Consequently, a semi-log plot of $[A_o^+]/[A_t^+]$ *versus* time should be a straight line of gradient k p.

If the ionic concentrations at various times are :

Time	$[A^+]$	$[C^+]$
0	$[A_o^+]$	[0]
t	$[A_t^+]$	$[C_t^+]$
∞	0	$[C_\infty^+]$

then $[A_o^+] \propto [C_\infty^+]$

and $[A_t^+] \propto [C_\infty^+ - C_t^+]$

Substitution of these quantities into expression (5-2) gives :

$$\ln \frac{C_\infty^+}{[C_\infty^+ - C_t^+]} = k\,p \qquad (5\text{-}3)$$

which allows determination of the rate constant for the increase of a product ion.

Clearly, the accuracy of this latter expression was largely dependent on the error in determining a value for C_∞^+ ; in most cases this could be adequately estimated, although this was not always possible. An alternative expression based on the time taken for one half of the reagent to react or one half of the product to be formed, may be derived as follows.

If $t_{\frac{1}{2}}$ is the time to 'half-concentration', i.e. at $t = t_{\frac{1}{2}}$:

$$[A_{t_{\frac{1}{2}}}^+] = [A_o^+]/2$$

then substitution in (5-2) gives :

$$\ln 2 = k\,p\,t_{\frac{1}{2}} \qquad (5\text{-}4)$$

This expression also holds for product ions.

If reaction (5-1) is the only one involving A^+ and C^+ occurring then $[A_o^+]$ and $[C_\infty^+]$ should be equal, with the curves crossing at $t_{\frac{1}{2}}$ for both species. Any significant deviation (i.e. exceeding system error) from this indicates the presence of additional reactions in which

A^+ or C^+, or both, are reacting or being produced.

Rate constants were determined by the following procedure. Sample was admitted to the system to give a fixed pressure, and the RF amplitude set to a given value. The storage time was also fixed, and the analyzer swept to give a conventional mass spectrum. The storage time was then increased, and the operation repeated. This was continued up to the maximum storage time available. Individual peak heights were measured, and expressed as a percentage of the total ionization (total peak height) for that spectrum. Finally the results were plotted on semi-log graph paper, and the rate constants evaluated using expressions (5-2) to (5-4).

Although zero storage time could be obtained by employing coincident creation and ejection pulses, the shortest time used in practice was 20μ S, zero storage time having been shown to give unreliable results. The reason for this was that ions created towards the end of the pulse were not ejected and reacted during the dead time. This effect was found to depend on the RF amplitude, as is illustrated by the methane spectra shown in Figure 5-14 (a) - (c). The relevant conditions were :

	RF Amplitude (Volts)	Sensitivity
(a)	450	x 1
(b)	675	x 10
(c)	800	x 10

As the RF potential was increased, the number of ions stored, and hence the number retained through the dead time, also increased. This is indicated by the increase of ion-molecule reaction products, although each spectrum was obtained at zero storage and identical pressures. Figure 5-14(a) shows only small ion-molecule product peaks, while (b) shows predominant peaks (at m/e 17, 27, 29) corresponding to products of the reactions :

Figure 5-14 (a) Methane Spectrum at zero storage time.

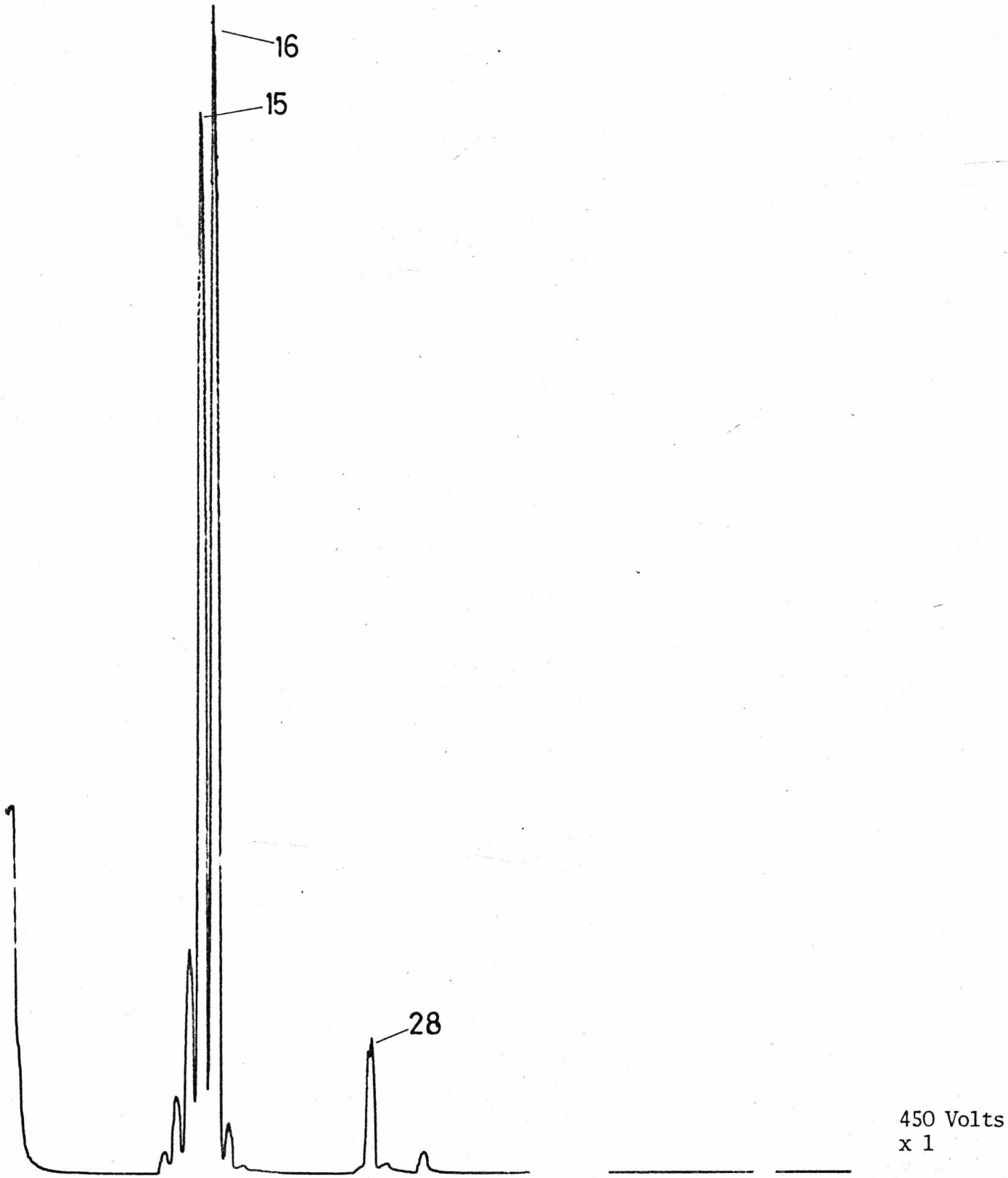

Figure 5-14 (b)

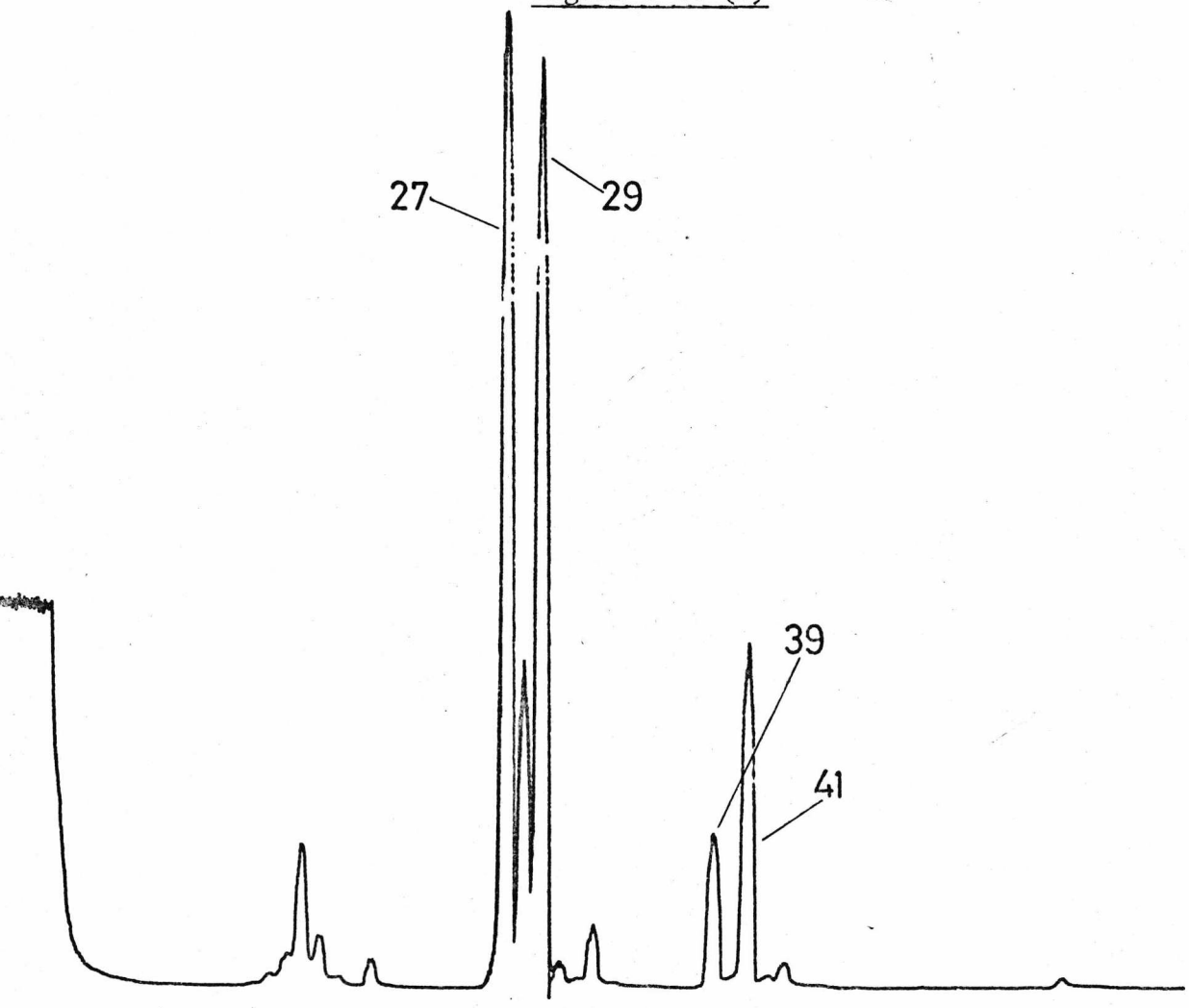

Figure 5-14 (c)

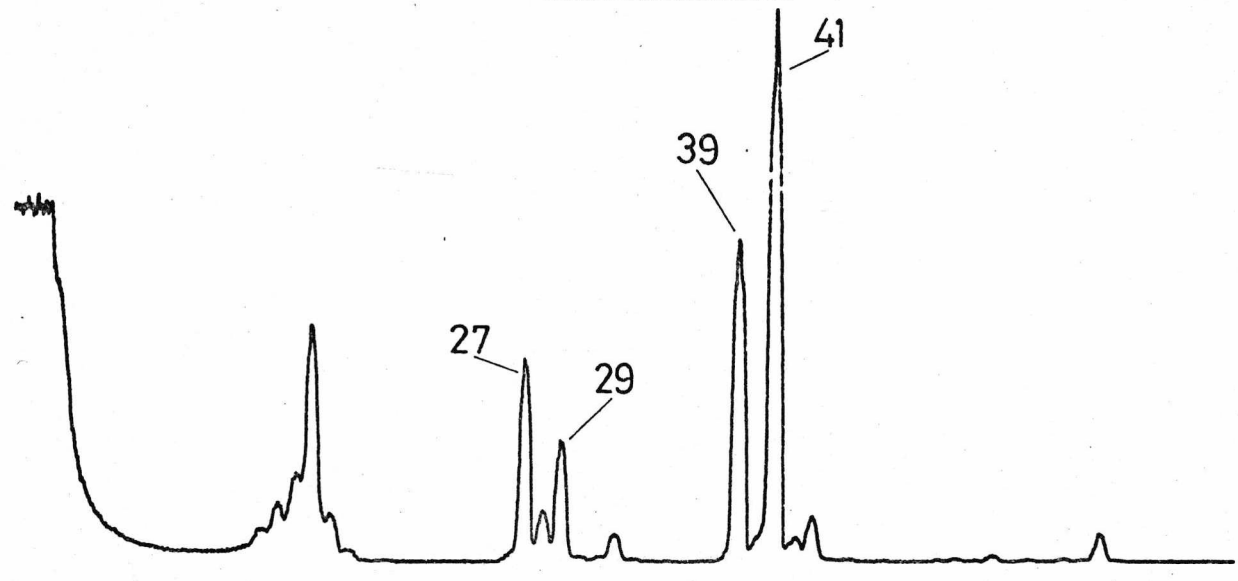

$$CH_4^+ + CH_4 \longrightarrow \begin{cases} CH_5^+ + CH_3 \\ CH_3^+ + H_2 \end{cases} \qquad (5\text{-}5)$$

$$CH_3^+ + CH_4 \longrightarrow C_2H_5^+ + H_2 \qquad (5\text{-}6)$$

$$CH_3^+ + CH_4 \longrightarrow C_2H_3^+ + 2H_2 \qquad (5\text{-}7)$$

$$CH_2^+ + CH_4 \longrightarrow C_2H_3^+ + H_2 + H \qquad (5\text{-}8)$$

and (c) shows that tertiary reactions have occurred, leading to peaks at m/e 39 and 41, and having the form :

$$C_2H_3^+,\ C_2H_5^+ \xrightarrow{CH_4} C_3H_3^+,\ C_3H_5^+ \qquad (5\text{-}9)$$

The higher mass peaks were also enhanced at the higher voltages due to the effects previously mentioned; since, however, these masses must have arisen from primary methane ions, the point that these were retained during the dead time is illustrated.

Before attempting to measure a rate constant by the method outlined above, it was important to ensure correct switching of the electron beam. If this was not the case, the storage time was unknown, since ions could be created at any time during a cycle. Correct gating was verified by observing ion pulses on the oscilloscope and ensuring that they disappeared when pulse generator A was switched off, thereby indicating that the negative voltage applied to the electron gate was of sufficient magnitude.

The accuracy of the rate constant determinations was dependent on the errors involved in measuring each of the quantities peak height, time and pressure. Some experimental observations and estimations of the possible errors in these are given below.

(i) Peak Height Errors

When using the oscilloscope to observe ion pulses, it was observed that the amplitude of the latter varied quite rapidly; this was in addition to a 100 Hz modulation introduced by the AC filament unit, and eliminated by employing the DC supply. It is believed that the rapid fluctuation was caused by the different, and random, phase of the RF at which the ejection pulses commenced. Dawson[105] and Whetten[56] have recently suggested that this parameter is important, and affects the efficiency of ion removal. Unfortunately, suitable pulse/RF synchronizing equipment was unavailable and so this could not be examined; any localized variation was probably reduced, however, by the averaging effect of the pen recorder over one or two hundred pulses. At fixed storage times, small peak height variations were observed, and to counteract these, two or more spectra were obtained at each storage time, allowing some estimation of the error. The error bars, indicated on semi-log plots throughout this work correspond, therefore, to two or more observations.

(ii) Timing Errors

These were dependent on two factors :

(a) the inaccuracy involved in setting a storage time, using the oscilloscope to measure the pulse separation,

(b) the error introduced by using pulses of finite width.

The oscilloscope graticule was calibrated in 1 cm. steps, from 0 to 10 cm, with 0.2 cm sub-divisions permitting an accuracy of better that 2%. As can be seen from Figure 5-15, the error introduced by the pulses is of the order of one pulse width and consequently the overall timing error was taken as the larger of 20 μS or 2%.

Clearly, the error is largest at short storage times, and so choice of pressure to give long reaction times (consistent with accurate

Figure 5-15. Diagram of Pulse Train, Showing Timing Errors

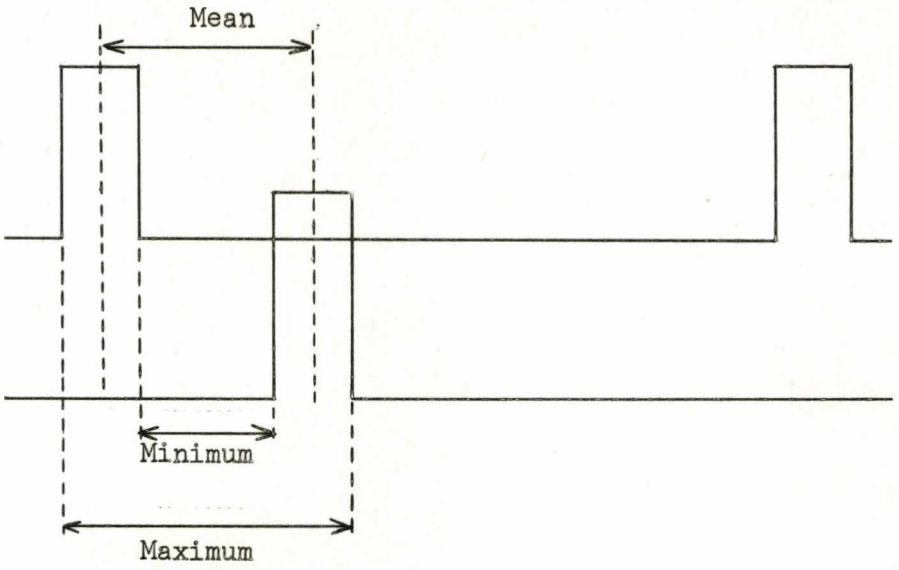

pressure measurements) was advantageous.

(iii) Pressure Errors

Pressure errors are usually the largest single source of inaccuracy in ion-molecule reaction studies; this arises because of the wide use of ion gauges which are invariably only calibrated for nitrogen, non-linear and extremely unreliable when contaminated. The advantage of ion gauges is that they are capable of measuring a wide range of pressures; McLeod gauges, although absolute, are not widely used because of the large size necessary to measure pressures less than 10^{-3} Torr, their incapacity to continuously monitor pressure and their inability to function correctly with condensable materials. In order to overcome this problem, some authors report calibrating their ion gauges against McLeod or Bourdon gauges (see reference 91, for example), although it is more common to employ the well-known reaction of CH_4^+ in methane (5-4) taking its rate

constant as $k = 12 \times 10^{-10} cm^3 molecules^{-1} sec^{-1}$.

In this work, it was at first decided to use ion gauge pressure readings, corrected using sensitivity factors, both measured and supplied by the manufacturer. To check that these quantities were similar, fixed amounts of nitrogen, indicated on the inlet system capsule gauge, were admitted to the vacuum system, allowed to stabilize and the pressure noted. This was repeated with a different sample and the pressure of sample plotted against that of nitrogen. Since the gauge was supposedly calibrated for nitrogen, the slope of such a curve should give the relative sensitivity for the particular substance. Two sets of results, for hydrogen and carbon dioxide, are presented in Figure 5-16; the measured relative sensitivities were 0.45 and 2.0 respectively. While the former was in excellent agreement with the manufacturer's value, the latter was vastly different from the quoted figure of 0.9. Examination of methane and propane yielded values in the region of 10.0, while the quoted value for hydrocarbons is ca. 1.4. These results suggested that the ion gauge was contaminated, and consequently this method of pressure measurement was abandoned to save having to calibrate the ion gauge before each experiment. As an alternative, the inlet system capsule gauge, capable of reading 0-20 Torr and insensitive to sample constituents, was calibrated for the decrease of CH_4^+ in methane, reaction (5-4). The rate of this reaction, but not the product distribution, is known to be fairly insensitive to ion kinetic energy,[116] at least up to 2 eV. The calibration was performed as follows. A fixed pressure of methane in the inlet system was admitted to the system, and the percentage of CH_4^+ of the total ion current recorded against storage time. A least squares method was used to determine the slope, and error, of the best straight line through these points from which the pressure necessary to produce such a slope was calculated

Figure 5-16. Indicated Pressures, Carbon Dioxide and Hydrogen vs. Nitrogen

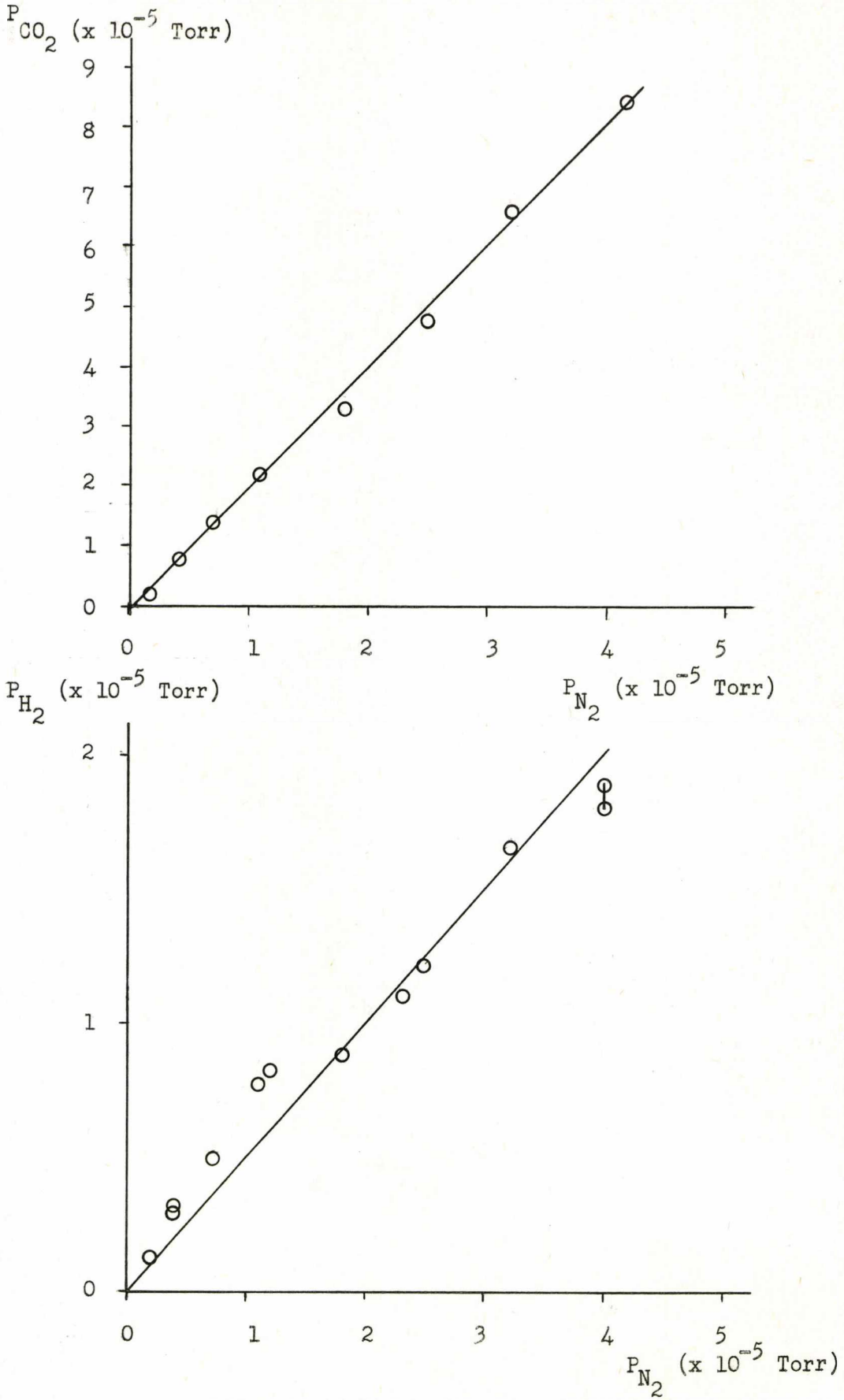

using expression (5-2). This was repeated for different inlet system pressures, P_I, the calculated pressures finally being plotted against P_I, as reproduced in Figure 5-17. Also included on this figure are two straight lines, calculated to minimize the square of the errors; the broken line was produced considering all points, whereas the solid line was for points in the region $10 < P_I < 20$ Torr. It was apparent from these that the capsule gauge was non-linear below about 5 Torr, and that for greatest accuracy pressures in the range 10 - 20 Torr should be used. It can also be seen that the errors in the calculated pressures increased as P_I; this was a result of timing errors, the reaction proceeding faster at higher values of P_I. As a check on these results, the kinetics of the methane system were examined as a function of pressure, rather than storage time. This was accomplished by arbitrarily fixing the storage time, in this case of 500 μS, and recording the percentage of CH_4^+ of the total ionization against the pressure of methane in the inlet system; the results are shown in Figure 5-18. Again the best straight line through these points (shown in Figure 5-18) was determined, and the pressure change equivalent to a change in the inlet system of 20 Torr, was calculated as $23.6 \pm 0.9 \times 10^{11}$ molecules cm^{-3}, in excellent agreement with the results shown in Figure 5-17.

From these results, the system pressure was known for a given pressure of methane in the inlet system, and it was assumed that this would be the same for other samples. This assumption introduced an error, since the rate of sample diffusion through the capillary was inversely dependent on the square-root of the mass. Consequently, the error was largest - and unknown - for a binary mixture of two samples of widely different molecular mass, for example the hydrogen/carbon dioxide system described later.

Figure 5-17 Pressure Calibration

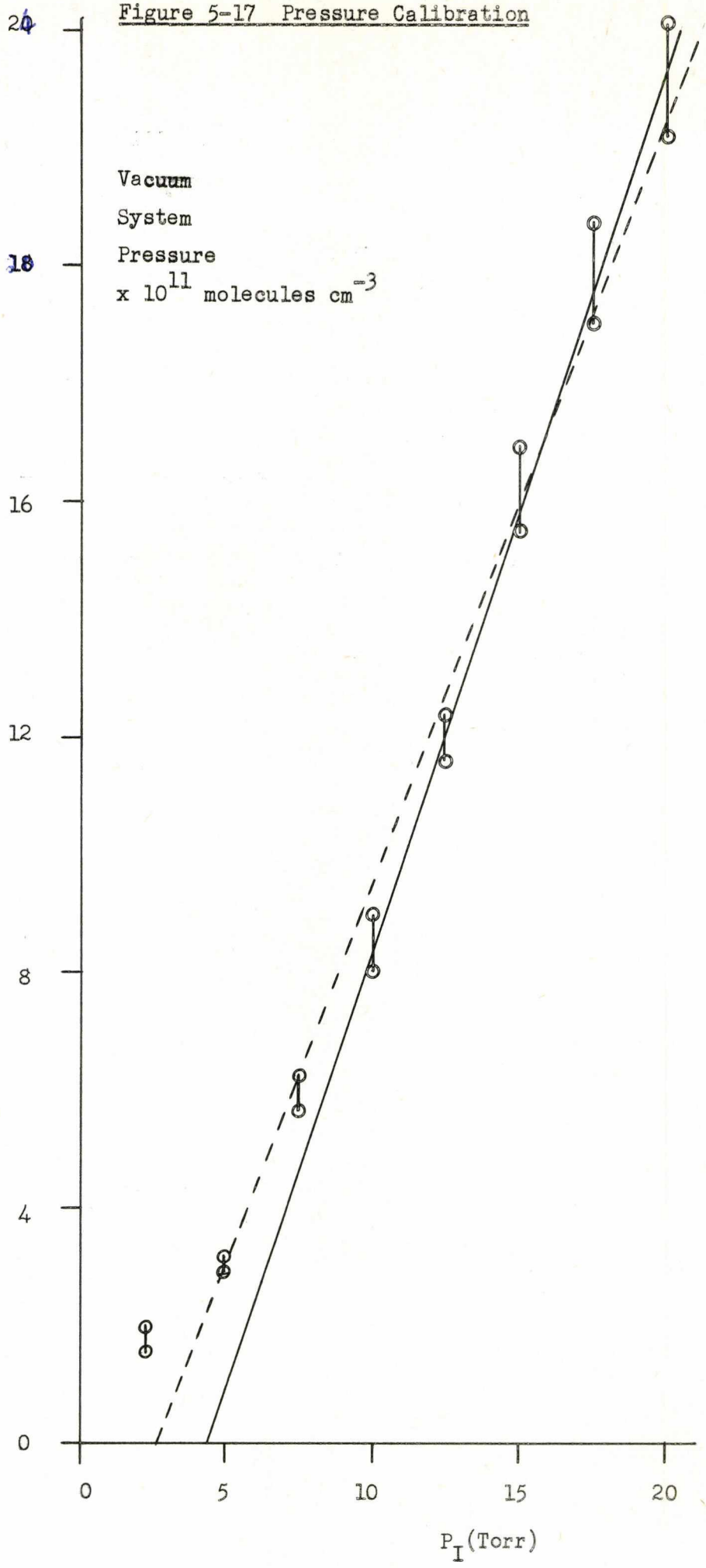

Figure 5-18. Percentage of CH_4^+ of Total Ionization vs. Pressure in Inlet System, P_I

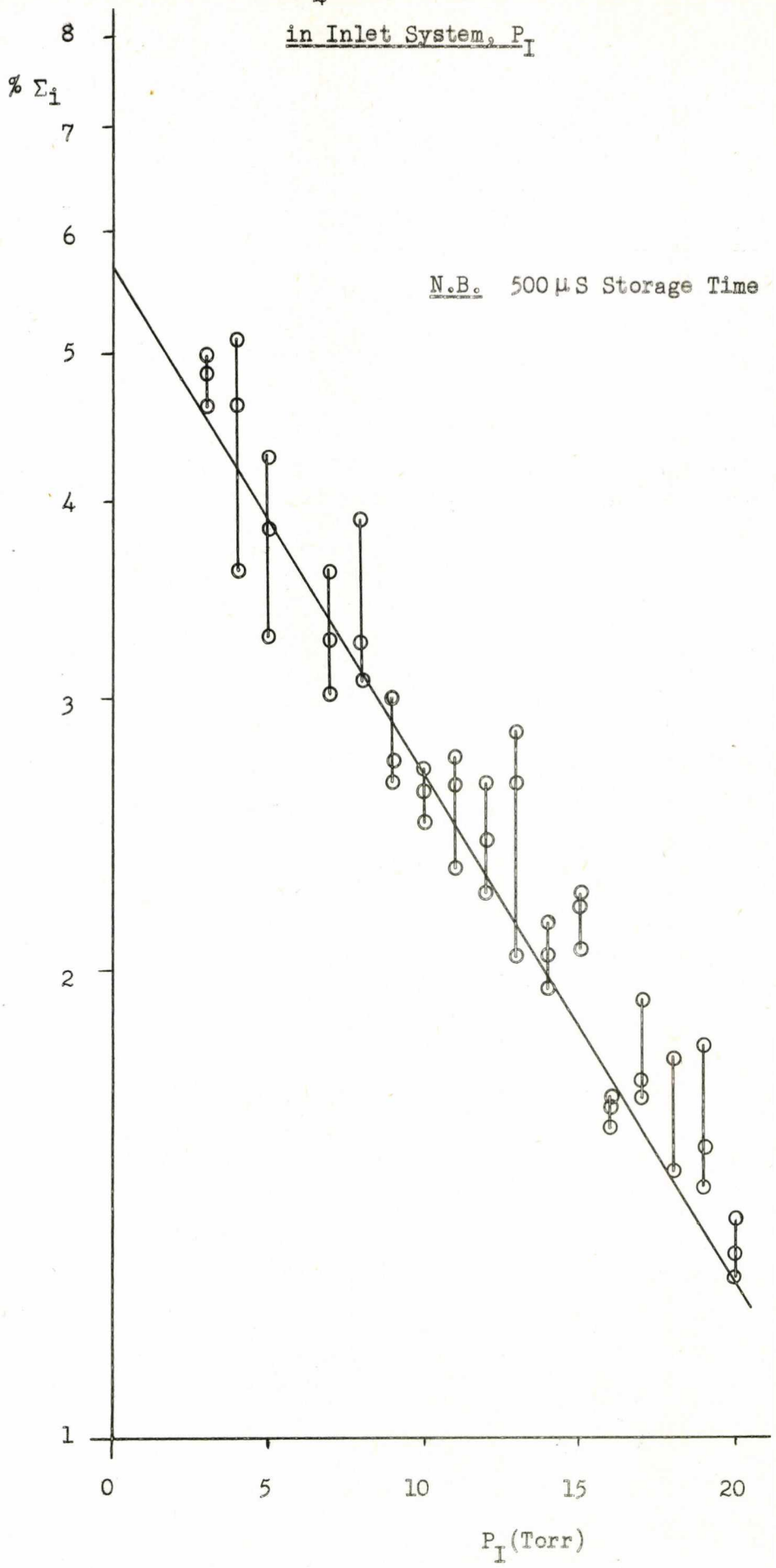

Throughout this work, samples employed were of the highest purity readily available. Rare gases were supplied by British Drug Houses (BDH) and were generally 99% pure, or better. Liquid samples were of Analytical Reagent (ANALAR) grade and were again better than 99% pure. Mixtures of known composition were made up in the inlet system, employing the capsule gauge to determine constituent partial pressures and Figure 5-17 to estimate the corresponding system pressures.

5.333 System Behaviour and Validity Checks

In view of the proposed use of the QUISTOR for the examination of types of ion-collision process, it was necessary to attempt to show that any change in such processes, caused by altering the RF amplitude, was solely a result of varying the primary ion kinetic energy. This was particularly important since the QUISTOR had shown considerable RF-dependent mass discrimination as a Static Source (see Section 5.32), and similar behaviour had been observed in the ion storage mode. It was felt that, because of the method of calculating rate constants, any change observed would arise from ion kinetic energy variations and this was supported by examination of two systems, in one of which major product distribution changes were expected with primary ion kinetic energy (methane) and the other in which little, or no change was expected, (hydrogen/carbon dioxide). In addition, the effect of varying the nature of the ion withdrawal pulse was investigated; this was clearly of fundamental importance since inadequate ion removal would result in reactions during the dead time, as for zero storage (see Section 5.332). To this end it was necessary to verify that ions were being ejected by the withdrawal pulse, before performing an experiment. This was checked by observing that the ion pulses, displayed on the oscilloscope with the analyzer monitoring one particular m/e, were coincident with the ion ejection pulse.

(i) Examination of the Effect of Varying the RF Amplitude

As has been previously indicated, large variations in recorded peak heights were observed on varying the RF amplitude, owing to competition between the number of ions that could be stored (increasing with RF amplitude) and the volume in which ions could be created and remain stable (decreasing with RF amplitude). These variations tend to accentuate the high mass ions at higher voltages, with ion current increases of 10-20 times. The method of calculating rate constants was, however, based on the intensity change of one ion, normalized with respect to all others, and not ratios of ion currents for different ions, and it was felt that any peak height increase should not, therefore, substantially alter the measured rate constants. In order to examine this, two systems were studied (carbon dioxide/hydrogen and methane) at RF amplitudes of 400 and 750 Volts, which encompassed the range generally used.

Carbon Dioxide/Hydrogen

This system is known to undergo three ion-molecule reactions :

$$CO_2^+ + H_2 \longrightarrow CO_2H^+ + H \qquad (5\text{-}10)$$

$$H_2^+ + CO_2 \longrightarrow CO_2^+ + H_2 \qquad (5\text{-}11)$$

$$H_2^+ + CO_2 \longrightarrow CO_2H^+ + H \qquad (5\text{-}12)$$

A report published by Smith and Futrell[106] contains results which showed that reaction (5-10) was independent of CO_2^+ kinetic energy (at least up to 6 eV), which would have made it ideal from the point of examining whether altering the intensity (by varying the RF) affected the observed rate constant, without confusing ion kinetic energy dependences. Further examination of the literature, however, showed that this behaviour was not well established, other authors having

obtained data which supported an inverse dependence of the rate constant on the square root of the primary ion kinetic energy. (Such a dependence being in agreement with the predictions of Langevin's theory of ion-molecule collisions, as described by Giomousis and Stevenson[107]). The various literature values, represented graphically in Figure 5-19, are due to Fehsenfeld, Schmeltekopf and Ferguson[108] (flowing afterglow technique), Moran and Friedman[109] (high pressure mass spectrometer), Shannon and Harrison[110] (pulsed mass spectrometer) and Gubtier[111] (high pressure mass spectrometer). The values of Shannon and Harrison were corrected in a later report[112]. The thermal energy rate constants of Fehsenfeld et al and Moran and Friedman are in excellent agreement, the latter group having also demonstrated the inverse-square-root of the kinetic energy dependence.

The value of Gubtier, obtained at 0.25 eV CO_2^+ kinetic energy, is again in agreement with the thermal values, but does not suggest a decrease with kinetic energy as would be expected on the model of Langevin. The rate constant of Shannon and Harrison was obtained using a pulsed mass spectrometer, in which the ion kinetic energy is controlled by the repeller voltage. Some doubt has arisen as to the value that should be taken for the mean ion energy; in their original paper, Shannon and Harrison quote the ion exit energy, Ee, directly (in this case 3.7 eV) whereas McDaniel[2] quotes their rate constant as having been obtained at 1.85 eV, i.e. Ee/2, while in later reports the average ion energy is taken as Ee/3, based on the analysis of Warneck[113]. As a result, the rate constant of Shannon and Harrison is shown for a range of ion energies. The value of Smith and Futrell is in poor agreement with all these values, which is quoted as being due to the different ionic histories. Their explanation, however, seems somewhat inadequate: they compare ICR to the mass spectrometric methods, stating that ions

Figure 5-19. Summary of Published Rate Constants for Reaction (5-12)

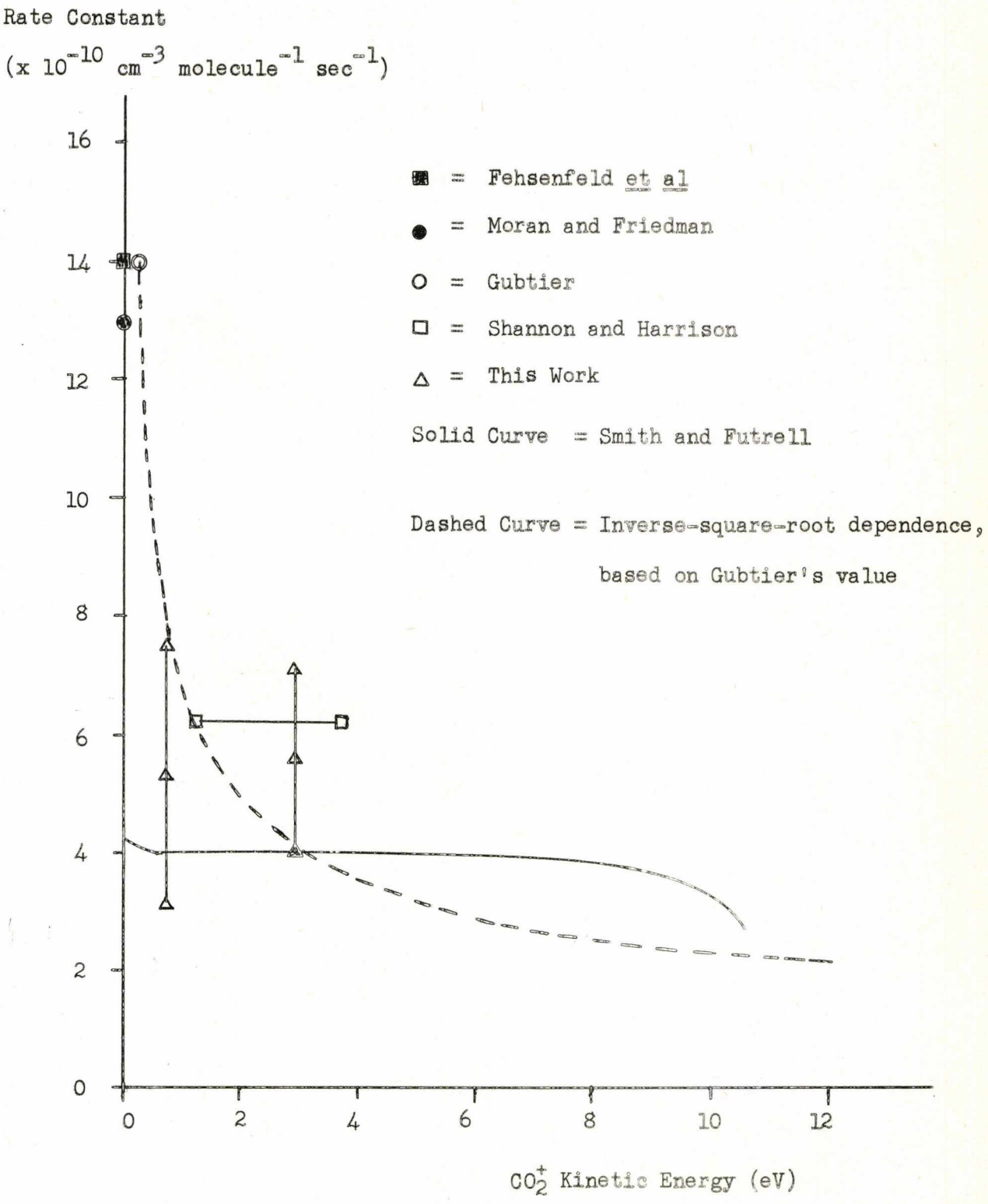

experience single collisions in both methods, and also to the afterglow, since ions are capable of vibrational relaxation in both instruments, while ignoring the significant, and excellent agreement between the mass spectrometric and flow tube values[108, 109]. It would appear more reasonable that ions in the ICR cell possess some internal or kinetic energy, possibly arising from the 1 - 4 Volt trapping supplies, or that they are not relaxed, which confuses the results at supposedly lower ion kinetic energies.

In attempting to study this system in the QUISTOR, several experimental difficulties were encountered, particularly involving the other possible reactions (5-11) and (5-12) and large pressure errors, Smith and Futrell[106] also reported that reactions (5-11) and (5-12) are 5 and 10 times larger, respectively, than that involving CO_2^+. In the QUISTOR, however, an RF amplitude of ca. 260 Volts was sufficient to produce a q-value for hydrogen(H_2) of 0.9. Consequently at the voltages employed here (400 and 750 Volts) the hydrogen ions were unstable and rapidly lost from the device. This was checked by examining the ion pulses on the oscilloscope, with the analyzer set to pass m/e 2, and verifying that they were coincident with the creation pulse. These ion pulses were, however, recorded, but were ignored when measuring peak heights. Although the H_2^+ species was unstable, the large values of the rate constants for its reactions allowed the possibility of reaction before complete ejection. Occurrence of these reactions was indicated by an initial hump in the CO_2^+ intensity, as shown in Figures 5-20 and 5-21 which are semi-log plots for m/e 44 (CO_2^+) and 45 (CO_2H^+) at different relative concentrations. The 'hump' was reduced by increasing the relative concentration of hydrogen, thereby reducing the probability of an H_2^+/CO_2 collision (see Figure 5-21); the probability of a CO_2^+/H_2 collision was correspondingly increased. The initial charge transfer

Figure 5-20. Carbon Dioxide/Hydrogen, 7:1 at 400 Volts

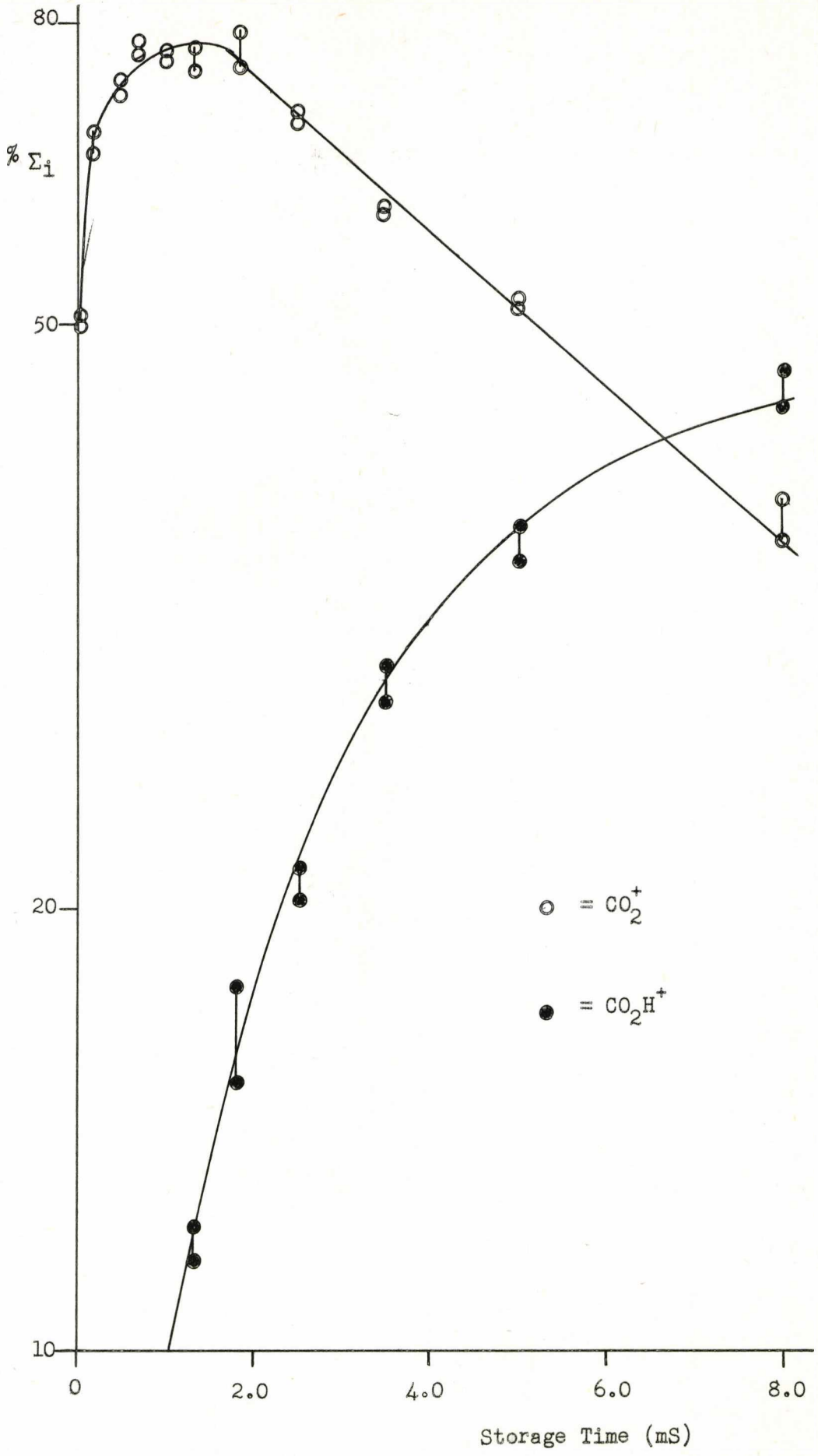

Figure 5-21. Carbon Dioxide/Hydrogen, 1:3 at 400 Volts

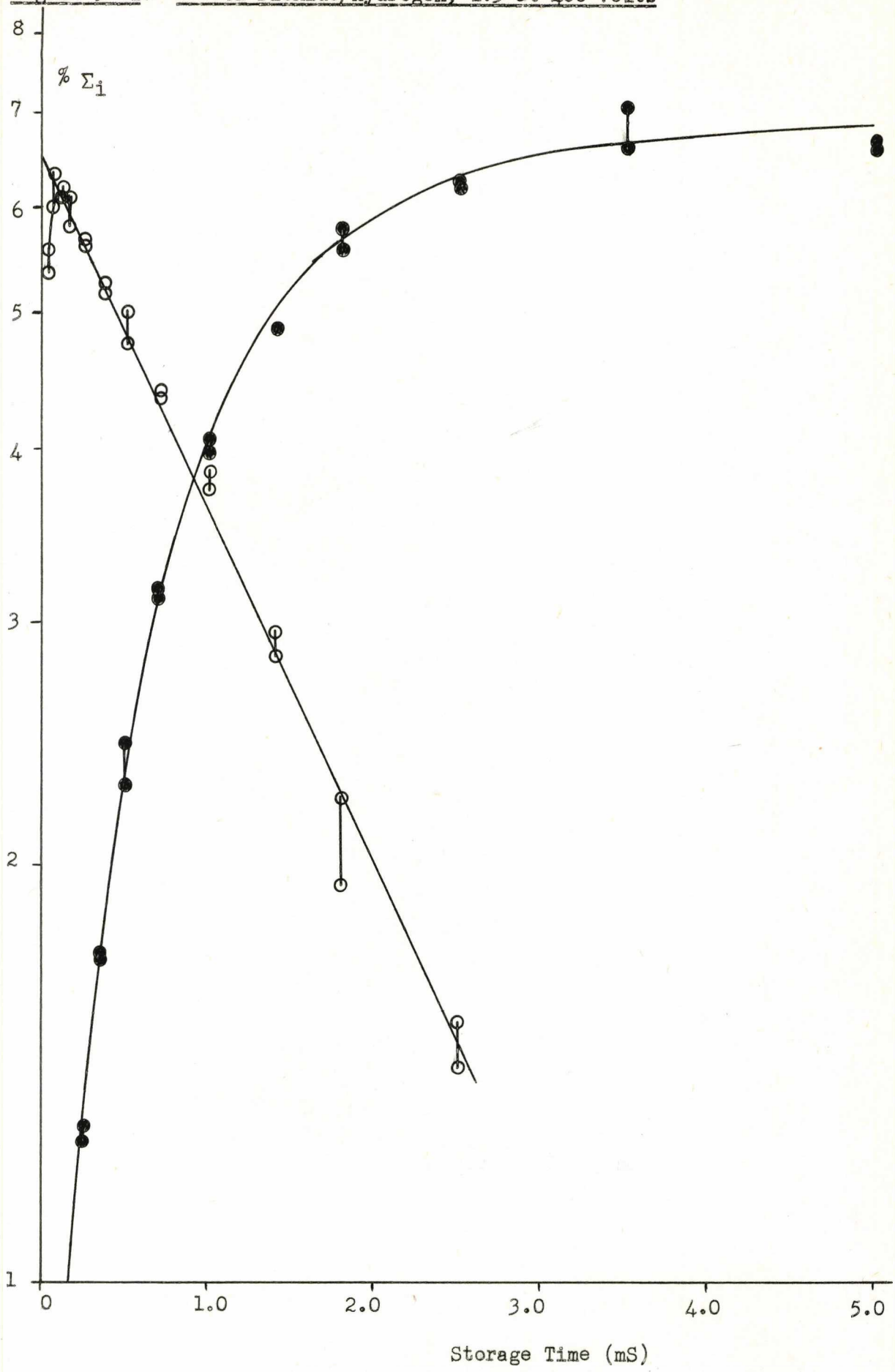

reaction (5-11) did not affect the subsequent reaction of CO_2^+ as long as the decreasing portion only was considered. It can be seen that the cross-over point did not occur at $t_{\frac{1}{2}}$ (marked for CO_2^+), indicating the presence of the additional reactions. Since their contribution could not be estimated, however, only the rate constant for reaction (5-10) was calculated. Values were obtained at several different relative concentrations, and these are summarized in Table 5-2; in each case the total pressure in the inlet system was 20 Torr, and the corresponding partial pressures employed to evaluate the system pressures, in conjunction with Figure 5-17.

Table 5-2. Measured Rate Constants for Reaction 5-12 at Different Relative Concentrations.

	$k \times 10^{10}$ cm^{-3} molecule^{-1} sec^{-1}	
Relative Concentration (H_2/CO_2)	400V	750V
1 : 19	7.2	7.2
1 : 7	7.5	6.2
1 : 1	5.8	6.3
1 : 1	-	3.9
1 : 1	-	4.1
3 : 1	3.8	-
7 : 1	3.1	-
9 : 1	4.2	-
19 : 1	5.3	-
Average k	5.3 ± 2.2	5.6 ± 1.6

The higher concentration of hydrogen systems (that is greater than 3 : 1) were examined in order to minimize the H_2^+ reactions, (5-11) and (5-12), and these results are in fair mutual agreement. Large pressure errors were inescapable here; at low hydrogen concentrations the capsule gauge was inaccurate, and a fractionating effect (caused by the different rates of diffusion - see Section 5.332) always resulted in an unknown relative concentration in the vacuum system.

As a result, no conclusions concerning the behaviour of the reaction :

$$CO_2^+ + H_2 \longrightarrow CO_2H^+ + H$$

with primary ion kinetic energy could be confidently drawn. Bearing in mind the large - and essentially unknown - pressure errors, the rate constants were in good agreement at the two voltages, indicating little change with RF amplitude, even though the sensitivity at 750 Volts was 10 times that at 400 Volts. Furthermore, these results show that the ion energies, calculated as described in Chapter 3, were certainly of the right order of magnitude.

Methane

As has been mentioned, the major reactions occuring in the methane system at thermal ion energies are :

$$CH_4^+ + CH_4 \longrightarrow CH_5^+ + CH_3 \qquad (5\text{-}13)$$

$$CH_3^+ + CH_4 \longrightarrow C_2H_5^+ + H_2 \qquad (5\text{-}14)$$

$$CH_2^+ + CH_4 \longrightarrow C_2H_3^+ + H_2 + H \qquad (5\text{-}15)$$

$$CH^+ + CH_4 \longrightarrow C_2H_2^+ + H_2 + H \qquad (5\text{-}16)$$

In addition, the following endothermic reactions become important at higher energies :

$$CH_4^+ + CH_4 \longrightarrow CH_3^+ + ? \qquad (5\text{-}17)$$

$$CH_3^+ + CH_4 \longrightarrow C_2H_3^+ + 2H_2 \qquad (5\text{-}18)$$

The latter two reactions have primary ion kinetic energy thresholds of ca. 1.5 eV, for ground state CH_4^+ and CH_3^+ [114].

The behaviour of this system, with kinetic energy, has been studied by the various groups shown in Table 5-3. In ICR and TMS studies, the pairs of reactions (5-13), (5-17), and (5-14), (5-18) can be separated and studied individually; this was not possible in the QUISTOR, but these reactions are nevertheless discussed separately.

(a) Reactions of the CH_4^+ Ion

Although there is little doubt that the primary product of CH_4^+ is CH_5^+, and that any secondary CH_3^+ occurs by dissociation of this latter species, there is, however, a possibility that the CH_3^+ species is formed directly from the CH_4^+ without prior formation of CH_5^+. Generally, the reaction of CH_4^+ is written as :

$$CH_4^+ + CH_4 \longrightarrow \begin{cases} CH_5^+ + CH_3 \\ \searrow\ CH_3^+ + H_2 \end{cases} \qquad (5\text{-}19)$$

In any event, whatever the mechanism, dissociation of the precursor of CH_3^+ must result from internal energy, transferred to it from the kinetic energy of the CH_4^+. For the case of ground state CH_4^+ ions, the reaction producing CH_3^+ is endothermic by ca. 1.4 eV, and McDaniel[4], considering the reaction to proceed as in (5-19), states that CH_3^+ ions are not observed for CH_4^+ energies of less than 2.8 eV, since the transfer process will only be approximately 50% efficient for entities of comparable mass. Nevertheless, CH_3^+ ions are often observed at CH_4^+ kinetic energies below the threshhold value, owing to the presence of excited CH_4^+ ions; the degree of excitation may be estimated from the

Table 5-3. Summary of Groups Who Have Examined the Reactions in Methane with Variations of the primary ion kinetic energy

$CH_4^+ + CH_4 \longrightarrow CH_3^+$ or CH_3^+

Group	Method	Ref.
Giardini-Guidoni and Friedman	MS	114
Abramson and Futrell	TMS	115,116
Harrison, Nagy, Chin and Herod	MS	23

$CH_3^+ + CH_4 \longrightarrow C_2H_5^+$ or $C_2H_3^+$

Group	Method	Ref.
Abramson and Futrell	TMS	115
Anders	ICR	117
Clow and Futrell	ICR	80
Harrison, Nagy, Chin and Herod	MS	23

Key : MS = Mass spectrometer ion source.

TMS = Tandem mass spectrometer.

ICR = Ion cyclotron resonance.

appearance potentials of CH_4^+ and CH_3^+ in methane, which differ by 1.2 eV, suggesting that CH_4^+ ions can be formed with vibrational energy in the range $0 \longrightarrow 1.2$ eV.

In this work, methane was examined at 400 and 750 Volts in order to determine whether the expected product distribution change occurred. At these voltages, the mean CH_4^+ kinetic energies were calculated as being 1.85 and 6.76 eV, respectively, indicating that little CH_3^+ should be observed at 400 Volts, but should be distinctly formed at 750 Volts.

The results are summarized in Figure 5-22, which shows a semi-log plot of the data obtained for the CH_3^+, CH_4^+ and CH_5^+ ions at 400 and 750 Volts. It is apparent, that the CH_3^+ curves were different at the two voltages owing to the enhanced production of this ion at the higher voltage. Comparison of the rate constants for loss of CH_4^+ and CH_3^+ at 400 Volts gives :

$$\frac{k_{CH_3^+}}{k_{CH_4^+}} = 0.41$$

which was considerably lower than the literature thermal energy value of 0.9, suggesting the presence of excited ions, and production of CH_3^+ in the QUISTOR at 400 Volts; since the calculated energies are mean values, there will also be more energetic ions present. The rate of CH_3^+ loss at the higher voltage was decreased, and accompanied by a drop in final intensity of the CH_5^+. these results were in agreement with those of the workers listed in Table 5-3, and again support the ion energy calculations.

(b) Reactions of the CH_3^+ Ion

It is generally accepted[115] that the CH_3^+ species reacts with methane molecules *via* a complex, $C_2H_7^+$, the products of which depend on the internal energy transferred during a collision. The various reports on

Figure 5-22 Reaction of CH_4^+ and CH_3^+ in Methane

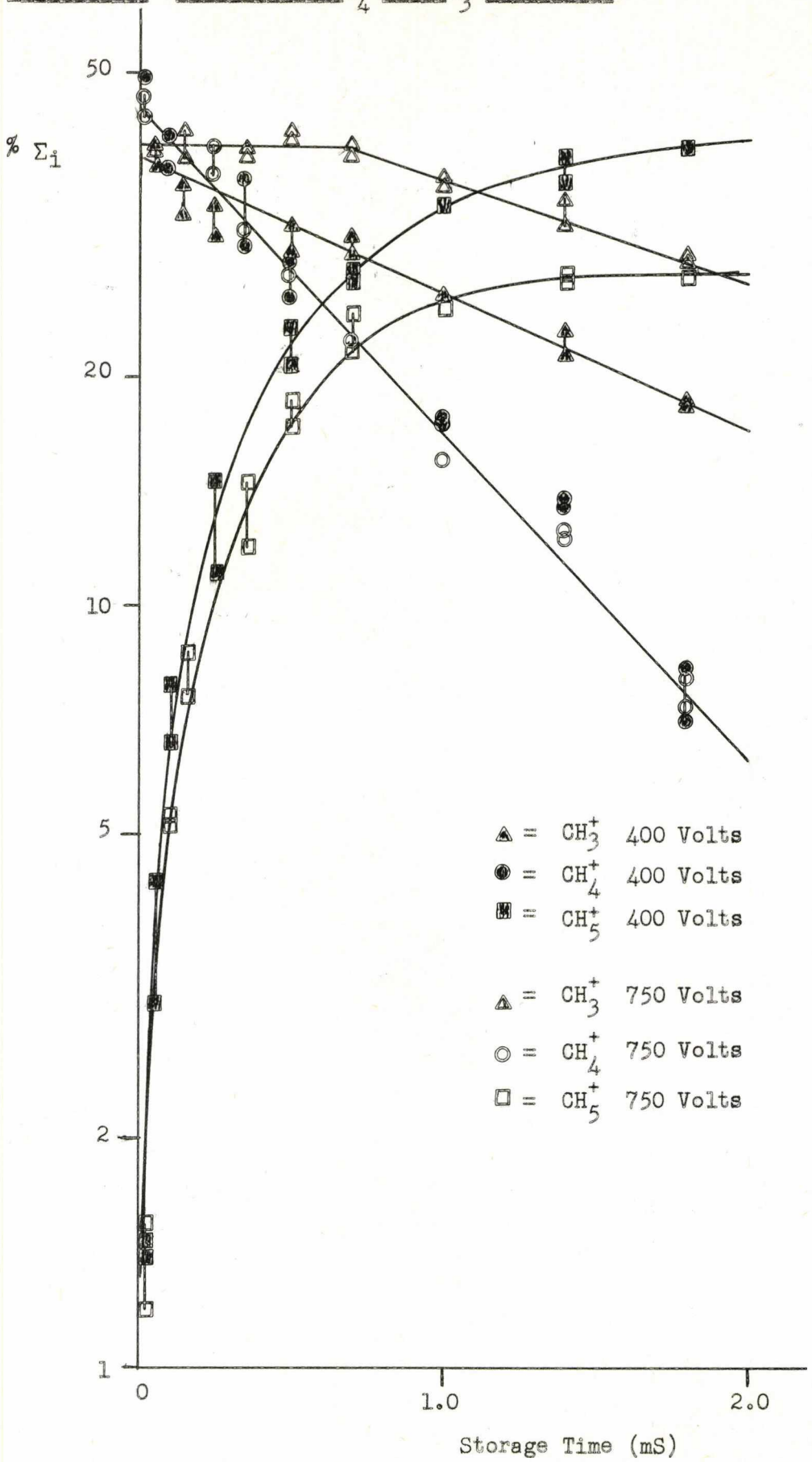

this system, summarised in Figure 5-23, have expressed the percentage of $C_2H_3^+$ of the total C_2 products as a function of the kinetic energy of the CH_3^+ ion. Again - as for the carbon dioxide/hydrogen system - there is a discrepancy between ICR and the other methods. The ICR studies do not report that the $C_2H_3^+$ intensity ever exceeds that of $C_2H_5^+$, whereas the other methods have indicated crossings at fairly low CH_3^+ energies (approximately 3 eV). Anders[117] reports that the reaction producing $C_2H_3^+$ is 1.6 eV endothermic and, if this is so, then the non-ICR results are suggestive of the presence of excited ions. Harrison et al[23] have again used the repeller field to control the ion energy, which may result in errors; similarly the TMS study of Abramson and Futrell[115] may possess some errors, since the energy spread of the ion beam increases at low energies.

The relevant semi-log plots obtained from the QUISTOR, again at 400 and 750 Volts corresponding to mean CH_3^+ kinetic energies of 1.68 and 4.91 eV, are shown in Figure 5-24, and included in the summarized data, Figure 5-23. At the lower energy the relative intensity of $C_2H_3^+$

Figure 5-23. Summary of Literature Distributions of Products from CH_3^+.

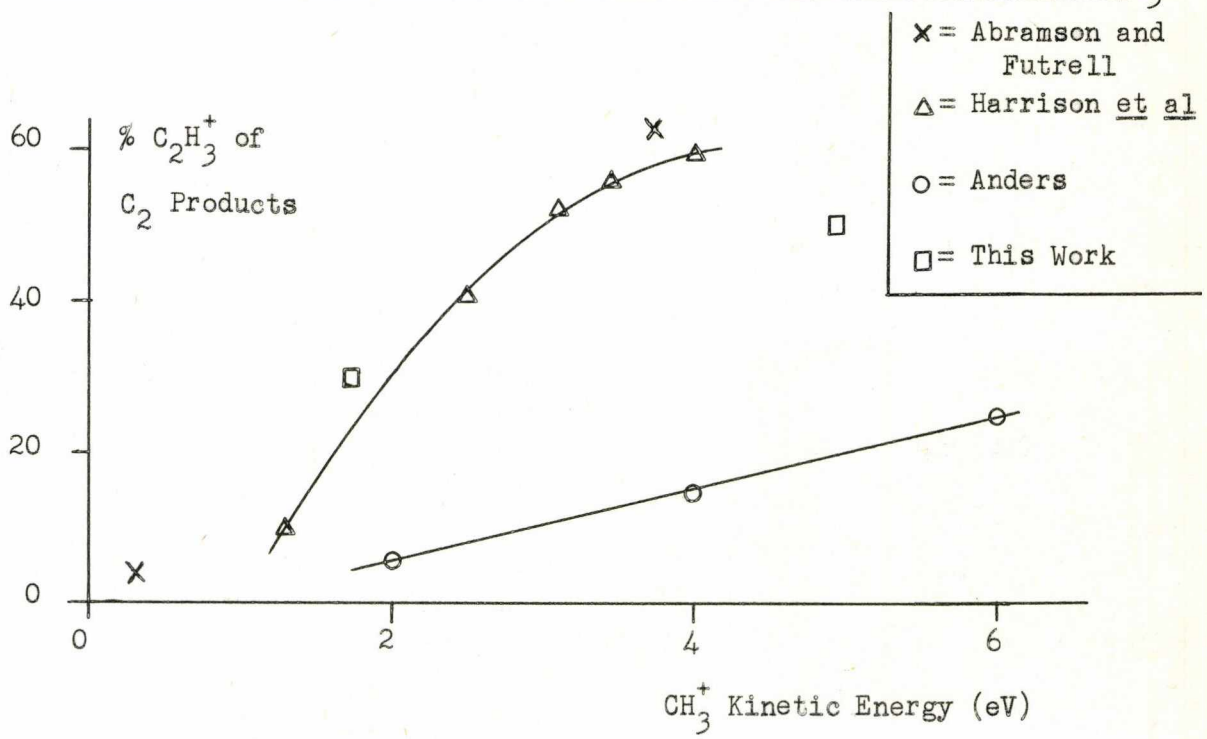

Figure 5-24 Reaction of CH_3^+ Ion in Methane

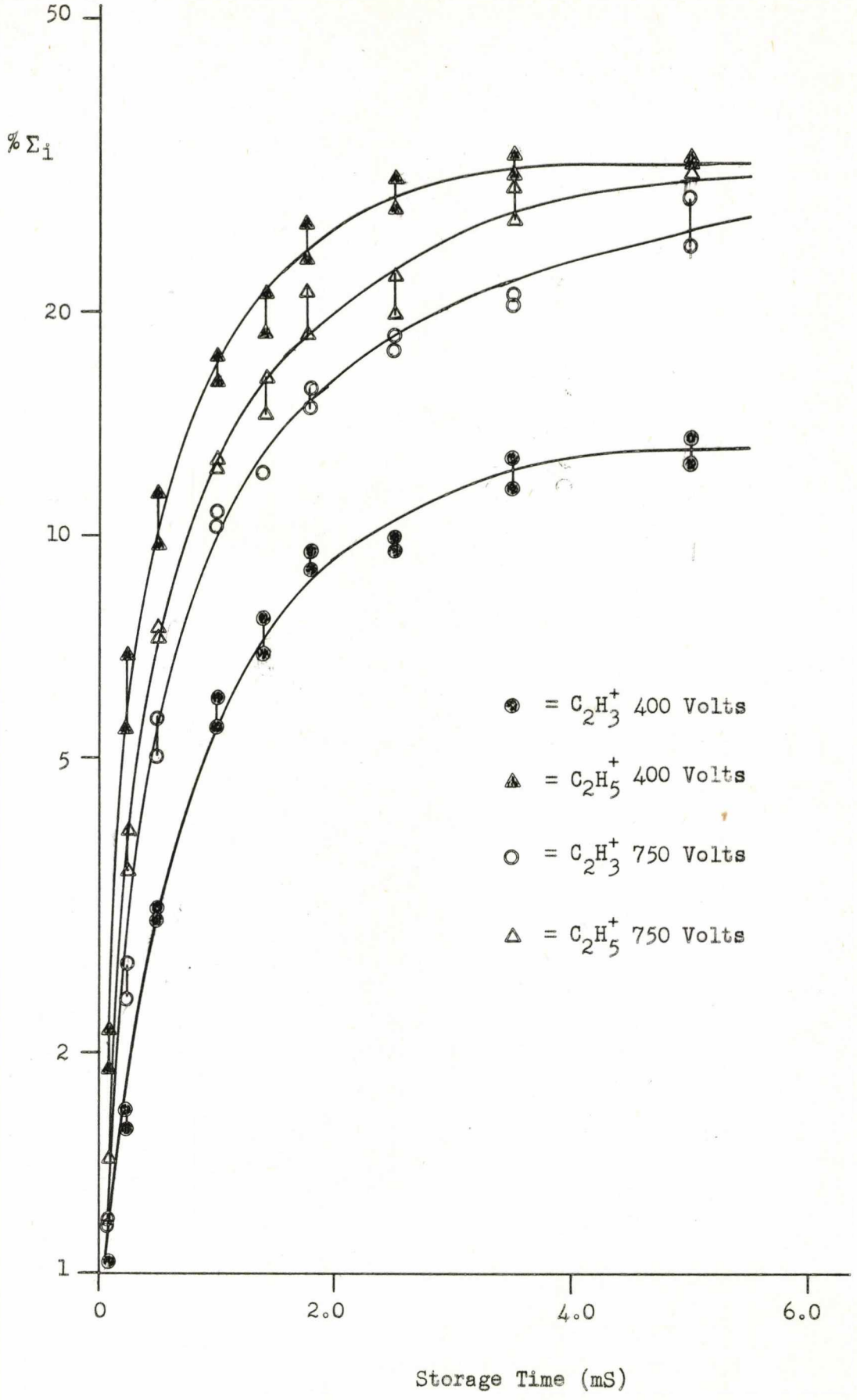

was 30%, rising to approximately 50% at 4.91 eV. These results were in fair agreement with the other reports, and lie between the results from ICR and other studies.

(ii) Comparison of Attractive and Repulsive Ion Extraction

As mentioned earlier, it was important to ensure that the trap was completely emptied by the ion withdrawal pulse, otherwise the storage time was indeterminate. Evidence for incomplete ion-ejection was the presence of abnormally large product ion peaks at short storage times. In order to investigate the effect of different extraction pulse voltages and polarities, an inert gas - argon - was studied to remove the possibility of confusing ion-molecule reactions. The apparatus was operated at fixed RF voltages with the left-hand end-cap, Figure 5-13, earthed and negative pulses applied to the right-hand end-cap. The ion current was recorded and plotted against the voltage of the applied pulse. This was repeated with positive pulses applied to the left-hand end-cap, and at different RF amplitudes.

The results obtained at 400 and 750 Volts of RF are illustrated in Figure 5-25, and showed several interesting features :

(a) Both 'attractive' curves were of similar shape, as were the 'repulsive' curves. The attractive curves exhibit a sharp initial rise, followed by a more gradual increase to a maximum. For the repulsive curves, the initial rise is slower and the maximum ion current, less. The difference between a repulsive and attractive curve, at any one voltage, is believed to be a result of focussing effects which, although unknown, may be estimated in a rather a priori manner as follows. Figure 5-26 shows a schematic diagram of the QUISTOR, the lower end-cap being perforated to allow ions to pass through. If negative pulses were applied to the lower end-cap (attractive mode) then ions would be drawn towards the perforations, this motion is represented by solid

Figure 5-25 Peak Height (Arbitrary Units) vs. Ion Expulsion Pulse Height at 400 and 750 Volts of RF

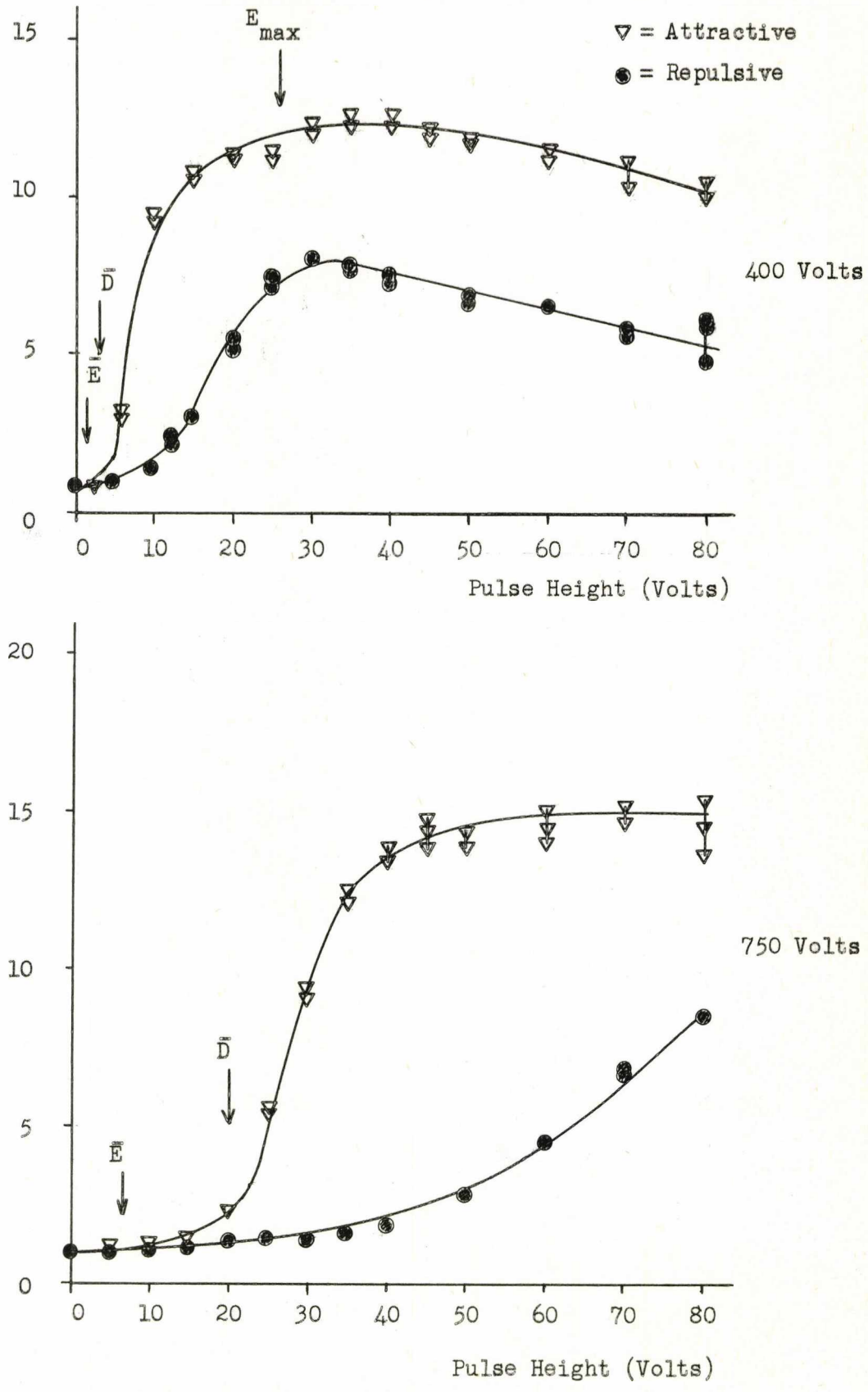

Figure 5-26. Representation of Ion Withdrawal Conditions

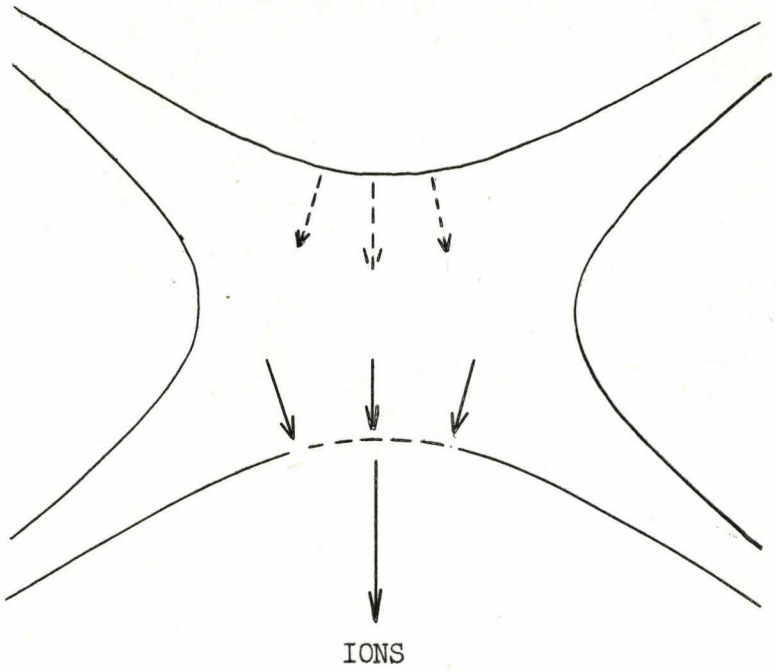

arrows in Figure 5-26. Alternatively, the application of positive pulses to the upper end-cap (repulsive mode) causes the ions to move away from this electrode (dashed lines) rather than towards the lower. Consequently fewer ions would be observed in the latter mode, and this is supported by Figure 5-25.

(b) At low pulse amplitudes the attractive and repulsive curves tended to the same value, indicating that some ions were ejected without the application of an extraction pulse. It is believed that this phenomenon was a result of 'self-ejection' as reported by Dawson and Whetten[34], where ions leave the trap because of space-charge repulsion. Dawson and Whetten were able to measure the frequency at which self-ejection

occurred and, by considering the ion cloud as a plasma undergoing self-oscillation, were able to estimate the ion density in their trap. An attempt to measure the self ejection frequency in this work proved impossible owing to the large swamping effect of the RF pick-up.

(c) As the RF amplitude was increased, the onset of the sharp rise in the attractive curve was delayed; from Dehmelt's model, this appears to be because the pseudo-potential well depth, and hence the ion energy, increased making removal of the ions more difficult. For the sake of comparison, calculated values for the mean ion energy ($\bar{E}$), the pseudo-potential well depth ($\bar{D}$) and the absolute maximum ion energy (calculated from equation (3-38) and represented by E_{max}), are shown in Figure 5-25. E_{max} for 750 Volts RF occurred at 93.8 eV, and is not included. It may be seen that E_{max} represents some measure of the extraction voltage required to remove most of the ions.

From these curves it was apparent that large extraction voltages, preferably attractive, should be used to ensure trap emptying and best signals. The width of the ejection pulse was found to have little effect, unless it was reduced below ca. 5 μS when incomplete trap emptying occurred.

(iii) Comparison of the QUISTOR Storage Capabilities with those of other Quadrupole Ion Traps

Dawson, Hedman and Whetten[36] have given an expression for the rate of change of the number of ions in a quadrupole trap with time :

$$\frac{dN}{dt} = k_1 p - k_2 N^2 - k_3 N p \qquad (5\text{-}20)$$

where : N = number of ions

p = pressure of neutral molecules

k_1 = rate constant for ion creation

k_2 = rate constant for ion-ion scattering

k_3 = rate constant for ion-molecule scattering.

Solution of this equation provides the three rate constants k_1, k_2, k_3 which determine the storage characteristics of the device. The behaviour of expression (5-20) is represented in Figure 5-27 from which it may be seen that the device saturates at a value of N equal to N_∞, for which dN/dt = 0 and :

$$k_1 p = k_2 N_\infty^2 + k_3 N_\infty p \qquad (5\text{-}21)$$

that is the rate of ion loss (by scattering) is equal to the rate of ion creation. If at a time t_1 the ionizing beam is switched off, then N decays according to the equation :

$$\frac{dN}{dt} = - k_2 N^2 - k_3 N p \qquad (5\text{-}22)$$

with the initial condition :

$N = N_o$ when $t = t_1 = 0$ (for the decay process)

Harden and Wagner[42] integrated this equation (5-22) and curve-fitted a set of decay data to the resulting expression, obtaining numerical values for k_2 and k_3. The integration may be performed as follows :

On re-arrangement, (5-22) gives :

$$\frac{dN}{N(k_3 p + k_2 N)} = -dt \qquad (5\text{-}23)$$

Comparison with the standard integral :

$$\int \frac{dx}{x(a+bx)} = \frac{-1}{a} \ln\left(\frac{a+bx}{x}\right)$$

Figure 5-27. Representation of Ion Build-up

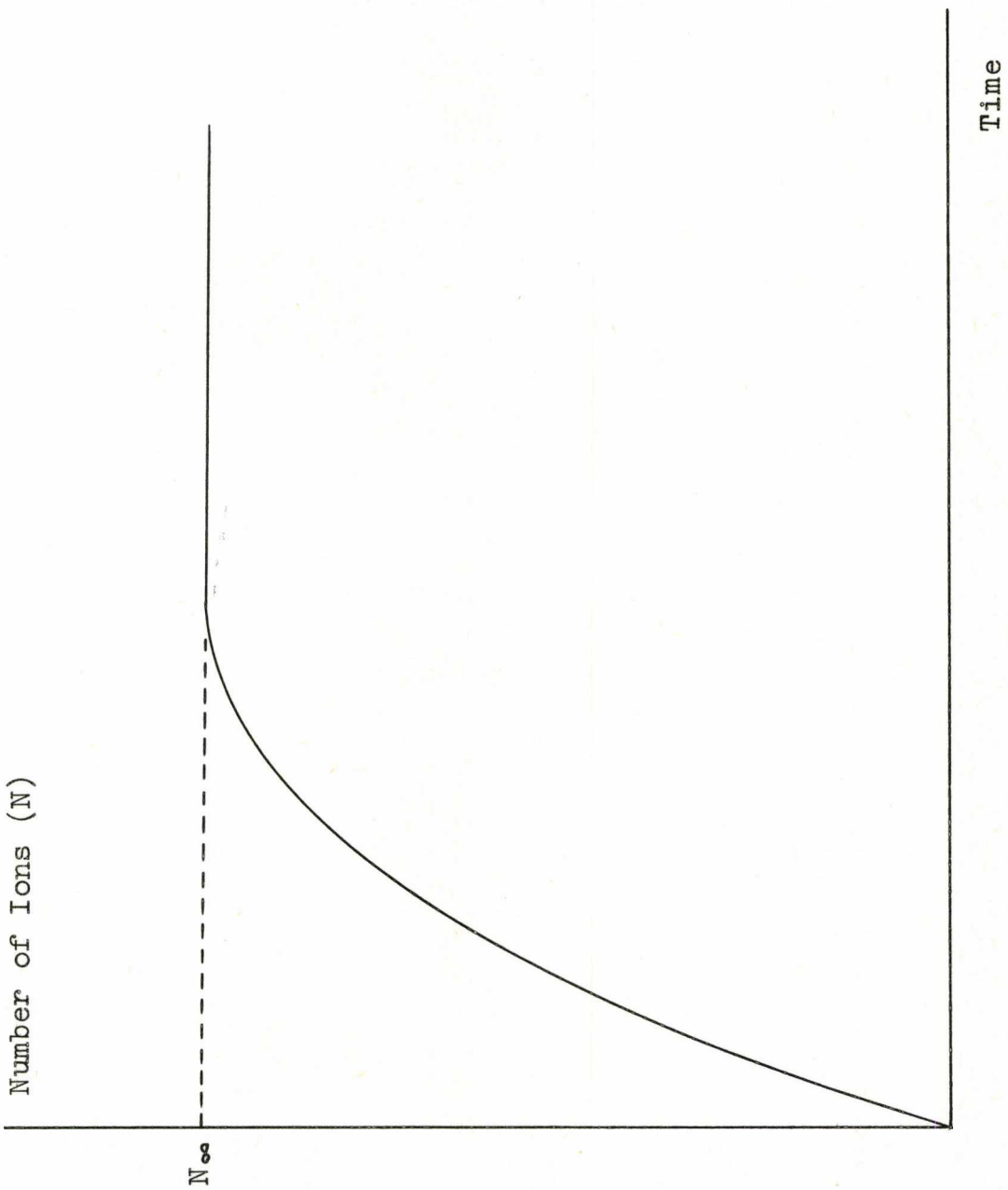

shows that (5-25) may be integrated :

$$\frac{1}{k_3 p} \ln\left(\frac{k_2 N + k_3 p}{N}\right) = t + c'$$

where the constant of integration, c', may be evaluated by applying the initial condition :

$$N = N_o \quad \text{when} \quad t = 0$$

which yields :

$$c' = \frac{1}{k_3 p} \ln\left(\frac{k_2 N_o + k_3 p}{N}\right)$$

and therefore :

$$\frac{1}{k_3 p} \ln\left(\frac{N_o(k_2 N + k_3 p)}{N(k_2 N_o + k_3 p)}\right) = t$$

Whence :

$$\frac{N_o(k_2 N + k_3 p)}{N(k_2 N_o + k_3 p)} = \exp(k_3 p t)$$

which may be re-arranged :

$$N = \frac{k_3 p N_o}{[(k_3 p + k_2 N_o)\exp(k_3 p t) - k_2 N_o]}$$

This equation is unsuitable for curve-fitting, but on inverting both sides :

$$\frac{1}{N} = \frac{(k_3 p + k_2 N_o)\exp(k_3 p t) - k_2 N_o}{k_3 p N_o}$$

$$= \left(\frac{k_3 p + k_2 N_o}{k_3 p N_o}\right)\exp(k_3 p t) - \frac{k_2}{k_3 p} \qquad (5\text{-}24)$$

an expression is obtained which can be fitted to the general form of

an exponential equation :

$$y = a \exp(bx) + c \qquad (5\text{-}25)$$

with :

$$a = \frac{k_3 p + k_2 N_o}{k_3 p N_o}$$

$$b = k_3 p \qquad (5\text{-}26)$$

and $$c = \frac{k_2}{k_3 p}$$

An expression for k_1 may be obtained by consideration of equation (5-20) and Figure 5-27, as follows. It is apparent that as $t \rightarrow 0$, then $N \rightarrow 0$ and hence $k_3 N_p \rightarrow 0$ and $k_2 N^2 \rightarrow 0$, therefore in the limit :

$$\frac{dN}{dt} = k_1 p \qquad (5\text{-}27)$$

Thus k_1 may be evaluated from the initial slope of a plot such as that shown in Figure 5-27.

Generally, k_1 will vary for different traps, since it depends on the electron beam optics, but the other parameters - k_2, k_3 and N_{∞} - should be fairly constant, irrespective of the actual device.

In attempting to measure these quantities in this work, two major experimental difficulties were encountered.

(i) Pressure errors; nitrogen was used as a sample, since the ion gauge was supposedly calibrated for this gas, but gauge contamination probably resulted in large errors (see Section 5.332).

(ii) In order to calculate N as a number of ions, some measurement of the number of ions in the trap corresponding to a given output at the pen recorder was necessary.

Figure 5-28 shows a schematic representation of the apparatus; the various transmission efficiencies or gains of each stage could be readily measured, with exception of the transfer efficiency from QUISTOR to analyzer. Based on the work of Dr. Lawson[37], this quantity was estimated as 1×10^{-3}. Utilizing these values, the number of ions in the trap corresponding to a voltage output at the pen recorder of V volts was estimated in the following manner.

The output voltage, V, was the result of averaging several pulses of height V' Volts and width 20μS over the time between pulses, i.e. 10 mS at 100 Hz. Consequently, V' was given by :

$$V' = \frac{10 \times 10^{-3}}{20 \times 10^{-6}} \times V = 500\ V$$

This voltage was caused by a current pulse, of height I, flowing through the input impedance of the pen recorder, R_I, which, from Ohm's Law was :

$$I = \frac{V'}{R_I} \text{ Amps.}$$

which was : $I = V \times 5 \times 10^{-4}$ Amps, as $R = 1\ M\Omega$.

The height of each pulse, I_p, arriving at the electron multiplier first dynode, D_I, was therefore given by I/Gm, where Gm was the multiplier gain, measured as 3×10^4.

Therefore :

$$I_p = \frac{I}{3 \times 10^4} = V \times 1.66 \times 10^{-8} \text{ Amps.}$$

The continuous rate of ion arrival, I_A, equivalent to this peak current is given by multiplying I_p by a factor of $1/1.6 \times 10^{19}$ ions sec^{-1}, so :

$$I_A = V \times \frac{1.66}{1.6} \times 10^{11} \text{ ions } sec^{-1}.$$

Figure 5-28. Schematic Diagram of Apparatus

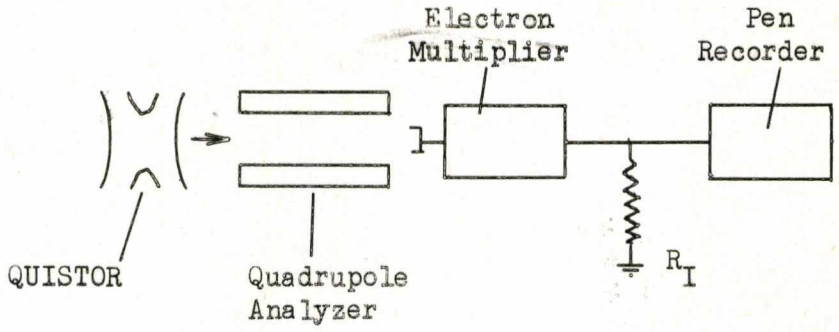

Since, however, the pulse of ions was only 20 μS wide, the number of ions per pulse, N_p, was found from :

$$N_p = V \times \frac{1.66}{1.6} \times 10^{11} \times 2 \times 10^{-5}$$

$$= V \times \frac{1.66}{1.6} \times 2 \times 10^{6}$$

The transmission efficiency of the quadrupole analyzer was measured as 10^{-2}, for the conditions of the experiment by comparing total pressure (100% transmission) and resolved signals. Combined with the estimated QUISTOR/analyzer transfer efficiency of 10^{-3}, this indicated that the number of ions in the trap, N, producing an output signal of V Volts was given by :

$$V \text{ Volts} = V \times 1.04 \times 2 \times 10^{6} \times 10^{5} \text{ ions}$$

$$= V \times 2.08 \times 10^{11} \text{ ions} \qquad (5\text{-}28)$$

The experimental procedure adopted was to operate the QUISTOR with a duty cycle of 100 Hz, at 2.75 MHz (to ensure ion trapping) and a fixed RF amplitude of 350 Volts. The width of the electron gating pulse was gradually increased, maintaining the ejection pulse (attractive and 80 Volts) immediately after it. In this way the output voltage was obtained as a function of t, and eventually saturated, as illustrated in Figure 5-27. The electron pulse width was then fixed and the time between it and the ejection pulse (storage time) increased, to allow a decay durve to be obtained. The decay data was fitted to an exponential expression, of the form of (5-27), and k_2 and k_3 evaluated; k_1 and N_∞ were calculated from the initial slope and saturation value respectively.

A typical build-up graph is shown in Figure 5-29, obtained at an indicated pressure of 5×10^{-5} Torr, and the corresponding decay curves in Figure 5-30. Each of the latter curves corresponds to decay from a fixed ionizing pulse width, which is indicated on the diagram. The recorded peak heights are in milli-volts, the correction factor being applied after curve-fitting. The error bars are large, and when combined with the pressure errors gave overall inaccuracies of at least one order of magnitude.

Table 5-4 compares the values obtained in this work with those of other workers. The values for k_1, k_2, k_3 and N_∞ are in ions $cm.^{-3}$, the volume of the trap having been estimated from the equation for the volume of a oblate spheroid :

$$V = \frac{4}{3} \pi r_o^2 z_o$$

as 3 cm^3.

Figure 5-29 Ion Build-up at 5×10^{-5} Torr

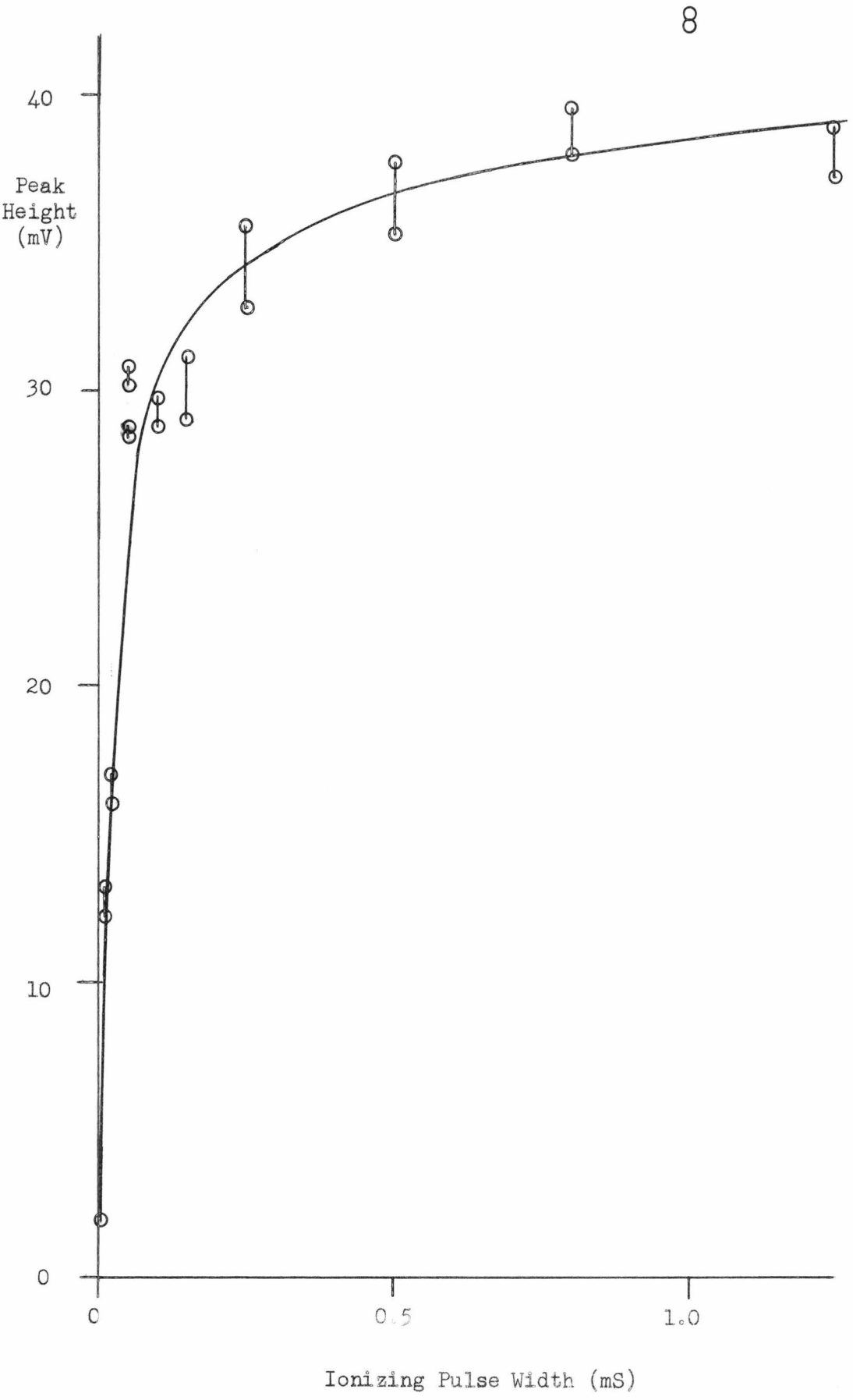

Table 5-4 Comparison of Three-Dimensional Quadrupole Storage Characteristics

	This Work	G. Lawson[37]	Dawson[36] et al	Harden and Wagner[42]
r_o (cm)	1.0	1.0	1.7	1.414
Species Examined	N_2^+	Propane	N_2^+	N_2^+
Pressure (Torr)	5×10^{-6} - 2×10^{-4}	7×10^{-5}	10^{-8} - 10^{-5}	10^{-6}
RF Frequency (MHz)	2.75	3.3	1.0	.2 → .315
RF Voltage (Volts)	350	500	300	70
DC (Volts)	0	0	79*	9*
k_1 ($cm^{-3}Torr^{-1}sec^{-1}$)	4.7×10^{14} - 6.7×10^{15}	1.1×10^{15}	2.15×10^{15}	2.14×10^{12}
k_2 (cm^3sec^{-1})	1.2×10^{-8} - 2.4×10^{-6}	-	2×10^{-5}	1.29×10^{-5}
k_3 ($Torr^{-1}sec^{-1}$)	2×10^8 - 4×10^8	3.7×10^5	1.7×10^8	1.25×10^{10}
N_∞ (ions cm^{-3})	3.2×10^8 - 2.8×10^9	3×10^9	1.5×10^7	9.7×10^8 *
$\bar{D}$ (Volts)	0.89	1.58	3.38	4.26

* This datum was not quoted by the authors, and has been estimated here for the sake of completeness.

Values for the pseudo-potential well depth, $\bar{D}$, are given since according to Dehmelt[49] the maximum number of ions stored should be proportional to this quantity.

Although definite conclusions could not be drawn from these results, owing to the large errors, some useful comparisons could be made. Any variation in k_1 (the ion creation rate constant) is to be expected, as this is dependent on the ion optics, and consequently the agreement with the values of Dawson *et al* and Dr. Lawson is surprisingly good. It was also interesting to note that the accurate stainless steel traps (Harden and Wagner and this work) gave lower values than the mesh traps (Dawson *et al* and Dr. Lawson), for k_2 but higher values for k_3. From the former observation it might appear that ions were trapped more efficiently in the accurate devices (as would be hoped), but this was not supported by the k_3 values. To compare the relative magnitudes of ion loss processes due to ion-ion and ion-molecule scattering the quantities k_2 and k_3 must be multiplied by N^2 and N_p respectively, assuming a pressure of 10^{-5} and a saturation value (N_∞) of 10^9 ions cm^{-3} the values obtained here give :

$$k_2N^2 = 5 \times 10^9 - 9 \times 10^{11} \text{ ion sec}^{-1}$$

$$k_3N_p = 2 \times 10^{12} - 4 \times 10^{12} \text{ ion sec}^{-1}$$

These values suggest that, under these conditions, major ion losses from the QUISTOR were caused by ion-molecule scattering; this conclusion is in agreement with the more detailed study of Dawson *et al* who found ion-molecule scattering to be the dominant process at pressures greater than 10^{-7} Torr. It is apparent from Figure 5-30 that, under the normal QUISTOR operating condition of *ca*. 10 μS electron beam pulse width, the ion loss was quite small and could be easily counteracted by basing calculated rate constants on percentage total ionization measurements

Figure 5-30 Ion Decay at Various Electron Beam Pulse Widths

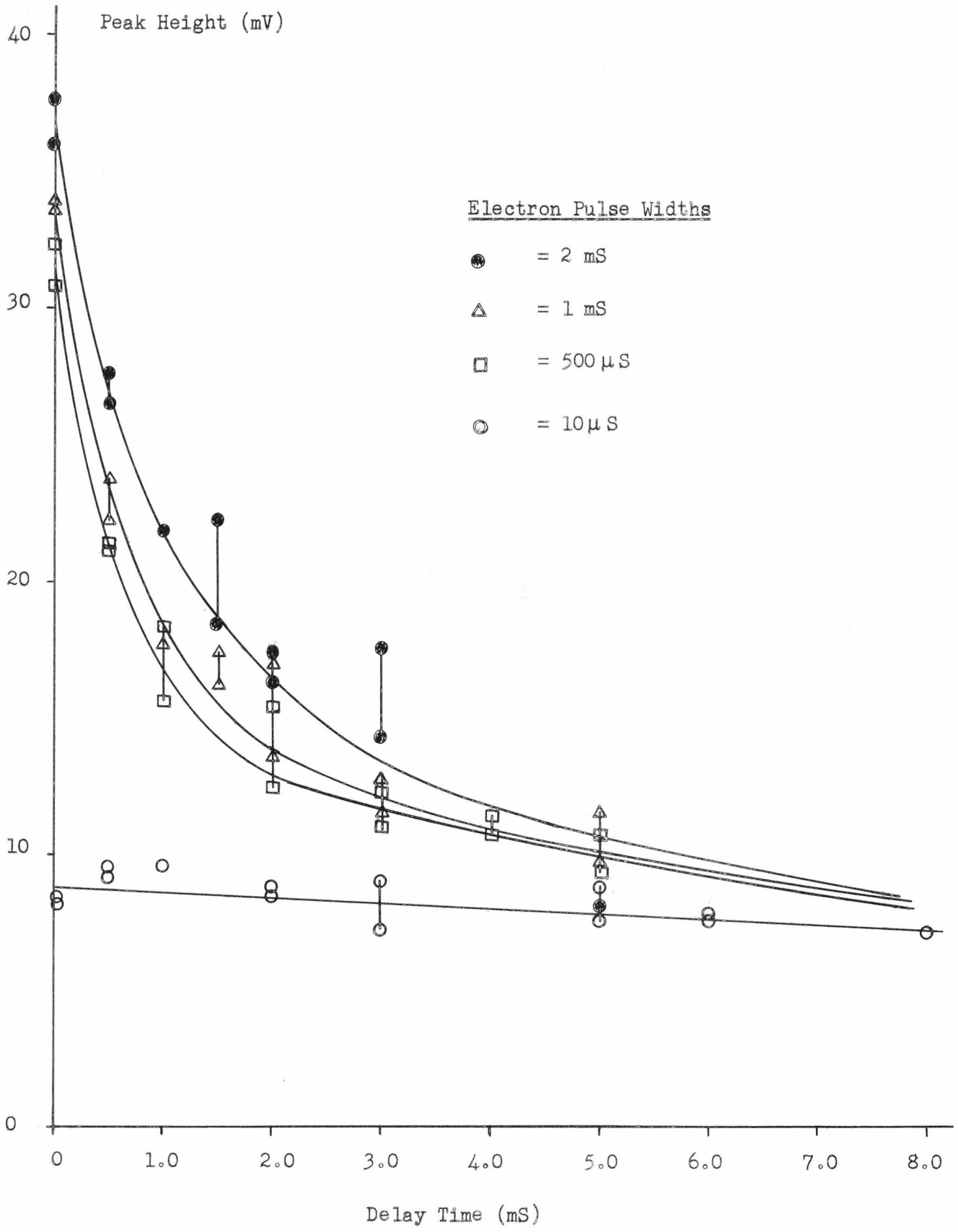

(see Sections 5.332 and 5.333(i)). At first sight the N_{∞} values bear little relationship to the $\bar{D}$ values; insufficient data is available for a meaningful comparison, however, since the Harden and Wagner N_{∞} value has been estimated, and the pressure at which the value of Dawson et al was obtained was not quoted. Since the N_{∞} values are also dependent on pressure, this quantity is important. It can be seen, however, that in this work, even though $\bar{D}$ was small, the calculated N values are comparable to the other results, suggesting that the accurate trap was more efficient than the mesh instruments. The value of N_{∞} estimated from Harden and Wagner's report is also fairly high, considering that their pressure was an order of magnitude lower than that used in this work, or in the work of Dr. Lawson.

5.4 Conclusion

In summary, this chapter has described the experiments performed in order to characterize the stainless steel QUISTOR and electron gun. In particular, attention was given to the behaviour at different RF frequencies and amplitudes, it being shown that most efficient storage occurred at 2.75 MHz and that, although altering the observed signal intensities, the main effect of altering the RF amplitude was to alter the ion kinetic energy. Evidence was also gathered supporting the ion energy calculations, see Chapter 3, and indicating that they were at least correct within an order of magnitude. The necessary checks, to ensure correct storage, and the optimum operating conditions were evaluated, and the major of these are summarised below.

(i) The device had to be clean for storage to be realized.

(ii) Because of the energy spread in the electron beam it was advisable to maintain a large negative potential difference between the filament and electron gate (at least 50 Volts). The RF voltage applied to the ring did not seriously affect the beam, other than to reduce its intensity by partial switching.

(iii) It was vital to ensure correct electron beam switching, failing which the storage time was indeterminate. This was checked by observing the ion pulses with the oscilloscope and confirming that these were reduced to zero when the electron gating pulse generator was switched off.

(iv) Operation at 2.75 MHz was also essential, otherwise ions were ejected.

(v) It was shown that zero storage, that is with coincident creation and expulsion pulses, gave misleading results owing to the possibility of incomplete ion ejection with consequent reactions during the dead time.

(vi) Operation with attractive ion removal gave better signal strengths than did repulsive, owing to better focussing. Further, large pulse voltages were necessary to completely empty the trap.

(vii) The RF amplitude was chosen to give a specific ion energy, or (particularly in the case of the Chemical Ionization work described in the following chapter) was 'optimized', that is, selected to give maximum product ion signal strength, at a given storage time, consistent with obtaining no products at 20 μS storage time.

(viii) Pressures were related to a known pressure in the inlet system, this being calibrated using the known rate of reaction of the CH_4^+ ion in methane :

$$CH_4^+ + CH_4 \longrightarrow CH_5^+ \quad \text{or} \quad CH_3^+$$

(ix) Ion currents, to be plotted against storage time, were normalized by expressing them as a percentage of the total ionization (total ion current) to overcome the slight ion loss.

(x) Although not conclusively proven, the storage characteristics suggested that the stainless steel QUISTOR was more efficient at storing ions than the mesh device that had been used previously;[37] this observation was supported by the greater ion currents generally encountered in this work.

The preceding conditions and tests were employed in all the experimental work described in the next chapter.

CHAPTER 6

Ionic Processes Observed in the QUISTOR

6.1 Introduction

This chapter contains a description of the various ionic processes that have been observed in the QUISTOR, and these are discussed under several headings, viz. Chemical Ionization, Spectrum Simplification, Ion-molecule Reactions, Metastable Ion Decay and Sequential Mass Spectrometry. These classifications are somewhat arbitrary, for example, the process of Spectrum Simplification is basically a series of ion-molecule reactions, and the order of their presentation in no way represents the chronological order in which the experimental work was performed. In fact this section of the examination proceeded on several fronts more or less simultaneously, with the underlying aims always being borne in mind. Essentially, these aims were to examine the adaptability of the QUISTOR to various studies and applications from both academic and technological/industrial view points. In respect of the latter, the particular possible application envisaged was as a detector for 'trace' components, for example, atmospheric pollutants. The result of such a wide investigation was, inevitably, that most of the above categories were studied in a rather cursory manner, detailed examination of any one topic being left to future workers. In particular, the Chemical Ionization studies are already being continued by Mr. R. E. Mather, who is also investigating the possibility of incorporating such a device into a large, magnetic sector mass spectrometer, in this case an A.E.I. MS 902.

In order to bring some degree of unity to these various sections they are preceded by a brief account of the reasoning process behind the experiments.

It is worth mentioning the main theories that have been proposed to explain ion-molecule reactions, since these are often mentioned in this

chapter in connection with experimental studies.

The first theory was described by Langevin as reported by Giomousis and Stevenson[107], for the simple case in which a long-range interaction between an ion and a molecule was assumed to induce a dipole in the latter with consequent mutual attraction and, if the initial separation perpendicular to the direction of the ion was suitably small, orbiting and reaction. This method gave rise to a simple expression for the capture cross section involving the polarizability of the molecule, the charge on the ion and the reduced mass of the system. As experimental techniques improved, however, it was realized that the cross-sections predicted by this theory were often too small, particularly if the molecule possessed a permanent dipole. Consequently Theard and Hamill[124] and Moran and Hamill[125] introduced an additional term to allow for the attraction between the ion and dipole, and made the simplifying assumption that the molecule rotated in order to maintain the orientation of the dipole towards the ion, the so-called 'locking-on' of the dipole. This theory, which has been termed the 'Locked Dipole Orientation' Theory, (LDO), has been found to predict cross-sections which, in contrast to Langevin's theory, were too large, and it was suggested by Gupta, Jones, Harrison and Myher[126] that 'locking-on' did not necessarily occur. At present an alternative theory, proposed by Su and Bowers (see refs. 127 and 128 for example and further references) and known as the 'Average Dipole Orientation' Theory (ADO), is being evaluated. In this the 'average orientation' of the ion and dipole is introduced, to allow for hindering of the molecular rotation by the ion and the random orientation at large separations, and is used to determine the cross section. Preliminary results (see ref. 128) indicate that the agreement between predicted and experimental cross sections is extremely good.

6.2 Ionic Processes in the QUISTOR

Although it had already been shown[37] that ion-molecule reactions could be examined in a wire mesh QUISTOR, further systems were studied during this work for a variety of reasons :

(i) Ion-molecule reactions are in themselves of great theoretical and practical interest, as has been indicated above and in Chapter 2; from studies of this kind, data has been obtained on basic collision processes and the understanding of topics involving ion chemistry, such as upper atmosphere conditions, and products from plasma and combustion, has been enlarged.

(ii) As many ion-molecule reactions are strongly dependent on the primary ion kinetic energy, their study also permits estimation of this quantity in the QUISTOR, by comparison with published data. This kind of investigation has been partially described in the preceding chapter.

(iii) The study of ion-molecule reactions led directly to the development of Chemical Ionization, and may be used to evaluate the potential of different gases for use as reagents in this technique.

(iv) The use of atmospheric ion-molecule reactions is often inherent in the design of atmospheric pressure ion sources and low-level concentration detecting equipment, which frequently rely on reactions of species such as H_3O^+ and OH^-.

In this work, the data obtained concerning the ion-molecule reactions occurring in a particular system was often exploited in several of the above areas; for example the water system was originally examined to determine its viability as a Chemical Ionization reagent, but the results were also used to support the kinetic energy calculations.

Having shown that ion-molecule reactions occurring in the QUISTOR, under suitable RF conditions, yielded predominantly the CH_5^+ and $C_2H_5^+$ species, the observation of Chemical Ionization (CI) was thought to be

distinctly likely, and was in fact observed. In many respects CI is a technique for detecting low-level concentrations, since only a spectrum due to the sample is observed even though it is only ca. 1% of the total material present in the ion source, and consequently was of interest. Clearly, so far as the detection of atmospheric pollutants is concerned, the use of air as a reagent gas would be advantageous, and this was also found to be possible. In turn this prompted an examination of the ion molecule reactions that can occur in air and water; the latter is of interest because the employment of air as a CI reagent gas relies on charge transfer from species such as N_2^+ or O_2^+, and proton transfer from H_3O^+, produced by the well-known ion-molecule reaction :

$$H_2O^+ + H_2O \longrightarrow H_3O^+ + OH$$

The reactions of water and similar substances, for example ammonia, are also of interest in the study of gas phase acidities and basicities.

During the studies of some systems an interesting phenomena, which has been termed 'Spectrum Simplification', was observed; this again relies on a series of ion-molecule reactions which result in only one ionic species being observed as the storage time is increased, owing to collision, and reaction, of the fragment ions with neutral molecules.

Much of the work described in the following sections was of a quantitative nature, the RF was not usually set to give a specific ion kinetic energy, but more often to 'optimize' the observed reactions (see Section 5.4); at all times the conditions and tests, described at the end of the preceding chapter, were employed.

6.3 Chemical Ionization (CI)

Since first being reported by Munson and Field[3] in 1966, CI has become one of the most widely used techniques in analytical mass spectrometry, particularly for high molecular weight samples, such as biochemicals. The reason for this extremely rapid development is that

CI is a much 'gentler' form of ionization than conventional Electron Impact (EI), and consequently results in greater abundances of the molecular ion and less fragmentation. As originally described, the technique involved subjecting a small amount of sample, mixed with a large excess of reagent gas (methane) so that the total source pressure was 1 - 2 Torr, to electron impact ionization; the methane was preferentially ionized and, owing to the high pressure, underwent sequential ion-molecule reactions producing predominantly CH_5^+ and $C_2H_5^+$ ions, (see Section 5.333). These species in turn underwent reactions with the sample molecules, AH, resulting usually in either proton transfer :

$$CH_5^+ + AH \longrightarrow AH_2^+ + CH_4$$

or hydride ion (H^-) abstraction :

$$CH_5^+ + AH \longrightarrow A^+ + CH_4 + H_2$$

leading to ions at (M + 1) or (M - 1), where M is the molecular weight of AH. Conventional EI ionization employs 70 eV electrons, and results in odd-electron positive ions which frequently experience extensive fragmentation to re-distribute the internal energy transferred. With CI however, the reactions depicted above involve low energy (< 5eV) methane secondary ions, and result in even-electron species with correspondingly little fragmentation being observed. Since the introduction of this technique the use of many reagent gases has been reported, some of which are summarised in Table 6-1 along with the stable reagent ions produced, and have been reviewed in detail elsewhere[1,129]. The use of NH_3, NO, Ar/H_2O, N_2/H_2O and ozone[130] has been pioneered by Hunt and colleagues in what is essentially gas-phase organic chemistry (see references 129 and 131 for examples and further references). Hunt[131] has pointed out that with CI the mass spectrum obtained is dependent on the nature of both sample and reagent, and consequently much structural information may

Table 6-1. Some CI Reagent Gases

Reagent Gas	Stable Ions Formed
CH_4	CH_5^+, $C_2H_5^+$
C_3H_8	$i-C_3H_7^+$
$i-C_4H_{10}$	$t-C_4H_9^+$
H_2	H_3^+
Rare Gases (R)	R^+
N_2	N_2^+
H_2O	H_3O^+, $(H_2O)_2H^+$ etc.
CH_3OH	$CH_3OH_2^+$, $(CH_3OH)_2H^+$, etc.
NH_3	NH_4^+, $N_2H_7^+$ etc.
NO	NO^+
Ar/H_2O *	H_3O^+, Ar^+, Ar_2^+
N_2/H_2O *	H_3O^+, N_2^+, N^+

* In the case of these mixtures, Hunt[131] also reports the presence of excited argon and nitrogen atoms and abundant slow electrons which may contribute to the CI spectrum.

be obtained by the use of several reagent gases. As an example, he quotes the fragmentation induced by proton transfer to a sample from hydrogen, methane and tertiary butane; in these cases the Brönsted acidity decreases in the order given, and is accompanied by a decrease in the kinetic energy transferred to the sample molecule, and hence also in the resulting fragmentation. Although for identification of an unknown sample, determination of the molecular weight, and hence abundant molecular ions, are of great use, some fragmentation is also desirable if structural information is required. To this end Hunt has suggested that argon-water and nitrogen-water mixtures are of greatest use as CI reagents, since sample molecules encountering H_3O^+ ions are protonated with little fragmentation, while those experiencing charge transfer from Ar^+, Ar_2^+, N_2^+ or N^+ undergo similar fragmentation to that observed in EI sources, the ionization potentials of these species being larger than those of most organic compounds. The result is a mass spectrum which shows abundant molecular and fragment ions, and has the appearance of an addition of a CI (methane) and EI spectra. The only advantage of nitrogen-water over argon-water mixtures, according to Hunt, is the cheapness of the former, which is also of interest here because of its similarity to the 'moist' air CI observed in the QUISTOR.

Instrumentally, the employment of CI entails a fair degree of modification to the mass spectrometer, particularly the inclusion of differential pumping and a fairly gas-tight ion source, with a small ion exit aperture, to allow the analyzer to be maintained at ca. 10^{-5} - 10^{-6} Torr, while the source is at 1 - 2 Torr. Since, for conventional EI, large ion exit apertures are advantageous the two techniques would appear difficult to incorporate into one instrument; by careful design, and often mechanical slit-moving, several workers[132] have, however, reported such instruments. In addition the various design considerations of CI sources have been examined by Yinon[133].

6.31 Chemical Ionization Processes Observed in the QUISTOR

Undoubtedly the most widely used CI reagent gas is methane, the technique depending on the production of CH_5^+ and $C_2H_5^+$ ions; since these species had been also observed to predominate in the ion-molecule reactions of methane observed in the QUISTOR (see Section 5.333), CI with methane as a reagent gas seemed probable. In order to examine this a 3 : 1 mixture of methane and methanol was admitted to the system and spectra obtained at various storage times; a selection of the results are shown in Figure 6-1, and the operating conditions are summarized below :

Figure 6-1	Storage Time (mS)	Sensitivity Factor
(a)	-	x 1
(b)	0.5	x 10
(c)	1.0	x 10
(d)	2.0	x 10

The RF amplitude was 600 Volts in all cases.

The spectrum shown in Figure 6-1(a) was obtained under the conditions previously known[37] as 'continuous ionization', that is as a static source with RF applied and ion removal by space charge repulsion. Under conventional EI, methanol yields the ions whose relative abundances are listed in Table 6-2. The major ions, m/e 32, 31 and 29, can be seen in spectrum (a), Figure 6-1, which also shows a typical methane fragmentation pattern. As the storage time was increased the methane ions disappeared, by reaction, producing ions at m/e 27, 29, 31, 32 and 33. Of these m/e 27 corresponded to $C_2H_3^+$ produced from methane, m/e 29 probably to a joint contribution of $C_2H_5^+$, from methane, and CHO^+ from methanol, the other ions resulting from methanol. The ions at m/e 31 and 32 were attributed to CH_3O^+ and CH_3OH^+, present in the EI spectrum of methanol, while the ion

Figure 6-1. Methane Methanol 3:1

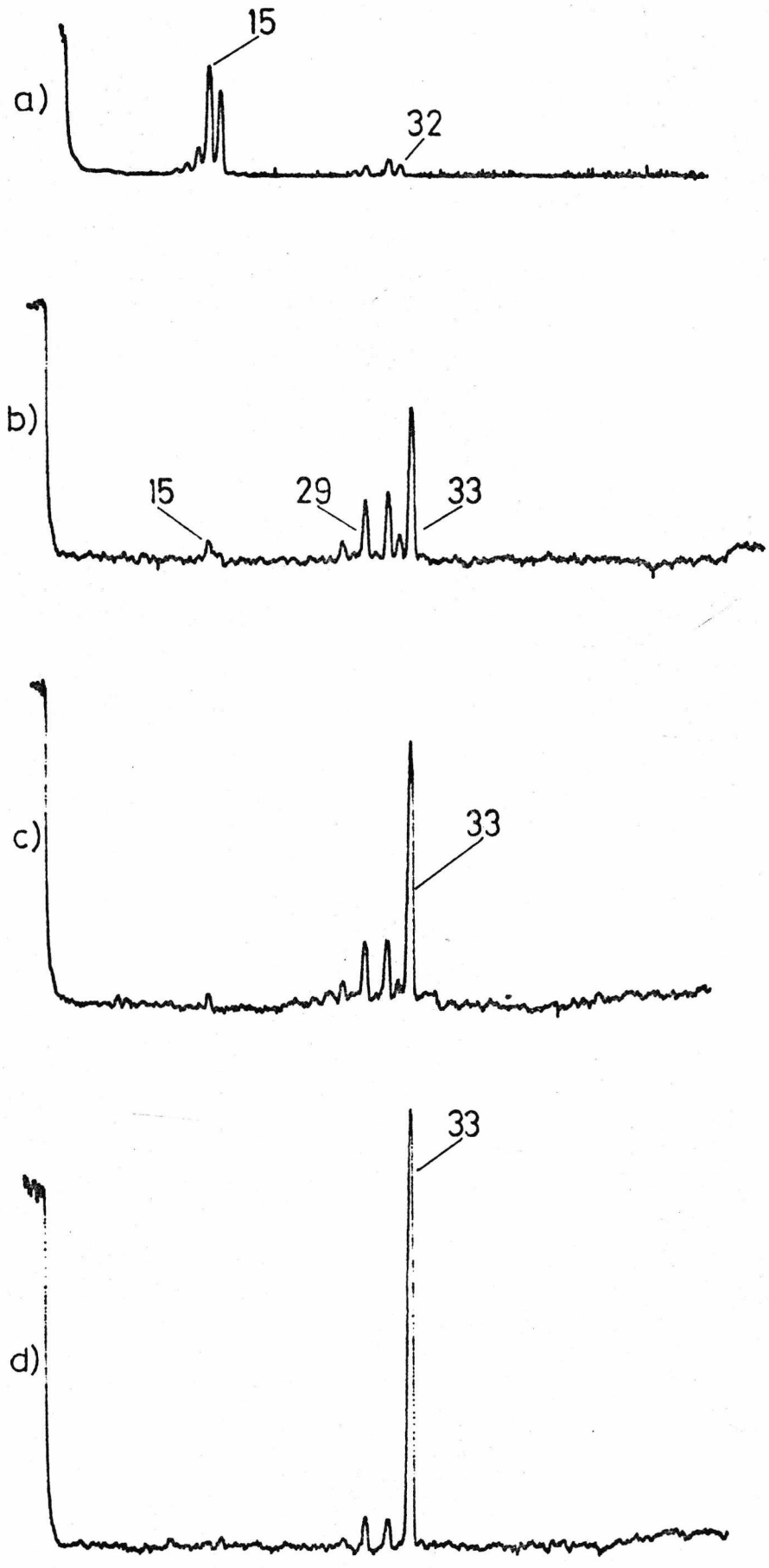

Table 6-2. EI Mass Spectrum of Methanol

m/e	Abundance %
33	1.0
32	66.7
31	100.0
30	0.8
29	64.7
28	6.4
18	1.9

Data obtained from the American Petroleum Institute (API) 'Tables of Mass Spectral Data', Spectrum Serial Number 363, originally obtained with a Consolidated Engineering Corporation (CEC) 21-102 Magnetic sector mass spectrometer.

---

at m/e 33, $CH_3OH_2^+$, was produced by proton transfer from methane, e.g.:

$$CH_3OH + CH_5^+ \longrightarrow CH_3OH_2^+ + CH_4$$

being the dominant ion even at 0.5 mS storage, and the only significant ion at longer storage times (Figure 6-1(d)).

Having thus demonstrated that CI could be observed in mixtures of sample and reagent in similar proportions, the excess of methane was increased until a normal CI ratio was obtained, that is less than 1% sample. Accurate mixtures were made by successively diluting known pressures of methanol with methane in the inlet system. The results obtained for a 400 : 1 mixture of methane and methanol are shown in Figure 6-2, the relevant conditions being :-

Figure 6-2. Methane/Methanol 400:1

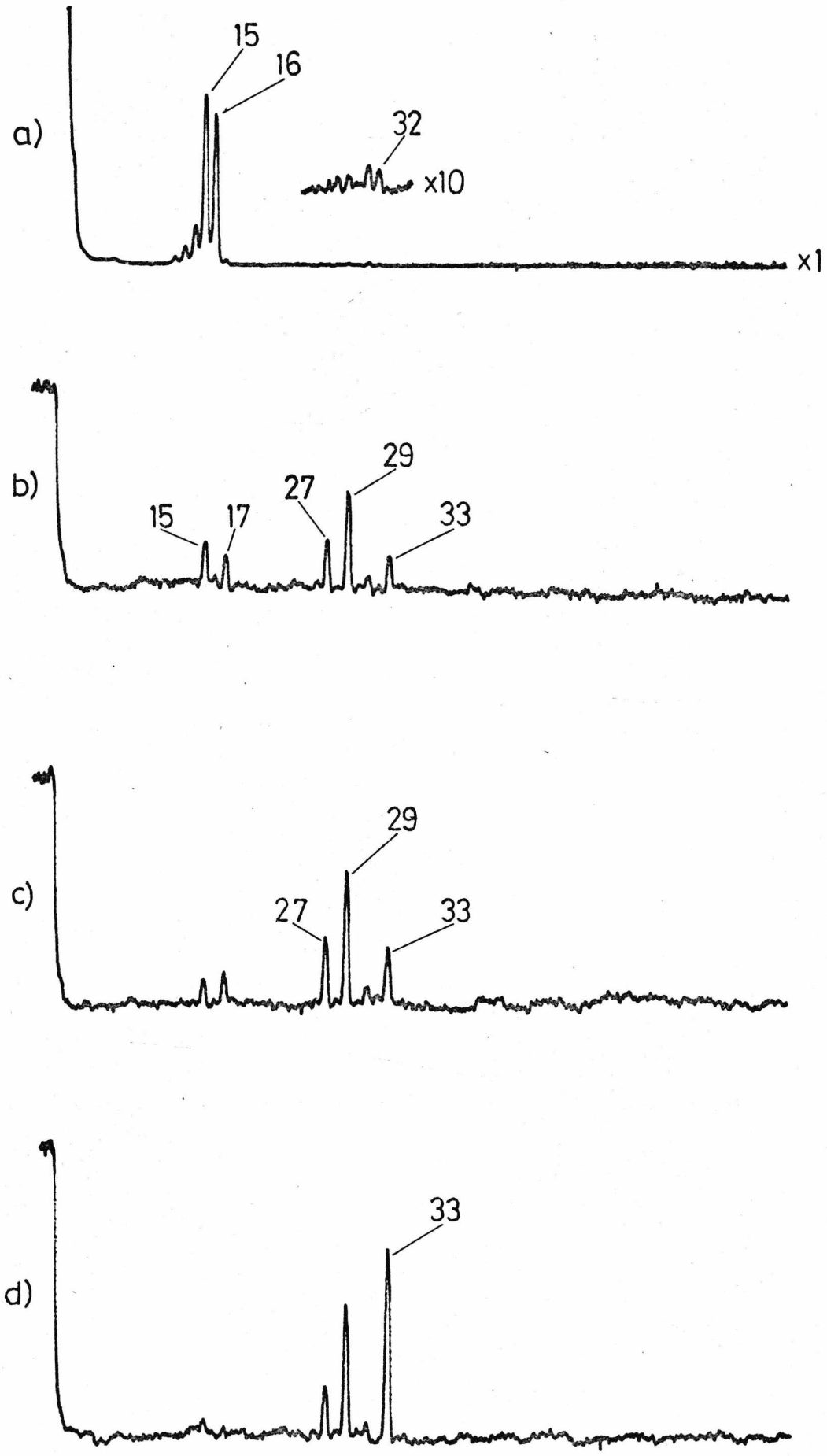

Figure 6-2	Storage Time (mS)	Sensitivity Factor
(a)	-	x 1
(b)	0.5	x 10
(c)	1.0	x 10
(d)	3.5	x 10

Spectrum (a) was again obtained with the QUISTOR functioning as a static source, as previously described, the insert shows the methanol peaks at an extra gain of 10. The behaviour observed was generally the same as for the 3 : 1 mixture, with the exception that the processes were slower, as was expected owing to the lower concentration of methanol. The methane product ions were clearly visible at m/e values of 15, 17, 27 and 29. Similar spectra obtained with an 8000 : 1 mixture of methane and methanol indicated that m/e 33 was again being produced but even more slowly, necessitating longer storage times to observe complete degradation of the spectrum to one peak; as an increase in storage time could only be achieved by reducing the repetition rate, and consequently the ion currents, this was not performed. Ion clusters of the form $(CH_3OH)_2H^+$, which have been reported by other workers[1], were not observed here; this is believed to be due to the fairly high kinetic energy of ions causing instability of such clusters, since the strength of hydrogen bonds is generally accepted as being less than 1 eV.

An ethanol/methane mixture, studied under the same conditions as methanol/methane, also yielded a base peak at (M+1), in this case m/e 47; with iso-propanol, however, cleavage of a methyl group was found to be extremely fast, causing a peak at (M-14), that is loss of methyl but addition of a proton.

As mentioned before, the possibility of CI using air was of great interest, and consequently mixtures of air and methanol were made and

subjected to ion storage, the results being depicted in Figures 6-3 and 6-4. The conditions under which both figures were obtained were :

	Storage Time (mS)	Sensitivity Factor
(a)	-	x 1
(b)	0.1	x 10
(c)	1.0	x 10
(d)	3.5	x 10

As before, both spectra (a) were obtained in the static mode. These figures also demonstrate the effect of altering the RF amplitude: Figure 6-3 was obtained at 625 Volts, to give maximum m/e 33 intensity at 3.5 mS storage time, while Figure 6-4 was with 575 Volts RF for maximum m/e 28 intensity at 20 μS storage. The final spectra, (d), were very similar, showing major peaks at m/e 31 (CH_3O^+) and 33 ($CH_3OH_2^+$), the slight differences arising because of the different intensity of the m/e 28, 29 and 31, 33 groups of ions. The reactions producing these ions were by no means clear; it seemed reasonable, however, that m/e 33 was produced by proton transfer from H_3O^+, thus :

$$CH_3OH + H_3O^+ \longrightarrow CH_3OH_2^+ + H_2O$$

which in turn was produced by the reaction :

$$H_2O^+ + H_2O \longrightarrow H_3O^+ + OH$$

The species with m/e 31, CH_2OH^+ or CH_3O^+, could be produced by a charge transfer reaction from N_2^+ or O_2^+, followed by fragmentation through loss of an hydrogen atom :

$$CH_3OH + \begin{matrix} O_2^+ \\ N_2 \end{matrix} \longrightarrow CH_3OH^+ \xrightarrow{-H} \begin{matrix} CH_2OH^+ \\ CH_3O^+ \end{matrix} \qquad (6\text{-}1)$$

in a similar manner to that in which m/e 31 must be produced in a conventional EI spectrum. The ionization potentials[134] for molecular oxygen, nitrogen, methanol and the appearance potential for the CH_3O^+

Air/MeOH 8000/1 1250 Volts RF(pk-pk).

Figure 6-3.

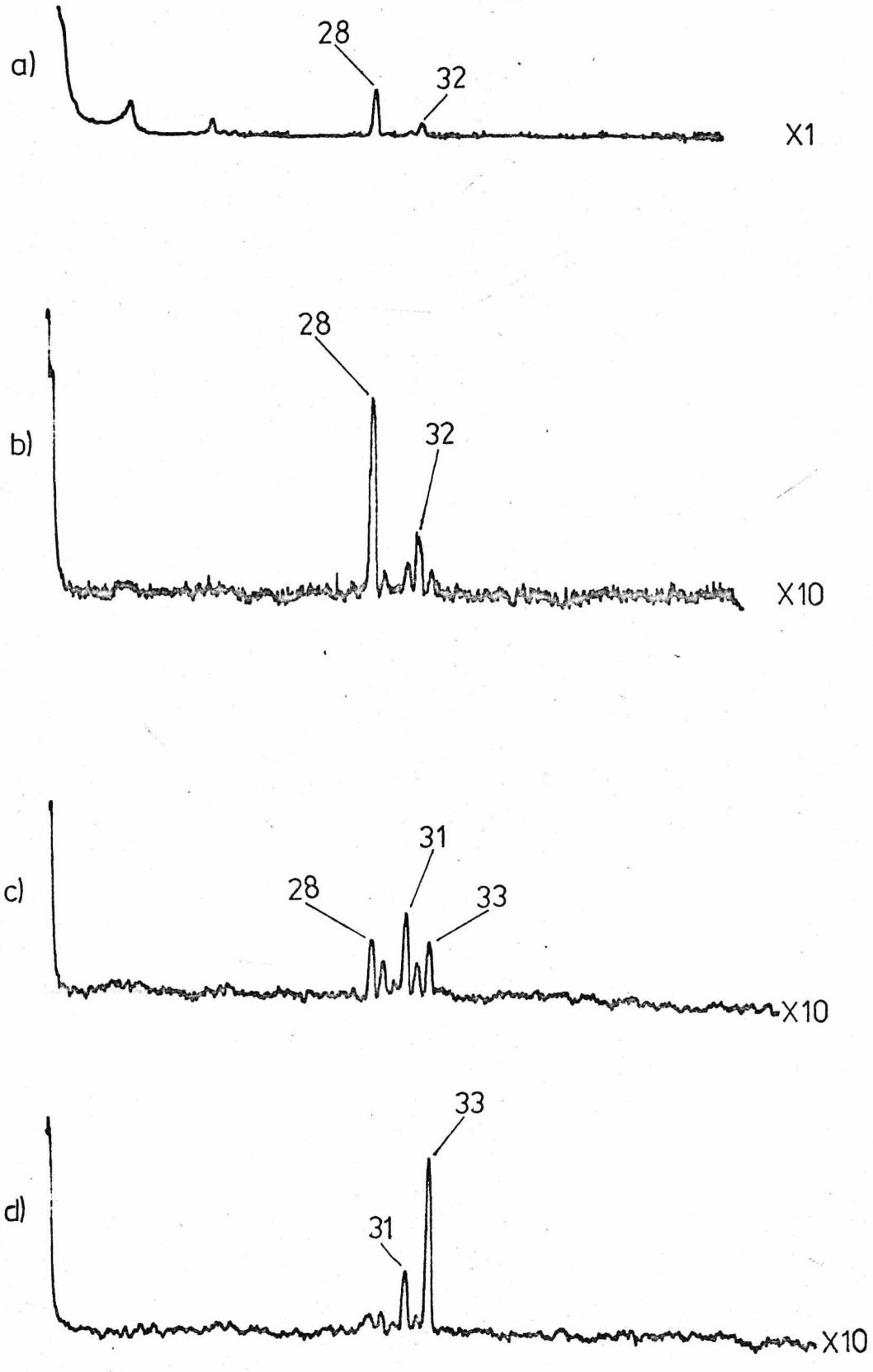

Air/MeOH. 8000/1 1050 Volts RF(pk-pk).

Figure 6-4.

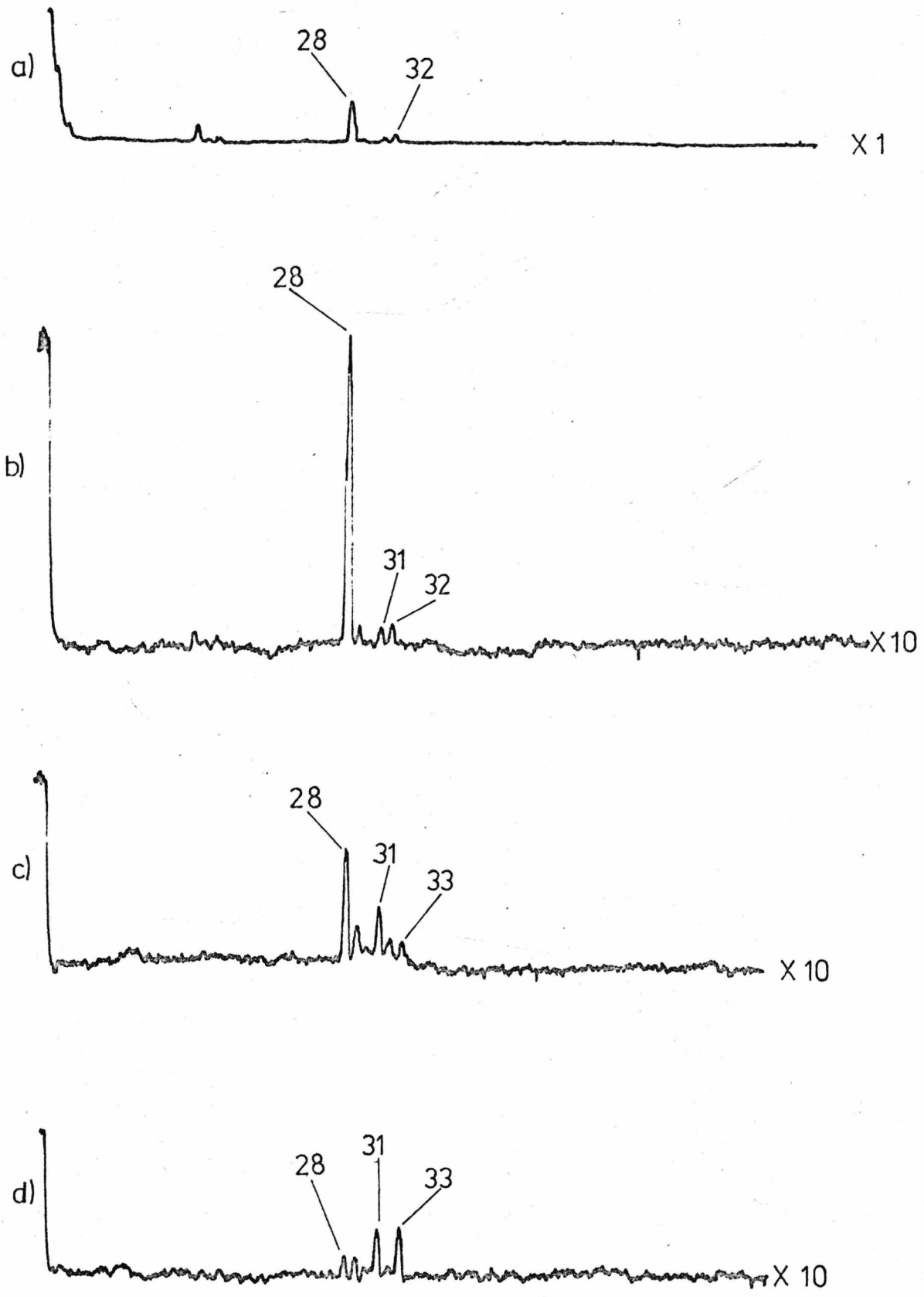

species (from methanol), listed below, suggested that reactions of this kind were energetically feasible.

Species	Ionization/Appearance Potential (eV)
N_2^+	15.5 - 23.6
O_2^+	12.0 - 12.5
CH_3OH^+	ca. 11.0
CH_3O^+	ca. 12.2

In addition a relatively small peak at m/e 29 was observed; this may have either been CHO^+ produced by a pathway similar to (6-1) above, or COH^+ or N_2H^+ produced by proton transfer to CO or N_2 in air (see Section 6.51). The possibility of using 'moist' air as a reagent gas has also been reported by Karasek and Cohen[135,136], who have employed a Plasma Chromatrograph. This instrument operates at atmospheric pressure and relies on ion-molecule reactions between nitrogen, oxygen, water and trace components to form observable ion intensities of the latter. They have reported the observation of water cluster ions, cf. methane, of the form :

$$(H_2O)n\ H^+, \text{ with } n = 1 \text{ to } 7.$$

These were not observed in the QUISTOR, nor reported by Hunt[131]; it seems probable that cluster ions are unstable in the QUISTOR and mass spectrometer because of the high ion energies, whereas the thermalization of ions at high pressures permits their formation. The Plasma Chromatographic studies did not indicate that charge transfer from oxygen or nitrogen had been observed, this is somewhat surprising considering that the ionization potentials of these substances (listed above) are generally higher than those of organic compounds. From this work, and that of others, it would appear that the use of 'moist' air - or an air/water

mixture - as a CI reagent gas could be advantageous both from the point of view of sample identification and also atmospheric pollutant detection, and certainly deserves further study.

6.4 Spectrum Simplification

This phenomenon, the observation of which has also been indicated by Harden and Wagner[42], was encountered during investigations of the methanol and ethanol systems, the results obtained being shown in Figures 6-5 and 6-6, respectively. In these systems ion-molecule reactions occur between fragment ions and neutral alcohol molecules, resulting in proton transfer and the production of a species at (M+1). As the storage time was increased the intensity of this peak followed until all the ionization was effectively 'concentrated' into one species. The methanol system has also been studied by McIver[88] and Bowers, Su and Anicich[128] with similar results. Bowers et al have examined this system in order to obtain data for comparison with the predictions of the ADO theory of ion-molecule reactions, developed by them (see Section 6.1), and for this reaction :

$$CH_3OH + CH_3OH^+ \longrightarrow CH_3OH_2^+ + CH_3O$$

the experimental variation of the rate constant with kinetic energy is in excellent agreement with the theoretical prediction. The rate constant, from the data of Bowers et al, tends to a value of 10×10^{-10} cm^3 $molecule^{-1}$ sec^{-1} at kinetic energies in excess of 0.5 eV. For the sake of comparison the methanol results obtained in this work were plotted on semi-log graph paper, Figure 6-7, and the rate constant determined. The experiment was performed with 15 Torr of methanol in the inlet system, corresponding to $16.5 \pm .8 \times 10^{11}$ molecules cm^{-3} in the vacuum system, and the calculated rate constant was $7 \pm 1 \times 10^{-10}$ cm^3 $molecule^{-1}$ sec^{-1}, which was in fair agreement with the results of Bowers et al, and supplied further support for the inlet system capsule gauge calibration described

Figure 6-5. Spectrum Simplification in Methanol.

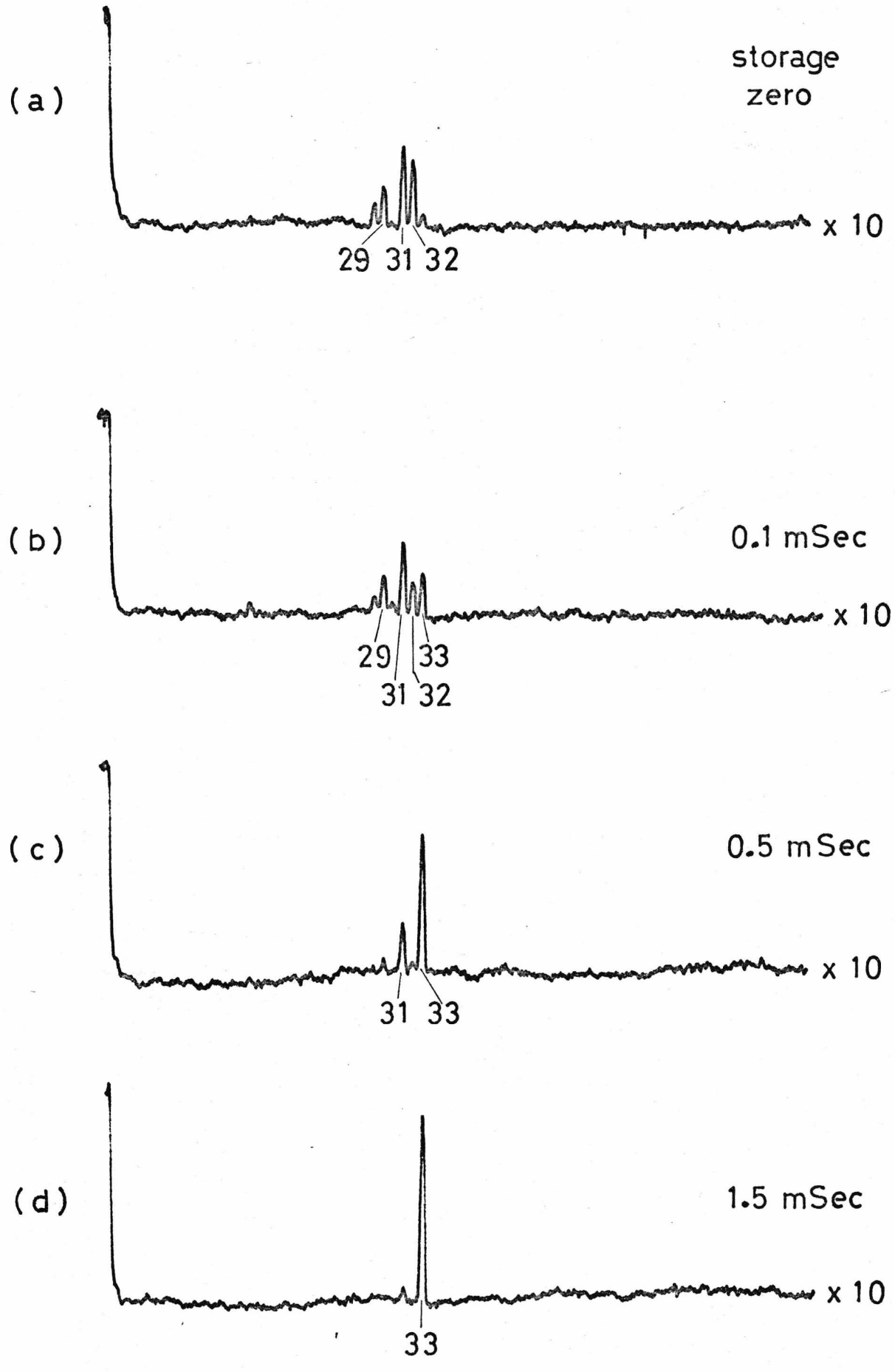

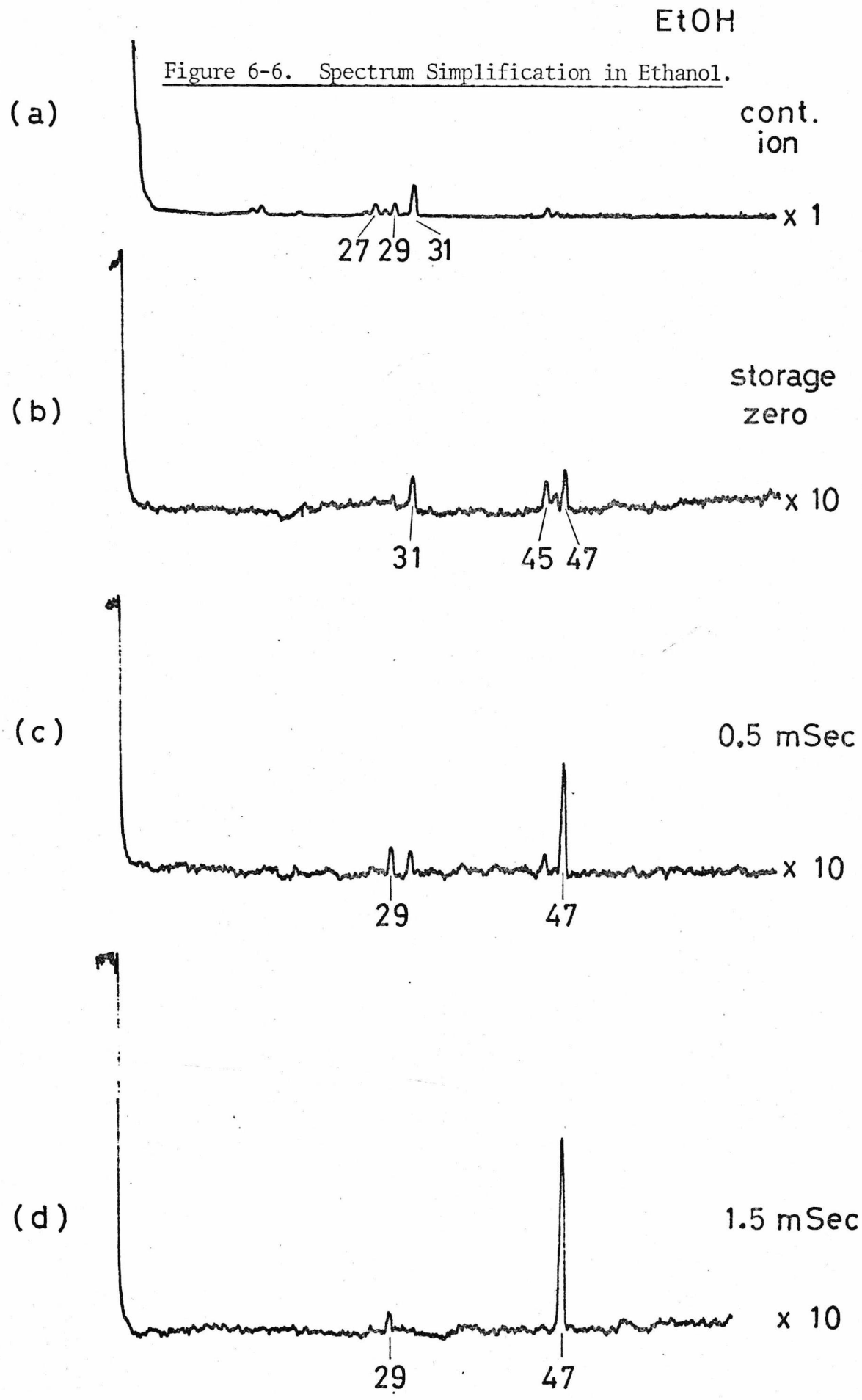

Figure 6-6. Spectrum Simplification in Ethanol.

Figure 6-7. Percentage Total Ionization vs. Storage Time for Methanol.

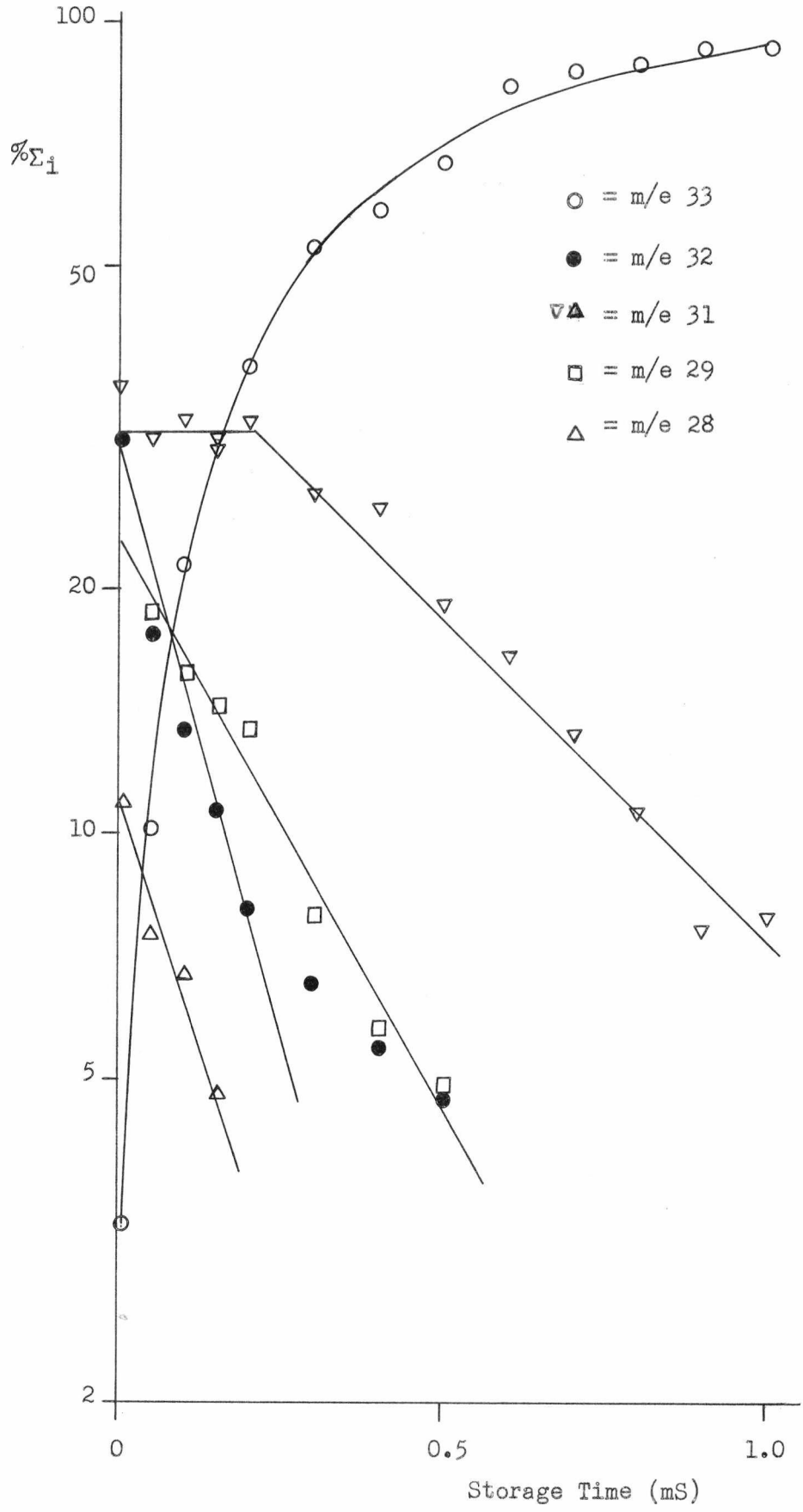

in the previous chapter.

6.5 Ion-molecule Reactions

As has been indicated, the ion-molecule reactions occurring in several systems were studied during this work for several reasons, but particularly to assess their potential as CI reagent gases, and to provide a comparison with the data of other workers to enable the ion energy calculations to be experimentally checked. Examination of methane and carbon dioxide/hydrogen (Chapter 5) having demonstrated that data obtained with the QUISTOR yielded viable rate constants, and suggested an ion energy in the range 1 - 3 eV. The ion-molecule reactions in air and water were examined in order to determine the ion pattern as the storage time increased, and the water data was also used to support the ion energy calculations. Furthermore the previous observation that cluster ions in water, based on hydrogen bonding, did not occur was verified. The study of water led to examination of a similar gaseous base, ammonia, and information on charge transfer processes was obtained from the fairly well studied argon/methane system.

6.51 Ion-molecule Reactions in Air

The results obtained from this system are presented in Figure 6-8 which shows a semi-log plot of the ion intensities (expressed as a percentage of the total ionization) against storage time. It is evident that several reactions were occurring, notably those causing a decrease in m/e 28 and an increase in m/e 32; high resolution studies[161] of vacuum chamber background gases have shown that a significant fraction of m/e 28 is due to CO^+ , in addition to N_2^+, and hence it was probable that at least three main reactions contributed to the decrease of m/e 28 intensity :

(i) Reaction of CO with background hydrogen producing COH^+ :

Figure 6-8. Percentage Total Ionization vs. Storage Time for Air.

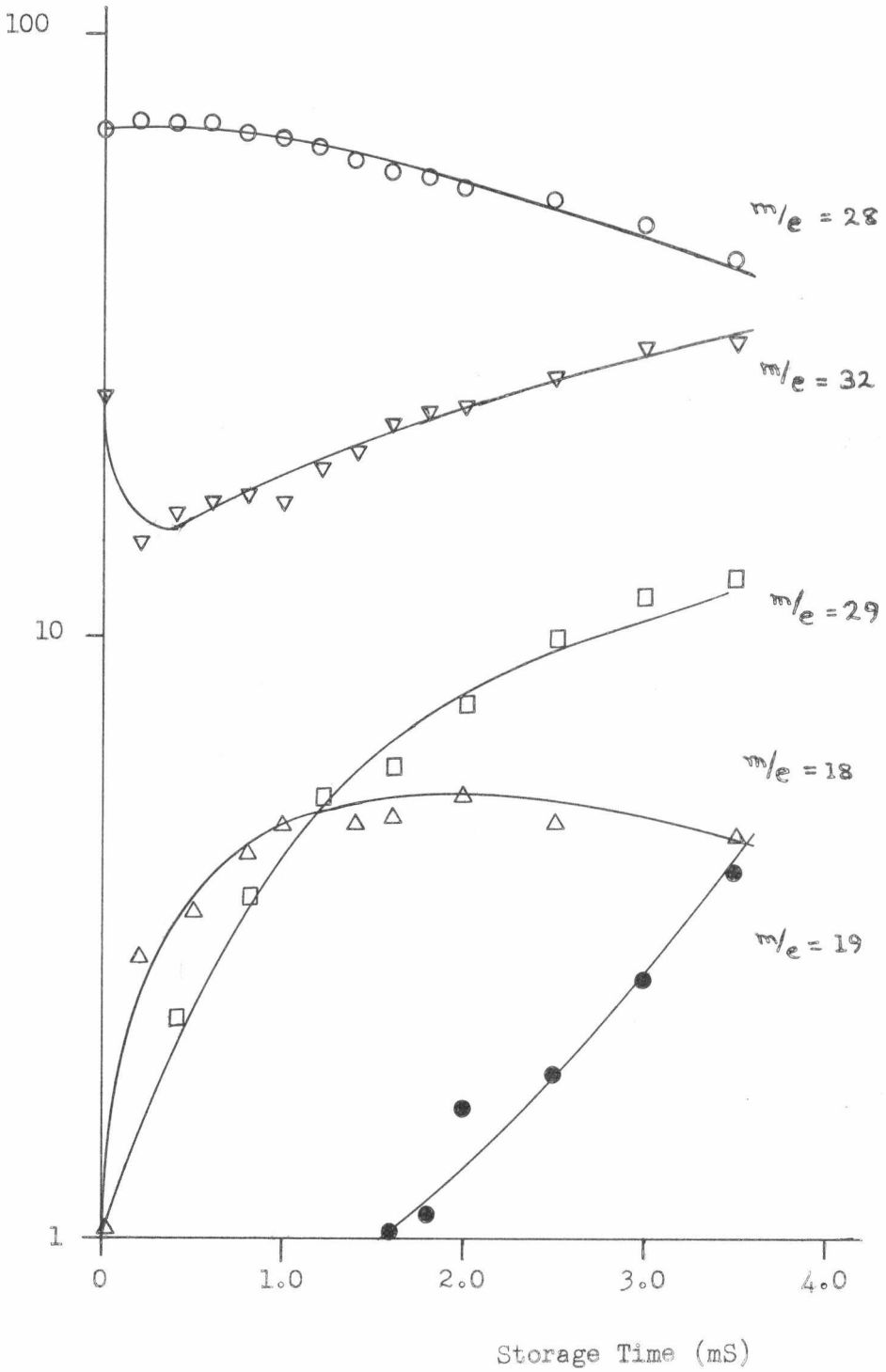

$$CO^+ + H_2 \xrightarrow{k_2} COH^+ + H \qquad (6\text{-}2)$$

$$H_2^+ + CO \xrightarrow{k_3} COH^+ + H \qquad (6\text{-}3)$$

These reactions are known to occur[108,109,137] and have an apparent rate constant, k_{app}, of 11 x 10^{-10} cm^3 $molecule^{-1}$ sec^{-1}, k_{app} having been defined by McAllister[137] as $k_2 + k_3/2.3$. Rettinghaus[39] assumed that reaction (6-2) occurred in order to explain the appearance of an ion at m/e 29 at long storage times in his studies on the use of a three-dimensional quadrupole ion trap as a partial pressure gauge.

(ii) Similar reactions between nitrogen and hydrogen are also known[137,138,139]:

$$N_2^+ + H_2 \xrightarrow{k_5} N_2H^+ + H \qquad (6\text{-}4)$$

$$H_2^+ + N_2 \xrightarrow{k_6} N_2H^+ + H \qquad (6\text{-}5)$$

having an apparent rate constant $k_{app} = k_5 + k_6/2.26$, ref 135) in the range 14.1 - 29.9 x 10^{-10} cm^3 $molecule^{-1}$ sec^{-1}.

(iii) Charge transfer from the more abundant N_2^+ ions to O_2 and H_2O neutrals. The latter reaction has not been reported in the literature, but its occurrence seemed likely from the build-up of m/e 18 in Figure 6-9. There are many known reactions between nitrogen and oxygen, and those involving the molecular forms include :

$$N_2^+ + O_2 \xrightarrow{k_7} N_2 + O_2^+ \qquad (6\text{-}6)$$

$$N_2^+ + O_2 \xrightarrow{k_8} NO_2^+ + N \qquad (6\text{-}7)$$

$$N_2^+ + O_2 \xrightarrow{k_9} NO^+ + NO \qquad (6\text{-}8)$$

Several workers have studied the ion-molecule reactions of these substances because of their importance in the chemistry of the upper atmosphere and it would appear, from the published results, that reaction (6-6) was most probable as it has a thermal rate constant of

Figure 6-9. Percentage Total Ionization vs. Storage Time for Water

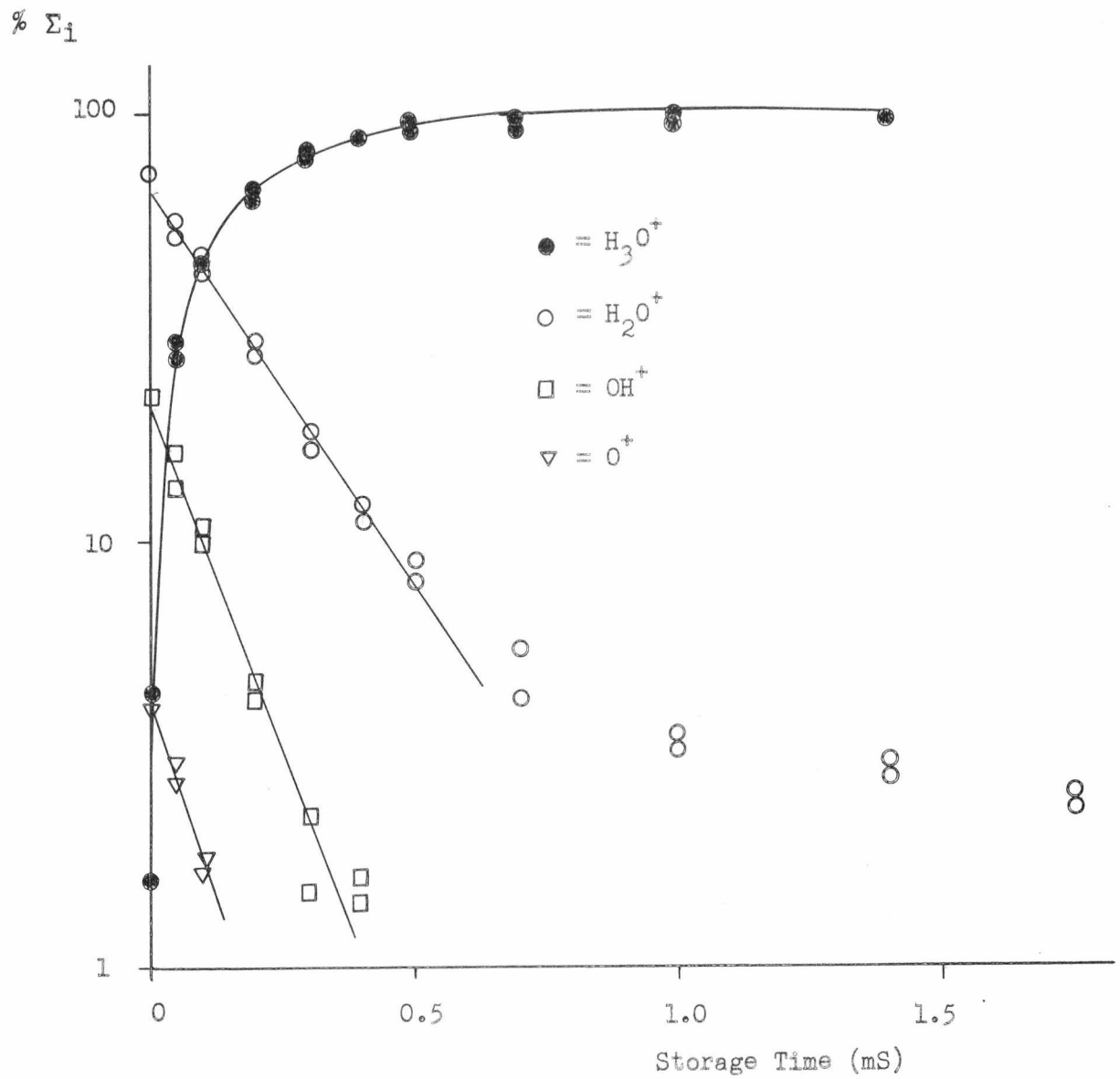

ca. 1×10^{-10} cm^3 $molecule^{-1}$ sec^{-1} (ref. 140), (6-7) and (6-8) having rate constants of less that 2×10^{-13} cm^3 $molecule^{-1}$ sec^{-1} (refs. 141, 142). These figures were supported quantitatively by this work where condensation-type products, that is the nitrogen oxides, were not observed.

The definitions of k_{app} quoted in (i) and (ii) above, were given by McAllister[137] for the rate of increase of product species, under the conditions of equal reagent concentrations. If this assumption is valid then the observed rate of reaction depends on the individual rate constants and the number of ions of each species created. This latter quantity depends on the relative ionization cross sections, and gives rise to the numerical factors in these definitions; the values for the ionization cross sections were obtained from the data of Lampe, Franklin and Field[143]. Since in this work the hydrogen concentration was low, ionization of this species was unlikely and reactions (6-2) and (6-4) predominated; consequently the values for k_{app} were not strictly relevant, but are included for the sake of comparison. The rate constant from (ii) suggests that :

$$N_2^+ + H_2 \longrightarrow N_2H^+ + H$$

was more likely than :

$$CO^+ + H_2 \longrightarrow COH^+ + H$$

especially as the concentration of N_2 was probably greater than that of CO. This could have been true of the work reported by Rettinghaus although under the ultra high vacuum conditions he employed (ca. 10^{-10} Torr) CO may have been the dominant species. In either case high resolution would be required to determine the actual reaction occurring.

In addition to these species, the ion at m/e 19 was probably H_3O^+ formed by the reaction :

$$H_2O^+ + H_2O \longrightarrow H_3O^+ + OH$$

which is described later (see Section 6.53).

In general then, the pattern of ions observed in air as the storage time was increased, was as expected from the CI studies using air as a reagent gas, and also accounted for the appearance of an ion at m/e 29 in these latter experiments.

6.52 Charge Transfer in Argon-methane Mixtures

The system was investigated in order to obtain data concerning the belief that charge transfer from nitrogen could occur in mixtures containing air. Argon-methane was chosen since it has been studied by other workers[144], and Hunt[131] has described the similarity between argon-water and nitrogen-water in his studies. The rate constants were not determined in this work since the pressure errors were felt to be large.

Field, Franklin and Head[145] have reported that the major process occurring in this system is charge transfer from argon to methane, followed by fragmentation of the latter due to the accompanying internal energy transfer (the relevent ionization potentials are argon 15.7 - 16 eV and methane 12.7 - 14.7 eV[134]) thus :

$$Ar^+ + CH_4 \longrightarrow Ar + CH_4^+ \longrightarrow CH_3^+ , CH_2^+ \qquad (6\text{-}9)$$

In addition they reported having observed ion-molecule reaction products of the form $Ar\,H^+$, $Ar\,C^+$, $Ar\,CH_2^+$ and $Ar\,CH_3^+$. These products were not observed in the experiments with the QUISTOR, it being found that the decrease of Ar^+ was entirely accounted for by production of CH_2^+, CH_3^+ and ion-molecule products from these species. Comparison with earlier work on the methane system indicated that any CH_4^+ and CH_5^+ produced arose directly from ionization and reaction of the methane molecules.

These results supported the belief that charge transfer from N_2^+,

and similar species, was viable in systems containing air.

6.53 Ion-molecule Reactions in Water

The first detailed study of the ion-molecule reactions occurring in water was reported by Lampe, Field and Franklin[145], but they only considered the reaction :

$$H_2O^+ + H_2O \xrightarrow{k_{10}} H_3O^+ + OH \qquad (6\text{-}10)$$

as had previous workers (see references cited by Lampe et al). The assumption that this was the only reaction was based largely on the similarity between the appearance potentials of H_2O^+ and H_3O^+ but, as has been pointed out by Gupta, Jones, Harrison and Myher[126], such measurements are unreliable where other reactions become possible at higher kinetic energies. Thynne and Harrison[146], using a pulsed high pressure mass spectrometer with an ion exit energy of 3.7 eV, measured the rate constant of reactions (6-10) and :

$$OH^+ + H_2O \xrightarrow{k_{11}} H_3O^+ + O \qquad (6\text{-}11)$$

but were unable to find evidence for a third reaction :

$$OH^+ + H_2O \longrightarrow H_2O^+ + OH \qquad (6\text{-}12)$$

although this reaction had been proposed by Baxendale and Gilbert[147] to account for their results on the -radiolysis of water. The results of Thynne and Harrison were later found to be inaccurate, owing to a large pressure error, and corrected values were given by Gupta et al.[126]
In addition to these reactions, Kebarle and colleagues[148,149] have demonstrated the formation of water cluster ions (see Section 6.3 and refs. 135 and 136). These were observed at high pressures (ca. 1-200 Torr), and were investigated primarily because of their known occurence in the upper atmosphere. Originally they were thought to be formed by equilibrium reactions of the form :

$$H_3O^+ + n\,H_2O \longrightarrow H^+(H_2O)_{n+1} \qquad (6\text{-}13)$$

where n = 1 to 8, but more recently[149] they have been thought to originate from hydration of O_2^+ ions. Ryan[150] has published the results of a careful study of this system, using a high pressure mass spectrometer similar to that of Gupta et al[126], which are in marked disagreement with the values of these workers. The results of Gupta et al, obtained at thermal energy and with 3.4 eV ion exit energy, see Section 5.333 (i), are summarised below :

	Rate Constant (x 10^{-10} cm^3 $molecule^{-1}$ sec^{-1})	
	Thermal	3.4 eV ion exit energy
k_{10}	16.0	19.6
k_{11}	15.3	19.2

The similarity between k_1 and k_2 at different energies was also used to infer that reaction (6-12) was not significant. In contrast, Ryan obtained a sharp decrease, by ca. 50%, in rate constant (from a thermal energy value of 26.2 x 10^{-10} cm^3 $molecule^{-1}$ sec^{-1}.) up to ca.2 eV ion exit energy, above which he observed a gradual increase; these results having been acquired with 18 eV ionizing electrons to prohibit formation of OH^+ ions. The same general behaviour was observed with 40 eV electrons, except that the values now were higher (than the 18 eV values) up to an ion exit energy of 0.6 eV, but thereafter the two sets of results were similar. He initially postulated that the difference up to 0.6 eV was due to reaction (6-11) only being significant up to this energy, but was able to show that it in fact occurred at a fairly constant rate up to 3 eV, finally concluding that the difference was due to reaction (6-12) being significant at low energies. Ryan's thermal rate constants for reactions (6-10) and (6-11) are in fair agreement with those obtained in a very recent study by Huntress and Pinnizzotto[91], as shown overleaf :

	Rate Constant (x 10^{-10} cm^3 $molecule^{-1}$ sec^{-1})	
	Ryan[150]	Huntress and Pinnizzotto[91]
k_{10}	26.2[a], 30[b]	20.5 ± 1.0
k_{11}	20 ± 3	28.9 ± 2.7

a = 18 eV electrons; b = 40 eV electrons.

In order to check the validity of his experimental system and conclusions, Ryan examined the methane system and obtained results identical with those of Giardini-Guidoni and Friedman[114] (see Section 5.33(i)). It must be noted that the ion energies quoted by Ryan, and given above, are for an ion leaving the ion source and hence must be divided by 3 to obtain the average ion kinetic energy[113] (see Section 5.333(i)).

In the present work, the QUISTOR was operated at 800 Volts, and water vapour admitted to the system; the water was de-ionized and was thoroughly degassed in the inlet system before admission to the vacuum tank. The results obtained are depicted graphically in Figure 6-9, which is a semi-log plot; as in the previous work on air the formation of clusters was not observed. Separation of the three reactions was not possible, since the device was incapable of mass selective operation and the ionizing electron energy could not be reduced sufficiently to ensure no production of OH^+, although the electron energy was nominally set to 18 eV. A material balance did show, however, that the increase of m/e 19 was exactly reproduced by the m/e 17 and 18 losses, indicating that these ions did, in fact, react to give H_3O^+; the reaction of OH^+, which may have been through either pathway of :

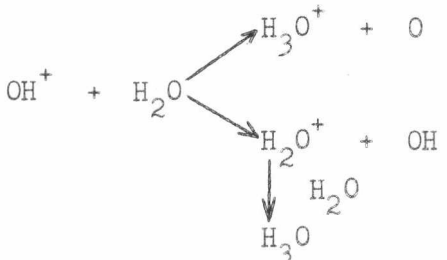

could not be determined. Consequently only rate constants for the loss of H_2O^+ and OH^+ were determined and found to be k 11.6 ± 1.5 x 10^{-10} cm^3 $molecule^{-1}$ sec^{-1} and k 26 ± 2.6 x 10^{-10} cm^3 $molecule^{-1}$ sec^{-1} respectively, the calculated mean ion kinetic energies being 2.15 eV (m/e 17) and 2.05 eV (m/e 18). The results for H_2O^+ loss are in good agreement with the values reported by Ryan of 12.6 x 10^{-10} cm^3 $molecule^{-1}$ sec^{-1} at 2 eV mean ion energy (i.e. 6 eV ion exit energy) after ionization with 18 eV electrons. Ryan's reported value for the rate of loss of OH^+ at 2 eV mean ion energy was 43.0 x 10^{-10} cm^3 $molecule^{-1}$ sec^{-1}, but he states that a large error of ± 15 was present, making the agreement with the results obtained from the QUISTOR quite reasonable.

It would appear that the formation of cluster ions is only possible at very high pressures and with low energy ions, since observation of these ions has only been reported under these conditions by Kebarle et al[148,151] and Karasek et al[135,136]. Ryan[150], Huntress and Pinnizzotto[91] and Gupta et al[126] did not report cluster ions, even at thermal ion energies, and they were not observed during this work.

6.54 Ion-molecule Reactions in Ammonia

The ion-molecule reactions occurring in ammonia are similar to those in water, and the major processes are :

$$NH_3^+ + NH_3 \xrightarrow{k_{14}} NH_4^+ + NH_2 \qquad (6\text{-}14)$$

$$NH_2^+ + NH_3 \xrightarrow{k_{15}} NH_4^+ + NH \qquad (6\text{-}15)$$

$$NH_2^+ + NH_3 \xrightarrow{k_{16}} NH_3^+ + NH_2 \qquad (6\text{-}16)$$

In addition, the resonant charge transfer reaction :

$$NH_3^+ + NH_3 \xrightarrow{k_{17}} NH_3 + NH_3^+ \qquad (6\text{-}17)$$

has been reported by one group of workers[151] to become important for translationally excited ammonia ions. As with water the earliest

studies of ammonia[152,153] considered only reaction (6-14), and a later study by Derwish, Galli, Giardini-Guidoni and Volpi[154] considered only reactions (6-14) and (6-16). This latter group did, however, suspect that either reaction (6-15) or :

$$NH^+ + NH_3 \longrightarrow NH_4^+ + N \qquad (6\text{-}18)$$

occurred, since a material balance indicated that up to 5% of the NH_4^+ species could not be accounted for by reaction (6-14). Fortunately they measured the rate constants for loss of each of the ammonia ions (NH_3^+, NH_2^+, NH^+, N^+) and their results are therefore of value; in addition they observed to formation of condensation-like products, $N_2H_5^+$, $N_2H_4^+$, $N_2H_3^+$, $N_2H_2^+$, N_2H^+, which must have arisen because of their very high pressure conditions (2.5×10^{-3} - 6.5×10^{-2} Torr) since the occurrence of the species has not been reported by other workers. In the more recent studies by Harrison and Thynne[155] (corrected results in ref. 127), Ryan[156], Huntress et al[84,151], Marx and Mauclaire[83], and Huntress and Pinnizzotto[91] all three reactions (6-14) to (6-16) have been considered, although the experimental difficulties of separating the competing reactions has often led simply to values for the loss of NH_3^+ (i.e. k_{14}) and NH_2^+ ($k_{15} + k_{16}$) being published.

The reported literature rate constants for the rate of loss of NH_3^+ (reaction (6-14)) at the various ion kinetic energies employed, are summarised graphically in Figure 6-10, which also shows the data of Huntress et al[151] for reaction (6-17), represented by closed triangles. In order to compile this figure, and also Figure 6-11, the kinetic energies of Ryan[156] and Harrison and Thynne[155] have been converted to mean ion energies, by dividing their quoted ion exit energies by a factor of three[113]. The ion energy conditions employed by Derwish et al[154] were not explicitly stated, but the ion exit energy has been estimated as 1.75 eV and the resulting mean energy as 0.58 eV, from experimental

Figure 6-10. Summary of Literature Rate Constants for Loss of NH_3^+ in Ammonia

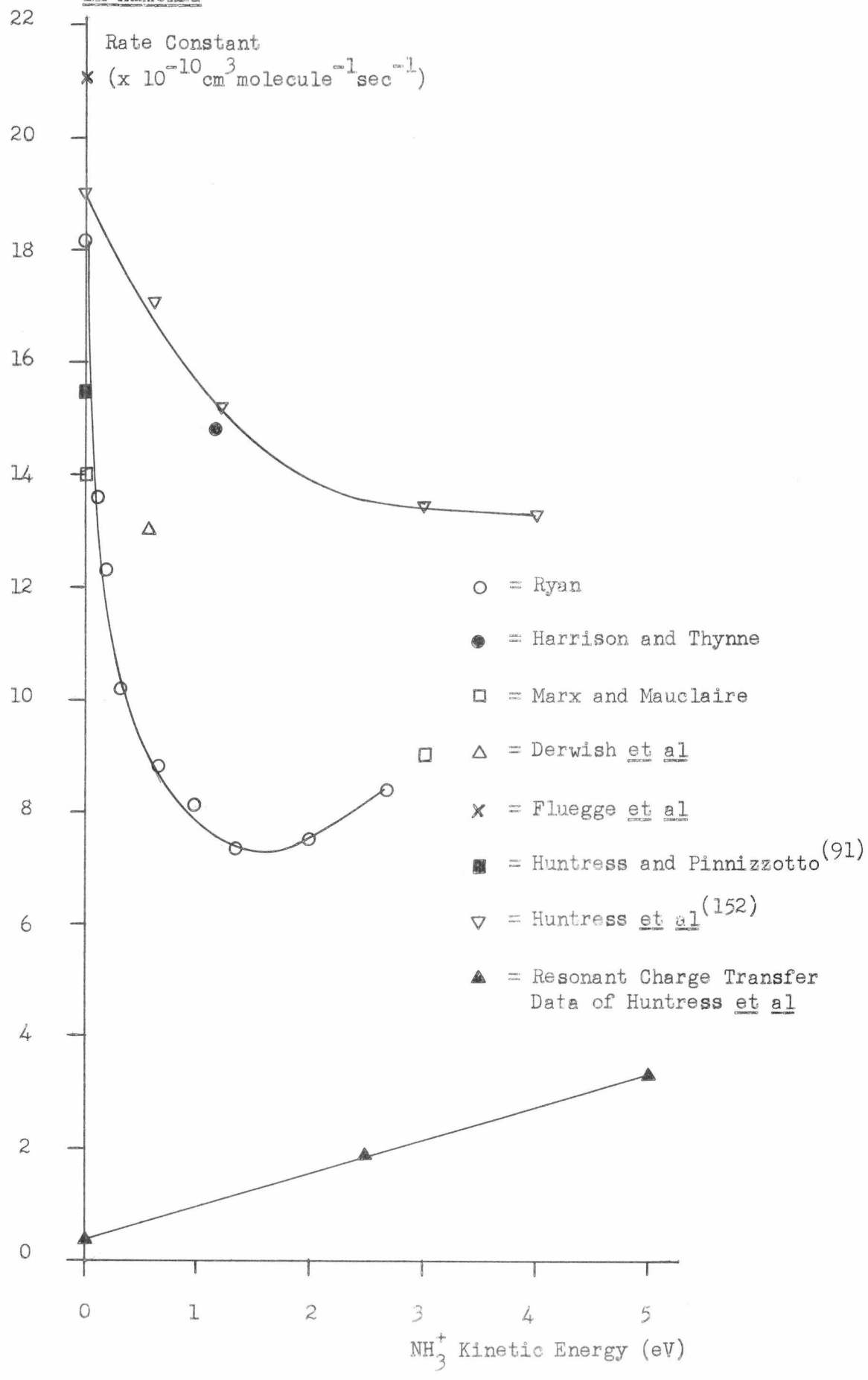

Figure 6-11. Summary of Literature Rate Constants For Loss of NH_2^+ in Ammonia

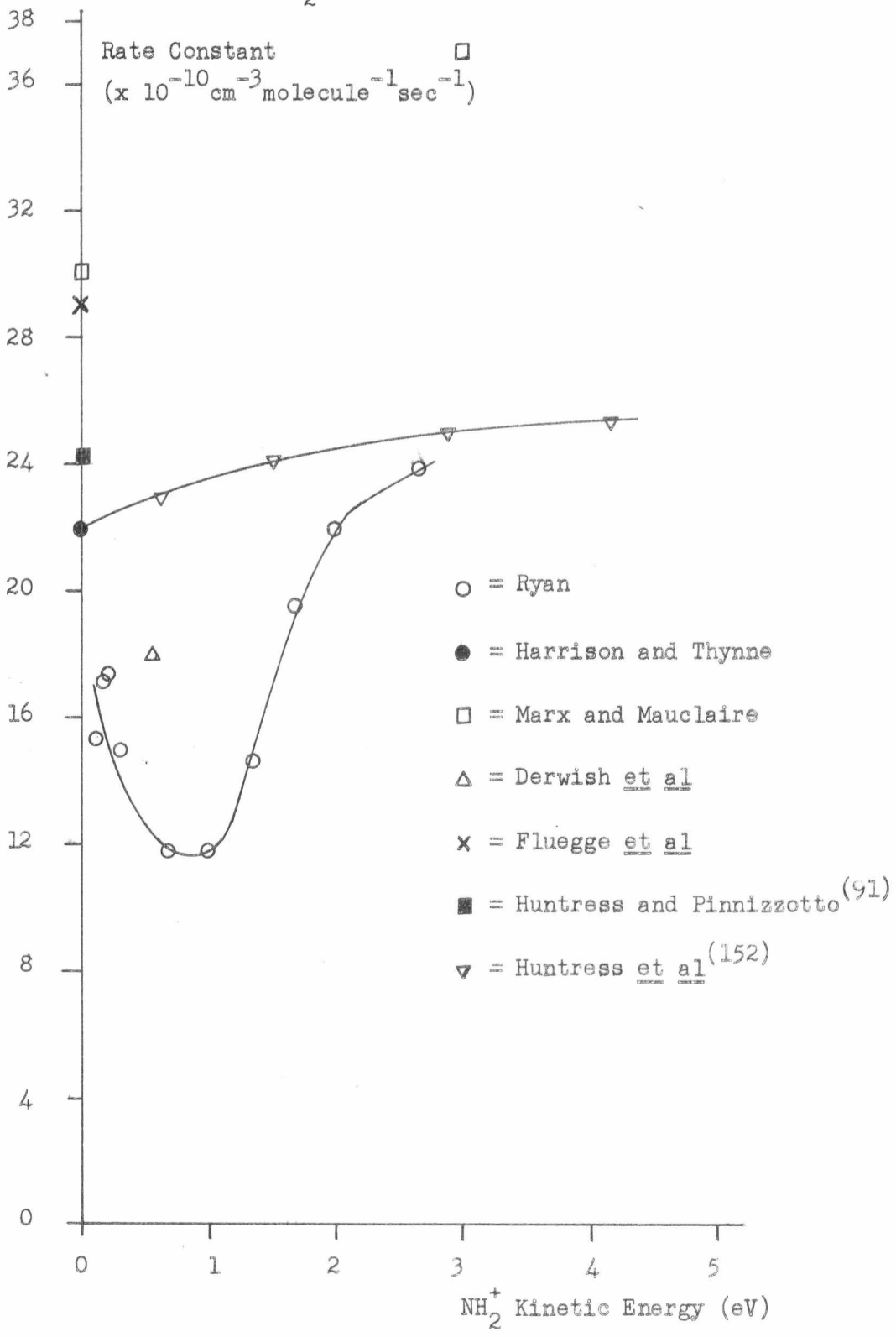

data supplied in their report. The two major studies, by Ryan and Huntress et al[151], indicate similar behaviour, differing mainly in the magnitudes of the measured rate constants. More interesting are the large discrepancies obtained by different groups using a similar technique; Ryan[156] and Harrison and Thynne[155] both used pulsed mass spectrometers, operated at moderate pressures, while Huntress and Pinnizzotto[91] used the recent technique of Pulsed ICR, and Huntress et al[84,151] and Marx and Mauclaire[83] have used ICR with source ejection. These latter two groups have disputed the relative merits of their respective results in the literature, each accusing the other of incomplete source ejection, and therefore deriving misleading results. In addition, Harrison and Thynne show an increase in rate constant with kinetic energy, in marked disagreement with all other results. Consequently, it would appear that the data of Ryan might be most reliable, particularly since he was able to duplicate the methane results of Giardini-Guidoni and Friedman[114], as mentioned earlier (see Section 6-53). Similar discrepancies are apparent in the published rate constants for the loss of NH_2^+, depicted in Figure 6-11. Unfortunately, data from the work of Harrison and Thynne is unavailable for the higher energy they employed (3.7 eV ion exit energy) since only the rate constant for reaction (6-15) was given at this energy; their value for this quantity of 9.7×10^{-10} cm^3 $molecule^{-1}$ sec^{-1}, is however in good agreement with the value obtained by Huntress et al[151]. Although the results of this latter group and of Ryan tend towards the same values at ion energies in excess of 2 eV, the initial sharp decrease in rate constant observed by Ryan was not reported by Huntress et al. Ryan has postulated this decrease as arising from a change in the reaction mechanism, the permanent dipole attraction (see Section 6.1) being dominant below 1 eV, and its importance decreasing with increasing ion energy, and the induced dipole dominating above 1 eV, and imparting

a constant or slightly increasing effect on the rate constant. Huntress *et al* were able to separate reactions (6-15) and (6-16), and their report shows that (6-15) undergoes a steady drop in rate constant above 1 eV, while (6-16) experiences an increase which results in the overall rate of loss of NH_2^+ remaining fairly constant, as shown in Figure 6-11. Doubt might again be cast on these results if their source ejection was incomplete, furthermore the use of 1-3 Volts source trapping voltages would confuse the results at supposedly low ion energies (see also the carbon dioxide/hydrogen discussion in Section 5.333). Marx and Mauclaire[83] also failed to observe the sharp drop, and reported rate constants for the loss of NH_2^+ were 30 x 10^{-10} cm^3 $molecule^{-1}$ sec^{-1} at thermal energies and 37 x 10^{-10} $cm^3 molecule^{-1} sec^{-1}$ at 3 eV.

As with water, the results obtained in this work were for the rate of loss of NH_3^+ and NH_2^+, since it was impossible to separate the reactions of this latter species. A typical set of results is shown in Figure 6-12, and it is apparent from these that the NH_2^+ ions are contributing to both NH_3^+ and NH_4^+, since a 'plateau' is observed for the former species at short storage times, and the increase of NH_4^+ can only be reproduced by addition of the losses of NH_2^+ and NH_3^+ (see also Figure 7-3). For the rate of loss of NH_3^+, values for the rate constant of 11.9 $\pm$ 0.5, 12.9 $\pm$ 1.5 and 12.2 $\pm$ 0.5 x $10^{-10} cm^3 molecule^{-1} sec^{-1}$ were obtained, the calculated mean ion kinetic energy being 2.15 eV. For the loss of NH_2^+, values of 29.7 $\pm$ 0.5, 34.5 $\pm$ 1.5 and 35.4 $\pm$ 0.5 x $10^{-10} cm^3 molecule^{-1} sec^{-1}$ were obtained at 2.18 eV. The rate constant for NH_3^+ loss lay almost exactly mid-way between the values of Huntress *et al*[151] and Ryan[156] but if, as was suspected, the results of Ryan are more reliable, then the figures suggest that a reasonable proportion of the ions had energies in excess of the calculated mean. This was not really surprising since the calculation of a mean energy must imply that there is a distribution

Figure 6-12. Percentage Total Ionization vs. Storage Time for Ammonia

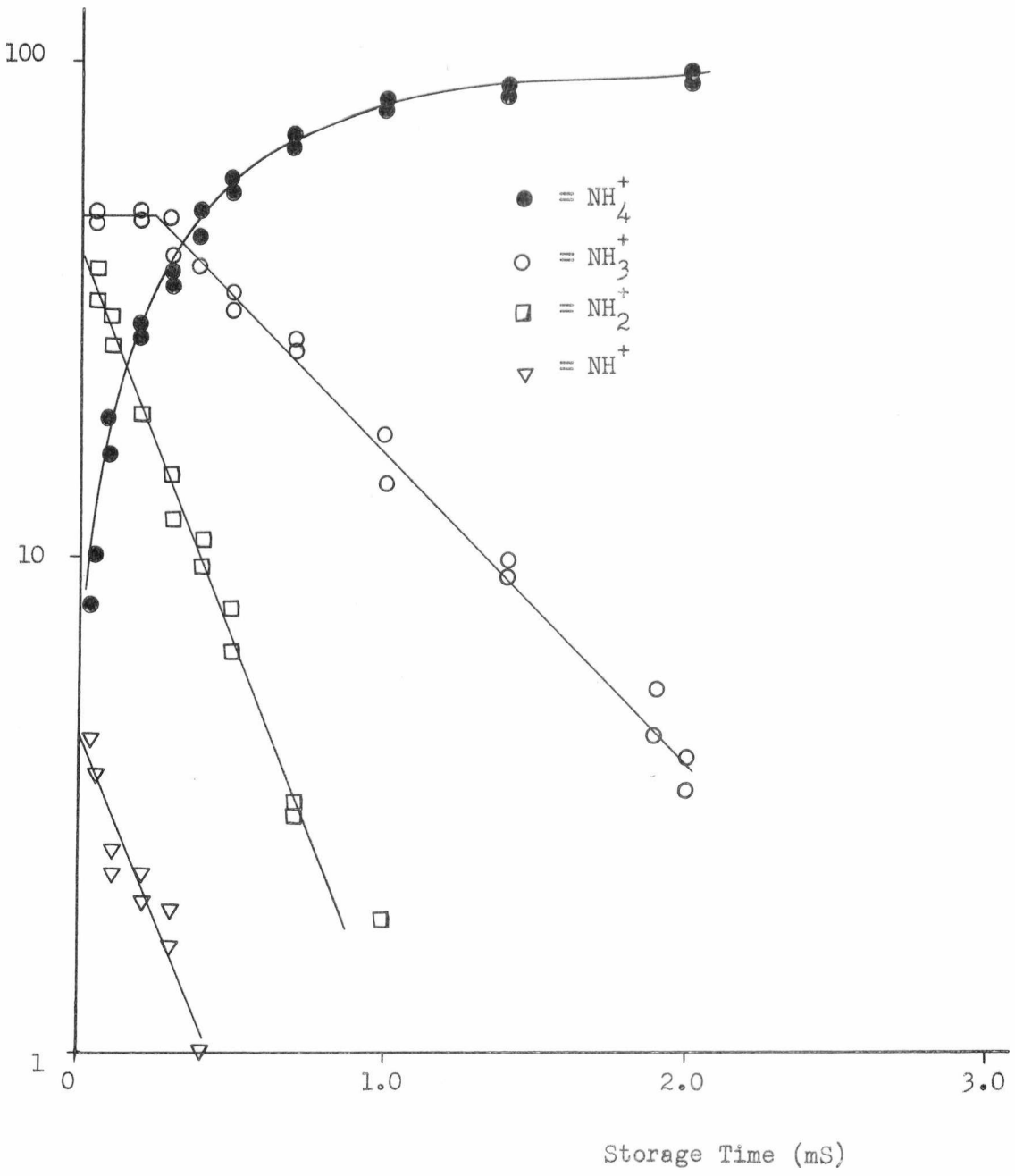

of energies, which may be large as suggested by Figure 5-25; in addition, it was fairly certain that some of the ions possessed internal energy, as discussed in Section 5.333. This conclusion was also supported by the extremely large rate constant for the loss of NH_2^+, which is in agreement only with the results of Marx and Mauclaire[83].

6.6 Metastable Ion Decay

Some preliminary investigations of hexafluoroethane, C_2F_6, showed that examination of processes of this kind were also viable in the QUISTOR. From the results, shown in Figure 6-13, it was apparent that the major ion in the spectrum, CF_3^+, slowly decayed, by loss of one or two atoms, forming CF_2^+ and CF^+. The mechanism of this reaction was not investigated, but could have occurred in one of two ways :

(i) Metastable decay of CF_3^+ ions.

(ii) Collisionally induced decay of the CF_3^+ ions.

If the reaction occurred by mechanism (ii) then the rate of decay would be pressure dependent, whereas this would not be the case if mechanism were operative.

In the examination of this type of reaction, which would certainly appear to merit further study, the use of the QUISTOR was comparable to the method of Tartarczyk and von Zahn[157], in which an energy and mass selected ion beam was passed through a 314 cm long quadrupole mass filter before analysis by a second, smaller mass filter. The first quadrupole, which functioned solely as a reaction chamber, was operated in the total pressure mode, and the available reaction time varied by altering the ion energy. Using the QUISTOR it should be possible to employ longer storage times, but the ion kinetic energy would be known with less accuracy.

6.7 Sequential Mass Spectrometry

The technique known as Sequential Mass Spectrometry, described in greater detail in Chapter 2, essentially involves storing ions in the

Figure 6-13

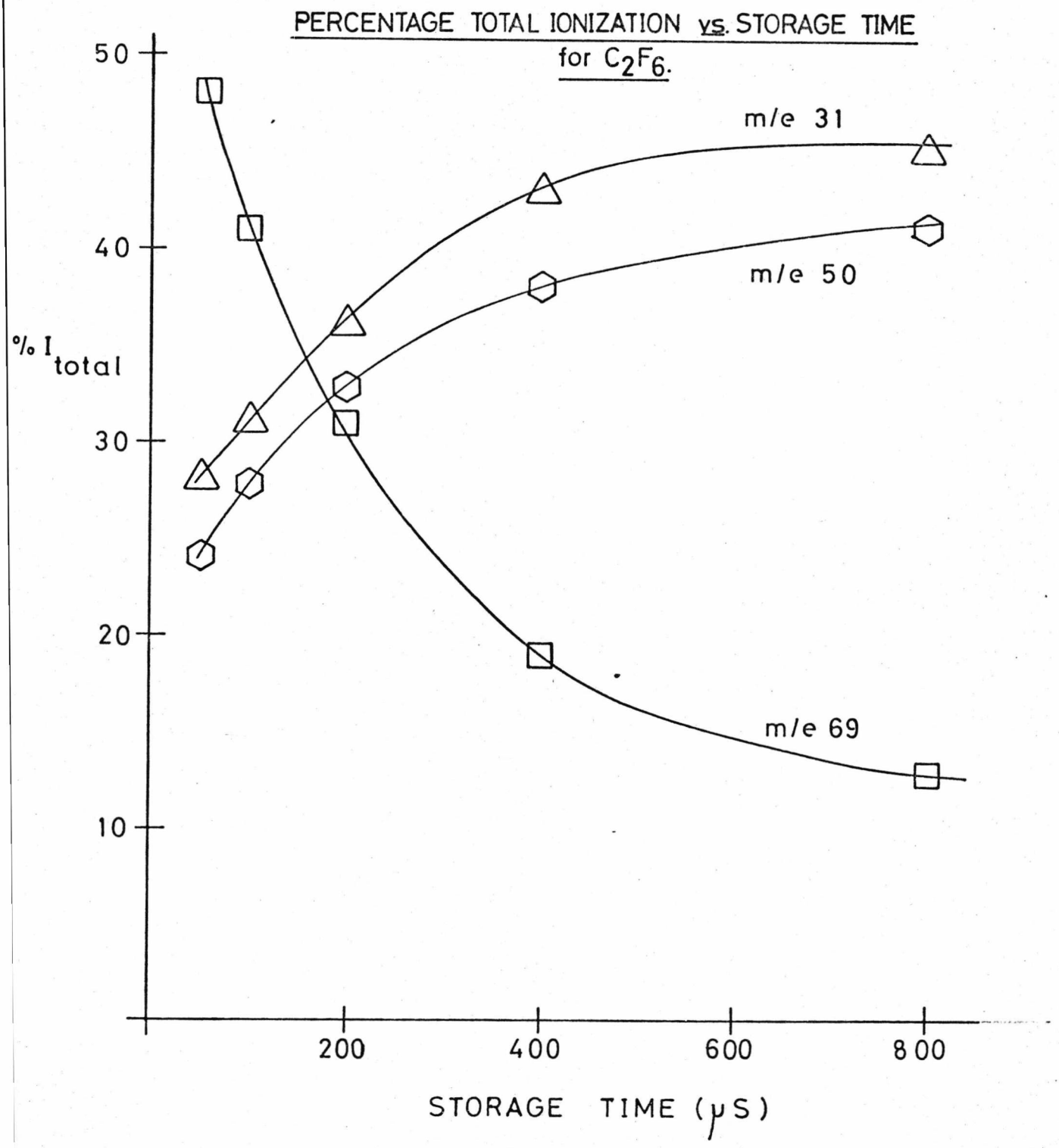
PERCENTAGE TOTAL IONIZATION vs. STORAGE TIME
for C_2F_6.
m/e 31
m/e 50
m/e 69
% I_{total}
50
40
30
20
10
200
400
600
800
STORAGE TIME (μS)

presence of an electron beam so that they undergo several ionizing collisions, resulting in the formation of multiply charged ions. The multiplicity of the collisions is ensured by maintaining the energy of the ionizing beam below the second, and bigger, ionizing potentials of the substance under investigation. The occurrence of this type of reaction had previously been observed in the mesh QUISTOR[37] by double pulsing the ion creation generator, that is creating a burst of ions, storing them for a given time and then admitting another pulse of electrons. During this investigation, Sequential Mass Spectrometry was observed under two sets of conditions :

(i) With the device operating as a static source with RF applied (see Section 5.32), under conditions of low ion extraction voltage so that some storage occurred.

(ii) Under ion storage conditions with long ionizing pulse widths, as employed in Section 5.333(iii).

In both cases the intensity of doubly charged ions was found to increase with the storage time (decrease of the ion extraction voltage in (ii)). If it were desired to use the QUISTOR for further studies of this kind, some re-designing of the electron gun in order to stabilize the electron energy, would be advisable.

CHAPTER 7

Conclusion and Discussion

7.1 Summary of This Work

As mentioned in the introduction to the previous chapter one of the fundamental aims of this work was to explore the possibilities of the QUISTOR as an ion source, from both academic and technological points of view. Clearly, before an examination of the possible uses, a detailed characterisation of the device was required and this was performed. During the course of the experimental studies, a brief theoretical and numerical analysis of the ionic motion within the QUISTOR was carried out in order to attempt to explain some of the observed behaviour and to derive expressions for the mean ion kinetic energy.

It was shown that, operating as an ion source, the QUISTOR provided an extremely versatile experimental tool, since it could be operated in a manner comparable to a conventional source or in the ion storage mode, permitting observation of ionic collision reactions. Of particular interest was the observation of Chemical Ionization at low pressures (ca. 10^{-5} - 10^{-4} Torr) and with air as a reagent gas.

Alteration of the operating mode was accomplished by interchanging the power supply connections to the device which, in a more sophisticated piece of equipment, could be achieved by direct switching. The disadvantages and advantages of the QUISTOR which were experienced during this work are summarized below.

Disadvantages

(i) The particular device used in this work was fabricated from stainless steel, and machined to an accuracy of $\pm$ 0.001 inches; this is a costly and time-consuming process. It was not conclusively proved, however, that this model had any great advantages over the cheaper wire

mesh model used previously[37], although the stainless steel version did appear to generate higher ion currents.

(ii) The power supplies required, particularly for ion storage operation, were large and expensive; namely, at least two pulse generators, capable of at least 100 Volts output, a high voltage RF oscillator and a filament power supply.

(iii) The QUISTOR tended to show RF-dependent mass discrimination. This was not disastrous in the observation of ion-molecule reactions, owing to the method of calculation employed (see Section 5.332), but is certainly undesirable in a conventional source. It may, however, be put to good use when employing the QUISTOR as a CI source, as it allows the mass spectrum obtained to be 'tuned' for maximum information.

(iv) Although the mean ion energies, calculated as in Chapter 3, were shown to be reasonable, the energy spread was unknown and likely to be fairly large. In addition the energy spread in the ionizing beam was found to be large, due to adverse affects of the RF voltage. These factors, while not greatly harming the operation as a static or CI source, are undesirable in an ion-molecule reaction chamber, since they are fundamental parameters in the investigation of such reactions.

Advantages

(i) The device was extremely versatile, being capable of examining several types of ionic reaction in addition to operating as a normal source. Furthermore changing between modes of operation was easily accomplished by re-connection of the applied voltages.

(ii) The QUISTOR is inherently capable of very long storage times (see for example Table 2-1 and the description of the three-dimensional quadrupole ion trap in Chapter 2). This should permit the observation of slow processes.

(iii) The various ionic processes occur at low pressures thereby

avoiding the need for complex vacuum systems.

(iv) It is conceivable that the mass discrimination effects may be turned to good usage by allowing the storage of one ion followed by relaxation to store all its products. This would provide a method of uniquely determining reaction pathways which is not available at present.

Based on the above brief comments and the observations made during this work, it was possible to make some suggestions for experimental improvement and possibly profitable areas of further study. These are described in the final section.

7.2 Instrumental Improvements and Suggestions for Further Investigation

During the writing of this thesis, a Boxcar Integrator, supplied by BROOKDEAL ELECTRONICS INC. and comprising a Model 9425 Scan Delay Generator and a Model 9415 Linear Gate, became available and was incorporated into the apparatus as shown in Figure 7-1. The Scan Delay Generator was

Figure 7-1 Incorporation of Boxcar Integrator into Detection Circuitry.

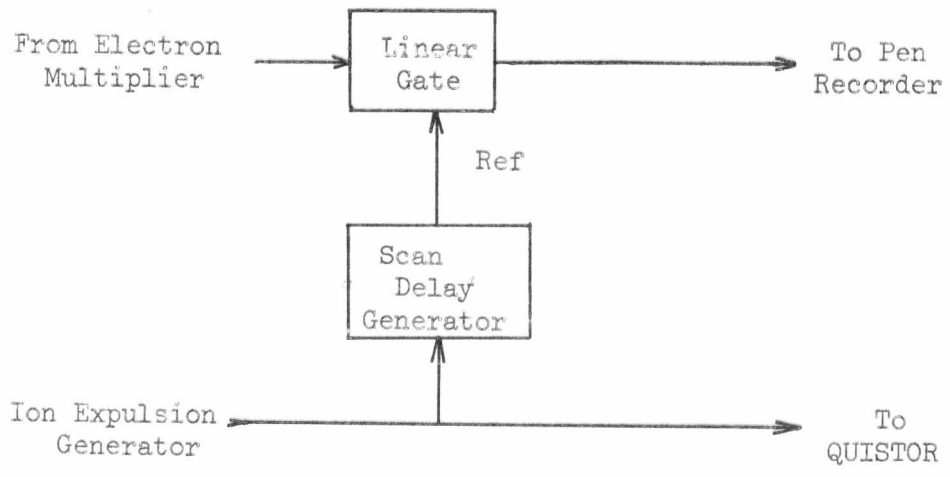

triggered by the ion expulsion pulse and supplied a one volt pulse, of variable width, a predetermined time after this. The second pulse 'opened' the Linear Gate, which in turn supplied a steady DC voltage proportional to the signal input during the time the Gate was open. As a result of this steady DC voltage, the averaging effect of the pen recorder was nullified resulting in an increase in signal strength of 10^3 - 10^4 times. The reference pulse was delayed after the ion expulsion pulse by ca. 5 μS, roughly the time taken for ions to reach the electron multiplier, and consequently only ions arriving during this period were detected. More particularly, ions arriving elsewhere in the duty cycle, as a result of being unstable, were not detected and the spectrum obtained was, therefore, due only to stored ions.

It was also found that the capabilities of these units could be further exploited by using the Scan Delay Generator to scan the storage time over a fixed range at a given rate. In this arrangement, shown in Figure 7-2, the Scan Delay Generator was triggered by the ion creation

Figure 7-2 Experimental Arrangement for Storage Time Scanning.

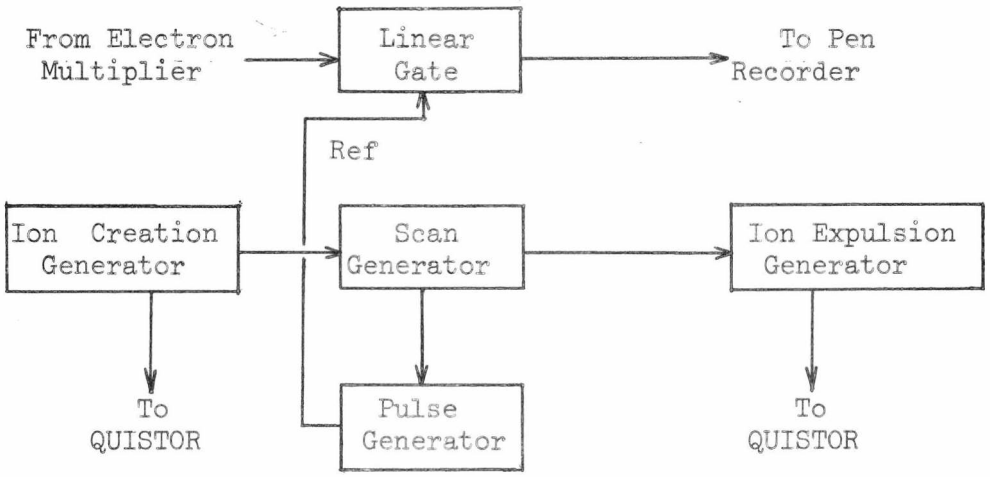

pulse generator, and supplied a pulse with slowly increasing delay time, to trigger the ion expulsion generator and a third pulse generator which in turn triggered the Linear Gate. Operating in this mode, the analyzer was set to a particular m/e value and the scan initiated allowing the behaviour of that mass with storage times to be recorded directly. (The Scan unit also supplies a linearly ramped voltage to drive the X-axis of the X-Y recorder). A preliminary example of this type of operation is shown in Figure 7-3 for the ammonia system; the horizontal scale is storage time from zero to 500 μS, and the vertical scale, peak height, is in arbitrary units. In this particular example the signal to noise ratio is rather bad, as a result of the hastily improvised system.

These units are obviously of great use for several reasons : they increase the signal strength and signal-to-noise ratio, thereby permitting the use of longer storage times; they also provide a spectrum which is known to result solely from stored ions; lastly, they are capable of generating a storage time scan, easing the problem of data retrieval.

With regard to the rest of the apparatus, several areas could be profitably re-designed or improved :

(i) Any desired investigation of higher molecular weight samples in the ensuing studies, clearly of particular importance in CI examinations, would entail re-designing the sample inlet system particularly to include heating and closer positioning of the capillary to the QUISTOR.

(ii) Re-positioning of the electron gun so that the electron beam was injected through an end-cap, rather than the ring electrode, might well cause a reduction of the energy spread in the electron beam. This would be advantageous in further studies on ion-molecule reactions. Alternatively, pulsed photo-ionization could be employed.

(iii) It would probably be advantageous to modify the RF oscillator circuitry, to permit greater flexibility of operation. Since only one

Figure 7-3. Example of Storage Time Scan.

Peak Heights in Ammonia vs Storage Time.

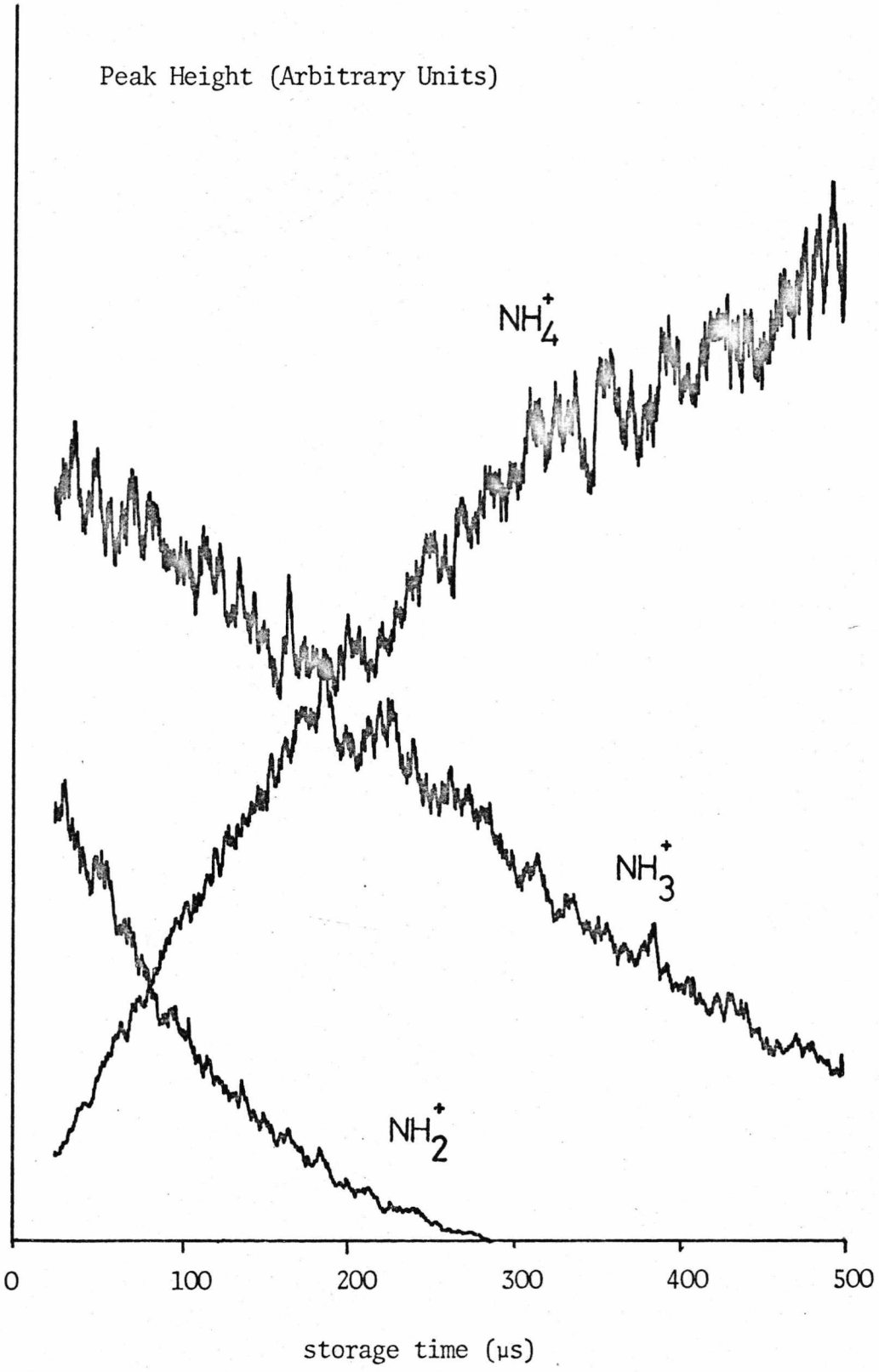

polarity of RF is required, this modification could take the form of a single-ended, high power linear amplifier[158] driven by a selection of low-voltage, solid-state oscillators. The latter would need to be extremely stable, crystal controlled or LC designs[158], and could be frequency and amplitude stabilized; any desired scanning or modulation could also be introduced at a low level.

(iv) Following the suggestion of Dawson and Lambert[105], the synchronization of the ion expulsion pulses to the phase of the RF should be investigated, and may well aid ion extraction.

The design of an RF oscillator similar to that outlined above, would also permit easy implementation of mass selective operation of the QUISTOR, which could be achieved in one of two ways :

(i) A recent report by Richards, Huey and Hiller[159] has indicated that mass resolution can be obtained in quadrupole devices by employing rectangular, rather than sinusoidal, waveforms without DC levels being required. In particular, for the ion trap, the conventional stability diagram (Figure 3-11) becomes distorted as the duty cycle ratio (the time the rectangular wave is positive to the time it is negative) is reduced. Eventually, a stability diagram having an apex intersecting the q-axis, as shown in Figure 7-4, is obtained.

This apex may be used to obtain resolution and, since it intersects the q-axis, no DC level is required. It is thus possible to operate a device for reaction pathway determination by storing one ion, and observing all products, viz. the QUISTOR is operated with a rectangular wave of suitable amplitude and duty cycle such that only the desired ion is stored. A burst of ions is created, stored to allow undesired ions to be lost on the electrodes and the wave-form altered to have a 1 : 1 duty cycle (square wave). This is equivalent to conventional total pressure operation, and consequently all ions having $0 < q < 0.9$ are stored;

Figure 7-4 Stability Diagram Obtained Using rectangular Waves.

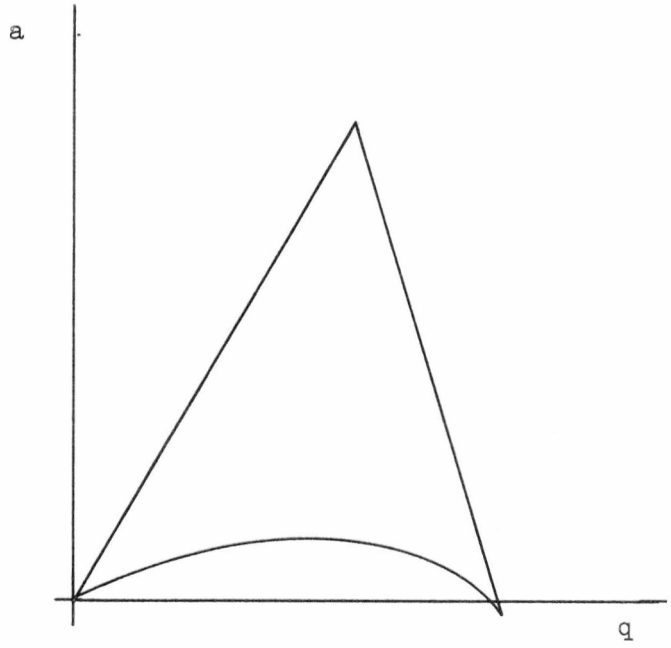

N.B. Not Drawn To Scale.

after a given storage time the ions are pulsed from the device for analysis.

(ii) Alternatively, the device could be operated under fixed RF and DC conditions, and the frequency selected to give the desired ion a- and q- values placing it in an apex of a conventional stability diagram. After removing all undesired ions (as above) the frequency is altered to again permit a range of m/e values to be stored.

The implementation of either of these methods would be considerably eased if they could be at low voltages, as in (iii) above, the low-level oscillators required being rectangular wave and frequency modulated respectively.

It may also be of interest to use a six-electrode quadrupole ion trap, constructed with planar electrodes as in Figure 2.7 . This device, although requiring a three phase oscillator would appear to possess several advantages over the three-electrode version:

(i) The planar electrodes would aid ion removal in both the static and storage modes, permitting higher ion currents to be extracted.

(ii) Injection of the electron beam and sample would be eased, particularly if the electrodes were fabricated from wire mesh.

A recent report by Walls and Dunn[160] has demonstrated the use of a static three-dimensional quadrupole as an ion store for studying the re-combination of ions and electrons. Essentially this device is the same as a conventional ion trap, except that DC only is applied to the ring and the instrument is placed in a magnetic field (parallel to the z-axis). Since the device is passive, ions of extremely low kinetic energies (e.g. 15 meV) can be stored. In many ways this instrument is an extension of ICR, as the ions follow circular trajectories in a plane at right angles to the magnetic field, and it would appear to have the advantage over the QUISTOR of permitting the use of accurate ion and electron energies, and would be worth investigating.

From the point of further research using the present apparatus, several ideas can be suggested :

(i) Investigation of the ion-energy spread in the QUISTOR by employing a well-known reaction, for example :

$$CH_4^+ + CH_4 \longrightarrow CH_5^+ + CH_3$$

and comparing the differences in rate constants at calculated ion energies with the values of other workers.

(ii) Further study of the QUISTOR as a CI source, particularly examining the use of 'moist' air as a reagent gas and the possibility of atmospheric pollutant detection.

Undoubtedly the implementation of all, or any, of these ideas and suggestions will depend on the interest of future researchers and the availability of finance.

BIBLIOGRAPHY

1. Field, F.H., 'Chemical Ionization Mass Spectrometry' in Franklin, J.L. (ed.) 'Ion-Molecule Reactions', Butterworths, 1972.

2. Franklin, J.L., 'Ion-Molecule Reactions', Vol. I and II, Butterworths, 1972.

3. Munson, M.S.B. and Field, F.H., J. Amer. Chem. Soc. 88, 2621 (1966). 'Chemical Ionization Mass Spectrometry. I. General Introduction'.

4. McDaniel, E.W., Čermak, V., Dalgarno, A., Ferguson, E.E. and Friedman, L., 'Ion-Molecule Reactions', Wiley-Interscience, 1970.

5. McDaniel, E.W., 'Collision Phenomena in Ionized Gases', Wiley, 1964.

6. Field, L.M., Spangenberg, K. and Helm, R., Elec. Commun. 24, 108, (1947). ' Control of Electron-Beam Dispersion at High Vacuum by Ions'.

7. Linder, E.G. and Hernqvist, K.G., J. Appl. Phys. 21, 1088 (1950). 'Space Charge Effects in Electron Beams and their Reduction by Positive Ion Trapping'.

8. Plumlee, R.H., Rev. Sci. Instrum. 28, 830 (1957). 'Space Charge Neutralization Trap in the Ionizing Beam of a Mass Spectrometer'.

9. Baker, F.A. and Hasted, J.B., Phil. Trans. Roy. Soc. London A. A261, 33 (1966). 'Electron Collision Studies with Trapped Positive Ions'.

10. Baker, F.A. and Hasted, J.B., Advan. in Mass Spectrom. 4, 727 (1968). 'Ionization Processes in Hydrogen and Helium'.

11. Hasted, J.B., 'Sequential Mass Spectrometry' in Bonnett, R. and Davies, J.G. (eds.) 'Some Newer Physical Methods in Structural Chemistry', United Trade Press, London, 1967.

12. Redhead, P.A., Can. J. Phys. 45, 1791 (1967). 'Multiple Ionization of the Rare Gases by Successive Electron Impact'.

13. Redhead, P.A. and Feser, S., Can. J. Phys. 46, 865, (1968). 'Multiple Ionization of the Rare Gases by Successive Electron Impacts (0-250eV). II. 1s-2s Transitions in $^{3}He^{+}$.'

14. Redhead, P.A. and Feser, S., Can. J. Phys. 46, 1905 (1968). 'Multiple Ionization of Mercury by Successive Electron Impacts'.

15. Daly, N.R. and Powell, R.E., Proc. Phys. Soc. (London) 89, 273 (1966). 'Electron Collisions in Nitrogen'.

16. Daly, N.R. and Powell, R.E., Proc. Phys. Soc. (London) 89, 281 (1966). 'Electron Ionization of He^{+} and the Destruction of He^{2+} by Charge Transfer Processes in a Space-charge Trap'.

17. Daly, N.R. and Powell, R.E., Proc. Phys. Soc. (London) 90, 629 (1967). 'Electron Collisions in Oxygen'.

18. Cuthbert, J., Farren, J., Prahallada Rao, B.S. and Preece, E.R., Proc. Phys. Soc. (London) 88, 91 (1966). 'Appearance Potentials and Transition Probabilities for Electron Impact Ionization of CO and CO^{+}'.

19. Cuthbert, J., Farren, J., Prahallada Rao, B.S. and Preece, E.R., Proc. Phys. Soc. (London) 91, 63 (1967). 'Sequential Mass Spectrometry: Nitrogen and the Determination of Appearance Potentials'.

20. Cuthbert, J., Farren, J., Prahallada Rao, B.S. and Preece, E.R., J. Phys. B. 1, 62 (1968). 'Sequential Mass Spectrometry. III. Ions and Fragments from Carbon Dioxide and Disulphide'.

21. Bourne, A.J. and Danby, C.J., J. Sci. Instrum. Ser. 2. 1, 155 (1968). 'A Technique for Ion-Trapping in Pulsed-Source Mass Spectrometry'.

22. Herod, A.A. and Harrison, A.G., Int. J. Mass Spectrom. Ion Phys. 4, 415 (1970). 'Bimolecular Reactions of Ions Trapped in an Electron Beam Space Charge'.

23. Harrison, A.G., Nagy, G.P., Chin, M.S. and Herod, A.A., Int. J. Mass Spectrom. Ion Phys. 9, 287 (1972). 'Kinetic Energy Effects on Product Yields from Ion-molecule Reactions'.

24. McAskill, N.A. and Harrison, A.G., Int. J. Mass Spectrom. Ion Phys. 5, 193 (1970); Harrison, A.G., ibid 6, 297 (1971); Blair, A.S. and Harrison, A.G., Can. J. Chem. 51, 703 (1973); Harrison, A.G. and Blair, A.S., Int. J. Mass Spectrom. Ion Phys. 12, 175 (1973); Blair, A.S. and Harrison, A.G., Can. J. Chem. 51, 1645 (1973).

25. Hartnagel, H., Proc. Inst. Elec. Eng. 111, 57 (1964). 'Electrostatically Focussed Electron Gun for Hollow Beams'; ibid, 111, 1821 (1964). 'Toroidal Hollow-Beam Gun'.

26. Hartnagel, H. and Herkmann, J., J. Vac. Sci. Technol. 10, 539 (1973). 'Electron Optical Aspects of a Sequential Mass Spectrometer'.

27. Hartnagel, H., Int. J. Electron. 21, 277 (1966). 'Some Considerations about Ion Trapping by Tubular Electron Beams for Collision Experiments'.

28. Hasted, J.B. and Awad, J.L., J. Phys. B. 5, 1719 (1972). 'Electron Impact Ionization of Ions Trapped in a Hollow Electron Beam'.

29. Hasted, J.B. and Hamdun, M., Private Communication.

30. Schulz, G.J., Phys. Rev. 116, 1141 (1959). 'Measurement of Excitation of N_2, CO and He by Electron Impact'.

31. Paul, W., Osberghaus, O. and Fischer, E., Forschungsbereichte des Wirtschafts und Vekehrsministeriums Nordheim-Westfalen, No. 415 (1958). 'Das Ionenkäfig'.

32. Fischer, E., Z. Phys. 156, 1 (1959). 'Die Dreidimensionale Stabiliserung von Ladungsträgern in einem Vierpolfeld'.

33. Paul, W. and Steinwedel, M., Z. Naturforsch, 8A, 448 (1953). 'Ein Neues Massenspektrometer ohne Magnetfeld'.

34. Dawson, P.H. and Whetten, N.R., J. Vac. Sci. Technol. 5, 1 (1968). 'Ion Storage in Three-Dimensional, Rotationally Symmetric, Quadrupole Fields. I. Theoretical Treatment'.

35. Dawson, P.H. and Whetten, N.R., J. Vac. Sci. Technol. 5, 11 (1968). 'Ion Storage in Three-Dimensional, Rotationally Symmetric, Quadrupole Fields. II. A Sensitive Mass Spectrometer'.

36. Dawson, P.H., Hedman, J.W. and Whetten, N.R., Rev. Sci. Instrum. 40, 1444 (1969). 'A Simple Mass Spectrometer'.

37. Lawson, G., Ph.D. Thesis, University of Kent at Canterbury, 1972. 'Some Studies in Mass Spectrometry'.

38. Lawson, G., Bonner, R.F. and Todd, J.F.J., J. Phys. E. 6, 357 (1973). 'The Quadrupole Ion Store (QUISTOR) as a Novel Source for a Mass Spectrometer'.

39. Rettinghaus, G., Z. Angew. Phys. 22, 321 (1967). 'Nachweis Niedriger Partialdrucke mit dem Ionenkäfig'.

40. Dawson, P.H. and Whetten, N.R., Int. J. Mass Spectrom. Ion Phys. 2, 45 (1969). 'Non-Linear Resonances in Quadrupole Mass Spectrometers due to Imperfect Fields. I. The Quadrupole Ion Trap'.

41. Harden, C.S. and Wagner, P.E., Edgewood Arsenal Special Publications EASP-100-93. 'The Three-Dimensional Quadrupole Mass Analyzer. I. General Description'.

42. Harden, C.S. and Wagner, P.E., Edgewood Arsenal Technical Report EATR 4545. 'A Three-Dimensional Quadrupolar Mass Analyzer. II. Operational Characteristics'.

43. Sheretov, E.P., Zenkin, V.A. and Boligatov, O.I., Instr. Exp. 14, 195 (1971). 'Three Dimensional Quadrupole Mass Spectrometer with Ion Storage'.

44. Sheretov, E.P. and Zenkin, V.A., Sov. Phys.-Tech. Phys. 17, 160 (1972). 'Shape of the Mass Peak in a Three-dimensional Quadrupole Mass Spectrometer'.

45. Sheretov, E.P., Zenkin, V.A. and Samodurov, V.F., Sov. Phys.-Tech. Phys., 18, 262 (1973). 'Three-dimensional Accumulation Quadrupole Mass Spectrometer'.

46. Mastoris, S., University of Toronto, Institute of Aerospace Studies, Technical Note 172. 'The Three Dimensional Quadrupole Mass Spectrometer'.

47. Holme, A.E., Thatcher, W.J. and Leck, J.H., J. Phys. E. 5, 429 (1972). 'An Investigation of the Factor Determining Maximum Resolution in a Quadrupole Mass Spectrometer'.

48. Kubicek, P., Czech. J. Phys. B19, 17 (1969). 'Approximate Calculation of the Resolving Power of a Quadrupole Mass Filter as a Function of the Number of Ion Oscillations'.

49. Dehmelt, H.G., Advan. in Atom. Mol. Phys. 3, 53 (1967). 'RF Spectroscopy of Stored Ions. I. Storage'.

50. Dehmelt, H.G., Advan. in Atom. Mol. Phys. 5, 109 (1969). 'RF Spectroscopy of Stored Ions. II. Spectroscopy'.

51. Church, D.A., Ph.D. Thesis, University of Washington, 1969. 'Storage and Radiative Cooling of Light Ion Gases in Radio-frequency Traps'.

52. Schuessler, H.A., Fortson, E.N. and Dehmelt, H.G., Phys. Rev. 187, 5 (1969). 'Hyperfine Structure of the Ground-State of $^3He^+$ by the Ion-storage Collision-exchange Technique'.

53. Bonner, R.F., Lawson, G. and Todd, J.F.J., Int. J. Mass Spectrom. Ion Phys. 10, 197 (1972/3). 'Ion-molecule Reaction Studies with a Quadrupole Ion Storage Trap'.

54. Bonner, R.F., Lawson, G. and Todd, J.F.J., J.C.S. Chem. Commun. 1179 (1972). 'A Low-pressure Chemical Ionization Source: An Application of a Novel Type of Ion Storage Mass Spectrometer'.

55. Wuerker, R.F., Shelton, M. and Langmuir, R.V., J. Appl. Phys. 30, 342 (1959). 'Electrodynamic Confinement of Charged Particles'.

56. Whetten, N.R., J. Vac. Sci. Technol. 11, 515 (1974). 'Macroscopic Particle Motion in Quadrupole Fields'.

57. Karras, T.W. and Lindman, E., J. Appl. Phys. 36, 18 (1965). 'RF Breakdown in a DC Parabolic Potential Field'.

58. Vedder, J.F., Rev. Sci. Instrum. 34, 1175 (1963). 'Charging and Accelerating of Microparticles'.

59. Langmuir, D.B., Langmuir, R.V., Shelton, M. and Wuerker, R.F., U.S. Patent No. 3,065,640. 'Containment Device'.

60. Byrne, J. and Farago, P.S., Proc. Phys. Soc. 86, 801 (1965). 'On the Production of Polarized Electron Beams by Spin Exchange Collisions'.

61. Benilan, M-N., and Audon, C., Int. J. Mass Spectrom. Ion Phys. 11, 421 (1973). 'Confinement d'Ions par un Champ Electrique de Radio-Frequence dans une Cage Cylindrique'.

62. Staubel, M., Acta. Phys. Austraca. 13, 265 (1960). 'Die Stabiliserung Elektrisch geladener Teilchen im Wechselfeddern'.

63. Berg, O.T. and Gaulker, T.A., Amer. J. Phys. 37, 1013 (1969). 'Apparatus for the Study of Charged Particles and Droplets'. See also ibid. 37, 859 (1969).

64. Berg, O.T. and Gaulker, T.A., J. Atmos. Sci. 26, 675 (1969). 'Electrification Experiments with AgI in the System: Water Vapour, Liquid Water and Ice'.

65. Dehmelt, H.G. and Walls, F.L., Phys. Rev. Lett. 21, 127 (1968). '"Bolometric" Technique for the RF Spectroscopy of Stored Ions'.

66. Church, D.A., J. Appl. Phys. 40, 3127 (1969). 'Storage-ring Ion Trap Derived from the Linear Quadrupole Radio-Frequency Mass Filter'.

67. Wuerker, R.F., Goldenberg, H.M. and Langmuir, R.V., J. Appl. Phys. 30, 441 (1959). 'Electrodynamic Containment of Charged Particles by Three-Phase Voltages'.

68. Zaritskii, A.A., Zakharov, S.D. and Kryukov, P.G., Sov. Phys.-Tech. Phys. 16, 174 (1971). 'Electrodynamic Confinement of Solid Particles'.

69. Waniek, R.W. and Jarmuz, P.J., Appl. Phys. Lett. 12, 52 (1968). 'Acceleration of Microparticles by Laser-induced Vapour Emission'.

70. Haught, A.F. and Polk, D.M., Phys. Fluids 9, 2047 (1966). 'High-temperature Plasmas Produced by Laser Beam Irradiation of Single Solid Particles'.

71. McDaniel, E.W., J. Chem. Phys. 52, 3931 (1970). 'Possible Sources of Large Error in Determinations of Ion-molecule Reaction Rates with Drift Tube Mass Spectrometers'.

72. Futrell, J.H., 'Ion Cyclotron Resonance Mass Spectrometry' in Price, D. (ed) 'Dynamic Mass Spectrometry', Vol. 2, Heyden and Sons, London, 1971.

73. Henis, J.M.S., 'Ion Cyclotron Resonance Spectrometry' in Franklin, J.L. (ed.) 'Ion-molecule Reactions', Vol. 2, Butterworths and Co., England, 1972.

74. Drewery, C.J., Goode, G.C. and Jennings, K.R., 'Ion Cyclotron Resonance Mass Spectrometry' in Macoll, A. (Volume Ed.) 'Mass Spectrometry', Volume 5 of the MTP International Review of Science, Buckingham, A., (ed.) Physical Chemistry, Series 1.

75. Sommer, H., Thomas, H.A. and Hipple, J., Phys. Rev. 76, 1877 (1949). 'A Precise Method for Determining the Faraday by Magnetic Resonance'.

76. Sommer, H. and Thomas, H.A., Phys. Rev. 78, 806 (1950). 'Detection of Magnetic Resonance by Ion Resonance Adsorption'.

77. Sommer, H., Thomas, H.A. and Hipple, J., Phys. Rev. 82, 697 (1951). 'The Measurement of $^{e}/m$ by Cyclotron Resonance'.

78. Blauth, E.W., 'Dynamic Mass Spectrometers', Elsevier Publishing Co., 1966.

79. Anders, L.R., Beauchamp, J.L., Dunbar, R.C. and Baldeschwieler, J.D., J. Chem. Phys. 45, 1062 (1966). 'Ion Cyclotron Double Resonance'.

80. Clow, R.P. and Futrell, J.H., Int. J. Mass Spectrom. Ion Phys. 4, 165 (1970). 'ICR Study of the Kinetic Energy Dependence of Ion-molecule Reaction Rates. I. Methane, Hydrogen and Rare Gas-Hydrogen Systems'.

81. Goode, G.C., Ferrer-Correia, A.J. and Jennings, K.R., Int. J. Mass Spectrom. Ion Phys. 5, 229 (1971). 'The Interpretation of Double Resonance Signals in Ion Cyclotron Resonance Mass Spectrometry'.

82. Beauchamp, J.L. and Armstrong, J.T., Rev. Sci. Instrum. 41, 123 (1969). 'An Ion Ejection Technique for the Study of Ion-molecule Reaction Rates with Ion Cyclotron Resonance Spectrometry!

83. Marx, R. and Mauclaire, G., Int. J. Mass Spectrom. Ion Phys. 10, 213 (1973). 'ICR Study of Positive and Negative Ion-Molecule Reactions in Ammonia'.

84. Huntress, W.T., Int. J. Mass Spectrom. Ion Phys. 11, 495 (1973). 'On Ion-molecule Reactions in Ammonia'.

85. McIver, R.T., Rev. Sci. Instrum. 41, 555 (1970). 'A Trapped Ion Analyzer Cell for Ion Cyclotron Resonance Spectrometry'.

86. McIver, R.T., U.S. Patent No. 3,742,212. 'Apparatus and Method for Pulsed Ion Cyclotron Resonance Spectroscopy'.

87. McIver, R.T. and Dunbar, R.C., Int. J. Mass Spectrom. Ion Phys. 7, 471 (1971). 'Pulsed Ion Cyclotron Resonance for the Study of Ion-molecule Reactions'.

88. McIver, R.T., Rev. Sci. Instrum. 44, 1071 (1973). 'Solid-State Marginal Oscillator for Pulsed Ion Cyclotron Resonance Spectroscopy'.

89. Bowers, M.T., Ave, D.H., Webb, H.M. and McIver, R.T., J. Amer. Chem. Soc. 93, 4314 (1971); McIver, R.T. and Eyler, J.R., ibid. 93, 6334; McIver, R.T., Scott, J.A. and Riveros, J.M., ibid. 95, 2706 (1973); McIver, R.T. and Silvers, J.M., ibid. 95, 8642 (1973).

90. McMahon, T.B. and Beauchamp, J.L., Rev. Sci. Instrum. 43, 509 (1972). 'A Versatile Ion Cell for Ion Cyclotron Resonance Spectroscopy'.

91. Huntress, W.T. and Pinnizzotto, R.F., J. Chem. Phys. 59, 4742 (1973). 'Product Distributions and Rate-Constants for Ion-Molecule Reactions in Water, Hydrogen Sulfide, Ammonia and Methane'.

92. Huntress, W.T. and Pinnizzotto, R.F., Int. J. Mass Spectrom. Ion Phys. 13, 331 (1974). 'Reactions of Fragment Ions in Methane: Ion-molecule Reactions in Methane and Helium-Methane Mixtures'.

93. McLachlan, N.W., 'Theory and Applications of Mathieu Functions'. Dover Publications Inc., 1964.

94. Arscott, P.M., 'Periodic Differential Equations'. Pergammon Press, 1964.

95. Tamir, T., Math. Computations 16, 100 (1962). 'Characteristic Exponents of Mathieu Functions'.

96. Denison, D.R., J. Vac. Sci. Technol. 8, 266 (1971). 'Operating Parameters of a Quad in a Grounded Cylindrical Housing'.

97. von Zahn, U., Rev. Sci. Instrum. 34, 1 (1963). 'Monopole Spectrometer, a New Electric Field Mass Spectrometer'.

98. Lever, R.F., IBM Journal, 10, 26 (1966). 'Computation of Ion Trajectories in the Monopole Mass Spectrometer by Numerical Integration of Mathieu's Equation'.

99. Chisholm, T. and Stark, A.M., J. Phys. D. 3, 1717 (1970). 'A Technique for the Compuation of Charged Particle Trajectories in a Radio-frequency Quadrupole Device'.

100. Powell, H.M., Ph.D. Thesis, Vanderbilt University, 1966. Disser. Abs. 27, 2071B (1967).

101. Kondo, T., Mass Spectrom. (Japan) 17, 589 (1970). 'Analog Computation of Ion Trajectories in a Mass Filter'.

102. Yinon, J. and Klein, F.S., Vacuum 21, 379 (1971). 'The Quadrupole and its Application in Vacuum Technology and Mass Spectrometry'.

103. Dawson, P.H. and Whetten, N.R., Advan. in Electron. Electron. Phys. 27, 59 (1969). 'Mass Spectrometry Using RF Quadrupole Fields'.

104. Dawson, P.H. and Whetten, N.R., Air Force Cambridge Research Laboratories Report No. AFCRL-69-0185, 1969. '3-D Quadrupole Ion Trap Mass Spectrometer'.

105. Dawson, P.H. and Lambert, C., Private Communication, to be published. 'Pulse-out Synchronization in the Quadrupole Ion Trap'.

106. Smith, D.L. and Futrell, J.H., Int. J. Mass Spectrom. Ion Phys. 10, 405 (1972/3). 'Ion Molecule Reactions in the CO_2/H_2 System by Ion Cyclotron Resonance'.

107. Giomousis, G. and Stevenson, D.P., J. Chem. Phys. 29, 294 (1958). 'Reactions of Gaseous Molecule Ions with Gaseous Molecules. V. Theory'.

108. Fehsenfeld, F.C., Schmeltekopf, A.L. and Ferguson, E.E., J. Chem. Phys. 46, 2802 (1967). 'Thermal-Energy Ion-Neutral Reaction Rates. VII. Some Hydrogen-atom Abstraction Reactions'.

109. Moran, T.F. and Friedman, L., J. Chem. Phys. 42, 2391 (1965). 'Cross Sections and Intramolecular Isotope Effects in AB-HD Ion-molecule Reactions'.

110. Shannon, T.W. and Harrison, A.G., J. Chem. Phys. 43, 4206 (1965). 'Concurrent Ion-molecule Reactions. II. Reactions in $X-D_2$ Mixtures'.

111. Gubtier, von H., Z. Naturforsch.12a, 499 (1957). 'Massenspektrometische Untersuchung der Reaktion $X^+ + H_2 \longrightarrow HX^+ + H$'.

112. Harrison, A.G. and Myher, J.J., J. Chem. Phys. 46, 3276 (1967). 'Ion-molecule Reactions in Mixtures with D_2 or CD_4'.

113. Warneck, P., J. Chem. Phys. 46, 513 (1967). 'Studies of Ion-neutral Reactions by a Photo-ionization Technique. II. Charge-transfer Reactions of Argon Ions at Near-thermal Energies'.

114. Giardini-Guidoni, A. and Friedman, L., J. Chem. Phys. 45, 937 (1966). 'Energy Transfer in Ion-molecule Reactions in the Methane System'.

115. Abramson, F.P. and Futrell, J.H., J. Chem. Phys. 45, 1925 (1966). 'Ion-molecule Reactions in Methane'.

116. Abramson, F.P. and Futrell, J.H., J. Chem. Phys. 46, 3264 (1967). 'On the Reaction of CH_4^+ with CD_4'.

117. Anders, L.R., J. Phys. Chem. 73, 469 (1969). 'Study of the Energetics of Ion-molecule Reactions by Pulsed Ion Cyclotron Double Resonance'.

118. Paul, W. and Raether, M., Z. Phys. 140, 262 (1965). 'Das Elektrischen Massenfilter'.

119. Paul, W., Reinhard, H.P. and von Zahn, U., Z. Phys. 152, 143 (1968). 'Das Elektrische Massenfilter als Massenspektrometer und Isotopentrenner'.

120. Busch, F.V. and Paul, W., Z. Phys. 164, 581 (1961). 'Isotopentrennung mit dem Elektrischen Massenfilter'.

121. Busch, F.V. and Paul, W., Z. Phys. 164, 588 (1961). 'Über Nichtlineare Resonanzen in Elektrischen Massenfilter als Folge Feldfehlern'.

122. Dawson, P.H. and Whetten, N.R., 'Quadrupole Mass Spectrometry' in Price, D. (ed.) 'Dynamic Mass Spectrometry', Vol. 2, Heyden and Sons, London, 1971.

123. Ball, G.W., Lawson, G. and Todd, J.F.J., 'The Application of Dynamic Mass Spectrometers to Problems in Residual Gas Analysis' in Price, D. (ed.) 'Dynamic Mass Spectrometry', Vol. 3, Heyden and Sons, London, 1972.

124. Moran, T.F. and Hamill, W.H., J. Chem. Phys. 39, 1413 (1963). 'Cross Sections of Ion-permanent-dipole Reactions by Mass Spectrometry'.

125. Theard, L.P. and Hamill, W.H., J. Amer. Chem. Soc. 84, 1134 (1962). 'The Energy Dependence of Cross Sections of Some Ion-molecule Reactions'.

126. Gupta, J.K., Jones, E.G., Harrison, A.G. and Myher, J.J., Can. J. Chem. 45, 3107 (1967). 'Reactions of Thermal Energy Ions. V. Hydrogen-Transfer Ion-molecule Reactions Involving Polar Molecules'.

127. Su, T. and Bowers, M.T., J. Chem. Phys. 58, 3027 (1972). 'Theory of Ion-polar molecule Collisions. Comparison with Experimental Charge Transfer Reactions of Rare Gas Ions to Geometric Isomers of Difluorobenzene and Dichloroethylene'.

128. Bowers, M.T., Su, T. and Anicich, V.G., J. Chem. Phys. 58, 5175 (1973). 'Theory of Ion-polar Molecule Collisions. Kinetic Energy Dependence of Ion-polar Molecule Reactions: $CH_3OH^+ + CH_3OH \longrightarrow CH_3OH_2^+ + (H_3O^*)$'.

129. Hunt, D.F., Advan. In Mass Spectrom. 6, 517 (1974). 'Reagent Gases for Chemical Ionization Mass Spectrometry'.

130. The use of ozone as a reagent gas was described during the presentation of Reference 129 at the Sixth International Conference on Mass Spectrometry, Edinburgh, 1973, but is not included in the published version of this paper.

131. Hunt, D.F., Private Communication. to be published in Progress in Anal. Chem. 'Selective Reagents for Chemical Ionization Mass Spectrometry'.

132. See Advan. in Mass Spectrom., Volume 6 for examples and further references.

133. Yinon, J., to be published in Vacuum. 'Instrumentation and Vacuum Aspects of Chemical Ionization Mass Spectrometry'.

134. Franklin, J.L., Dillard, J.G. and Field, F.H. 'Ionization Potentials, Appearance Potentials and Heats of Formation of Gaseous Positive Ions'. National Bureau of Standards, 1969.

135. Cohen, M.J. and Karasek, F.W., J. Chromatographic Sci. 8, 330 (1970). 'Plasma Chromatography - A New Dimension for Gas Chromatography and Mass Spectrometry'.

136. Karasek, F.W., Anal. Chem. 43, 1982 (1971). 'Plasma Chromatography of the Polychlorinated Biphenyls'.

137. McAllister, T., Int. J. Mass Spectrom. Ion Phys. 9, 127 (1972). 'Ion-molecule Reaction Kinetics by Ion Cyclotron Resonance Mass Spectrometry'.

138. Bowers, M.T. and Elleman, D.D., J. Chem. Phys. 51, 4606 (1969). 'Kinetic Analysis of the Concurrent Ion-Molecule Reactions in Mixtures of Argon and Nitrogen with H_2, D_2 and HD utilizing Ion-ejection Ion-cyclotron-resonance Techniques'.

139. Bowers, M.T., Elleman, D.D. and King, J.J., J. Chem. Phys. 50, 1840 (1969). 'Kinetic Analysis of the Ion-molecule Reactions in Nitrogen-Hydrogen Mixtures using Ion Cyclotron Resonance'.

140. Golden, P.D., Schmeltekopf, A.L., Fehsenfeld, F.C., Schiff, H.I. and Ferguson, E.E., J. Chem. Phys. 44, 4095 (1966). 'Thermal Energy Ion-neutral Reaction Rates. II. Some Reactions of Ionospheric Interest'.

141. Ryan, K.R., J. Chem. Phys. 51, 4136 (1969). 'Ionic Collision Processes in Gaseous Mixtures of Oxygen and Nitrogen'.

142. Galli, A., Giardini-Guidoni, A. and Volpi, G.G., J. Chem. Phys. 39, 518 (1963). 'Ion-molecule Reactions leading to NO^+ Formation'.

143. Lampe, F.W., Franklin, J.L. and Field, F.H., J. Amer. Chem. Soc. 79, 6129 (1957). 'Cross Sections for Ionization by Electrons'.

144. Field, F.H., Head, H.N. and Franklin, J.L., J. Amer. Chem. Soc. 84, 1118 (1962). 'Reactions of Gaseous Ions. XI. Ionic Reactions in Krypton-Methane and Argon-Methane Mixtures'.

145. Lampe, F.W., Field, F.H. and Franklin, J.L., J. Amer. Chem. Soc. 79, 6132 (1957). 'Reaction of Gaseous Ions. IV. Water'.

146. Thynne, J.C.J. and Harrison, A.G., Trans. Farad. Soc. 62, 2468 (1966). 'Reactions of Thermal Energy Ions. Part 3. Ion-molecule Reactions in H_2O and D_2O'.

147. Baxendale, J.M. and Gilbert, G.P., Disc. Farad. Soc. 36, 186 (1963). 'The γ-Radiolysis of Water Vapour'.

148. Kebarle, P. and Hogg, A.M., J. Chem. Phys. 42, 798 (1965). 'Heats of Hydration and Solvation by Mass Spectrometry'.

149. Good, A., Durden, D.A. and Kebarle, P., J. Chem. Phys. 52, 222 (1970). 'Mechanism and Rate Constants of Ion-molecule Reactions leading to Formation of $H^+(H_2O)n$ in Moist Oxygen and Air.'

150. Ryan, K.R., J. Chem. Phys. 52, 6009 (1970). 'Ionic Collision Processes in Water Vapour'.

151. Huntress, W.T., Moseman, M.M. and Elleman, D.D., J. Chem. Phys. 54, 843 (1970). 'Relative Rates and their Dependences on Kinetic Energy for Ion-molecule Reactions in Ammonia'.

152. Lampe, F.W. and Field, F.H., Tetrahedron 7, 189 (1959). 'Reactions of Ions with Molecules in the Gas Phase'.

153. Dorfman, L.M. and Noble, P.C., J. Phys. Chem. 63, 980 (1959). 'Reactions of Gaseous Ions. Ammonium Ion Formation in Ionized Ammonia'.

154. Derwish, G.A.W., Galli, A., Giardini-Guidoni, A. and Volpi, G.G., J. Chem. Phys. 39, 1599 (1963). 'Ion-molecule Reactions in Gaseous Ammonia'.

155. Harrison, A.G. and Thynne, J.C.J., Trans. Farad. Soc. 62, 2804 (1966). 'Reactions of Thermal Energy Ions. Part 4. Ion-molecule Reactions in Ammonia and Hydrazine'.

156. Ryan, K.R., J. Chem. Phys. 53, 3844 (1970). 'Ionic Collision Processes in Gaseous Ammonia'.

157. Tartarczyk, H. and von Zahn, U., Z. Naturforch 20a, 1708 (1965). 'Nachweis metastabilier Ionen mit langen Lebensdauern'.

158. Designs for such electronic equipment abound in Amateur Radio texts; see for example 'The Communication Handbook', The Radio Society of Great Britain, London, 1968.

159. Richards, J.A., Huey, R.M. and Hiller, J., Int. J. Mass Spectrom. Ion Phys. 12, 317 (1973). 'A New Operating Mode for the Quadrupole Mass Filter'.

160. Walls, F.L. and Dunn, G.H., Physics Today, August 1974, Page 30. 'Storing Ions for Collision Studies'.

161. Fite, W.C. and Irving, P., J. Vac. Sci. Technol. 11, 351 (1974). "High Resolution Residual Gas Analysis'.

162. Smith, C., 'Conic Sections', Macmillan and Co., 1910.

APPENDIX

Papers Published as a Result of this Work

Published Reports

Bonner, R.F., Lawson, G. and Todd, J.F.J.

Int. J. Mass Spectrom. Ion Phys. 10, 197 (1972/73).

'Ion-molecule Reaction Studies with a Quadrupole Ion Trap (QUISTOR).'

Bonner, R.F., Lawson, G. and Todd, J.F.J.

J. Chem. Soc. Chem. Commun. 1179 (1972).

'A Low-pressure Chemical Ionization Source: An Application of a Novel Type of Mass Spectrometer'.

Lawson, G., Bonner, R.F. and Todd, J.F.J.

J. Phys. E. (J. Sci. Instrum.) 6, 357 (1973).

'The Quadrupole Ion Store (QUISTOR) as a Novel Source for a Mass Spectrometer'.

Bonner, R.F., Lawson, G., Todd, J.F.J. and March, R.E.

Advan. in Mass Spectrom. 6, 377 (1974).

'Ion Storage Mass Spectrometry - Applications of the Study of Ionic Processes and Chemical Ionization Reactions'.

Lawson, G., Bonner, R.F., Todd J.F.J. and March, R.E.

J. Chem. Soc. Faraday I. - submitted for publication.

'The Quadrupole Ion Store (QUISTOR). Part I. Ion-molecule Reactions in Methane, Water and Ammonia'.

Papers Presented at Conferences

Bonner, R.F.*, Lawson, G. and Todd, J.F.J.

'Chemical Ionization and Charge Transfer Studies with a Quadrupole Ion Store (QUISTOR)'.

Presented at the 6th Annual Meeting of the Mass Spectrometry Group, Swansea, U.K. 1972, Abstract No. 9.

Bonner, R.F., Lawson, G., Todd, J.F.J.*and March, R.E.

'Ion Storage Mass Spectrometry - Applications in the Study of Ionic Processes and Chemical Ionization Reactions'.

Presented at the 6th International Conference on Mass Spectrometry, Edinburgh, 1973. Abstract No. 39.

* Paper presented by this Author.